

УНИВЕРЗИТЕТ ЦРНЕ ГОРЕ
МЕТАЛУРШКО-ТЕХНОЛОШКИ
ФАКУЛТЕТ

Цетињски пут б.б.
81000 Подгорица,
Црна Гора

UNIVERSITY OF MONTENEGRO
FACULTY OF METALLURGY AND
TECHNOLOGY

Cetinjski put b.b.
81000 Podgorica
MONTENEGRO



www.ucg.ac.me/mtf

Тел/Факс: +382(0)20 245-406

e-mail: mtf@ucg.ac.me

Жиро рачун: 510-2435-10

ПИБ: 02016702

ПДВ: 30/31-03951-6

Број 643/1

Подгорица, 20.03.2024.

UNIVERZITET CRNE GORE

SENAT

ODBOR ZA DOKTORSKE STUDIJE

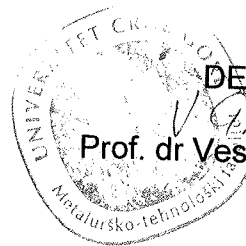
Podgorica

PREDMET: Predlog Komisije za ocjenu DD
kandidata MSc Aleksandre Gezović

Poštovani,

U prilogu akta dostavljamo odluku Vijeća Metalurško-tehnološkog fakulteta od 20.03.2024. godine, o imenovanju Komisije za ocjenu doktorske disertacije: „*Ekološki polianjonski katodni materijali na bazi fosfata za primjenu u litijum/natrijum-jonskim baterijama*“, kandidata MSc Aleksandre Gezović, sa pretećom dokumentacijom, na dalji postupak.

Srdačan pozdrav,



DEKAN,

V. Grudić
Prof. dr Veselinka Grudić

Broj 643
25-03 24
Podgorica, 20... god.

Na osnovu člana 64 Statuta Univerziteta Crne Gore („Bilten UCG“ br. 337/2015 i br. 447/2018), a u vezi sa čl. 41 Pravila doktorskih studija Univerziteta Crne Gore, Vijeće Metalurško-tehnološkog fakulteta u Podgorici, na sjednici održanoj 20.03.2024. godine, donijelo je -

ODLUKU

Predlaže se Komisija za ocjenu doktorske disertacije: „*Ekološki polianjonski katodni materijali na bazi fosfata za primjenu u litijum/natrijum-jonskim baterijama*“, kandidata MSc Aleksandre Gezović, u sastavu:

1. Prof. dr Veselinka Grudić, redovni profesor, UCG - MTF, Podgorica, mentor,
Naučna oblast: *Fizička hemija*
2. Dr Milica Vujković, naučni savjetnik, UB - Fakultet za fizičku hemiju i gostujući predavač Centra za interdisciplinarnu i multidisciplinarnu studiju UCG,
Naučna oblast: *Fizička hemija (komentor)*
3. Prof. dr Ivana Bošković, redovni profesor, UCG - MTF, Podgorica, član
Naučna oblast: *Fizička hemija*
4. Dr Miloš Milović, viši naučni saradnik, Institut tehničkih nauka, SANU, Beograd, Naučna oblast: *Fizička hemija, Elektrohemija, Kristalografija*
5. Prof. dr Martin Čalasan, vanredni profesor, UCG - ETF, Podgorica,
Naučna oblast: *Električne mašine i pogoni*

DOSTAVLJENO:

- Odbor za doktorske studije,
- Sekretar,
- Dosije,
- a/a.

UNIVERZITET CRNE GORE
METALURŠKO-TEHNOLOŠKI FAKULTET
DEKAN
Prof. dr Veselinka Grudić

ISPUNJENOST USLOVA DOKTORANDA

OPŠTI PODACI O DOKTORANDU			
Titula, ime, ime roditelja, prezime	MSc, Aleksandra Radovan Gezović		
Fakultet	Metalurško-tehnološki fakultet		
Studijski program	Hemijska tehnologija		
Broj indeksa	1/18		
NAZIV DOKTORSKE DISERTACIJE			
Na službenom jeziku	„Ekološki polianjonski katodni materijali na bazi fosfata za litijum/natrijum-jonske baterije”		
Na engleskom jeziku	„Ecologically polyanionic cathode materials based on the phosphates for lithium/sodium-ion batteries”		
Naučna oblast	Fizička hemija - Elektrohemija		
MENTOR/MENTORI			
Prvi mentor	Prof. dr Veselinka Grudić	Metalurško-tehnološki fakultet, Univerzitet Crne Gore, Crna Gora	Fizička-hemija, Elektrohemija
Drugi mentor	Dr Milica Vujković	Fakultet za fizičku hemiju, Univerzitet u Beogradu, Srbija	Fizička-hemija, elektrohemija
KOMISIJA ZA PREGLED I OCJENU DOKTORSKE DISERTACIJE			
Prof. dr Ivana Bošković (predsjednik)	Metalurško-tehnološki fakultet, Univerzitet Crne Gore, Crna Gora	Fizička-hemija	
Prof. dr Veselinka Grudić	Metalurško-tehnološki fakultet, Univerzitet Crne Gore, Crna Gora	Fizička-hemija, Elektrohemija	
Dr Milica Vujković	Fakultet za fizičku hemiju, Univerzitet u Beogradu, Srbija	Fizička-hemija, Elektrohemija	
Prof. dr Martin Čalasan	Elektrotehnički fakultet, Univerzitet Crne Gore, Crna Gora	Električne mašine i pogoni	

Dr Miloš Milović	Institut tehničkih nauka, SANU, Srbija	Fizička-hemija, Elektrohemija, Kristalografija
Datum značajni za ocjenu doktorske disertacije		
Sjednica Senata na kojoj je data saglasnost na ocjenu teme i kandidata	09.07.2019. godine	
Dostavljanja doktorske disertacije organizacionoj jedinici i saglasnost mentora	18.03.2024. godine	
Sjednica Vijeća organizacione jedinice na kojoj je dat prijedlog za imenovanje komisija za pregled i ocjenu doktorske disertacije	20.03.2024. godine	
ISPUNJENOST USLOVA DOKTORANDA		
U skladu sa članom 38 pravila doktorskih studija kandidat je/nije cjelokupna ili dio sopstvenih istraživanja vezanih za doktorsku disertaciju publikovao u časopisu sa (SCI/SCIE)/(SSCI/A&HCI) liste kao prvi autor.		
Spisak radova doktoranda iz oblasti doktorskih studija koje je publikovao u časopisima sa (SCI/SCIE)		
a) Aleksandra Gezović , Miloš Milović, Danica Bajuk-Bogdanović, Veselinka Grudić, Robert Dominko, Slavko Mentus, Milica J. Vujković, An effective approach to reaching the theoretical capacity of a low-cost and environmentally friendly $\text{Na}_4\text{Fe}_3(\text{PO}_4)_2(\text{P}_2\text{O}_7)$ cathode for Na-ion batteries, <i>Electrochimica Acta</i> , 476 (2024) 143718 https://doi.org/10.1016/j.electacta.2023.143718 (IF=6.6)		
b) A. Gezović[#] , M.J. Vujković ^{#,*} , M. Milović, V. Grudić, R. Dominko, S. Mentus, Recent developments of $\text{Na}_4\text{M}_3(\text{PO}_4)_2(\text{P}_2\text{O}_7)$ as the cathode material for alkaline-ion rechargeable batteries: challenges and outlook, <i>Energy Storage Materials</i> , 37 (2021) 243-273 https://doi.org/10.1016/j.ensm.2021.02.011 (IF=20.4)		
Obrazloženje mentora o korišćenju doktorske disertacije u publikovanim radovima		

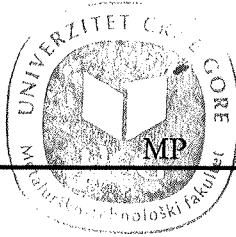
Doktorand je u konsultacijama sa mentorom i komentorom došao na ideju da se prvi dio doktorske disertacije predstavi i publikuje kroz pregledni rad. Za početak je akcenat bio isključivo na jedinjenju opšte formule $\text{Na}_4\text{Fe}_3(\text{PO}_4)_2\text{P}_2\text{O}_7$, koje predstavlja i glavni cilj projekta stipendije. Međutim, nakon pregleda rada od strane mentora/komentora došlo se na ideju da bi bilo veoma značajno proširiti pregled literature sa ciljem da se osim jedinjenja $\text{Na}_4\text{Fe}_3(\text{PO}_4)_2\text{P}_2\text{O}_7$, detaljnije prodiskutuje i o njemu izostrukturalnim jedinjenjima iz grupe polianjonskih miješanih katodnih materijala, opšte formule $\text{Na}_4\text{M}_3(\text{PO}_4)_2\text{P}_2\text{O}_7$ (gdje je $\text{M}=\text{Co}, \text{Mn}$ i Ni). Radom je obuhvaćena retrospektiva postupaka sinteze, kinetike i mehanizma reakcija sodijacije/desodijacije, zasnovanih na eksperimentalnim i teorijskim rezultatima. Prvenstveno su rezimirane strukturne osobine ovih jedinjenja i to u pogledu njihovih električnih, vibracionih i površinskih osobina. U drugom dijelu su hronološki povezane metode sinteze i performanse skladištenja natrijuma/litijuma. Kao zaključak pregleda literature izdvojene su prednosti i slabosti ovih miješanih polianjonskih katodnih materijala. Unapređenje performansi navedenih katodnih materijala je i suština eksperimentalnog dijela disertacije. Time je prvobitno publikovani rad ujedno i uvodni dio doktorske disertacije, o čijoj važnosti najbolje govori veoma visoki impakt faktor časopisa u kojem je isti publikovan (20.4).

Nakon navedene publikacije uočeno je da su najveće poteškoće vezane za sintezu ove faze. Tačnije, prema saznanjima, do tada nije bilo istraživanja koja su u postupku metode sagorijevanja gela koristili fosfate i pirofosfate zasebno kao reaktante. Zbog toga je drugi objavljeni rad obuhvatio upravo eksperimentalni dio disertacije gdje je osnova bila da se miješanjem navedenih komponenti, prateći stehiometriju $\text{Na}_4\text{Fe}_3(\text{PO}_4)_2\text{P}_2\text{O}_7$ faze, zajedno s određenom količinom limunske kiseline uvidi uticaj na krajnji fazni sastav dobijenog materijala. Kako je pH u ovom slučaju podešavan limunskom kiselinom i izmjeren oko 3, utvrđeno je da pri ovim uslovima nije moguće dobiti čistu $\text{Na}_4\text{Fe}_3(\text{PO}_4)_2\text{P}_2\text{O}_7$ fazu, već se suprotno u mnogo većem procentu dobija $\text{Na}_2\text{FeP}_2\text{O}_7$ faza. Time je glavni cilj rada dalje usmjeren na dobijanje $\text{Na}_4\text{Fe}_3(\text{PO}_4)_2\text{P}_2\text{O}_7$ u odsustvu $\text{Na}_2\text{FeP}_2\text{O}_7$ faze. Dalje su kroz eksperimentalni rad modifikacijom sinteze u smislu povećanja pH suspenzije, prilagođeno određenom količinom limunske kiseline ili amonijum-hidroksida, postignute promjene reakcionog puta, čime je upravo i postignuto da se povećava relativna količina miješane NFPP faze. Osim povećanja NFPP faze sa porastom pH od 2 do 6, kada se postigne vrijednost $\text{pH} \approx 7$, ova faza se oslobađa od individualnih pirofosfata. Sve navedeno je obrazloženo i potvrđeno sa više metoda karakterizacije, što je prikazano u drugom publikovanom radu. Osim toga, publikacija sadrži i krajnji cilj disertacije a to je dalje ispitivanje dobijenih materijala sa stanovišta primjene u vodenim Naciononskim baterijama. Postignute su teorijske vrijednosti kapaciteta pri relativno visokim strujama od 8 C, a uz to je postignuta i sposobnost podnošenja visokih brzina u oba elektrolita, posebno u onom koji sadrži Na^+ jone, za miješane fosfate-pirofosfate.

Stoga, oba rada su obuhvatila istraživanje u okviru disertacije, kroz koje je iznijeta suština istraživanja, sa jasnom identifikacijom problema, kao i njihovim rješenjem.

Datum i ovjera (pečat i potpis odgovorne osobe)

U Podgorici,
25.03.2024. godine

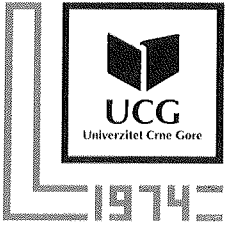


DEKAN

V. Gručić

Prilog dokumenta sadrži:

1. Potvrdu o predaji doktorske disertacije organizacionoj jedinici
2. Odluku o imenovanju komisije za pregled i ocjenu doktorske disertacije
3. Kopiju rada publikovanog u časopisu sa odgovarajuće liste
4. Biografiju i bibliografiju kandidata
5. Biografiju i bibliografiju članova komisije za pregled i ocjenu doktorske disertacije sa potvrdom o izboru u odgovarajuće akademsko zvanje i potvrdom da barem jedan član komisije nije u radnom odnosu na Univerzitetu Crne Gore



УНИВЕРЗИТЕТ ЦРНЕ ГОРЕ
МЕТАЛУРШКО-ТЕХНОЛОШКИ
ФАКУЛТЕТ

Цетињски пут б.б.
81000 Подгорица,
Црна Гора

www.ucg.ac.me/mtf

Тел/Факс: +382(0)20 245-406

e-mail: mtf@ucg.ac.me

UNIVERSITY OF MONTENEGRO
FACULTY OF METALLURGY AND
TECHNOLOGY

Cetinjski put b.b.
81000 Podgorica
MONTENEGRO



Жиро рачун: 510-2435-10

ПИБ: 02016702

ПДВ: 30/31-03951-6

Број

589

Подгорица,

18. 03. 2024.

Na osnovu člana 33 Zakona o upravnom postupku („Sl. list CG“ br. 56/14, 20/15, 40/16 i 37/17), a u vezi sa odredbama Pravila doktorskih studija na Univerzitetu Crne Gore i nakon uvida u službenu evidenciju, Metalurško-tehnološki fakultet izdaje-

P O T V R D U

MSc Aleksandra Gezović, student doktorskih studija na Metalurško-tehnološkom fakultetu u Podgorici, dostavila je ovom Fakultetu doktorsku disertaciju pod nazivom „*Ekološki polianjonski katodni materijali na bazi fosfata za primjenu u litijum/natrijum-jonskim baterijama*“, dana 18.03.2024. godine, na dalje postupanje.

Potvrda se izdaje u skladu sa Pravilima doktorskih studija na Univerzitetu Crne Gore, kao dokaz da je student dostavio radnu verziju doktorske disertacije u štampanoj i elektronskoj formi, i u druge svrhe se ne može upotrijebiti.

SEKRETAR,

Seka Šekularac-Petrović
Seka Šekularac-Petrović



UNIVERZITET CRNE GORE
METALURŠKO-TEHNOLOŠKI FAKULTET

Na osnovu člana 37. Pravila doktorskih studija Univerziteta Crne Gore, dajem sledeću

SAGLASNOST

UNIVERZITET CRNE GORE
METALURŠKO-TEHNOLOŠKI FAKULTET

Rad pod nazivom "**Ekološki polianjonski katodni materijali na bazi fosfata za litijum/natrijum-jonske baterije**" autorke Msc Aleksandre Gezović, saradnice u nastavi na Metalurško-tehnološkog fakulteta Univerziteta Crne Gore, zadovoljava kriterijume doktorske disertacije propisane Statutom Univerziteta Crne Gore i Pravilima doktorskih studija.

Na osnovu člana 37. Pravila doktorskih studija Univerziteta Crne Gore, dajem sledeću

MENTOR

18.03.2024.

V Grudić

Prof. dr Veselinka Grudić

KOMENTOR

M Vujković

Dr Milica Vujković

18.03.2024.

U Podgorici, 18.03.2024. godine

Prof. dr Veselinka Grudić

KOMENTOR

Dr Milica Vujković

Dr Veselinka Grudić

Dr Milica Vujković



Recent developments of $\text{Na}_4\text{M}_3(\text{PO}_4)_2(\text{P}_2\text{O}_7)$ as the cathode material for alkaline-ion rechargeable batteries: challenges and outlook

Aleksandra Gezović^{a,#}, Milica J. Vujković^{b,#,*}, Miloš Milović^c, Veselinka Grudić^a, Robert Dominko^{d,e}, Slavko Mentus^{b,f}

^a Faculty of Metallurgy and Technology, University of Montenegro, Cetinjski put bb, 81000 Podgorica, Montenegro

^b Faculty of Physical Chemistry, University of Belgrade, Studentski trg 12-14, 11158 Belgrade, Serbia

^c Institute of Technical Sciences of Serbian Academy of Sciences and Arts, Knez Mihajlova 35/IV, 11158 Belgrade, Serbia

^d National Institute of Chemistry, Hajdrihova 19, SI-1000 Ljubljana, Slovenia

^e FKKT, University of Ljubljana, Večna pot 117, 1000 Ljubljana, Slovenia

^f Serbian Academy of Sciences and Arts, Knez Mihajlova 35, 11158 Belgrade, Serbia

ARTICLE INFO

Keywords:

Polyanionic material
 $\text{Na}_4\text{M}_3(\text{PO}_4)_2(\text{P}_2\text{O}_7)$
 Sodium-ion batteries
 Synthesis procedures
 Sodium redox processes

ABSTRACT

Sodium ion batteries (SIB) present one of the most perspective post lithium technology and their progress strongly depends on the development of compounds having the structure which enables fast sodium insertion/deinsertion reactions. Polyanion compounds have been widely investigated as cathode materials for SIBs where they compete effectively to the usually used layered oxides. This survey is focused on the development of specific family of isostructural polyanion phases encompassed by the common chemical formula $\text{Na}_4\text{M}_3(\text{PO}_4)_2(\text{P}_2\text{O}_7)$. The comprehensive retrospective of their synthesis procedures, the kinetics and mechanism of sodiation/desodiation reactions, based on both experimental and theoretical results, is provided. First, the review summarizes the structural properties of variety of $\text{Na}_4\text{M}_3(\text{PO}_4)_2(\text{P}_2\text{O}_7)$ compounds in terms of its electrical, vibrational and surface properties. Then, the synthesis methods and sodium/lithium storage performance, of each type of $\text{Na}_4\text{M}_3(\text{PO}_4)_2(\text{P}_2\text{O}_7)$ compounds, are chronologically presented and discussed. Finally, the strengths and weaknesses of these mixed polyanion cathodes are outlined, with the aim to explain some discrepancies and unclarified issues encountered in the literature. Besides, this survey will make room for future development. It can be very useful for the future design of high-performance mixed polyanionic compounds as cathodes for alkaline-ion rechargeable batteries.

1. Introduction

An increased utilization of intermittent renewable energy sources requires expansion of electrochemical energy storage systems (EES) to a large scale, suitable to be integrated with renewable energy source devices into electrical grid. The state-of-the-art Li-ion batteries (LIBs) play the pivotal role, due to the capability of storing a large amount of energy, which is favorable for various applications such as portable electronics, electric vehicles and grid power stabilization units [1–9]. However, the demand for electrochemical storage devices keeps getting higher and higher, thus leading to an increased lithium consumption from limited resources and its steep price. To slow down this growth and control lithium supply, extensive studies on alternative systems, based on Na, Zn, Al, Mg, Ca, etc. [10–17], have been launched. The focus of these studies is actually on the development of cost-effective

and environmentally friendly energy storage systems which would be capable of replacing Li-ion batteries, at least in the field where weight and/or volume are not a limiting factor. Among them, sodium-ion batteries (SIBs) have the great economic and energetic potential for grid-scale energy storage systems, due to the low cost and high sodium abundance in Earth's crust. Although SIBs theoretically possess less specific energy than Li ion batteries (the lower redox potential of Na^+/Na than Li^+/Li), the similarity between Li and Na chemistry and "rocking-chair" working principle caused their booming in recent years. Numerous studies have concentrated on the development of electrode materials and electrolytes through different synthesis methods and strategies, trying to get the best performance [18–25]. As a result, different anodes (hard carbon, metal oxides/sulfides...) [16,17,22,26] and cathode materials (oxides, polyanionic compounds...) [20,23,27–32] have been developed, which show not only ultra-fast sodium rate perfor-

* Corresponding author at: University of Belgrade, Faculty of Physical Chemistry, Studentski trg 12–14, 11158 Belgrade, Serbia
 E-mail address: milica.vujkovic@ffh.bg.ac.rs (M.J. Vujković).

Contributed equally

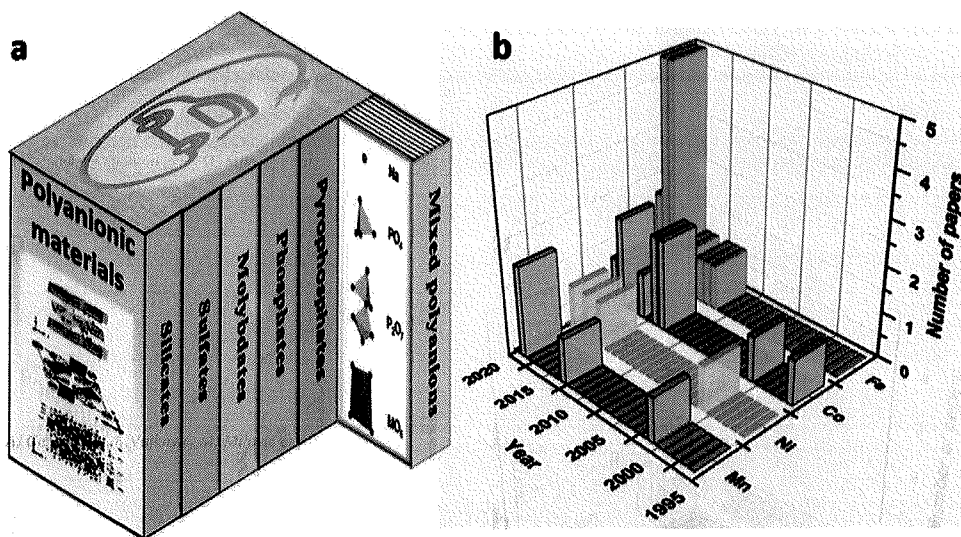


Fig. 1. The mixed-polyanionic compounds: a) the classification b) the recent development of $\text{Na}_4\text{M}_3(\text{PO}_4)_2(\text{P}_2\text{O}_7)$ where $\text{M}=\text{Co}, \text{Fe}, \text{Mn}$ and Ni .

mance, but also the capability of storing larger amount of sodium than lithium ions.

Since Goodenough introduced LiFePO_4 olivine into the world of Li ion batteries [33–35], polyanionic-type materials (Fig. 1a) have been widely examined as cathode materials. Their three-dimensional framework, built on tetrahedral anions $(\text{XO}_4)^{n-}$ or their derivatives $(\text{X}_m\text{O}_{3m+1})^{n-}$ ($\text{X}=\text{P}, \text{Si}, \text{S}, \text{Se}, \text{Mo}, \text{W}, \dots$) and corner- or edge-sharing MO_6 polyhedrons ($\text{M}=\text{transition metal}$), is suitable for diffusion of alkaline ions during charging/discharging and sufficient structural stability [30,36]. Sodium intercalation polyanionic structures based on phosphates (NaMPO_4 , Nasicon type - $\text{Na}_3\text{M}_2(\text{PO}_4)_3$), fluorophosphates ($\text{Na}_2\text{MPO}_4\text{F}$, $\text{Na}_3\text{M}_2(\text{PO}_4)_2\text{F}_3$, $\text{Na}_3(\text{VO})_2(\text{PO}_4)_2\text{F}$...) and pyrophosphates ($\text{Na}_2\text{MP}_2\text{O}_7$...), where M is $\text{Fe}, \text{Mn}, \text{Co}, \text{V}, \dots$, have experienced a huge expansion in the research field of alkaline-ion batteries [20,30,36–41]. The importance of investigating NaFePO_4 [31,32,39,40] should not be emphasized too much, bearing in mind the popularity of the commercial LiFePO_4 cathode material. Further, fluorine doping of phosphates is an effective way to increase redox potential via inductive effect and improve the kinetic of electrochemical reaction [30,42,43]. Also, pyrophosphates appear as promising cathode materials, possessing advantages over MFePO_4 in terms of offering 2D pathways for M^+ diffusion, higher voltage and higher thermal stability. On the other hand, their lower capacity, when compared to MFePO_4 compounds, can cause the lower energy density, if not compensated by the increased voltage [44,45].

Another group of pyrophosphates/phosphates with a mixed polyanionic group and a general formula of $\text{Na}_4\text{M}_3(\text{PO}_4)_2\text{P}_2\text{O}_7$ [46–48], have attracted an increased attention as novel Na-ion cathodes (Fig. 1b), due to low barrier for Na-ion diffusion and advantages over individual phosphate and pyrophosphate compounds.

This mixed compound offers higher operating voltage and less volume changes than individual phosphates and pyrophosphate structures. For instance, the $\text{Fe}^{2+}/\text{Fe}^{3+}$ redox potential increases following the order FePO_4 , NaFePO_4 , $\text{Na}_2\text{FeP}_2\text{O}_7$ or $\text{Na}_2\text{FePO}_4\text{F}$, $\text{Na}_4\text{Fe}_3(\text{PO}_4)_2\text{P}_2\text{O}_7$, amounting to 2.4, 2.7, 3 and 3.2 V versus Na^+/Na , respectively [36,49,50], as illustrated in Fig. 2a–c. The reason for the higher voltage of the mixed polyanionic compound agrees with the change of the M–O covalency strength via inductive effect from the neighboring polyanionic groups. The introduction of polyanionic units, in the structure, results in more resonance forms, thus causing a weaker (covalent) M–O bond and a shorter distance between bonding and antibonding orbitals. As a result, system with more polyanionic units will have a slightly higher voltage [51], despite the same nature of metal and polyanionic group. The control of electronegativity via polyanionic groups is an op-

erative way to tune redox properties of the polyanionic cathode. The replacement of Fe in the mixed polyanion by some other transition metals such as $\text{Mn}, \text{Co}, \text{Ni}$, leads to the increase of the redox potential. In addition, the small volume change during Na^+ insertion/deinsertion is observed for $\text{Na}_4\text{Fe}_3(\text{PO}_4)_2\text{P}_2\text{O}_7$ (below 4 %) [47], which is close to that for $\text{Na}_2\text{FeP}_2\text{O}_7$ ($\sim 2\%$) [52,53], but significantly less than that for NaFePO_4 ($\sim 17\%$) [54]. Furthermore, the issue of pyrophosphates' degradation, caused by reaction with moisture or CO_2 , as one of the crucial complications of pyrophosphates [55], is not pronounced for this type of mixed polyanion compounds.

Although these mixed phosphates have a higher molecular weight than individual phosphate or pyrophosphates, their three-dimensional (3D) channels could allow fast diffusion of sodium ions with low migration barrier (0.2–0.24 eV), while one Na^+ participates into electrochemical reaction of NaMPO_4 and $\text{Na}_2\text{MP}_2\text{O}_7$, thus diffusing through 1D and 2D channels, respectively [44,54,56]. Still, it should be noted that the Na^+ ion diffusion along the three principal axes of the $\text{Na}_2\text{MP}_2\text{O}_7$ material is also reported [57]. However, the diffusion barrier of mixed polyanionic compound (0.2–0.24 eV) [58] is lower than those calculated for other polyanionic structures such as NaMPO_4 (for Fe 0.32 eV and 0.65 eV for Mn) [59,60], $\text{Na}_2\text{MP}_2\text{O}_7$ (0.49 eV or 0.54 eV for Fe and 0.58 for Mn pyrophosphates) [56,57], $\text{Na}_2\text{FePO}_4\text{F}$ (0.3 eV) [61] and $\text{Na}_3\text{V}_2(\text{PO}_4)_3$ (0.35 eV) [62], Fig. 2d. Based on the Arrhenius equation ($D = v e^{-E_a/k_bT}$, D is diffusion coefficient, E_a is the activation diffusion barrier, k_b is Boltzmann constant and v is the pre-exponential factor), this can be explained by the higher diffusion coefficients of mixed polyanionic compounds when compared to other polyanion structures. By using molecular dynamic (MC) simulations, Islam et al. [58] calculated a high diffusion coefficient value of NFPP and NMPP amounting to 6.1×10^{-11} or $3.1 \times 10^{-10} \text{ S cm}^{-1}$, which is in accordance with the experimentally obtained values ranging from 10^{-9} to 10^{-11} [63,64]. Experimental diffusion coefficients of some other polyanionic-type materials were found to be $\sim 10^{-15} \text{ S cm}^{-1}$ for NaFePO_4 [32], $\sim 10^{-12} - 10^{-13}$ for $\text{Na}_2\text{FePO}_4\text{F}$ [65], 2.79×10^{-13} for $\text{Na}_2\text{FeP}_2\text{O}_7$ [44] and $6 \times 10^{-13} - 2 \times 10^{-15} \text{ S cm}^{-1}$ for $\text{Na}_3\text{V}_2(\text{PO}_4)_3$ [66].

Phosphates/fluorophosphates have higher theoretical capacity than pyrophosphates (129 mAh g^{-1} vs. 97 mAh g^{-1} for Fe-based compounds) [23,44,67]. Nevertheless, this value is slightly lower than that for NaMPO_4 (129 mAh g^{-1} vs. 154 mAh g^{-1} for Fe) due to large differences in the molecular weights. If the mixed-polyanion has theoretical ability to exchange all four Na^+ [68,69], its capacity will be higher than that of NaMPO_4 . The first principle calculation shows that the exchange of all Na^+ ions is possible in the case of $\text{Na}_4\text{Co}_3(\text{PO}_4)_2(\text{P}_2\text{O}_7)$, whereas deinsertion process of the last Na ion is followed by the electron trans-

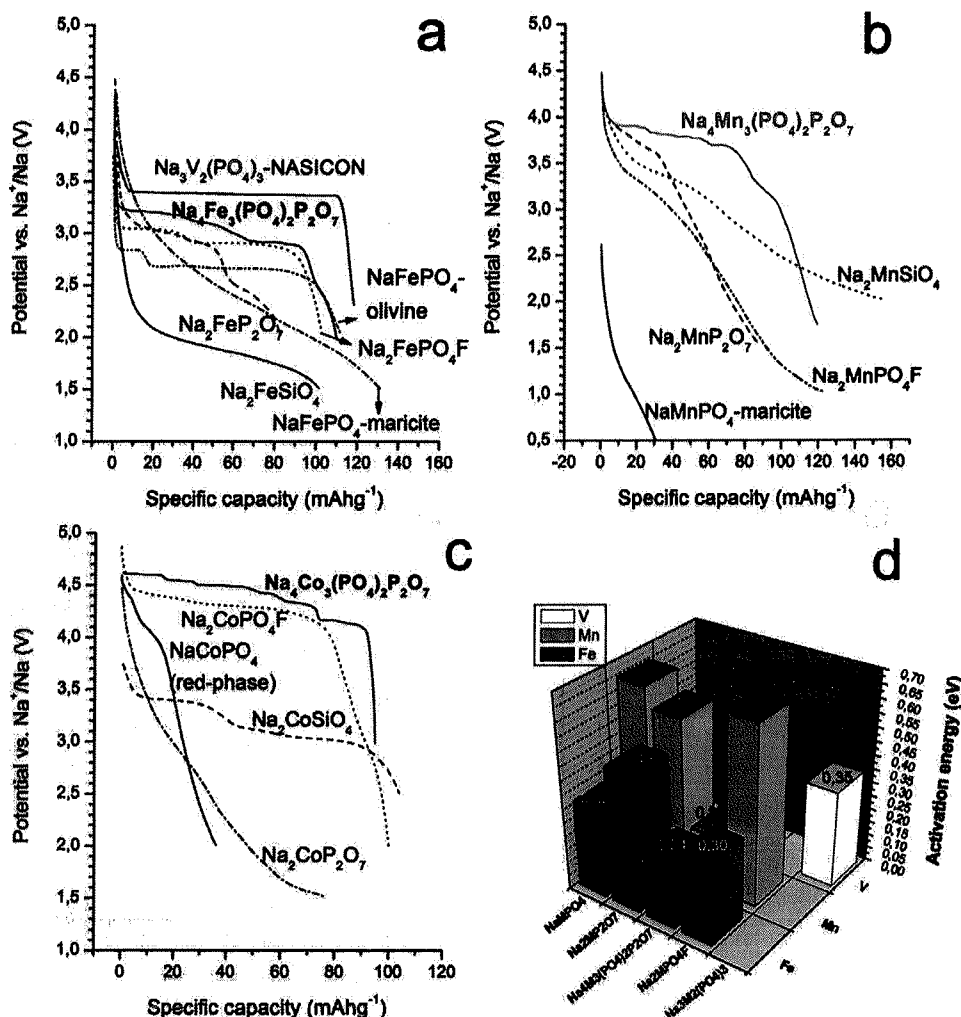


Fig. 2. Typical discharge profiles at low current densities ($\leq C/10$) of $\text{Na}_4\text{M}_3(\text{PO}_4)_2\text{P}_2\text{O}_7$ versus other polyanionic cathodes of Fe (a), Mn (b) and Co (c). Calculated activation barriers of Na^+ migration in various polyanionic compounds of Fe and Mn (d). Profiles are replotted with permission from [50] ($\text{Na}_4\text{Fe}_3(\text{PO}_4)_2\text{P}_2\text{O}_7$), [72] (NaFePO_4 -olivine), [73] (NaFePO_4 -maricite), [56] ($\text{Na}_2\text{FeP}_2\text{O}_7$), [74] ($\text{Na}_2\text{FeSiO}_4$), [75] ($\text{Na}_3\text{V}_2(\text{PO}_4)_3$ -NASICON), [76] ($\text{Na}_2\text{FePO}_4\text{F}$), [77] ($\text{Na}_4\text{Mn}_3(\text{PO}_4)_2\text{P}_2\text{O}_7$), [78] (NaMnPO_4 -maricite), [79] ($\text{Na}_2\text{MnP}_2\text{O}_7$), [80] ($\text{Na}_2\text{MnPO}_4\text{F}$), [81] ($\text{Na}_2\text{MnSiO}_4$), [68] ($\text{Na}_4\text{Co}_3(\text{PO}_4)_2(\text{P}_2\text{O}_7)$), [82] (NaCoPO_4 red-phase), [83] ($\text{Na}_2\text{CoP}_2\text{O}_7$), [84] ($\text{Na}_2\text{CoSiO}_4$) and [85] ($\text{Na}_2\text{CoPO}_4\text{F}$). DFT activation energy data are taken from [58] ($\text{Na}_4\text{Fe}_3(\text{PO}_4)_2\text{P}_2\text{O}_7/\text{Na}_4\text{Mn}_3(\text{PO}_4)_2\text{P}_2\text{O}_7$), [59] (NaFePO_4), [60] (NaMnPO_4), [57] ($\text{Na}_2\text{FeP}_2\text{O}_7$), [56] ($\text{Na}_2\text{MnP}_2\text{O}_7$), [61] ($\text{Na}_2\text{FePO}_4\text{F}$) and [62] ($\text{Na}_3\text{V}_2(\text{PO}_4)_3$ -NASICON).

fer from the oxygen sublattice rather than the oxidation of Co^{3+} to Co^{4+} [70]. However, the process is found to be difficult due to channel's narrowing upon the last Na ion deinsertion. Moreover, the final extraction of the Na ion causes large volume changes, while the process itself occurs at very high potentials (4.93 V vs. Na^+/Na) where the electrolyte stability is the main issue. Nevertheless, theoretical capacity of NCPP is taken to be 170 mAh g^{-1} due to possible exchange of all four Na ions. So, this value would be larger than the one calculated for NaCoPO_4 amounting to 154 mAh g^{-1} . On the other hand, the cycling stability upon possible deinsertion of all four Na ions would be very challenging. Regarding $\text{Na}_4\text{Fe}_3(\text{PO}_4)_2(\text{P}_2\text{O}_7)$ structure, if the exchange of four Na^+ ions was possible, the oxidation of Fe^{2+} up to Fe^{4+} would happen. However, this process is not identified (so far at least). Moreover, Kim et al. [71] observed that Na tunnels narrowed upon extraction of the third Na ion (Fe^{3+} - Fe^{3+} repulsion at the composition of $\text{NaFe}_3(\text{PO}_4)_2(\text{P}_2\text{O}_7)$), thus preventing further extraction of the last Na ion, which acts as a pillar. That is why the capacity of NFPP is calculated per three Na ions (based on $\text{Fe}^{2+}/\text{Fe}^{3+}$ redox couple) and amounts to 129 mAh g^{-1} . If the extraction of all Na^+ ions was achievable in real system (which in our opinion is not impossible), it would probably occur at such high potentials, while the structural collapse (due to removal of Na pillar) present the issue.

Anyhow, all these comparative properties of these mixed polyanion compounds, emphasized as their strong and weak points are elaborated through this overview. Numerous review papers on the topic of sodium-ion batteries provide a general picture of all existing cathode materials [27–30,49,86–94]. Some of them are exclusively focused on the sur-

vey of polyanionic compounds [86,87,92–94] including novel cathode structures, such as these mixed phosphates. However, due to a large number of covered polyanionic structures in those studies, main points, related to the $\text{Na}_4\text{M}_3(\text{PO}_4)_2(\text{P}_2\text{O}_7)$ are outlined very briefly, thus leaving plenty of room for deeper discussion, more detailed insights and challenges for the specific structural composition. Therefore, this interesting $\text{Na}_4\text{M}_3(\text{PO}_4)_2(\text{P}_2\text{O}_7)$ structure containing 3d transition metals (such as Co, Fe, Mn and Ni) [46,48] needs to be further developed and improved as a cathode for SIBs. This paper offers the recent progress of each member of $\text{Na}_4\text{M}_3(\text{PO}_4)_2(\text{P}_2\text{O}_7)$ family ($M=\text{Co}$, Fe , Mn and Ni) starting from the synthesis methods, sodium insertion mechanism, to electrochemical behavior in both half-cells (vs. Na anode) and full coin-type configurations (vs. hard carbon anode). It summarizes the strengths and weaknesses of polyanionic cathodes and highlights main issues/contradictions from the literature, as directions for further research in this area.

2. Structure-to-property relations of $\text{Na}_4\text{M}_3(\text{PO}_4)_2\text{P}_2\text{O}_7$

2.1. Structure vs. electrochemistry

Sanz et al. [46,48] determined the crystal structure for different polymorphs of $\text{Na}_4\text{M}_3(\text{PO}_4)_2(\text{P}_2\text{O}_7)$. The $\text{Na}_4\text{M}_3(\text{PO}_4)_2\text{P}_2\text{O}_7$ compounds are isostructural and belong to orthorhombic space group No.33 ($Pn2_1a$) with similar lattice parameters and slight increase of the cell volume in order $\text{Ni}<\text{Co}<\text{Fe}<\text{Mn}$, as displayed in Table 1. It is the structure composed of alternating $\{\text{M}_3\text{P}_2\text{O}_{13}\}_n$ double layers built from edge- and

Table 1
Table comparing the unit cell parameters of $\text{Na}_4\text{M}_3(\text{PO}_4)_2(\text{P}_2\text{O}_7)$ ($\text{M}=\text{Co}, \text{Fe}, \text{Ni}, \text{Mn}$).

Space group		$\text{Pn}2_1\text{a}$			
Space group no.		33			
Crystal System		Orthorhombic			
M	Ref.	Cell parameters (Å)			Cell Volume (Å ³)
		a	b	c	
Ni	[47]	17.999(2)	6.4986(6)	10.4200(9)	1218.9(2)
Co	[49]	18.046(5)	6.533(2)	10.536(2)	1242.1(5)
Fe	[47]	18.07517(7)	6.53238(2)	10.64760(4)	1257.204(1)
Mn	[2]	17.991(3)	6.648(1)	10.765(2)	1287.6(3)

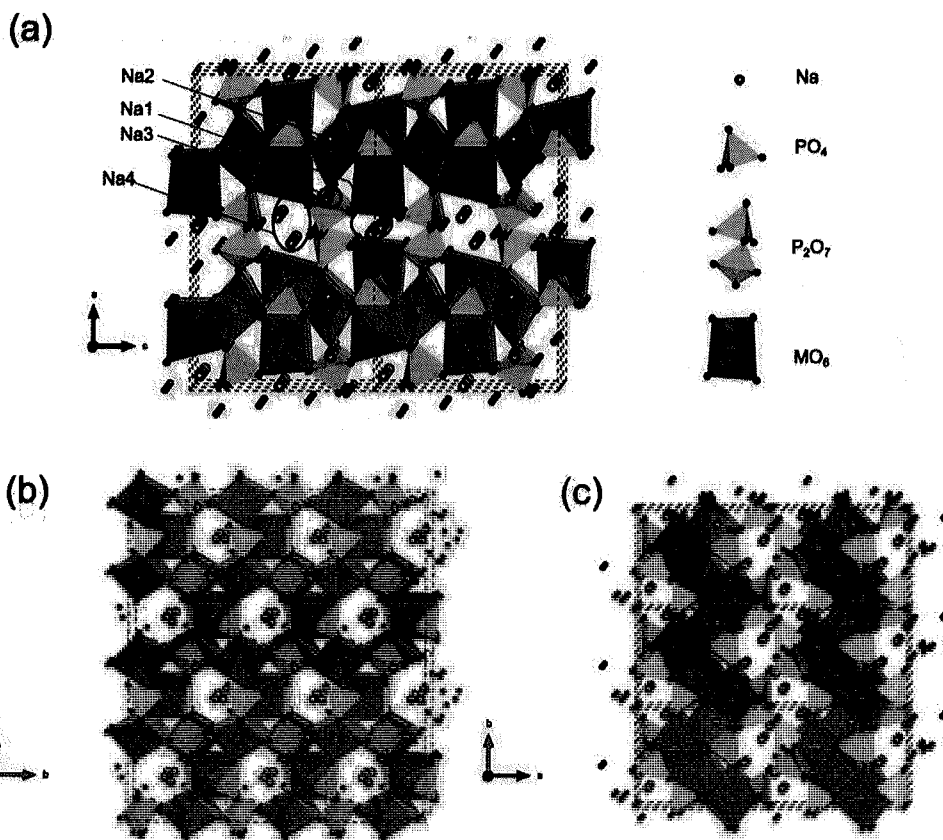


Fig. 3. The crystal structure of $\text{Na}_4\text{M}_3(\text{PO}_4)_2(\text{P}_2\text{O}_7)$ viewed along b-axis (a), a-axis (b) and c-axis (c); the structure is reproduced with permission from ref. [48].

corner-shared MO_6 octahedra and PO_4 tetrahedra (parallel to the b-c plane).

The $\{\text{M}_3\text{P}_2\text{O}_{13}\}_n$ layers are interconnected along a-direction by diphosphate P_2O_7 groups (acting as “pillars”) thus creating extensive tunnel network (along with three main crystallographic directions [100], [010] and [001]) that hosts Na cations. This stable framework is prone to small volume changes of just ~ 4 vol % (Fe) [71], ~ 7 vol % (Mn) [77], ~ 10 vol % (Co) [95] and ~ 2 vol % (Ni) [96] upon Na extraction. Three symmetrically distinguishable sites in octahedral coordination are reserved for a transition metal, while sodium ions are arranged in four crystallographic sites: Na(1), Na(2), Na(3) and Na(4), which are connected by channels (A, B and C) along all three axes (a, b, and c), as illustrated in Fig. 3. Na(2) atoms are located in the A1 channel, at the height of the $(\text{Co}_3\text{P}_2\text{O}_{13})_y$ sheet, while the intersection of two tunnels B2xC1, A1xC1, and B1xC1, accommodates Na(1), Na(3) and Na(4), respectively, with a low activation barrier for all diffusion paths [47,58]. While the pathways, involving Na2 and Na3 sites, are essentially linear, those including Na1 and Na2 are curved ones [58]. The Na^+ ion diffusion coefficient (D_{Na}) of Fe and Mn-based compound

is calculated to be in the range of 10^{-10} and $10^{-11} \text{ cm}^2 \text{ s}^{-1}$, respectively [47,58].

The coordination number of Na sites is a matter of debate in the literature with no consent (see ref. [47,50,63,71,97]) and ranges from 5 to 7, but the majority of authors agrees that the lower coordinated sodium ions are extracted first. Anyhow, small changes in the crystal field, around different sodium atoms, noticeably affect potential of sodium intercalation, which is reflected as the “stepped” discharge curve or as multiple redox peaks in cyclic voltammograms (or in dQ/dV profiles) of all $\text{Na}_4\text{M}_3(\text{PO}_4)_2(\text{P}_2\text{O}_7)$ compounds (4a,b). Except these small changes upon insertion, the discharge potential of $\text{M}^{2+}/\text{M}^{3+}$ pair in $\text{Na}_4\text{M}_3(\text{PO}_4)_2(\text{P}_2\text{O}_7)$ follows the trend $\text{Ni} > \text{Co} > \text{Mn} > \text{Fe}$ as a result of d-orbital splitting discrepancy, well-known from previous polyanion cathode compounds [51].

Reported ionic conductivities of the members of the $\text{Na}_4\text{M}_3(\text{PO}_4)_2(\text{P}_2\text{O}_7)$ family differ by several orders of magnitude (Fig. 4c). At 330 °C the ionic conductivity amounts to ~ 10^{-7} , ~ 10^{-6} and ~ $10^{-5} \text{ S cm}^{-1}$ for $\text{Na}_4\text{Ni}_3(\text{PO}_4)_2(\text{P}_2\text{O}_7)$, $\text{Na}_4\text{Co}_3(\text{PO}_4)_2(\text{P}_2\text{O}_7)$ and $\text{Na}_4\text{Mn}_3(\text{PO}_4)_2(\text{P}_2\text{O}_7)$, respectively [46].

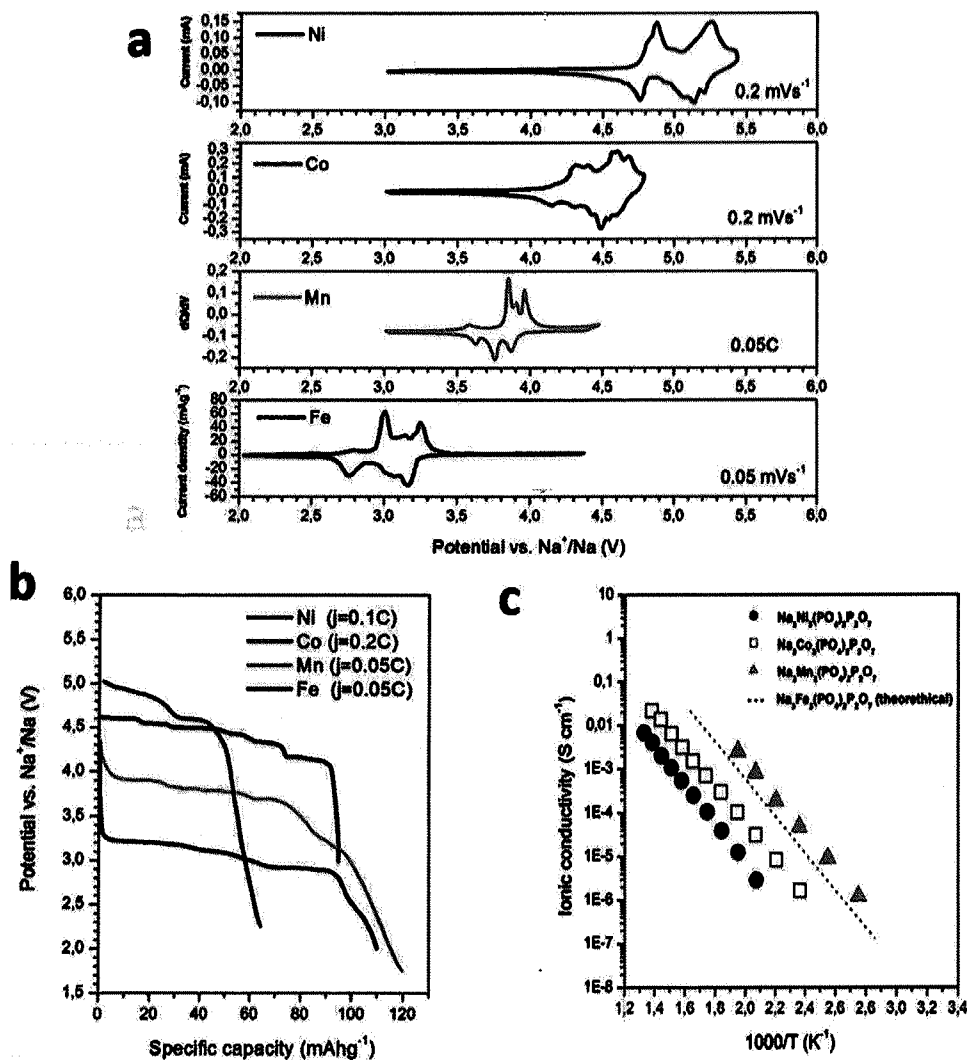


Fig. 4. a) Typical CV profile of $\text{Na}_4\text{M}_3(\text{PO}_4)_2(\text{P}_2\text{O}_7)$ ($\text{M}=\text{Ni}$, Co and Fe) and dQ/dV plot for $\text{M}=\text{Mn}$; b) Typical electrochemical discharge profile of $\text{Na}_4\text{M}_3(\text{PO}_4)_2(\text{P}_2\text{O}_7)$ ($\text{M}=\text{Ni}$, Co , Fe and Mn); the image is replotted with permission from [98] (for Ni), [67,68] (Co), [77] (Mn) and [50] (Fe); c) Arrhenius plots of the ionic conductivity of $\text{Na}_4\text{M}_3(\text{PO}_4)_2\text{P}_2\text{O}_7$ compounds; replotted with permission from [46] (for $\text{M}=\text{Co}$, Mn , Ni) and [58] (theoretically estimated for $\text{Na}_4\text{Fe}_3(\text{PO}_4)_2(\text{P}_2\text{O}_7)$).

Since diffusion of sodium dominantly takes place between $\{\text{M}_3\text{P}_2\text{O}_{13}\}_n$ layers in the bc-plane, the reported rise of conductivity is attributed to the increased dimensionality of the ionic conduction, i.e. to the facilitated transfer of sodium in a-direction and through $\{\text{M}_3\text{P}_2\text{O}_{13}\}_n$ layers. It is a result of channels' widening of the (larger Na-O and N3-O distances) that go along this axis [46]. To date, however, there are no experimental reports for ionic conductivity values of the pure $\text{Na}_4\text{Fe}_3(\text{PO}_4)_2(\text{P}_2\text{O}_7)$ compound. Still, theoretically calculated Arrhenius plots of Na^+ diffusion coefficients suggest slightly lower ionic conductivity for $\text{Na}_4\text{Fe}_3(\text{PO}_4)_2(\text{P}_2\text{O}_7)$ than for $\text{Na}_4\text{Mn}_3(\text{PO}_4)_2(\text{P}_2\text{O}_7)$ [58]. So, the theoretically estimated values of sodium ion conductivity for the composition $\text{Na}_4\text{Fe}_3(\text{PO}_4)_2(\text{P}_2\text{O}_7)$ are also shown in the Fig. 4c.

2.2. DFT approach

The calculations based on DFT are now widely used investigation method of electrode materials for alkali-ion batteries. For calculations, usually Quantum Espresso or Vienna ab-initio simulation package (VASP) are used. Both software packages are based on plane-wave pseudopotential method, what implies a choice of a suitable pseudopotential function in input file formulation. Several other input data are necessary to run the software. The necessary crystallographic data (i.e. the coordinates of constituting atoms) are usually provided by X-ray diffractometry. The calculations with alkali iron phosphates and pyrophosphates [58,79,86] were successively performed using generalized gradient ap-

proximation (GGA) with the Perdew-Burke-Ernzerhof (PBE) exchange correlation functional. The Brillouin-zone integration is performed under suitable choice of Monkhorst-Pack grid. The criterion of good choice of input data is the convergence of the system total energy to a minimum. As explained in a recent review by Chakraborty et al. [86] for a proposed crystallographic structure without or with defects, this method allows to determine the electronic structure, the enthalpy of formation of crystal lattice, the energy of formation of defects and the height of the ion migration barrier. Furthermore, assuming the closeness of enthalpy to the Gibbs free energy, one may calculate the open circuit potential for different charging degrees. Theoretical results could significantly save time for experiments serving as guidelines in materials engineering. As a good example, Park et al. [79] searched the reasons of admirable $\text{Na}_2\text{MnP}_2\text{O}_7$ sodiation/desodiation kinetics relative to the monoclinic $\text{Li}_2\text{MnP}_2\text{O}_7$ by means of first-principle calculations. The explanation was found in the corner-sharing triclinic structure of $\text{Na}_2\text{MnP}_2\text{O}_7$ enabling the locally flexible accommodation of Jahn–Teller distortions on charging. On contrary, the edge sharing geometry of monoclinic $\text{Li}_2\text{MnP}_2\text{O}_7$ requires much larger atomic rearrangements during charging reaction, which slows down the reaction kinetics.

Several theoretical or combined experimental/theoretical studies relate just to the $\text{Na}_4\text{M}_3(\text{PO}_4)_2(\text{P}_2\text{O}_7)$ materials [58,70,71,99].

By combining experimental studies and DFT calculations, Kim et al. [71,87,100] concluded that sodiation/desodiation reactions of the $\text{Na}_4\text{Fe}_3(\text{PO}_4)_2(\text{P}_2\text{O}_7)$ electrode proceed within a single phase. They ex-

perience very small volume change, less than 4 %, while the oxidoreduction reactions of $\text{Fe}^{3+}/\text{Fe}^{2+}$ redox couple compensate the charge carried by sodium ions. This behavior is in contrast to that of individual phosphates (NaFePO_4) and pyrophosphates ($\text{Na}_2\text{FeP}_2\text{O}_7$), which possess two-phase electrochemical reaction.

Islam et al. [58] studied sodium storage mechanism in mixed phosphates $\text{Na}_4\text{M}_3(\text{PO}_4)_2(\text{P}_2\text{O}_7)$ ($\text{M}=\text{Fe}, \text{Co}, \text{Mn}, \text{Ni}$), using molecular dynamics (MD) and DFT simulations. The results of atomistic energy minimization demonstrated for all compositions that the most energetically favorable type of intrinsic defect are the Na/M anti-site pair. By means of mean square displacement inside the long-scale MD simulations, the sodium diffusion coefficients for Fe and Mn materials were determined. The results suggest that Na ions tend to diffuse across 3D migration pathways with a low activation barrier of 0.20 – 0.24 eV, allowing relatively high Na^+ -diffusion coefficients of 10^{-10} – 10^{-11} $\text{cm}^2 \text{s}^{-1}$ at 325 K, suggesting good rate capability. The calculated trends of open circuit voltage for Ni doping in $\text{Na}_4\text{Fe}_{3-x}\text{M}_x(\text{PO}_4)_2(\text{P}_2\text{O}_7)$ show an increase in operational voltage from 3 to 4.9 V if x increases from 0 to 3.

Moriwake et al. [70] have also used the first principles DFT calculations to study the desodiation behavior of $\text{Na}_4\text{Co}_3(\text{PO}_4)_2\text{P}_2\text{O}_7$. Assuming a stepwise desodiation process, the removal of three Na ions (Na1, Na2 and Na4) down to $\text{NaCo}_3(\text{PO}_4)_2(\text{P}_2\text{O}_7)$ is found to be accompanied by oxidation of Co^{2+} to Co^{3+} . Further removal of the last Na (Na3) to give $\text{Co}_3(\text{PO}_4)_2(\text{P}_2\text{O}_7)$ requires oxidation of oxygen 2p orbitals in the P_2O_7 polyhedra instead of Co^{3+} being oxidized to Co^{4+} . Open circuit potentials have been calculated to increase from 4.05 to 4.33, 4.81 and 4.93 V (vs. Na^+/Na) for this stepwise desodiation.

Furthermore, Chen et al. [99] studied $\text{NaFe}_3(\text{PO}_4)_2(\text{P}_2\text{O}_7)/\text{C}$ composite as cathode material. Structural investigations indicated low volume change of 4.0 % on charging/discharging cycle. Density functional theory (DFT) as well as bond valence sum (BVS) calculations were used to unveil possible sodium diffusion pathways. The authors discovered that the Na^+ ions can be assigned to three different types, based on their binding energies. The diffusion energy barriers, within the same Na^+ ion type, were found to be 0.553 eV, 0.02 eV, and 0.365 eV, respectively. These low barriers along all crystallographic axes allow three-dimensional diffusion pathways.

More comprehensive overview of theoretical calculations, regarding Na storage sites, Na diffusion sequence during deinsertion/insertion and migration barriers, will be elaborated within the following section 3, for each type of $\text{Na}_4\text{M}_3(\text{PO}_4)_2(\text{P}_2\text{O}_7)$ separately. The comparison of theoretical data with the experimental observations will be discussed as well. We would like to get the ball rolling by pointing out discrepancies which occur between different theoretical and experimental approaches.

2.3. Spectroscopic Study

The structural characterization of $\text{Na}_4\text{M}_3(\text{PO}_4)_2(\text{P}_2\text{O}_7)$ compounds is usually examined by FTIR, Raman and XPS methods. Vibrational spectrum of these mixed phosphate compounds consists of the characteristic PO_4 and P_2O_7 bands [97,101], as presented in Fig. 5a,b. Vibrations of PO_4 group include symmetric and asymmetric stretching $\nu\text{P-O}$ and bending $\delta\text{O-P-O}$ modes. Vibrations of P_2O_7 (or $\text{O}_3\text{P-O-PO}_3$) are assembly of vibrations of PO_3 group and P-O-P bridges. The first one includes above mentioned $\nu\text{P-O}$ and $\delta\text{O-P-O}$ modes (as in PO_4) and the latter includes symmetric and asymmetric $\nu\text{P-O-P}$ vibrations. The overlap of certain modes complicates the precise interpretation of the $\text{Na}_4\text{M}_3(\text{PO}_4)_2\text{P}_2\text{O}_7$ spectrum. For the sake of simplicity, the spectral region (1400–450 cm^{-1}) can be divided into several regions [97,101], as shown in Fig. 5. The 1200–990 cm^{-1} spectral region includes asymmetric stretching vibrations $\nu_{\text{as}}(\text{P-O})$ in PO_3 and PO_4 , while corresponding symmetric stretching vibrations contribute to the 990–900 cm^{-1} region. Further, the multiple bands, in the lowest frequency range of 500–680 cm^{-1} , have been assigned to the bending O-P-O vibrational modes ($\delta_{\text{as}}\text{O-P-O}$). Also, Fe-O vibration mode of FeO_6 units contributes to this region. The position of this vibrational band is found to be 543 cm^{-1} , but for

isolated FeO_6 octahedra [99]. Two bands, belonging to symmetric and asymmetric P-O-P vibrations in P_2O_7 group appear in the frequency range 900–700 cm^{-1} . According to Kosova [97], these modes are located at $\sim 737 \text{ cm}^{-1}$ (ν_{s}) and $\sim 879 \text{ cm}^{-1}$ (ν_{as}). However, there are some divergences/shifting regarding the assignment of these modes, since their positions have been found either at 721 (ν_{s}) and 956 cm^{-1} (ν_{as}) [102] or at 710 and 905 cm^{-1} [63]. It can be concluded that interpretation of the spectrum strongly depends on the sample's composition, i.e. on the presence of small fraction of the secondary phases and their nature.

To the best of our knowledge, infrared spectra of Ni-, Co- and Mn-based compounds of this family have not been reported yet. Due to close structural similarities of the compounds, it is expected that their respective spectra practically match the spectrum of $\text{Na}_4\text{Fe}_3(\text{PO}_4)_2(\text{P}_2\text{O}_7)$. Fe replacement with a more electropositive metal shifts the bands towards lower wavenumber values, $\text{Ni} > \text{Co} > \text{Fe} > \text{Mn}$ (based on experience with phosphate [103] and pyrophosphate [104,105] family).

Raman spectroscopy and XPS are usually used for the surface characterization of the $\text{Na}_4\text{M}_3(\text{PO}_4)_2(\text{P}_2\text{O}_7)$. Raman spectra of Ni-based mixed polyanion (Fig. 5b) reveals characteristic modes of mixed phosphates, positioned at $\sim 1105 \text{ cm}^{-1}$, $\sim 1056 \text{ cm}^{-1}$ (the stretching modes of PO_4), $\sim 958 \text{ cm}^{-1}$, $\sim 718 \text{ cm}^{-1}$ (the bridge P-O-P modes), 570 cm^{-1} and 348 cm^{-1} (the deformation of PO_4 and P-O-P), which are barely detected in the composite with carbon [106]. However, one can notice inconsistencies regarding other assignments, performed for $\text{Na}_4\text{Fe}_3(\text{PO}_4)_2(\text{P}_2\text{O}_7)/\text{C}$ [63,99], which are not mutually consistent. For instance, Chen et al. [99] have identified typical Raman bands at 218.7 cm^{-1} , 288 cm^{-1} (belonging to stretching and banding vibrations of PO_4 units) and 402.1 cm^{-1} (belonging to the stretching vibrations of FeO_6 octahedra), while Pu et al. [63] have recognized typical bands of FeO_4 , PO_4 and P_2O_7 units at 451 cm^{-1} , 709 cm^{-1} and 1040 cm^{-1} , respectively. We are convinced that not only the quality of carbon layer contributes to these differences but also the chemical composition of the synthesized sample (in terms of the type and fraction of the secondary phase).

Furthermore, the typical XPS spectrum of the mixed polyanionic compound, such as $\text{NaNi}_3(\text{PO}_4)_2(\text{P}_2\text{O}_7)$ (Fig. 5c), shows that Ni 2p appears as a doublet of Ni 2p_{3/2} ($\sim 878.1 \text{ eV}$) and Ni 2p_{1/2} (860.2 eV), including satellite peaks at 866.3 eV and 883.3 eV as well. Each peak is resolved into two peaks, which correspond to Ni^{+2} and Ni^{+3} states. Also, Fe 2p splitting into two major peaks, at the binding energies of $\sim 711 \text{ eV}$ (Fe 2p_{3/2}) and $\sim 725 \text{ eV}$ (Fe 2p_{1/2}) [63,107], indicates a divalent state of Fe in the $\text{NaFe}_3(\text{PO}_4)_2(\text{P}_2\text{O}_7)$ sample. It should be emphasized that the Raman and XPS analyses, of these isostructural polyanionic compounds, have been focused on the carbon analysis [102,107], as the most intensive feature in the spectrum. In some Raman spectra, the main phase cannot even be recognized, due to its coverage by the surface carbon layer [102,107,108].

An overview of each $\text{Na}_4\text{M}_3(\text{PO}_4)_2(\text{P}_2\text{O}_7)$ compound ($\text{M}=\text{Co}, \text{Fe}, \text{Mn}$ and Ni), with the emphasis on the synthesis procedure, electrochemical behavior and sodium redox mechanism, will be provided in the following section.

3. The influence of the transition metal cations

3.1. $\text{Na}_4\text{Co}_3(\text{PO}_4)_2(\text{P}_2\text{O}_7)$ - NCPP

Although Sanz et al. [48] determined the structure of $\text{Na}_4\text{Co}_3(\text{PO}_4)_2(\text{P}_2\text{O}_7)$ (NCPP) in 1996, the electrochemical behavior of this mixed polyanionic material has been examined since 2013, when the interests in sodium-ion batteries began to attract attention once again. In this regard, the sol-gel is the most commonly used synthesis method [67–69,95,109,110], while the spray-drying process [111] has also been reported. Let us provide, chronologically, an overview of the $\text{Na}_4\text{Co}_3(\text{PO}_4)_2(\text{P}_2\text{O}_7)$ electrochemical behavior and its sodium redox mechanism (the sequence of sodium deinsertion/insertion, the type of phase transition, etc.), which strongly depends on the synthesis conditions (type of precursors, temperature, the carbon source, etc.).

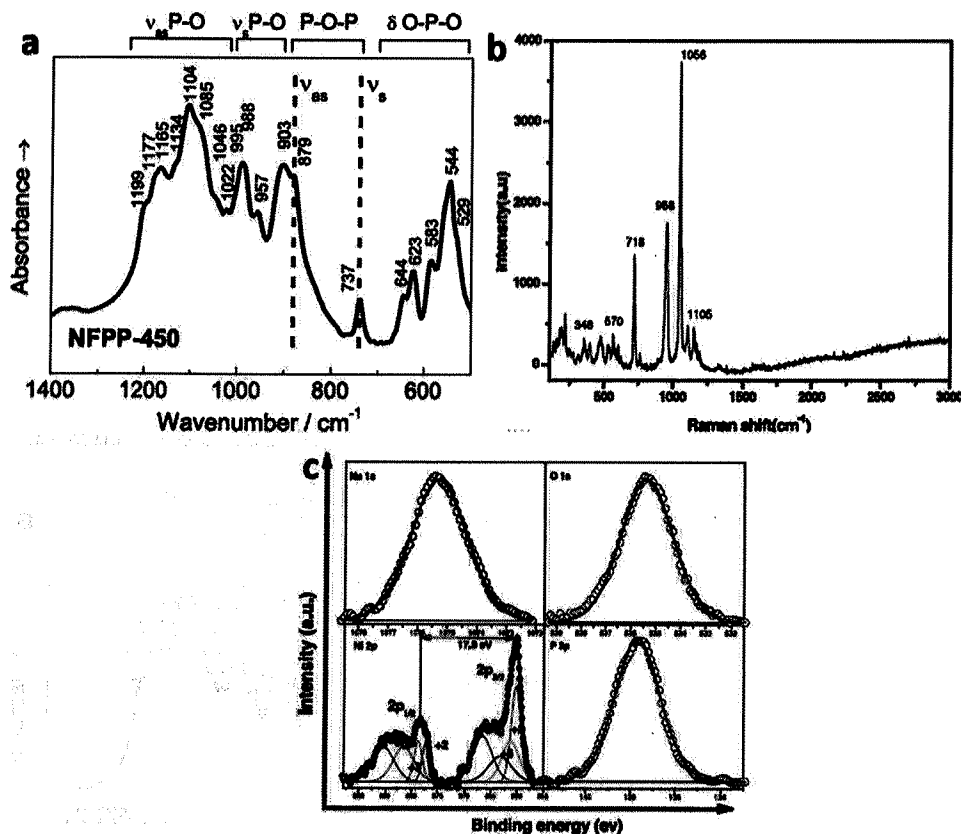


Fig. 5. a) FTIR spectrum of $\text{Na}_4\text{Fe}_3(\text{PO}_4)_2\text{P}_2\text{O}_7$, Reprinted with permission from ref. [97], Copyright 2018, Elsevier, b) Raman and c) XPS spectrum of $\text{Na}_4\text{Ni}_3(\text{PO}_4)_2\text{P}_2\text{O}_7$ Reprinted with permission from ref [106], Copyright 2015, Elsevier.

3.1.1. Sol-gel method

In 2013, Nose and co-workers [68,110] first reported the redox behavior of $\text{Na}_4\text{Co}_3(\text{PO}_4)_2(\text{P}_2\text{O}_7)$ (NCPP) for sodium ion batteries, by using the typical sol-gel method which includes mixing of the diluted nitrate solution of $(\text{CH}_3\text{COO})_2\text{Co}$, $\text{Na}_4\text{P}_2\text{O}_7$ and $\text{NH}_4\text{H}_2\text{PO}_4$ and glycolic acid (to suppress the particle growth). By heating the gel at 700°C , they have produced the $\text{Na}_4\text{Co}_3(\text{PO}_4)_2(\text{P}_2\text{O}_7)$ polycrystal ($\sim 3\mu\text{m}$ in diameter) consisting of submicron-sized primary particles, with the reversible capacity of 95 mAh g^{-1} (2.2 Na^+) at 34 mA g^{-1} (i.e. 0.2 C , based on the theoretical capacity for 4 Na^+ which corresponds to the value of 170 mAh g^{-1}) and an average potential of $4.5\text{ V vs. Na}^+/\text{Na}$. This comes from the multi redox peaks/plateaus, observed within the high potential region $4.1\text{--}4.7\text{ V vs. Na}^+/\text{Na}$ in $\text{NaPF}_6/\text{EC}+\text{DEC}$, which belong to $\text{Co}^{2+}/\text{Co}^{3+}$ redox process (Fig. 6a). The full capacity was considered unattainable due to activity of $\text{Co}^{3+}/\text{Co}^{4+}$ redox couple at potentials above $4.8\text{ V vs. Na}^+/\text{Na}$. In addition to negligible capacity decrease after 100 cycles, Nose et al. [68] have also demonstrated the high rate capability of NCPP ($10\text{ C} - 25\text{ C}$), as evidenced by reaching the capacity of $\sim 80\text{ mAh g}^{-1}$ at 25 C . A very small polarization of NCPP charge/discharge curves at these high current rates revealed its prominent advantage among reported Na^+ intercalation materials. By combining this material as a cathode, with a hard carbon as an anode, the authors have assembled 4 V -class sodium ion battery ($\text{C}/\text{NaPF}_6/\text{EC}+\text{DEC}/\text{Na}_4\text{Co}_3(\text{PO}_4)_2\text{P}_2\text{O}_7$), with the initial capacity of $\sim 90\text{ mAh g}^{-1}$ and long-term cyclability (93 % after 50 cycles and 83 % even after 100 cycles). By doping Co sites with Ni and Mn [69], through the same sol-gel procedure, they have further managed to procure improved electrochemical properties of polyanionic cathode, within the potential region of $3\text{--}5.1\text{ V}$ in $\text{NaPF}_6/\text{EC}+\text{DEC}$. The $\text{Na}_4\text{Co}_{2.4}\text{Mn}_{0.3}\text{Ni}_{0.3}(\text{PO}_4)_2\text{P}_2\text{O}_7$ compound (with accompanied traces of NaCoPO_4 amounting to 0.5%) was capable of delivering specific discharge capacity of 106 mAh g^{-1} at 2 C and 103 mAh g^{-1} at 5 C (1

$\text{C} = 170\text{ mA g}^{-1}$) (Fig. 6b). The capacity retention was 93 % and 88 % at 2 C and 5 C , although the authors showed only ten cycles. Unlike the multi-redox peaks of $\text{Na}_4\text{Co}_3(\text{PO}_4)_2\text{P}_2\text{O}_7$, two redox pairs of $\text{Na}_4\text{Co}_{2.4}\text{Mn}_{0.3}\text{Ni}_{0.3}(\text{PO}_4)_2\text{P}_2\text{O}_7$, narrow ($\sim 4.2\text{ V}$) and broad ($\sim 4.6\text{ V}$), were observed (Fig. 6b), as a consequence of mixing potentials of simultaneous Co, Mn and Ni redox processes ($\text{Co}^{2+}/\text{Co}^{3+}$, $\text{Mn}^{2+}/\text{Mn}^{4+}$ via Mn^{3+} and $\text{Ni}^{2+}/\text{Ni}^{3+}$).

In the next study, Nose et al. [109] showed that the lithiated form of the mixed polyanionic compound ($\text{Li}_4\text{Co}_3(\text{PO}_4)_2\text{P}_2\text{O}_7$) cannot be obtained chemically by the same sol-gel process. So, these authors have examined the lithium insertion capability of electrochemically desodiated form of $\text{Na}_4\text{Co}_3(\text{PO}_4)_2(\text{P}_2\text{O}_7)$, prepared by the deep anodic oxidation up to $4.8\text{ V vs. Na}^+/\text{Na}$ (corresponding to the capacity of 115 mAh g^{-1} or 2.6 Na^+). Such obtained $\text{Na}_{1.4}\text{Co}_3(\text{PO}_4)_2(\text{P}_2\text{O}_7)$ material shows the rapid Li^+ and Na^+ ion insertion capability. Its discharge capacity, measured in $\text{LiPF}_6/\text{EC}+\text{DEC}$ solution, is close to 100 mAh g^{-1} at 0.2 C and 80 mAh g^{-1} at 5 C (2.4 Li^+ and 1.9 Li^+ , respectively), while the corresponding discharge capacity in $\text{NaPF}_6/\text{EC}+\text{DEC}$ solution amounts to 99 mAh g^{-1} and 89 mAh g^{-1} , respectively. So, the lithium and sodium storage capacity of this Na-extracted material are comparable at 0.2 C , while the better Na vs. Li capacity retention (90 % vs. 80 %) with the current rate increase to 5 C was observed (Fig. 6c). The higher operating voltage of sodium versus lithium redox process and the faster kinetics (which is attributed to the stronger interaction of $\text{Li}^+-\text{O}^{2-}$ than $\text{Na}^+-\text{O}^{2-}$), have been verified. The lithium insertion capability (from the electrolyte) of this polyanionic compound is also proved in the full battery cell, which is composed of $\text{Na}_4\text{Co}_3(\text{PO}_4)_2(\text{P}_2\text{O}_7)$ as a cathode, $\text{Li}_4\text{Ti}_5\text{O}_{12}$ as an anode and $\text{LiPF}_6/\text{EC}+\text{EMC}+\text{DMC}$ solution as the electrolyte. Such 3 V -class hybrid battery delivers reversible capacities of $\sim 80\text{ mAh g}^{-1}$ at 0.2 C , $\sim 65\text{ mAh g}^{-1}$ at 2 C and $\sim 50\text{ mAh g}^{-1}$ at 5 C , with low coulombic efficiency at a low rate of 0.05 C (1–5 cycles), which is attributed to the irreversible decomposition of the organic electrolyte at the high poten-

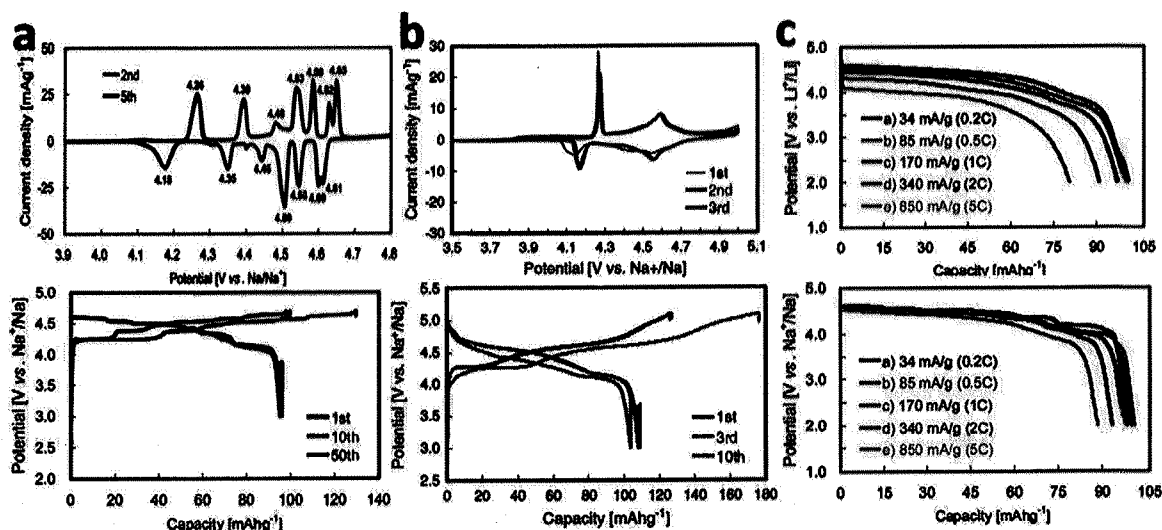


Fig. 6. a) CV and galvanostatic profiles of $\text{Na}_4\text{Co}_3(\text{PO}_4)_2(\text{P}_2\text{O}_7)$ measured at 0.01 mV s^{-1} and 0.2 C , respectively. (Reprinted with permission from ref [68], Copyright 2013, Elsevier.); b) CV and galvanostatic profiles of $\text{Na}_4\text{Co}_{2.4}\text{Mn}_{0.3}\text{Ni}_{0.3}(\text{PO}_4)_2\text{P}_2\text{O}_7$ in $\text{NaPF}_6/\text{EC} + \text{DEC}$ at 0.01 mV s^{-1} and 0.2 C , respectively (Reprinted with permission from ref [69], Copyright 2013, Elsevier.); c) Discharge profiles of $\text{Na}_{1.4}\text{Co}_3(\text{PO}_4)_2\text{P}_2\text{O}_7$ at various C-rates in Li- and Na-ion cells (Reprinted with permission from ref. [109], Copyright 2014, The Royal Society of Chemistry); ($1 \text{ C} = 170 \text{ mA g}^{-1}$).

tial of the positive electrode. An additional reason could be the deficit of Li ions since the electrolyte in this configuration is the only source of mobile ions.

With the aim to comprehend deeply the sodiation/desodiation behavior of this material, Moriwake et al. [70], in collaboration with Nose and co-workers, [68,109] have simulated each step of the $\text{Na}_4\text{Co}_3(\text{PO}_4)_2(\text{P}_2\text{O}_7)$ deinsertion process (the battery charging) by using the first principles calculations. They have reported the sequence of sodium deinsertion, from different sodium sites, as follows Na2, Na1 and Na4. Na2, The Na1 and Na4 deinsertion from $\text{Na}_4\text{Co}_3(\text{PO}_4)_2(\text{P}_2\text{O}_7)$, $\text{Na}_3\text{Co}_3(\text{PO}_4)_2(\text{P}_2\text{O}_7)$ and $\text{Na}_2\text{Co}_3(\text{PO}_4)_2(\text{P}_2\text{O}_7)$ phases, respectively, occurs at the potentials of 4.05, 4.33 and 4.81 V versus Na^+/Na , which reproduces experimentally obtained charge/discharge profile [68]. These authors have confirmed that these sodium deinsertion processes are accompanied by Co^{2+} to Co^{3+} oxidation (one third per each Na atom), with all Co^{3+} ions in highly spin state. The removal of the last Na atom (that is Na3 site occupied on $\text{A}1 \times \text{B}1$ tunnel intersection) from the $\text{NaCo}_3(\text{PO}_4)_2(\text{P}_2\text{O}_7)$ structure (happen at the highest potential of 4.93 V vs. Na) requires oxidation of oxygen 2p orbitals in the P_2O_7 polyhedra (verified through the formation of immobile holes at O^{2-} anions) rather than $\text{Co}^{3+} \rightarrow \text{Co}^{4+}$ oxidation. The absence of Co^{3+} to Co^{4+} oxidation, while the same one occurs in LiCoO_2 , is explained by the less-densely packed phosphate structure (Fig. 7a). Small structural parameter changes (less than 3%) have been calculated upon deinsertion of three sodium ions. The removal of the last Na ion (from Na3 site) causes the narrowing of the Na channel, which along with the holes' strong self-trapping in P_2O_7 units, is considered to render kinetics of desodiation at the highest potentials. This is an explanation for the difficult deintercalation of all four Na atoms from the structure and achievement of the full theoretical capacity. Unlike these DFT studies [70] which showed the full extraction of the specified Na ion upon each redox process, experimental observations carried out by Zarrabeitia et al. [95] revealed that all four Na ions were partially extracted during redox processes within the voltage range 4.0–4.7 V vs. sodium. These authors have observed four biphasic regions (α - β , β - γ , γ - δ , δ - ϵ) during redox process of $\text{Na}_4\text{Co}_3(\text{PO}_4)_2(\text{P}_2\text{O}_7)/\text{C}$ by the means of operando X-ray diffraction (XRD). That is evidenced by multiple-redox plateaus (more than three), which are followed by the solid-solution reaction at the highest potential (at the end of the charge), Fig. 7b. By using synchrotron XRD of the oxidized $\text{Na}_4\text{Co}_3(\text{PO}_4)_2(\text{P}_2\text{O}_7)/\text{C}$ (at 4.67 V), three phases (α , β and δ)

are evidenced (γ is not observable due to the used high current rate), where the sequence of Na^+ extraction is identified as follows: Na(4) progressively leaves the structure until it has been emptied in the δ phase (occ Na4 in α , β and δ phases is 0.68, 0.28 and 0), Na1 is simultaneously removed, but at lower rates since $\frac{1}{4}$ remains in δ phase (occ Na1 is 0.82, 0.66 and 0.23), while Na2 and Na3 deinserted simultaneously at certain Na content (occ Na2 is 1, 1 and 0.64 and occ Na3 is 0.68, 0.28 and 0 in α , β and δ phases, respectively), with the partial occupation of Na2 in δ phase. The proposed Na^+ extraction sequence including all four Na ions, which is not in line with DFT study of Moriwake [70], has been confirmed by using the theoretical, bond valence energy landscape (BVEL) approach. Additionally, very low values of charge transfer resistance, R_{ct} ($< 7 \Omega$) and its changes (2% variation between the lowest and the highest R_{ct} value) have been identified upon occurrence of mentioned successive structural transitions.

Furthermore, Kumar et al. [67] have prepared the composite of $\text{Na}_4\text{Co}_3(\text{PO}_4)_2(\text{P}_2\text{O}_7)$ with multiwalled carbon nanotubes (NCPP-CNT), with the particle size of 200 nm, by modifying procedure developed by Nose et al. [68]. They have used an aqueous solution instead of diluted nitric acid solution and the temperature of 650°C instead of 700°C . Also, the CNTs were added (instead of the glycolic acid) to provide ~16 wt.% of the carbon in the composite. The redox behavior of the composite was found to depend on the composition of used electrolyte such as 1 M $\text{NaPF}_6/\text{EC} + \text{DMC}$ and 1 M $\text{NaClO}_4/\text{PC} + 5\%$ fluoroethylene carbonate (FEC), due to the difference in their electrochemical stability window (1–6 V and 1–4.8 V, respectively). Six anodic/cathodic peaks, positioned at 4.3/4.15, 4.4/4.3, 4.5/4.42, 4.55/4.48, 4.6/4.53 and 4.7/4.6 V, which correspond to $\text{Co}^{2+}/\text{Co}^{3+}$ redox process are defined in CV of NCPP-CNT in $\text{NaPF}_6/\text{EC} + \text{DMC}$, while these peaks are poorly defined in $\text{NaClO}_4/\text{PC} + \text{FEC}$ (the explanation is provided in the section 5). As a result, the initial specific capacity of NFPP-CNT in $\text{NaPF}_6/\text{EC} + \text{DMC}$ solution was higher and amounted to 138 mAh g^{-1} (charge) and 92 mAh g^{-1} (discharge) at a current rate of 0.1 C (Fig. 7c). Unlike mentioned observations by Nose [68], these authors have estimated C_{theor} at 129 mAh g^{-1} , taking into account three Na^+ ions. The reversible specific capacity amounts to 80 mAh g^{-1} , thus retaining ~90% of its own value after 50 cycles of charging/discharging. The similar capacity value was measured at 55°C (78 mAh g^{-1} for 45 cycles), but with the lower coulombic efficiency (~85%) due to the accelerated kinetics, at elevated temperature, during the charging process. The discharge capacity of NFPP-CNT

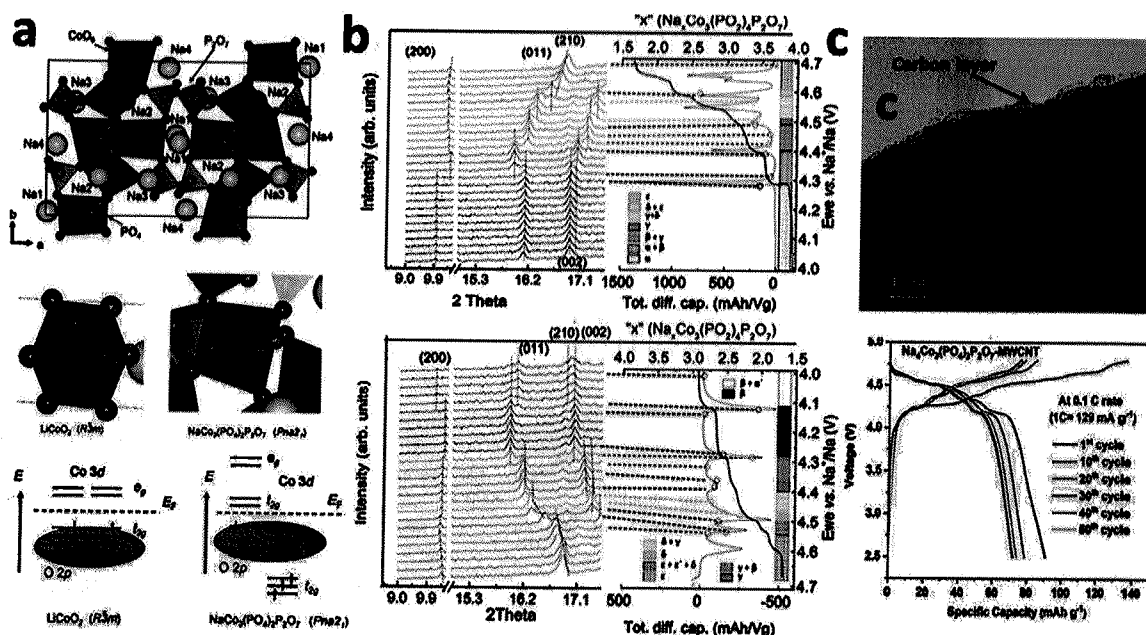


Fig. 7. a) Local environment of Co ions in LiCoO_2 and $\text{Na}_4\text{Co}_3(\text{PO}_4)_2(\text{P}_2\text{O}_7)$ structures and their Fermi energy, E_F (Reprinted from with permission ref. [70], Copyright 2016, Elsevier.) b) Combined operando XRD and EIS data which show the evolution of the phase transitions (Reprinted with permission from ref. [95], Copyright 2019, American Chemical Society); c) TEM of $\text{Na}_4\text{Co}_3(\text{PO}_4)_2(\text{P}_2\text{O}_7)$ -MWCNT and its galvanostatic profile measured in $\text{NaPF}_6/\text{EC}+\text{DMC}$ at 0.1 C, at room temperature ($1\text{ C} = 129\text{ mA g}^{-1}$). (Reprinted with permission from ref. [67], Copyright 2020, The Royal Society of Chemistry).

at higher current rate of 1, 2, 5, 10 and 20 C amounted to 55, 48, 39, 31 and 20 mAh g^{-1} , respectively. When the NCPP-CNT is used as cathode in the $\text{NaTi}_2(\text{PO}_4)_3\text{-MWCNT}/\text{NaPF}_6/\text{EC}+\text{DMC}/\text{NCPP-CNT}$ full cell, it is capable of delivering the capacity of 75 mAh g^{-1} (the initial value) and 50 mAh g^{-1} (after 40 cycles) at 0.2 C rate, with a very low coulombic efficiency of 85 %, which is probably due to the electrolyte degradation. Still, the measured capacities are below those observed by Nose [68] for the full SIB, using the pure NCPP as a cathode.

3.1.2. Spray-drying pyrolysis

One can see from previous studies that the sodium storage capacity of sol-gel synthesized NCPP lies noticeably below theoretical value (even if calculated for three Na ions), while the rate capability has been limited to 20 C and capacity retention to 100 cycles. Liu et al. [111] have improved both rate capability and cyclic stability of $\text{Na}_4\text{Co}_3(\text{PO}_4)_2(\text{P}_2\text{O}_7)$ by Al doping of Co sites (on account of Na^+ vacancy generation), through the spray-drying method using $\text{Co}(\text{NO}_3)_2$, $\text{Al}(\text{NO}_3)_3$, $\text{NaH}_2\text{PO}_4 \cdot 2\text{H}_2\text{O}$ and $\text{C}_6\text{H}_8\text{O}_7 \cdot \text{H}_2\text{O}$ as raw materials and CNT as the carbon source. The Al doping was found to increase a , b and c lattice parameters despite smaller Al^{3+} (0.535 Å) than Co^{2+} (0.65 Å) radius, while it improves ionic conductivity, charge transfer and structural stability thus maintaining the multiple redox behavior of an active phase (Fig. 8a-c). A moderate amount of Al increases the sodium storage properties (from 82.8 to 99.5 mAh g^{-1} at 0.5 C for $x=0.15$ in $\text{Na}_{4-x}\text{Co}_{3-x}\text{Al}_x(\text{PO}_4)_2(\text{P}_2\text{O}_7)$ (Fig. 8c, left), while the excessive Al dopant reduces the electrochemical activity (85 mAh g^{-1} at 0.5 C for $x=0.2$) (Fig. 8c, middle). The $\text{Al}_{0.15}$ -NCPP hollow microspheres (inset in Fig. 8c) with the size of 0.5–3 μm and shell thickness of 465 nm, composed of NCPP nanoparticles and CNT conductive network, can deliver the highest discharge capacity in $\text{NaPF}_6/\text{EC}+\text{DEC}+\text{FEC}$ electrolyte, amounting to 99.5, 93.2, 89.2, 85.8 and 83.2, 80.3, 77.7 and 73.4 mAh g^{-1} at 0.5, 1, 2, 5, 10, 20, 30 and 50 C ($1\text{ C} = 170\text{ mA g}^{-1}$). Its capacity retention of 98.4 % (after 800 cycles at 5 C) or 96.3 % (after 900 cycles at 10C) is higher than one observed for Al-free sample (91.1 % and 80.3 %, respectively). Superb capacity retention of 82.7 % was measured over 8000 cycles at an extremely high current rate of 30 C (Fig. 8c, right). Excellent rate capability of the full battery cell $\text{C}/\text{NaPF}_6/\text{EC}+\text{DEC}+\text{FEC}/\text{Al}_{0.15}$ -

NCPP (88.1 mAh g^{-1} at 5 C and 70.6 mAh g^{-1} at 30 C) and outstanding cycling stability (95 % of capacity maintaining after 200 cycles at 1 C), was also demonstrated. However, it should be taken into account that such a high rate capability is achieved under a quite small electrode loading (1.3 mg cm^{-2}). To meet the practical demands, such high C-rate properties need to be achieved under much higher loadings, which remains the challenge for this type of material.

It can be concluded that there is a need for further improvement of Co-based mixed polyanionic compound, especially at high current rates, through the development of different synthesis/strategies. They should primarily aim at reducing particles to nanodimensions. Besides, the issue of C-value should be addressed since the comparison of the specific capacity between different reported materials is not adequate due to different C-values taken.

3.2. $\text{Na}_4\text{Fe}_3(\text{PO}_4)_2(\text{P}_2\text{O}_7)$ - NFPP

3.2.1. Solid-state method

Solid-state synthesis of $\text{Na}_4\text{Fe}_3(\text{PO}_4)_2(\text{P}_2\text{O}_7)$ (NFPP) powder [47,71,97,112–115] usually employs $\text{Na}_4\text{P}_2\text{O}_7$, $\text{Fe}_2\text{C}_2\text{O}_4 \cdot 2\text{H}_2\text{O}$, and $\text{NH}_4\text{H}_2\text{PO}_4$ or $(\text{NH}_4)_2\text{PO}_4$ as Na, Fe and P sources. Kim et al. [47,71] have proposed the NFPP crystallized in the orthorhombic crystal structure (Pn2₁a space group) as a promising mixed-polyanionic cathode for Na rechargeable batteries (Fig. 9). Simple, two-step solid-state synthesis method (ball milling at 70 °C + solid-state reaction at 500 °C) was used to obtain NFPP particles (100–200 nm), with the small fraction of accompanied maricite NaFePO_4 phase (~4 %). While the NCPP phase can be obtained at 700 °C, NFPP undergoes thermal decomposition above 530 °C, thus producing different Na-rich and Na-poor phosphate or pyrophosphate phases, depending on the sodium content [71]. In NaClO_4/PC electrolyte, solid-state prepared NFPP showed an average operating voltage of ~3.2 V and the initial specific capacity of ~113 mAh g^{-1} at C/40 (~88 % of the C_{theor}) and ~106 mAh g^{-1} at C/20 (i.e. ~82 % of the C_{theor}). Authors showed only 15 cycles (the capacity is estimated per NFPP mass unlike that shown in Fig. 9c), respectively ($1\text{ C} = 129\text{ mA g}^{-1}$), Fig. 9b,c. The significant P_2O_7 distortion in lattice occurs at the last stage of charging (caused by Fe^{3+} - Fe^{3+} repulsion

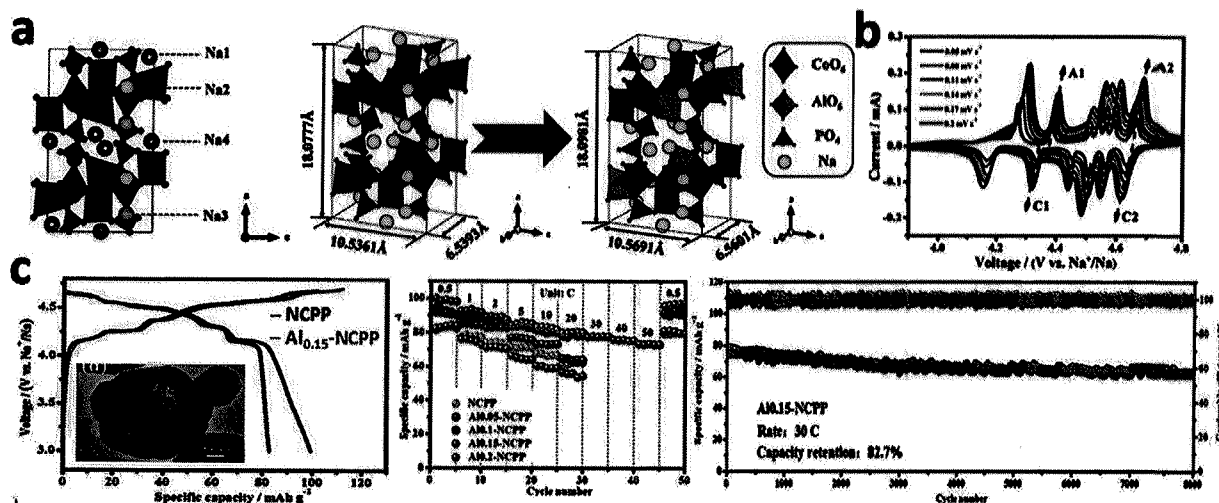


Fig. 8. a) The $\text{Na}_4\text{Co}_3(\text{PO}_4)_2(\text{P}_2\text{O}_7)$ and $\text{Na}_{3.85}\text{Co}_{2.85}\text{Al}_{0.15}(\text{PO}_4)_2\text{P}_2\text{O}_7$ ($\text{Al}_{0.15}\text{-NCPP}$) structures b) Cyclic voltammograms and c) Charge/discharge performance of $\text{Al}_{0.15}\text{-NCPP}$ performed in $\text{NaPF}_6/\text{EC}+\text{DEC}+\text{FEC}$ at different scan rates and current densities, respectively ($1\text{ C}=170\text{ mA g}^{-1}$); inset in c) shows $\text{Al}_{0.15}\text{-NCPP}$ hollow microspheres observed by TEM (Reprinted with permission from ref. [111], Copyright 2019, The Royal Society of Chemistry).

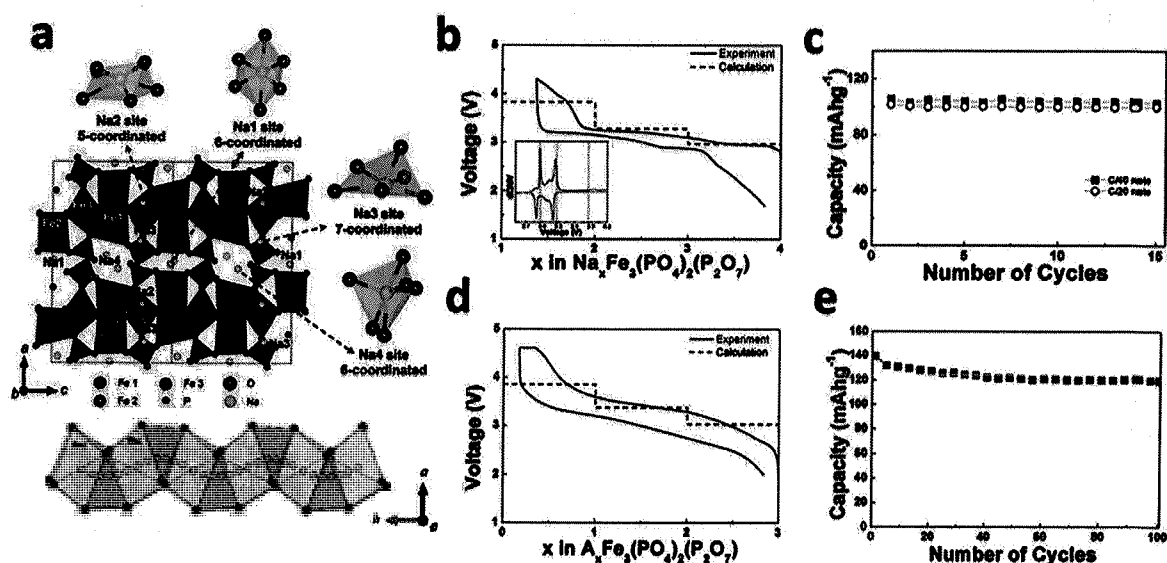


Fig. 9. a) Schematic representation of $\text{Na}_4\text{Fe}_3(\text{PO}_4)_2(\text{P}_2\text{O}_7)$ structure, its Na diffusion channel along the b-axis and different Na sites; b) Charge/discharge profile and c) cyclic performance of solid-state prepared $\text{Na}_4\text{Fe}_3(\text{PO}_4)_2(\text{P}_2\text{O}_7)$ in NaClO_4/PC at C/40 (b, c) and C/20 (b); ($1\text{ C}=129\text{ mA h g}^{-1}$); d, e) Charge/discharge profile and cycle performance of $\text{Li}_3\text{NaFe}_3(\text{PO}_4)_2(\text{P}_2\text{O}_7)$ in $\text{LiPF}_6/\text{EC}+\text{DMC}$ at C/20 ($\sim 25^\circ\text{C}$) and C/5 ($\sim 60^\circ\text{C}$), respectively. Reprinted with permission from ref. [47,71] Copyright 2012, 2013, American Chemical Society).

at the composition of $\text{NaFe}_3(\text{PO}_4)_2(\text{P}_2\text{O}_7)$, thus leading to a shift from edge to corner sharing of FeO_6 polyhedra between the Fe1 and Fe3 sites. It results in the contraction of Na diffusion tunnels and mobility reduction of the remaining Na ion [71]. That is why three Na ions from $\text{Na}_4\text{Fe}_3(\text{PO}_4)_2(\text{P}_2\text{O}_7)$ were found to participate in the electrochemical reaction during charging/discharging. Therefore, the theoretical capacity is calculated to be 129 mA h g^{-1} (based on possible exchange of three sodium ions). The same authors [47] also reported the $\text{Li}_3\text{NaFe}_3(\text{PO}_4)_2(\text{P}_2\text{O}_7)$, prepared by chemical Na-Li exchange of $\text{Na}_4\text{Fe}_3(\text{PO}_4)_2(\text{P}_2\text{O}_7)$ (three Na were exchanged by Li cations), with an average potential of 3.4 V and initial capacity of $\sim 119\text{ mA h g}^{-1}$ at C/20 measured in $1\text{ M LiPF}_6/\text{EC}+\text{DMC}$ (Fig. 9d). The lithium storage capacity of this electrode is capable of being improved to $\sim 140\text{ mA h g}^{-1}$ (at C/5) by increasing the temperature of the Li-cell to $\sim 60^\circ\text{C}$, thus retaining 86% of its value after 100 cycles (Fig. 9e). The high energy density of both Na-ion ($\text{Na}/\text{NaClO}_4\text{-PC}/\text{Na}_4\text{Fe}_3(\text{PO}_4)_2(\text{P}_2\text{O}_7)$) and Li-ion cells ($\text{Li}/\text{LiPF}_6/\text{EC}+\text{DMC}/\text{Li}_3\text{NaFe}_3(\text{PO}_4)_2\text{P}_2\text{O}_7$) amounted

to energy densities of 380 Wh kg^{-1} and 460 Wh kg^{-1} , respectively (based on the materials' level).

By investigating the electrochemical mechanism of $\text{Na}_x\text{Fe}_3(\text{PO}_4)_2(\text{P}_2\text{O}_7)$ ($1 \leq x \leq 4$) through combined computation and experiments, Kim et al. [71] showed that this material underwent one-phase $\text{Fe}^{2+}/\text{Fe}^{3+}$ electrochemical reaction (without formation of intermediate phase), with an exceptionally small volumetric change (less than 4%), unusual for larger Na ions. It is explained by the capability of P_2O_7 dimers to rotate and distort (provided by the open 3D framework) to accommodate structural changes. Four distinguishable Na sites, with a low activation barrier for all diffusion paths are identified, whereas the Na sinusoidal diffusion in the large tunnel along the b-axis (from Na1 site to another Na1 site) shows the lowest activation energy of 256 meV (Fig. 9a). Very low energy barrier for three-dimensional diffusion pathways of Na ions was also confirmed by Chen et al. [99], who calculated the values of 0.553 , 0.02 and 0.365 eV , thus revealing the barrier-less diffusion of Na^+ ions along a direction. Based on the first

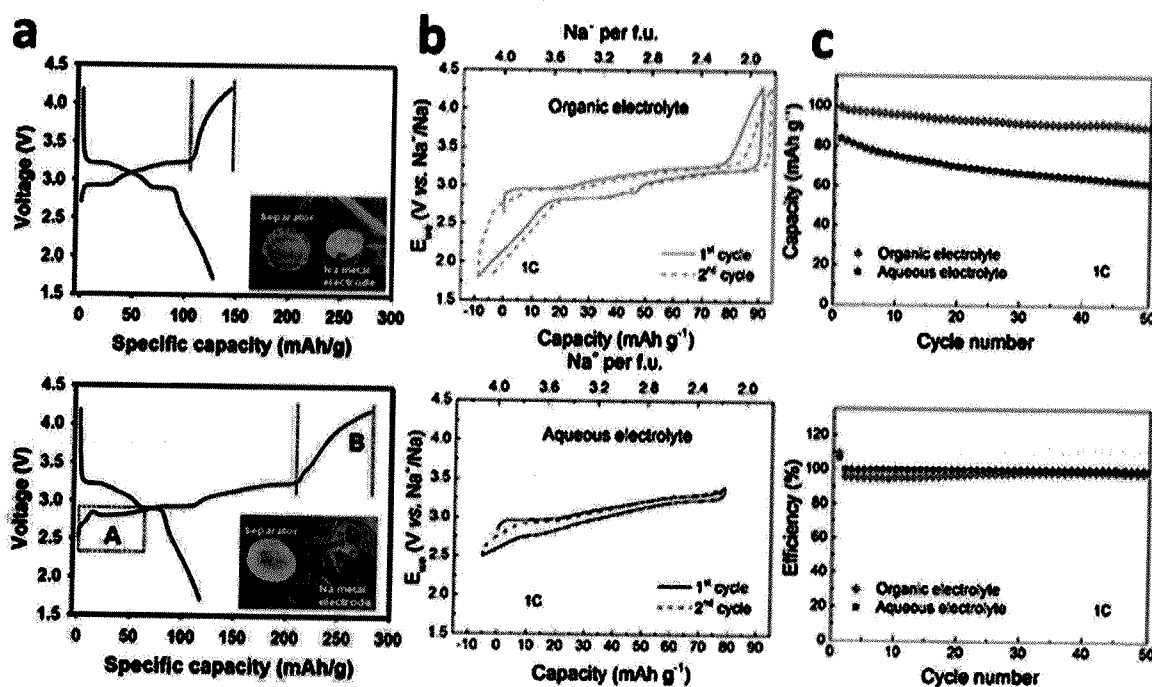


Fig. 10. a) The initial charge/discharge curves of solid-state prepared $\text{Na}_4\text{Fe}_3(\text{PO}_4)_2(\text{P}_2\text{O}_7)$ measured in $\text{NaClO}_4/\text{EC}+\text{PC}$ (top) and $\text{NaClO}_4/\text{EC}+\text{DEC}$ (bottom); (Reprinted with permission from ref. [112], Copyright 2014, Elsevier); b) galvanostatic profiles and c) cyclic performance of $\text{Na}_{3.97}\text{Fe}_3(\text{PO}_4)_2(\text{P}_2\text{O}_7)/3.04\text{wt.}\%\text{NaFePO}_4/7.8\text{wt.}\%\text{C}$ measured in an organic ($\text{NaClO}_4/\text{EC}+\text{PC}$) and aqueous electrolyte (Na_2SO_4), at a current rate of 1 C (1 C = 129 mAh g^{-1}); (Reprinted with permission from ref. [114], Copyright 2018, American Chemical Society).

principle calculations, Kim et al. [71] have determined the sequence of Na extraction: I. Na ions are first extracted from the Na2 site (5-coordinated); II. After their complete extraction, half of Na ions in both Na1 (6-coordinated) and Na4 sites (6-coordinated) are simultaneously extracted and III. The half of Na ions from Na3 site (7-coordinated) and remaining half of Na ions from Na1 site (6-coordinated) are deinserted thus leaving the half of Na ions in both Na3 and Na4 sites which do not participate in electrochemical reaction. Still, the exact order of the Na ion deinsertion/insertion is still unknown. Let us express some discrepancies here. Wu et al. [50] and Kosova et al. [97] have exposed different Na sites coordination and arrangement, pointing out the preference of extracting Na ions with lower coordination number. Based on the results of solid-state NMR spectroscopy, Wu et al. [50], reported the next Na extraction sequence: Na3 (five-coordinated) and Na1 (six-coordinated), followed by Na4 (six-coordinated), while the Na ions from seven-coordinated Na2 hardly participate in the electrochemical reaction. Furthermore, Kosova et al. [97] have confirmed "non-activity" of Na2 positions, thus suggesting (based on the Rietveld refinement of the XRD pattern) different coordination numbers of Na1, Na2, Na3 (6-coordinated) and Na4 sites (7-coordinated) than those in references [50,71] and indicating that the insertion of Na ions happens opposite to the deinsertion (i.e. the charging process), following the order Na4, Na1, Na3. These authors indicate an impurity of three Fe different sites (relying on the results of ⁵⁷Fe Mössbauer measurements), which does not go along with Kim's observations [71] based on equal distribution of Fe ions between three sites.

Solid-state synthesis procedure, developed by Kim, has been adopted in further studies [97,112–115] aimed at improving the electrochemical properties of NFPP, either through the selection of an appropriate electrolyte [112,115] or through the carbon addition/coating [97,113,114]. By using the mixture of ethylene carbonate and propylene carbonate (EC+PC), as a solvent for NaClO_4 , Jang et al. [112] measured the initial specific capacity of NFPP very close to the theoretical value, amounting to 128 mAh g^{-1} at C/20, as shown in Fig. 10a. About 97% of the initial capacity can be retained after 100 cycles of charg-

ing/discharging. The use of electrolytes with 1 M NaClO_4 in the combination with EC and PC solvents instead of EC and DEC in the Na/NFPP cell leads to the higher discharge capacity and columbic efficiency. This can be attributed to higher ionic conductivity, lower reactivity with Na metal and higher stability under high voltage conditions of 1M $\text{NaClO}_4/\text{EC}+\text{PC}$, when compared to 1 M $\text{NaClO}_4/\text{EC}+\text{DEC}$ (Fig. 10a). Roper et al. [114] modified the solid-state procedure [47,71,112] by adding the conducting carbon into reagent mixture, to produce the $\text{Na}_{3.97}\text{Fe}_3(\text{PO}_4)_2(\text{P}_2\text{O}_7)/3.04\text{wt.}\%\text{NaFePO}_4/7.8\text{wt.}\%\text{C}$ composite with an extended potential of application in terms of high current performance (up to 1 C) and aqueous batteries. Actually, the synthesized composite may deliver the initial discharge capacity of 99 mAh g^{-1} at 1 C in $\text{NaClO}_4/\text{EC}+\text{PC}$ (Na metal as an anode) and 84 mAh g^{-1} in an aqueous solution of 1 M Na_2SO_4 (the aqueous type of cell with AC as an anode), thus retaining 99% and 74% of the initial value after 50 cycles, respectively (Fig. 10b,c). The less capacity retention of NFPP in an aqueous than in an organic cell could be attributed to the material solubility in an aqueous electrolyte (more precisely the hydrolysis of pyrophosphates which lead to iron oxides and sodium phosphate) and the sample oxidation upon the discharge process. The sodium storage capacity of this mixed polyanionic cathode, in an aqueous electrolyte, exceeds the capacity of other materials such as $\text{Na}_2\text{FeP}_2\text{O}_7$ (55 mAh g^{-1}), NaFePO_4 (70 mAh g^{-1}), $\text{Na}_{0.5}\text{Ti}_{0.5}\text{Mn}_{0.5}\text{O}_2$ (46 mAh g^{-1}) and $\text{Na}_3\text{MnTi}(\text{PO}_4)_3$ (58 mAh g^{-1}), also measured in the aqueous-based electrolytes, while the capacity retention is below that measured for $\text{Na}_2\text{Fe}_2\text{P}_2\text{O}_7$ (86% after 300 cycles) or NaFePO_4 (90% after 30 cycles) [114].

Recently, Kang and his collaborators [115] have demonstrated an excellent NFPP performance in the highly concentrated aqueous electrolyte of NaClO_4 (17 M), capable of providing a high-voltage aqueous-type of sodium ion batteries. In both 1 M and 17 M NaClO_4 aqueous solutions the NFPP showed the discharge capacity of 90–100 mAh g^{-1} at 1 C and an average redox voltage of 3.2 V vs. Na^+/Na , which is very similar to the performance in an organic electrolyte. What is very important is that the oxygen evolution reaction (OER) at NFPP is not induced before 4.2 V vs. Na^+/Na in 17 M $\text{NaClO}_{4\text{aq}}$, while the oxygen evolution

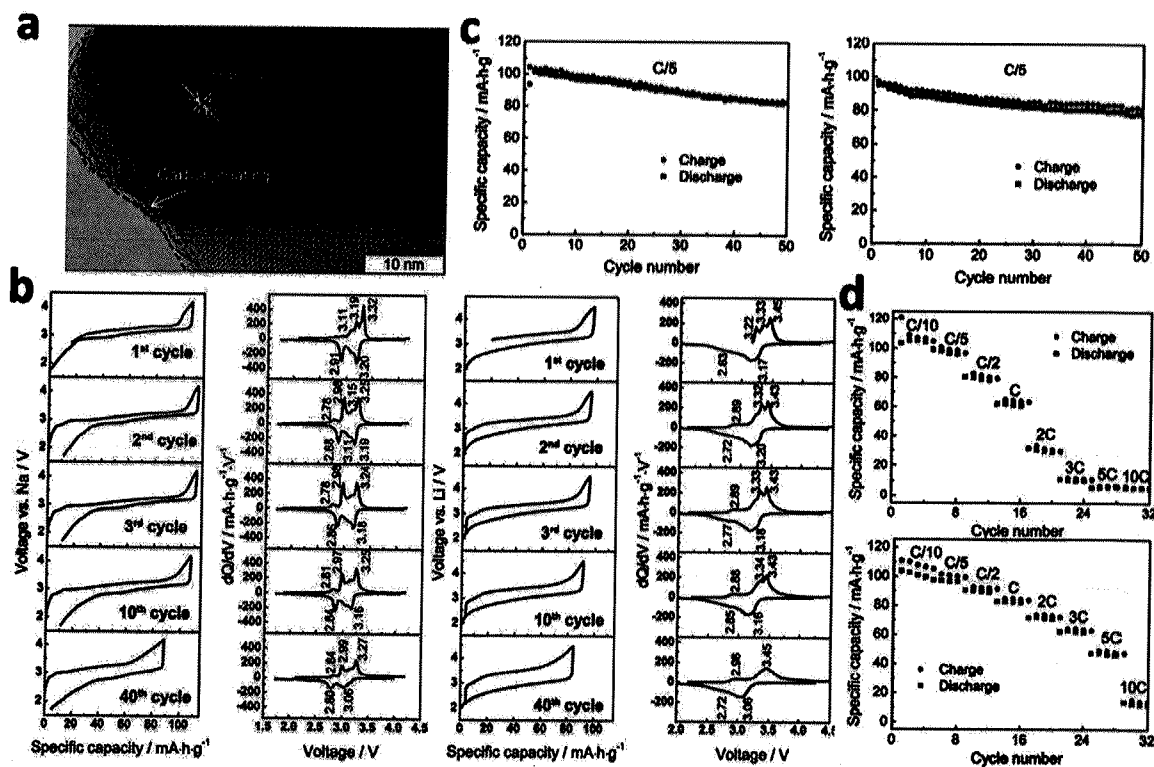


Fig. 11. a) TEM image of NFPP-450 sample; b) Galvanostatic and dQ/dV profile of NFPP-450 measured in $\text{NaClO}_4/\text{EC-PC}$ (left) and $\text{LiPF}_6/\text{EC-DEC}$ (right) at C/5 rate; c) Cyclic stability of NFPP-450 measured in Na-cell (left) and Li-cell (right); d) The specific capacity of NFPP-450 measured in Na-cell (top) and Li-cell (bottom) at different current rates up to 10 C (1 C = 129 mA h g^{-1}) (Reprinted with permission from ref. [97], Copyright 2018, Elsevier).

in $1 \text{ M NaClO}_{4\text{aq}}$ was observed at $3.9 \text{ V vs. Na}^+/\text{Na}$ (the theoretical oxygen evolution potential corresponds to $3.5 \text{ V vs. Na}^+/\text{Na}$). With the aim to demonstrate the practical application of NFPP in the aqueous Na-ion battery of an extended voltage, Kang's team constructed the cell containing NFPP as a cathode, $\text{NaTi}_2(\text{PO}_4)_3$ as an anode and the aqueous salt of NaClO_4 as an electrolyte. The capacity of this battery using $1 \text{ M NaClO}_{4\text{aq}}$ decreases rapidly, from the initial 44 to 8 mA h g^{-1} after 50 cycles (calculated per both anode and cathode masses) or from 87 to 17 mA h g^{-1} if the capacity is calculated per NFPP cathode mass. Poor capacity retention (18 %) and coulombic efficiency (from the initial 87 % up to 68 % after 50 cycles), measured in $1 \text{ M NaClO}_{4\text{aq}}$, are considerable disadvantages. However, notable improvement of this battery was achieved using $17 \text{ M NaClO}_{4\text{aq}}$ as the electrolytic solution, where the capacity retention after 200 cycles and coulombic efficiency were found to be 75 % and 99 % at 1C, respectively. The constructed $\text{NaTi}_2(\text{PO}_4)_3/17 \text{ M NaClO}_{4\text{aq}}/\text{Na}_4\text{Fe}_3(\text{PO}_4)_2(\text{P}_2\text{O}_7)$ full cell is capable of delivering an energy density such as 36 Wh kg^{-1} , outperforming the state-of-the-art experimental sodium batteries based on super-concentrated NaCF_3SO_3 electrolyte solution.

Kosova et al. [97,113] also adopted mechanochemically assisted solid-state method [47,71] to get $\text{Na}_4\text{Fe}_3(\text{PO}_4)_2(\text{P}_2\text{O}_7)$ particles (the average size of 100 nm) covered by carbon layer of $\sim 2\text{--}3 \text{ nm}$ (NFPPC) (Fig. 11a). Unlike the proposed synthesis procedure, in mentioned Kim's papers [47,71], the soot is used as a carbon source and the time of mechanical milling of reagent mixtures (under Ar atmosphere) is shortened to only 5 min. Kosova's study [97] indicates the strong influence of the synthesis conditions on the phase purity of targeted $\text{Na}_4\text{Fe}_3(\text{PO}_4)_2(\text{P}_2\text{O}_7)$ phase and its structural arrangement. First, the solid-state reaction, without mechanical treatment, does not cause the formation of $\text{Na}_4\text{Fe}_3(\text{PO}_4)_2(\text{P}_2\text{O}_7)$ phase (the mechanical milling facilitates the solid state-reaction). Second, the chemical composition of the solid-state reaction prepared sample significantly varies, depending on the temperature of heating. Actually, the temperature selection, within

Table 2

The chemical composition of the solid-state prepared NFPP determined by XRD Rietveld refinement; Replotted with permission from ref. [97].

Sample	XRD Rietveld refinement		
	NFPP, %	NaFePO_4 , %	$\text{Na}_2\text{FeP}_2\text{O}_7$, %
NFPP-600	56.7	25.3	18.0
NFPP-500	64.2	22.7	13.1
NFPP-450	89.1	10.9	-
NFPP-450 (quenching)	93.8	6.2	-
NFPP-400	61.8	28.9	9.3

the $400 - 600 \text{ }^\circ\text{C}$ range, determines the type and fraction of secondary phases in the sample, as shown in Table 2.

The highest fraction of NFPP phase and one type of secondary phase (maricite NaFePO_4) is obtained at $450 \text{ }^\circ\text{C}$ (NFPP-450). Third, the quenching of this sample leads to the increase of the NFPP fraction (94:6 = NFPP: NaFePO_4 for $450 \text{ }^\circ\text{C}$), but results in the higher structural distortion of FeO_6 octahedra (due to the partial $\text{Fe}^{2+} \rightarrow \text{Fe}^{3+}$ oxidation), as evidenced by X-ray, Mossbauer and FTIR measurements, and lower electrochemical performance.

The best electrochemical properties are obtained for the sample heated at $450 \text{ }^\circ\text{C}$ and cooled slowly (89 % NFPP / 11 % NaFePO_4), where the irreversibility upon the first charge process is observed due to the structural rearrangement. In a Na-cell, one can see three anodic/cathodic redox peaks of NFPP-450 (2.98/2.88, 3.15/3.11 and 3.25/3.19 V vs. Na^+/Na for the second cycle), which correspond to Na deinsertion/insertion from/in different crystallographic sites. In a Li-cell, one can see three anodic peaks at ~ 3.22 , 3.32 and $3.43 \text{ V vs. Li}^+/\text{Li}$ and one broader cathodic peak at $\sim 3.17 \text{ V vs. Li}^+/\text{Li}$ (the second cycle) belonging to simultaneous deinsertion/insertion of both Li and Na ions (Fig. 11b). The initial discharge capacity of NFPP-450, measured in $\text{NaClO}_4/\text{EC-PC}$ and $\text{LiPF}_6/\text{EC-DMC}$ solutions, reaches $\sim 90 \%$

($\sim 116 \text{ mAh g}^{-1}$) and $\sim 83 \%$ (107 mAh g^{-1}) of the theoretical value at the rate of C/5 (capacities are re-estimated per mass of NFPP phase) (Fig. 11c). Its sodium storage capacity is somewhat better than one for NFPP in NaClO_4/PC reported by Kim et al. (the latter is also $\sim 90 \%$ of C_{theor} but it is measured at significantly lower current rate of C/40) [47], however, it is lower than the value in $\text{NaClO}_4/\text{EC-PC}$ solution reported by Jang (~ 105 vs. $\sim 125 \text{ mAh g}^{-1}$ at C/10) [112]. Although slightly lower initial capacity of NFPP-450 was measured in Na than in Li-salt electrolyte, better cyclic and rate capability were evidenced in the Li cell (Fig. 11c,d). Namely, the specific capacity, after 50 cycles, is decreased by $\sim 21 \%$, in the Na-, and by $\sim 18 \%$, in the Li-salt electrolyte, while the capacity decrease with the cycling rate increase (from C/10 to 1 C) is almost two times less in the Li cell. The capability of NFPP, to withstand very high current rates (from 1 C to 10 C), was demonstrated for the first time in the Kosova' papers [97,113] (Fig. 11c), which is probably related to the carbon coating. Still, very small capacities were measured at 10 C.

By investigating the mechanism on Na-Li exchange within NFPP, these authors showed [97] that the full process of Na-Li exchange of $\text{Na}_4\text{Fe}_3(\text{PO}_4)_2(\text{P}_2\text{O}_7)$, either chemically or electrochemically, cannot be achieved, but it results in the formation of the mixed Li/Na compound. By the cycling of $\text{Na}_4\text{Fe}_3(\text{PO}_4)_2(\text{P}_2\text{O}_7)$ in Li electrolyte, one part of Na ions ($\sim 1.2 \text{ Na}^+$ ions per f.u) remains in the structure, acting as a pillar throughout cycling (according to the ref. [50,97] these ions belong to Na2 sites), the other part ($\sim 1.6 \text{ Na}^+$ ions per f.u) deinserts during the first charge cycle, thus remaining in the electrolyte, while the last part ($\sim 1.2 \text{ Na}^+$ ions per f.u) participates in the electrochemical reaction, together with the approximately same fraction of Li ions. This simultaneous Na/Li participation in electrochemical reaction improves electrochemical properties. By continuing the studies of the Li-Na redox mechanism, Kosova et al. [113] reveal that the addition of Na-salts into Li-salt electrolyte actually improves the capacity, especially rate capability of NFPP, since Na sites are not completely suitable for Li ions. This makes the composite an excellent cathode material for hybrid Li/Na batteries. Actually, the initial specific discharge capacities of the NFPP in Li electrolyte, the desodiated NFPP in Li electrolyte and the desodiated NFPP in mixed 0.9 Li - 0.1 Na electrolyte, measured at C/5, were found to be $\sim 95 \text{ mAh g}^{-1}$, $\sim 105 \text{ mAh g}^{-1}$ and $\sim 106 \text{ mAh g}^{-1}$, respectively (desodiated sample is obtained by the previous extraction of three Na ions upon the cell charging). The capacity drop, after 45 cycles, is 16.4 %, 33.4 % and 8.9 %, respectively. After cycling, the lowest capacity is obtained for the system with the lowest Na fraction, which confirms instability of the Li^+ ions in the NFPP structure. At higher current rates, the capacity of desodiated carbon coated NFPP in mixed 0.9 Li - 0.1 Na electrolyte is found to be 91 mAh g^{-1} (1 C) and 65 mAh g^{-1} (3 C). The capacity at 1 C is in the range of the capacity measured by Roper et al. [114] for NFPP (also modified with carbon), but these authors did not report the current rate above 1 C. Still, at lower current such as C/10, the capacity of this hybrid Li/Na battery is inferior to the capacity of Na battery reported by Jang et al. [112].

3.2.2. Solution combustion synthesis

Bascar et al. [116,117] have reported 200 nm thick pulsed laser deposited $\text{Na}_4\text{Fe}_3(\text{PO}_4)_2(\text{P}_2\text{O}_7)$ film as the promising electrode for thin sodium-ion microbatteries, due to its excellent rate-capability (125 mAh g^{-1} and 110 mAh g^{-1} at $\sim 2 \mu\text{A cm}^{-2}$ and $\sim 10 \mu\text{A cm}^{-2}$), cyclic stability (over 500 cycles) and high coulombic efficiency ($\sim 100 \%$). The pure $\text{Na}_4\text{Fe}_3(\text{PO}_4)_2(\text{P}_2\text{O}_7)$ powder (Fig. 12a), which is crystallized into orthorhombic structure, of $\text{Pn}2_1$ a space group, was firstly synthesized by the facile solution combustion process using $\text{Fe}(\text{NO}_3)_3 \cdot 9\text{H}_2\text{O}$, NaH_2PO_4 (as the Fe and P sources) and $\text{C}_6\text{H}_8\text{O}_6$ (as a fuel and carbon source) and then, in the form of pallet, subjected to the pulsed laser deposition to make the thin film, with a fairly smooth surface (the roughness is 11 nm) and the thickness of $\sim 220 \text{ nm}$, consisting of poorly agglomerated, well-crystallized grains (65–75 nm). The specific discharge capacity of such obtained NFPP film, measured in 1 M $\text{NaClO}_4/\text{EC}+\text{DMC}$, amounts

to $\sim 118 \text{ mAh g}^{-1}$ (stable upon 100 cycles), which is similar to the value of its carbon-coated $\text{Na}_4\text{Fe}_3(\text{PO}_4)_2(\text{P}_2\text{O}_7)$ parent obtained by the combustion route (126 mAh g^{-1} for the 1st and 121 mAh g^{-1} for 2nd cycle at 0.1 C), Fig. 12b. The charge/discharge plateaus, belonging to $\text{Fe}^{2+}/\text{Fe}^{3+}$ redox reactions, are better defined and more stable (during cycling) for 220 (three distinct plateaus at ~ 3.2 , ~ 2.9 and $\sim 2.5 \text{ V}$ vs. Na^+/Na) than for 300 nm thick film (plateaus merging), Fig. 12b. There is no capacity fade of $\sim 220 \text{ nm}$ thin film sample upon 500 cycles at 1 C, Fig. 12c.

In an additional study, Bascar et al. [118] have reported the reversible K^+ intercalation of the $\text{Na}_4\text{Fe}_3(\text{PO}_4)_2(\text{P}_2\text{O}_7)$ powder, prepared by the solution-combustion method. Compared to the sodium redox behavior, the larger number of redox peaks, corresponding to the K^+ insertion/deinsertion processes, is evidenced. The high irreversibility after the first charge cycle is the indication of structural arrangement caused by K^+ intercalation. The initial potassium storage capacity of the gel-combustion synthesized powder, measured in $\text{KPF}_6/\text{EC}+\text{DEC}$, amounts to 121 mAh g^{-1} at C/20, which is very close to the corresponding sodium storage capacity (126 mAh g^{-1} at C/20). Its value decreases in the second cycle to the value of 116 mAh g^{-1} (sodium discharge capacity in the second cycle is $\sim 121 \text{ mAh g}^{-1}$), thus remaining stable during ten consecutive charge/discharge cycles [118].

3.2.3. Sol-gel method

The use of sol-gel method for the NFPP synthesis has been reported firstly by Wu's group and further developed by other groups [99,107,119]. The synthesized sol-gel structures are capable of overcoming the barrier of solid-state prepared NFPP, related to the issue of the limited rate capability.

Wu and colleagues [50] have synthesized the NFPP/C particles (100–150 nm) of the orthorhombic structure ($\text{Pn}2_1$ a space group), using an stoichiometric ratio of Fe, citric acid and ethylene glycol as well as NaH_2PO_4 as the only source of phosphorus. These authors showed that the thermal stability of NFPP can be achieved within the temperature region 400 - 600 °C, while the excess of undesired pyrophosphate can be avoided with a stoichiometric ratio of phosphate and iron. The amorphous carbon (8.3 wt.% for 400 °C and 8.7 wt.% for 500 °C) is found to cover NFPP particles in the form of 7 - 8 nm layer (Fig. 13a). The characteristic redox profile of NFPP is recognized through the three galvanostatic plateaus/redox peaks and irreversible change in the first charge cycle. Nanocomposite, heated at 500 °C (NFPP/C-500), shows an excellent high rate performance (Fig. 13b), thus delivering the higher discharge capacity in 1 M $\text{NaClO}_4/\text{PC}+\text{FEC}$ solution (78 mAh g^{-1} at 25 °C and 81 mAh g^{-1} at 55 °C under 10 C) than that measured for the sample obtained by the solid-state synthesis [113]. This material can retain 89 % of the initial discharge capacity after 300 cycles of charging/discharging at 0.5 C. By using combined in-situ synchrotron-based time-resolved X-ray diffraction (Fig. 13c) and solid-state nuclear NMR measurements, Wu's group identified sequence of Na extraction (indicated above), thus suggesting that the sodium extraction from NFPP is an imperfect solid-solution (evidenced by the local lattice distortion at the end of the charge process) rather than an ideal solid-solution reaction.

By introducing graphene oxide into the reaction solution of the sol-gel process [50] (Fig. 13d) and heating the gel at 500 °C in $\text{Ar}/5\%\text{H}_2$, Ma et al. [107] have obtained amorphous carbon (AC)-coated $\text{Na}_4\text{Fe}_3(\text{PO}_4)_2(\text{P}_2\text{O}_7)$ particles (50 - 100 nm with 6 nm AC layer) embedded into cross-linked reduced graphene oxide ($\text{Na}_4\text{Fe}_3(\text{PO}_4)_2\text{P}_2\text{O}_7@\text{AC}/\text{rGO}$) (Fig. 12e), with improved sodium storage performance compared to that of NFPP@AC composite. Such improvement is more pronounced at high current rates (10 - 50 C) and low temperature ($-15 \text{ }^\circ\text{C}$), Fig. 13f. Cross-linked rGO network plays a pronounced role in the suppression of particles aggregation and the increase of both carbon content (10.8 % vs. 8.8 %) and porosity. As a result, the NFPP@AC/rGO is capable of withstanding ultra-fast diffusion of Na ions, thus delivering the high and stable sodium storage capacity in a wide temperature range. Its average discharge capacity

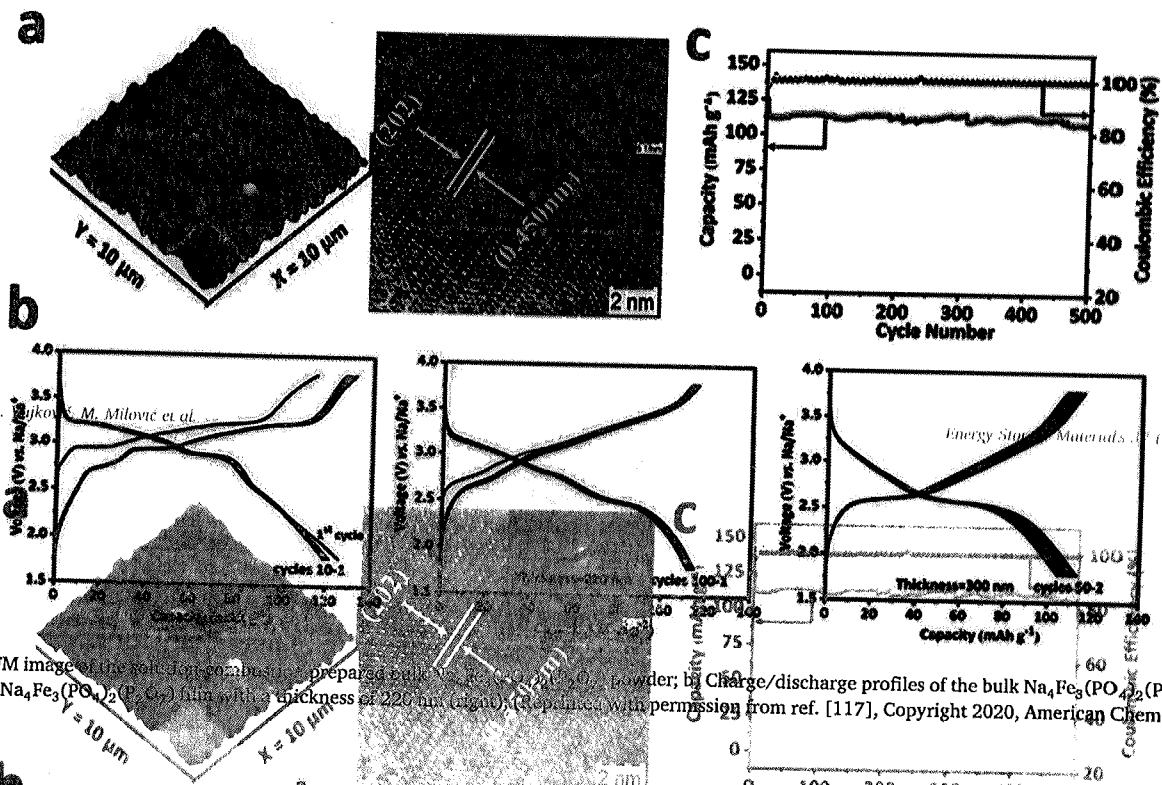


Fig. 12. a) AFM image of the sol-gel combustion prepared bulk $\text{Na}_4\text{Fe}_3(\text{PO}_4)_2(\text{P}_2\text{O}_7)$ powder; b) Charge/discharge profiles of the bulk $\text{Na}_4\text{Fe}_3(\text{PO}_4)_2(\text{P}_2\text{O}_7)$ powder (left) and thin $\text{Na}_4\text{Fe}_3(\text{PO}_4)_2(\text{P}_2\text{O}_7)$ film with a thickness of 220 nm (right); (Reprinted with permission from ref. [117], Copyright 2020, American Chemical Society).

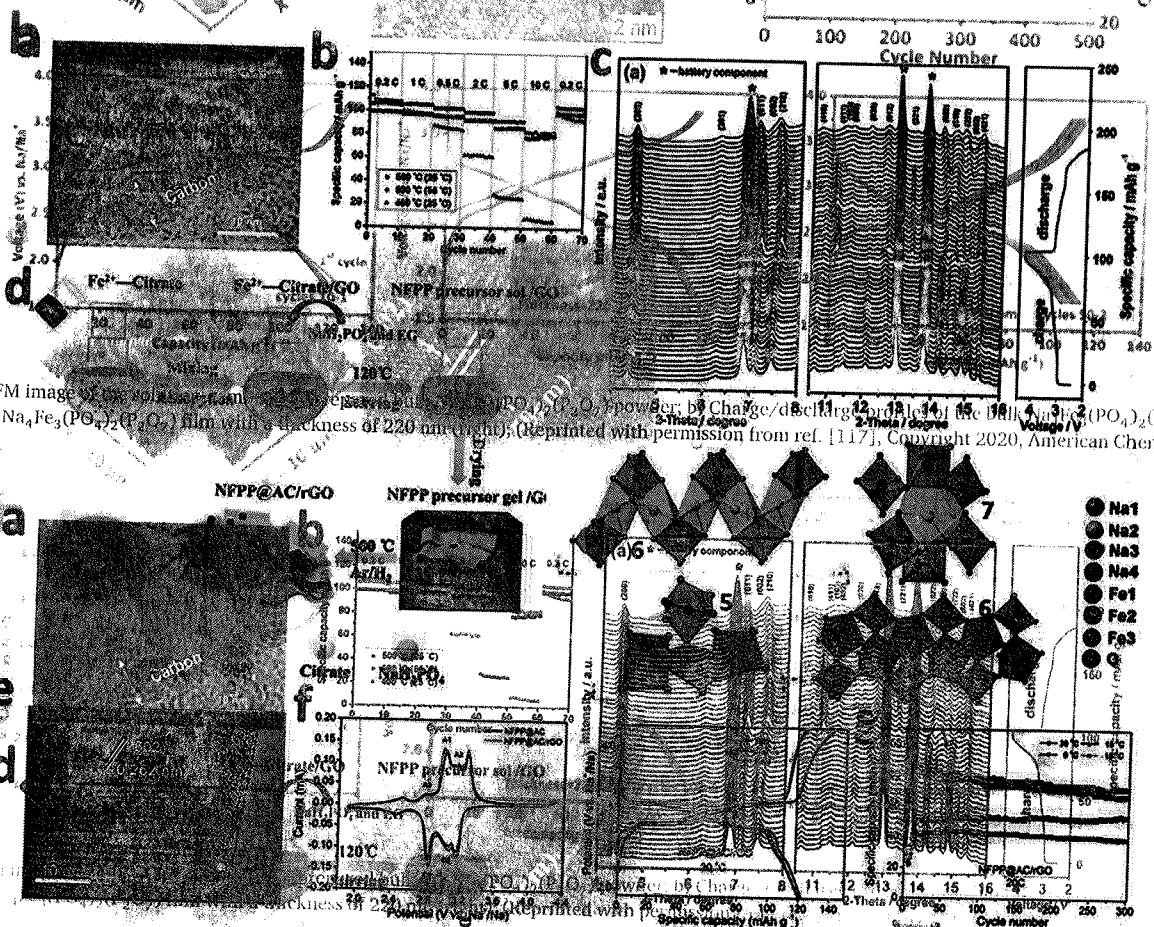


Fig. 13. a) TEM of the sol-gel prepared NFPP/C-500; b) The rate capability of the sol-gel prepared NFPP powders, heated at different temperatures; c) In-situ XRD patterns of NFPP/C-500 during the first charge-discharge cycle (Reprinted with permission from ref. [50], Copyright 2016, Elsevier); d) The scheme of the sol-gel procedure of NFPP@AC/rGO powder and e) its HRTEM image; f) Rate/Cyclic performances of NFPP@AC/rGO and NFPP@AC obtained in $\text{NaClO}_4/\text{PC}+\text{FEC}$ at different temperatures and scan rates (10, 20, 50, 100, 200, 500 mA h⁻¹ g⁻¹) (Reprinted with permission from ref. [107], Copyright 2018, American Chemical Society).

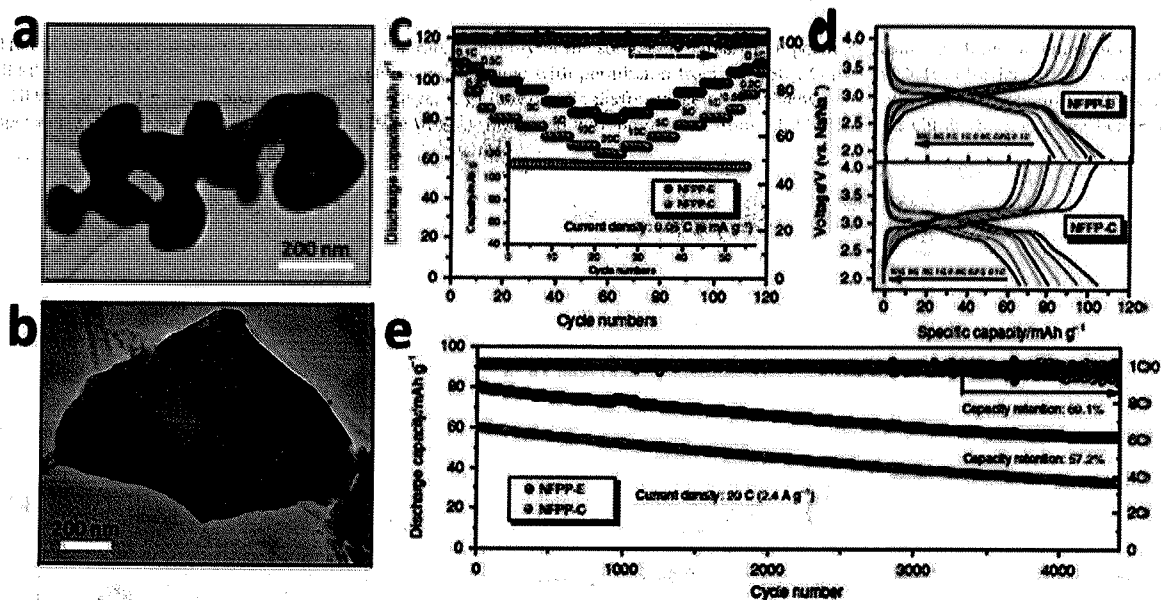


Fig. 14. SEM images of a) nanoplate-like $\text{Na}_4\text{Fe}_3(\text{PO}_4)_2(\text{P}_2\text{O}_7)$ (NFPP-E) and b) microporous $\text{Na}_4\text{Fe}_3(\text{PO}_4)_2\text{P}_2\text{O}_7$ (NFPP-C) particles; c, d) The comparison of cyclic performance of NFPP-E and NFPP-C, measured in $\text{NaClO}_4/\text{EC}+\text{PC}+\text{FEC}$ at different current rates; e) Long-term cyclic stability of both NFPP-E and NFPP-C measured at 20 C (2400 mA g^{-1}) over more than 4000 cycles. (Reprinted with permission from ref. [99], Copyright 2019, Nature Communication).

in 1 M $\text{NaClO}_4/\text{PC}+\text{FEC}$ solution amounts to 107, 99, 85, 78 and 66 mAh g^{-1} (at 30 ° C) and 97, 89, 53, 42 and 29 mAh g^{-1} (at -15 ° C), at 0.5, 1, 10, 20 and 50 C, respectively (Fig. 13f). These values are higher than the corresponding discharge capacities of NFPP@AC composite amounting to 95, 62, 51, and 37 mAh g^{-1} (at 30 ° C) and 60, 28, 18 and 9 mAh g^{-1} (at -15 ° C), respectively. The capacity retention of rGO-modified NFPP@AC after 300 cycles is 83 % (30 ° C) and 89 % (-15 ° C) at 20 C, which is also better than that measured for NFPP@AC amounting to 69 % and 61.2 %, respectively (Fig. 13g). Outstanding high-rate performance is the consequence of the high contribution of pseudocapacitive effects. The full battery with the composition of hard carbon/ $\text{NaClO}_4/\text{PC}+\text{FEC}/\text{NFPP@AC}/\text{rGO}$ is capable of powering 42 red light-emitting diode (LED) lights, thus delivering the average capacities of 95, 82, 64 and 50 mAh g^{-1} (calculated per mass of cathode) at 0.5, 1, 2 and 5 C, respectively. The energy density of this cell amounts to 250 Wh kg^{-1} , based on the mass of cathode active material. By developing simple sol-gel-based dip coating method, followed by heat treatment at 500 ° C under Ar/H_2 ($v/v=95:5$) atmosphere, Ma et al. [119] also have recently developed core-double shell structured $\text{Na}_4\text{Fe}_3(\text{PO}_4)_2\text{P}_2\text{O}_7/\text{NaFePO}_4/\text{C}$ composite grown on a carbon cloth (CC) substrate (NFPP@NFP@C-CC), with an improved rate capability (up to 100 C). This binder-free and self-supported cathode is capable of delivering capacities of 127, 118, 113, 104, 97, 89, 75 and 68 mAh g^{-1} in 1 M $\text{NaClO}_4/\text{PC}+5\% \text{ FEC}$, at current densities of 0.5, 1, 2, 5, 10, 20, 50 and 100 C, respectively. The capacity fade is not observed over 3000 cycles at the current rate of 10 C. The full battery cell, composed of NFPP@NFP@C-CC as cathode, HC as anode and 1 M $\text{NaClO}_4/\text{PC}+\text{FEC}$ solution as electrolyte, can deliver the initial charge/discharge capacity of 125 /114 mAh g^{-1} , thus retaining 97.2 % capacity after 110 cycles of charging/discharging [119].

Furthermore, Chen et al. [99] have successfully developed two types of $\text{Na}_4\text{Fe}_3(\text{PO}_4)_2(\text{P}_2\text{O}_7)$ powders with two different morphologies: i) nanoplate-like particles (NFPP-E), with the size of 150 nm (SSA is 3.52 m^2/g) and carbon content of 3.6 wt.% and ii) microporous $\text{Na}_4\text{Fe}_3(\text{PO}_4)_2\text{P}_2\text{O}_7$ particles (NFPP-C), with the particle size of 1 μm (SSA is 9.74 $\text{m}^2 \text{g}^{-1}$) and carbon content of 4.1 wt.%, via a facile one-step sol-gel method, Fig. 14a,b. They have used Na acetate and ammonium phosphate (mixed with glucose and stearic acid in water to give transparent solution A) as the source of sodium and phosphates and iron (II)

acetate (mixed with cetyltrimethylammonium bromide and ethylenediaminetetraacetic acid for NFPP-E or citric acid monohydrate for NFPP-C to give transparent solution B) as the source of iron. The evaporation of A+B mixture to the gel formation, followed by the heating at 500 ° C in Ar, results in the high phase purity powder (4 wt.% of maricite NaFePO_4 is still identified in both samples) and with the uniform carbon layer (4 nm for NFPP-E and 3 nm for NFPP-C).

Due to nanosized particles, the NFPP-E shows better high rate performance than NFPP-C. Its specific discharge capacity, measured at 20 C in $\text{NaClO}_4/\text{EC}+\text{PC}+\text{FEC}$ electrolyte, amounts to 80.3 mAh g^{-1} (Fig. 14c,d). An outstanding cyclic stability of this material (100 % after 50 cycles at C/20 and 69.1 % after 4400 cycles of charging/discharging at 20 C) is obtained, without morphological destruction and cracks' formation upon long-term cycling (Fig. 14e). While the specific capacity of NFPP-E, at lower scan rates (0.05 and 0.1 C), is in the range of other reported NFPP's prepared by solid-state reaction [47,97], its improvement is achieved at high rates such as 10 C and 20 C [50,107]. Its high sodium storage capability is also achieved at both low and high temperatures (-20 ° C and 50 ° C), with outstanding cyclic stability (92.1 % and 91.4 % capacity retention at 0.5 C, respectively). The structural stability of NFPP, upon exposure to both air atmosphere (three-month period) and cycling in Na-containing electrolyte (volume changes of 4 %), is confirmed by in-situ XRD and in-situ XANES. The practical use of NFPP-E material is also tested in two full-cell SIB configurations such as polypyrrole (PPy)-coated $\text{Fe}_3\text{O}_4/\text{NaClO}_4/\text{EC}+\text{PC}+\text{FEC}/\text{NFPP-E}$ and hard carbon/ $\text{NaClO}_4/\text{EC}+\text{PC}+\text{FEC}/\text{NFPP-E}$, which can deliver the initial discharge capacities of ~ 225 mAh g^{-1} and 170 mAh g^{-1} at 100 mA g^{-1} , with the capacity retention of ~ 77 % (after 500 cycles) and ~ 41 % (after 12 cycles), respectively.

3.2.4. Template and spray-drying methods

An adequate micro/nano structure of 3D polyanionic framework and its carbon coating, achieved by adjusting synthesis conditions through the solid-state reaction, sol-gel and combustion routes, is shown to provide the high rate capability of NFPP up to 20 C. The ultra-high rate capability (above 20 C) is not achieved by the sol-gel procedure itself. The reason could be in an insufficient purity of the synthesized NFPP since its formation is often accompanied by the appearance of some additional NaFePO_4 or $\text{Na}_2\text{FeP}_2\text{O}_7$ phases (they appear at least in traces,

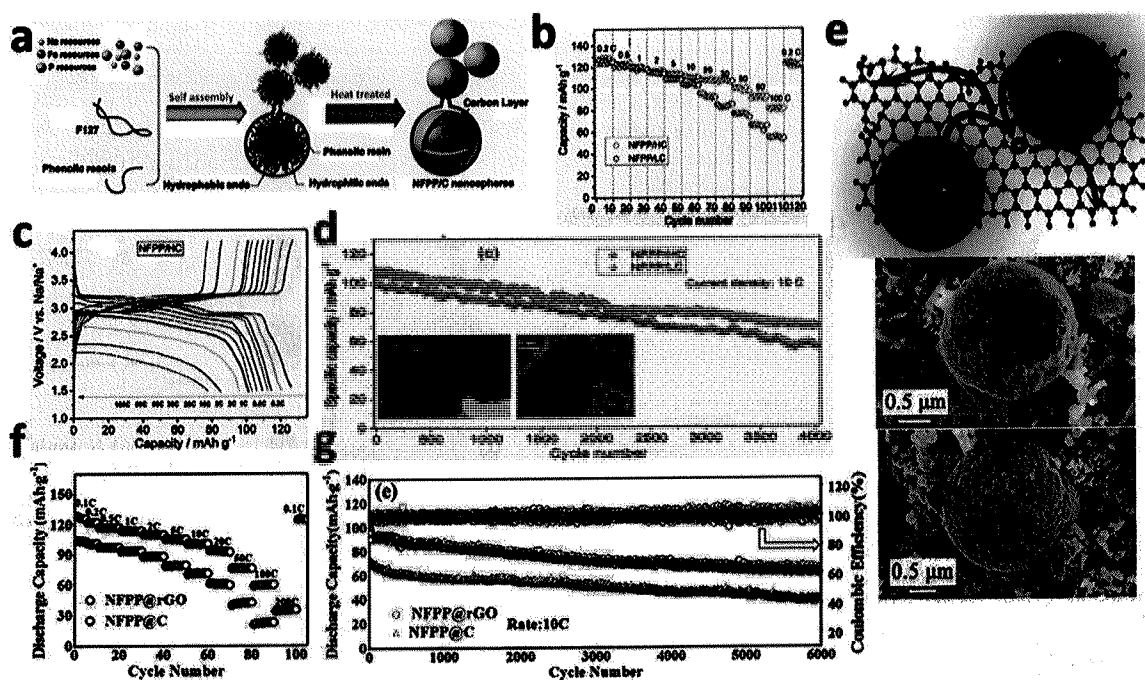


Fig. 15. a) Schematic design of the synthesis of NFPP/C nanospheres and their b-d) electrochemical performance in $\text{NaClO}_4/\text{EC-DEC}+\text{FEC}$ at different current rates and during long-term cycling at 10 C; Reprinted with permission from ref. [63], Copyright 2019, Elsevier); e) Schematic design of NFPP nanoparticles and rGO sheets and f, g) their electrochemical performance at different current rates and during long-term cycling at 10 C (Reprinted with permission from ref. [102], Copyright 2019, Elsevier) ($1\text{ C} = 129\text{ mA g}^{-1}$).

even under strictly controlled synthesis conditions) or electronic and ionic wiring. Still, the maricite is capable of showing the high electrochemical activity, when it is in the composite with NFPP, thus contributing to the high rate capability of the composite up to 100 C [119]. By demonstrating template [63] and ultra-spray method [102], these limitations have been overcome and the outstanding electrochemical properties of this material, (the rate capability up to 100–200 C and long-term cyclability up to 4000–6000 cycles) are achieved.

Pu et al. [63] have developed a novel template method to demonstrate ultra-high current capability of NFPP, evidenced by reaching the sodium storage capacity of 79 mAh g^{-1} at even 100 C (charge/discharge in 36 s). By introducing a nonionic triblock surfactant Pluronic-F127, as a template, and phenolic resinol into the mixture of reactants ($\text{Na}_4\text{P}_2\text{O}_7$, $\text{NH}_4\text{H}_2\text{PO}_4$ and $\text{Fe}(\text{NO}_3)_3 \cdot 9\text{H}_2\text{O}$), these authors prepared the pure uniform NFPP/C nanospheres (without traces of commonly identified maricite phase) with the average diameter of 29.3 nm (NFPP/HC sample with 14.3 wt.% C) and 56.8 nm (NFPP/LC sample with 9.4 wt.% C), coated by thin carbon layer (3 nm and 1.8 nm, respectively), Fig. 15a. The carbon content and thickness can be adjusted by varying the phenolic resinol amount. Both produced NFPP/LC and NFPP/HC nanospheres reach almost theoretical capacity ($\sim 128.5\text{ mAh g}^{-1}$) in $\text{NaClO}_4/\text{EC-DEC}+\text{FEC}$ at a current rate of 0.2 C (Fig. 15b). The specific capacity of NFPP/HC retains its high value at higher current rates (about 123, 120, 116, 114, 111, 108, 106, 91 and 79 mAh g^{-1} at 0.5, 1, 5, 10, 20, 30, 50, 80 and 100 C, respectively) and during cycling, where 63.5 % of the initial capacity is measured over 4000 cycles at 10 C (Fig. 15c,d). An ultra-high-power density of 24.1 kW kg^{-1} , at the energy density of 146.6 Wh kg^{-1} , is obtained for Na//NFPP/HC battery cell (based on the total active masses of both cathode and Na anode). This remarkable performance of NFPP/C, Pu et al. [63] attribute to the ultra-small particles and 3D continuous carbon network structure which facilitate both ions and electronic transport through the nanospheres.

By demonstrating the facile spray pyrolysis method, Yuan et al. [102] have synthesized NFPP nanoparticles (60 nm), homogeneously enwrapped by 3D interconnected rGO network (NFPP@rGO), Fig. 15e,

starting from aqueous solution of $\text{NaH}_2\text{PO}_4 \cdot 2\text{H}_2\text{O}$, $\text{Fe}(\text{NO}_3)_3 \cdot 9\text{H}_2\text{O}$ and $\text{C}_6\text{H}_8\text{O}_7 \cdot \text{H}_2\text{O}$. These particles are capable of providing not only the theoretical capacity, at low current rates ($\sim 128\text{ mAh g}^{-1}$ at 0.1 C), but also an impressive capacity value ($\sim 35\text{ mAh g}^{-1}$) at a very high current rate of even 200 C (discharge process can be accomplished within 18 s). Furthermore, $\sim 62\%$ of capacity retention upon over 6000 cycles at 10 C, is measured. Explicitly, the specific discharge capacity of NFPP@GO, containing 8.3 wt.% C (based on NFPP mass), measured in the $\text{NaClO}_4/\text{EC-DEC}+\text{FEC}$ electrolyte, amounts to 128, 122, 117, 114, 110, 105, 101, 93, 76, and 60 mAh g^{-1} , at different C rates of 0.1, 0.2, 0.5, 1, 2, 5, 10, 20, 50 and 100 C, respectively. The material keeps 88% of the initial capacity after 1300 cycles at 1 C, thanks to the high fraction of the surface stored charge (i.e. intercalation pseudocapacitance). The maximum power density of the full Na//NFPP@rGO cell ($\sim 52.3\text{ kW kg}^{-1}$ corresponding to $\sim 70.9\text{ Wh kg}^{-1}$) is substantially higher than the value of cells containing other reported iron-based mixed polyanionic cathodes. The beneficial role of 3D highly conductive graphene framework can be seen through the comparison of the sodium storage behavior between NFPP@rGO and NFPP@C composites (NFPP@C contains 7.8 wt.% C). The latter is also obtained by the spray-drying method, under the same synthesis conditions, where the only difference is seen in the replacement of rGO by an additional amount of citric acid. Poorer electrochemical performance of NFPP@C vs. NFPP@rGO ($129\text{ vs. }106\text{ mAh g}^{-1}$ at 0.1 C and $60\text{ vs. }23\text{ mAh g}^{-1}$ at 100 C) originates from the: i) 6 nm amorphous carbon layer of NFPP@C versus 2 nm fine graphene layer of NFPP@rGO ii) lower specific surface area ($8.38\text{ m}^2\text{ g}^{-1}$ vs. $28.68\text{ m}^2\text{ g}^{-1}$) and iii) the larger aggregation of NFPP particles when compared to NFPP@C ones. It should be added that the higher specific surface area of NFPP@rGO vs. NFPP@C contributes to the higher fraction of pseudocapacitance, as evidenced by the shape of their curves at the end of discharge.

Recently, Cao et al. [64] have also used the spray drying method to obtain $\text{Na}_4\text{Fe}_3(\text{PO}_4)_2(\text{P}_2\text{O}_7)$ nanoparticles (20–50 nm) growing on multi-walled carbon nanotubes (MCNTs). The NFPP@MCNTs sample shows slightly lower capacities in $\text{NaClO}_4/\text{EC}+\text{DEC}+\text{FEC}$ than those

measured for NFPP@rGO sample, which amount to 115.7, 103.3, 99.2, 96.7, 94, 90.5, 82.1 and 62.8 mAh g⁻¹ at current rates of 0.1, 0.5, 1, 2, 5, 10 and 20 C. Besides, the specific capacities of the full cell CHC//NaClO₄/EC+DEC+FEC//NFPP@MCNTs (based on the mass of both anode and cathode materials) were found to be very high at different currents of 0.1, 0.5, 1, 2 and 5 C amounting to 69.3, 60.5, 51.8, 40.1 and 35.2 mAh g⁻¹, respectively.

Unlike NCPP, more diverse synthesis methods of NFPP have been developed which resulted in its high rate properties. However, the issue of the lower voltage remains a great challenge, and the future research should be focused on the improvement of the operating voltage of this material.

3.3. Na₄Ni₃(PO₄)₂(P₂O₇) – NNPP

As we emphasized, NNPP is isostructural to NFPP and NCPP. Its crystal structure, determined by Sanz et al. [46,48], presents three-dimensional network of [Ni₃P₂O₁₃]_∞ layers, composed of NiO₆ octahedra and (PO₄³⁻) tetrahedra in the bc plane, which are bridged by (P₂O₇)⁴⁻ dimers in a way that create the large channels along b-axis available for Na-ion diffusion. Four distinguishable Na sites are identified, where Na1 and Na4 are positioned in the large channels parallel to the b-axis. Also, Sanz et al. [120] determined the crystal structure of the Na₄Ni₃(PO₄)₂(P₂O₇)₂.

3.3.1. Solution combustion synthesis

The electrochemical behavior of NNPP has been examined since 2015 [106]. Generally, Ni-phosphate and pyrophosphate compounds have been widely known as high voltage cathodes for Li-ion battery applications, but the achievement of their high performance is difficult due to the intrinsic sluggish kinetics caused by the low electronic and Li-ion conductivity. In 2015, Islam et al. [58] have predicted that Ni doping of NFPP leads to the increase of the cell voltage, while the high potential redox activity of NNPP in Na cell was experimentally evidenced somewhat later [96]. First, Senthilkumar et al. [106] revealed the Ni²⁺/Ni³⁺ redox activity in NNPP, at ~ 0.35/0.17 V vs. Ag/AgCl, in an aqueous solution of NaOH. These authors have reported the combustion synthesis of Na₄Ni₃(PO₄)₂(P₂O₇)/C, using three different types of fuel such as glycine, urea and hexamine, for the sake of examining their effect on physicochemical/electrochemical properties of composite. By using Na₄P₂O₇, NH₄H₂PO₄ and Ni(NO₃)₂ · 6H₂O as reactants and the mentioned fuels, they have synthesized the pure Na₄Ni₃(PO₄)₂(P₂O₇) phase (NNPP). This NNPP phase is obtained by heating at 600 °C (for 3 h in Ar atmosphere) and reveals its higher thermal stability compared to Na₄Fe₃(PO₄)₂(P₂O₇). Authors have shown that the use of hexamine as a fuel reduces NNPP particle size to nano dimension (50 - 300 nm) and forms more voids/pores for an easier access of electrolyte ions, with respect to both urea and glycine. As a result, the higher current response of NNPP is obtained in the case of hexamine-assisted synthesis. Also, the presence of amorphous coated carbon (~ 2.7 wt.% C) reduces the particle size and increases electronic conductivity of the composite electrode.

3.3.2. Solid-state and sol-gel methods

Passerini et al. [96] were the first who demonstrated the high potential of NNPP (4.8 V vs. Na⁺/Na) in the full Na-cell, using ionic liquid-based electrolyte (NaTFSI in Py₁₄FSI), which could provide better properties than typical carbonate-based electrolyte (1 M NaPF₆ in EC+DEC). High redox activity of NNPP/C is evidenced by three anodic (4.61, 4.67 and 5 V) and two cathodic (4.58 and 4.92 V) peaks, while the Ni redox activity in Na₂NiP₂O₇/C, under the same conditions, is not evidenced. When the submicrometric NNPP/C powder (~ 500 nm), obtained by citric-assisted solid state method + ball milling (using Na₄P₂O₇, Ni(OCOCH₃)₂ · 4H₂O, NH₄H₂PO₄ as Na, Ni and P sources), is used as the cathode in two-electrode cell, along with metal Na as the negative electrode, it delivers the initial discharge capacity of 63 mAh

g⁻¹ and 40 mAh g⁻¹ (@10 mA g⁻¹) in NaTFSI+Py₁₄FSI (3 - 5.1 V) and NaPF₆/EC+DEC (3 - 4.9 V), respectively. This is still inferior to Fe- and Co-based analogues due to lower ionic conductivity of Ni-based mixed polyanionic compound. Also, the collapse of [Ni₃P₂O₁₃]_∞ layers, occurring upon charge/discharge, causes its low sodium reversibility (1.3 Na⁺ vs. 2.6 Na⁺ in the first cycle) and consequently low coulombic efficiency. Based on ex-situ XRD, Na⁺ ions are proposed to be extracted first from Na1 and Na2 sites (positions in the large channels constructed by P₂O₇ dimers) at lower potentials, thus resulting in the decrease of a parameter and the volume change of 1.6 %. Afterwards, Na⁺ ions, belonging to both Na3 and Na4 sites, are regarded to leave the structure, at the highest potential of 5 V vs. Na⁺/Na, resulting in the rapid increase of the b parameter. Still, the total volume change during cycling is small and together with the high thermal stability, present advantage of this mixed polyanionic structure in terms of operating at high voltages.

Since the NNPP proved to be a high potential cathode material for SIBs, Passerini and collaborators [98] continue to study its electrochemical behavior trying to improve the electronic conductivity and prevent poor reversibility of sodium insertion. In this regard, composites of NNPP with carbon and reduced graphene oxide have been prepared [98] by the sol-gel synthesis procedure (starting from Ni(CH₃COO)₂ · 4H₂O, (NH₂)HPO₄ and Na₄P₂O₇ as reactants and graphene oxide and sucrose as the carbon source), followed by heating treatment at 700 °C under Ar for 24 h. The size of NNPP particles in these composites, which are covered by 7 nm carbon layer, is approximately 500 nm (for NNPP/rGO with 8.9 wt.% of C) and 600 nm (for NNPP-C with 8.45 wt.% of C), Fig. 16a. Both composites undergo sodium multistep reaction path as evidenced by well-defined CV redox peaks in 1 M NaPF₆/EC+DMC solution, Fig. 16b. Their specific capacity is found to be higher than that for the pure sol-gel prepared sample and one prepared by solid-state reaction [96].

The initial charge/discharge capacity, measured at 0.1 C (1 C = 127 mA g⁻¹) within the voltage range of 1.7 - 5.1 V, amounts to ~ 168/72 for NNPP-rGO and ~ 132/74 mAh g⁻¹ for NNPP-C, Fig. 16c. However, the poor reversibility during cycling has been observed for both composites, with only ~ 36 % of the capacity retention after 50 cycles due to the structural deformation upon third Na redox process (occurring at the highest voltage). It is attributed to the O₂ release from lattice at the fully charged state. Such assumptions have been confirmed through i) limited cycling of NNPP-C to insert/extract 1.3 Na⁺, which leads to stable capacity of 51 mAh g⁻¹ over 40 cycles at 0.1 C and ii) identification of structural changes after the first charge.

Further improvement of the performance of this high-voltage material, in terms of preventing structural changes upon cycling at high voltages (either through development of different strategies or new synthesis procedures), remains the challenge for the future research.

3.4. Na₄Mn₃(PO₄)₂(P₂O₇) – NMPP

3.4.1. Solid-state method

Numerous Mn-based compounds have been synthesized and examined electrochemically, due to the abundance and high accessibility of manganese. Based on this, the cost of the material production would be cheaper than that for Ni, Co and Fe-based compounds. NMPP polyanionic compound has been firstly synthesized by Kim et al. [77] via a conventional mechanochemically-assisted solid-state reaction, using Na₄P₂O₇, Mn₂C₂O₄ · 2H₂O and NH₄H₂PO₄ as reactants and pyromellitic acid as a carbon source. Such synthesized NMPP/C powder (with the particle size of 200 - 500 nm), heated at 600 °C (first in the air to get NMPP phase and then in Ar for 2 h to coat NMPP particles by carbon) is found to be isostructural to NFPP and NCPP, but with larger lattice constants due to larger ionic radius of Mn²⁺ ion (0.83 Å) compared to Fe²⁺ (0.78 Å) or Co²⁺ (0.745 Å), which follows Vegard's law. Typically, 3D open polyanionic framework of orthorhombic NMPP crystal structure (Pn21a) is composed of [Mn₃P₂O₁₃]_∞ layers along bc plane which are connected by P₂O₇ groups along the a-axis, with three crystallograph-

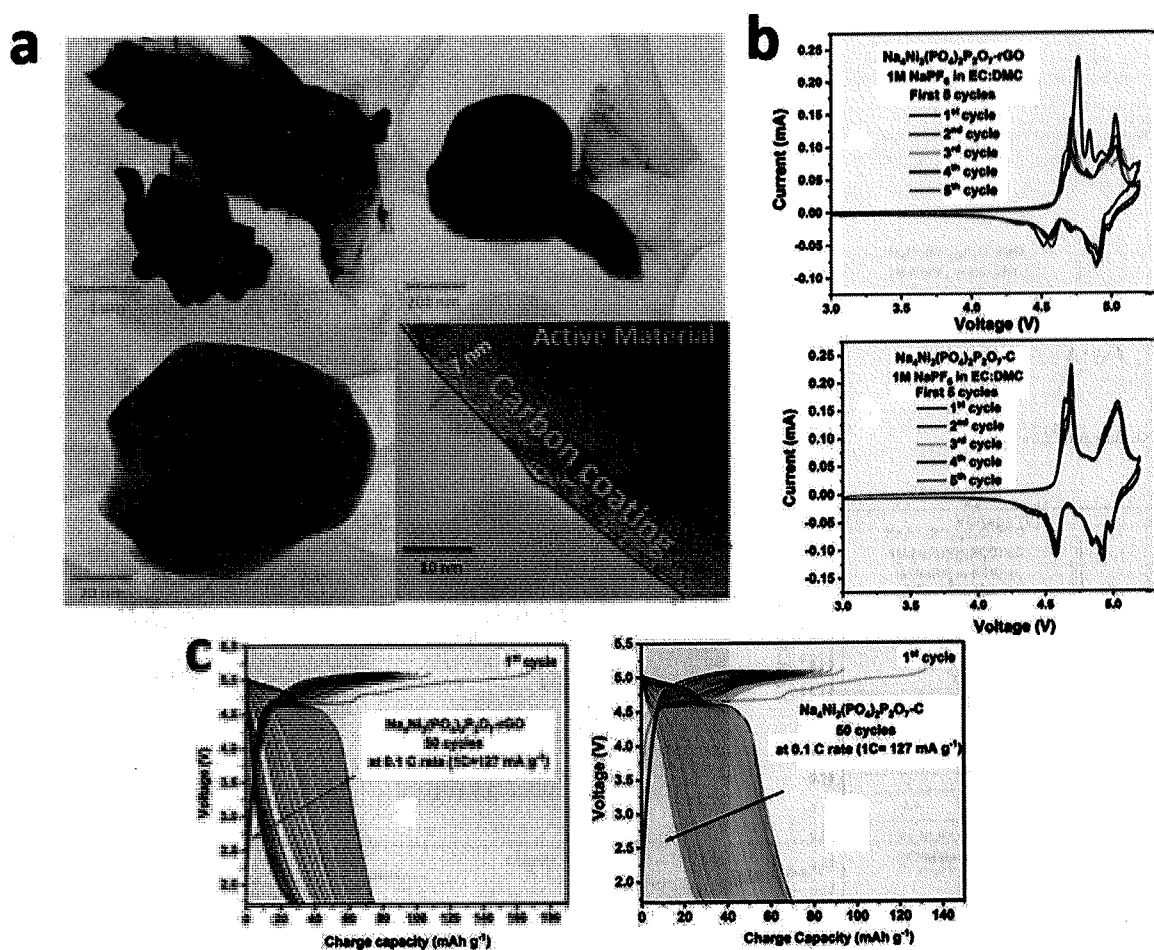


Fig. 16. a) TEM images of sol-gel prepared NNPP/rGO (top) and NNPP/C (bottom) composites and their b) CVs and c) Galvanostatic charge/discharge curves measured in NaPF₆/EC+DMC, The current rate is 0.1 C (1 C = 127 mA g⁻¹) (Reprinted with permission from ref. [98], Copyright 2019, Springer).

ically distinct edge and corner-shared Mn octahedra sites. NaMnPO₄ traces (< 4 wt.%) are also detected in the solid-state synthesized powder.

Kim et al. [77] demonstrated improved properties of NMPP compared to other manganese-based electrodes such as higher Mn²⁺/Mn³⁺ redox potential of 3.84 V vs. Na⁺/Na and larger energy density, amounting to 416 Wh kg⁻¹ (on the materials' level), thus revealing that both sodium-ion mobility and cycling stability are not deteriorated by Jahn-Teller distortion (Mn³⁺). Moreover, the typical Jahn-Teller distortion (Mn³⁺) during NMPP cycling is found to open Na diffusion channels (the activation barrier of most Na diffusion pathways is considerable decreased). As a result, the solid-state synthesized NMPP reaches almost theoretical capacity (129.5 mAh g⁻¹) upon the first charge in NaBF₄/EC+PC solution at a rate of C/20, while the 85 % of this capacity (109 mAh g⁻¹) is measured after the first discharge. The capacity retention, after 100 cycles, is found to be 82 % at C/20 and 86 % at C/5, with the coulombic efficiency of 98.5 %. The material can deliver the discharge capacity of 121 mAh g⁻¹ (93 % of its theoretical value) at elevated temperature of 60 °C (C/20), with the energy density of 416 Wh kg⁻¹ (that is the energy density of Na/NFPP cell), while the corresponding energy density at a room temperature reaches 385 Wh kg⁻¹. (the energy density is based on the cathode level). At a higher current rate of 2 C, the capacity of NMPPC amounts to ~ 83 mAh g⁻¹ (25 °C) and ~ 112 mAh g⁻¹ (60 °C), while the more than a half of the theoretical capacity is retained at 10 C (for both temperatures). The high rate capability and good cyclic performance of solid-state synthesized NMPP have been regarded as superior when compared to Mn-based compounds.

The NMPP experiences multi-phase reaction during the charge/discharge process (Fig. 17a), as evidenced by the existence of three anodic/cathodic peaks at 3.85/3.64 V, 3.89V/3.77V and 3.96/3.87 V vs. Na⁺/Na in measured dQ/dV curve. After solid-solution behavior of NMPP in the initial cycling (up to 3.86V vs Na⁺/Na), phase transition ($\alpha \rightarrow \beta$) is observed during further charging (up to 3.9 V vs. Na⁺/Na which corresponds to the extraction of approximately 1.6 Na ions), with the large difference in *a* and *b* parameters between α and β phase. Further deeper charging, above 4 V vs. Na⁺/Na, leads to the appearance of new γ phase (Na-poor phase). These multi-phase changes result in 7 % of total volume change which is still higher than that for the NFPP (which is 4 %), but it is lower than those volume changes observed for other manganese-based electrodes such as O3-NaNi_{0.5}Mn_{0.5}O₂ (18 %), P2-Na_xFe_{0.5}Mn_{0.5}O₂ (11 %) and olivine LiMnPO₄ (10 %) [77]. On the discharge, the additional δ phase is identified as intermediate phase of $\beta \rightarrow \alpha$ transition, most likely as the consequence of Na-vacancy ordering (Fig. 17a).

3.4.2. Spray-drying and solution combustion methods

Although improved properties of NMPP over other Mn-based electrodes are achieved [77], the reversible discharge capacity is still substantially below the theoretical limit (calculated for three Na ions), especially at higher currents. Because of that, further studies on NMPP have been focused on developing dual strategy for the improvement of the sodium storage behavior, including the partial Mn-Co substitution and carbon coating of NMPP particles [108,121] by selecting the highly conductive carbon nanotubes [108] and reduced graphene oxide [121].

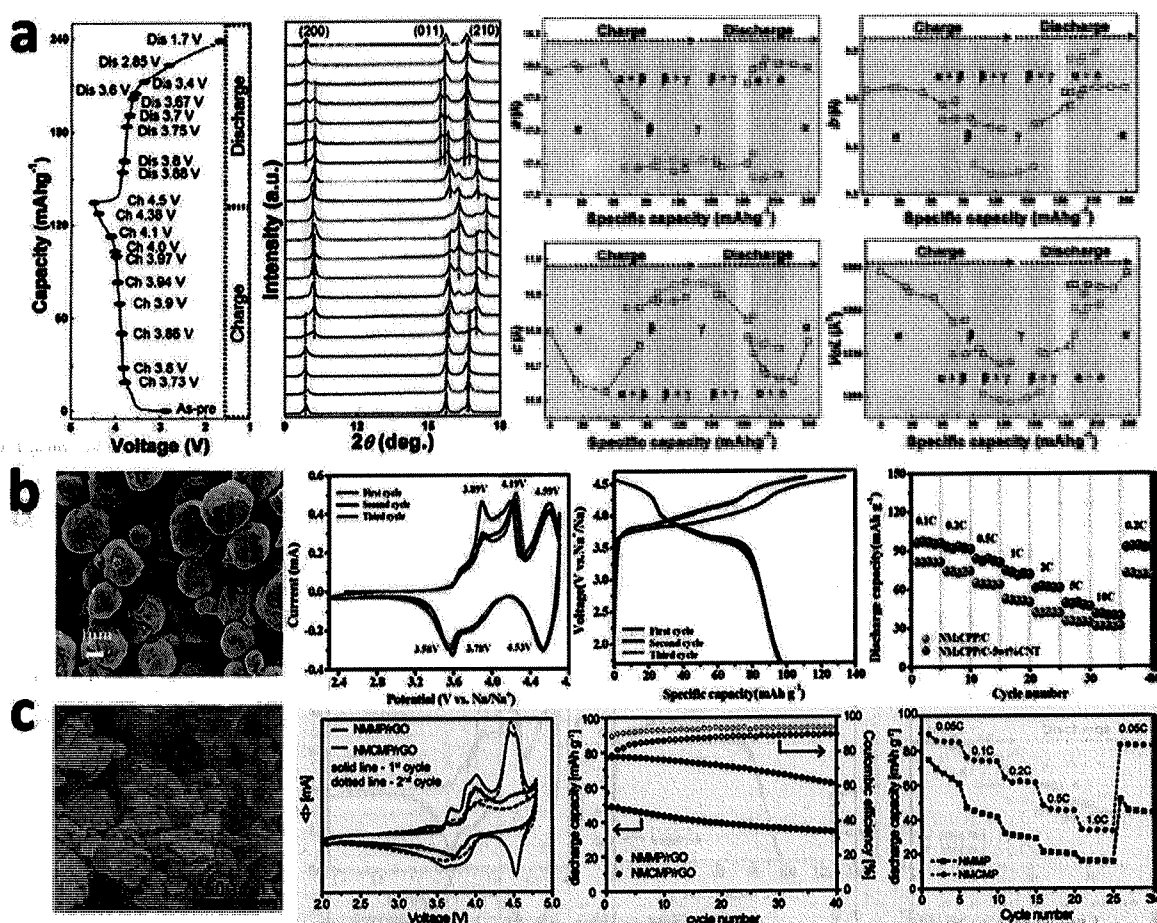


Fig. 17. a) Galvanostatic charge/discharge profile of solid-state prepared $\text{Na}_4\text{Mn}_3(\text{PO}_4)_2(\text{P}_2\text{O}_7)$ at C/20 (1 C = 130 mA g⁻¹) and in-situ XRD patterns obtained during its charge/discharge (Reprinted with permission from ref. [77], Copyright 2015, The Royal Society of Chemistry); b) SEM, CVs (the scan rate is 0.05 mV s⁻¹), galvanostatic charge/discharge profile (the current rate is 0.1 C, 1 C = 128.7 mA g⁻¹) and rate performance of CNTs-decorated $\text{Na}_4\text{Mn}_2\text{Co}(\text{PO}_4)_2(\text{P}_2\text{O}_7)/\text{C}$ ($\text{NM}_2\text{CPP}/\text{C}-5\text{wt.}\% \text{CNTs}$) measured in $\text{NaClO}_4/\text{EC}+\text{PC}+\text{FEC}$ (Reprinted with permission from ref. [108], Copyright 2019, American Chemical Society); c) SEM, CVs (the scan rate is 0.025 mV s⁻¹), cyclic performance (the current rate is 0.1 C, 1C = 130 mA g⁻¹) and rate performance of $\text{Na}_4\text{Mn}_{2.4}\text{Co}_{0.6}(\text{PO}_4)_2(\text{P}_2\text{O}_7)/\text{rGO}$ composite (NMCMP/rGO) measured in $\text{NaPF}_6/\text{EC}+\text{DEC}$ (Reprinted with permission from ref. [121], Copyright 2019, Elsevier).

Both ways can improve kinetics of the electrochemical reaction. Besides, the partial Mn substitution by Co results in smaller volume cell owing to smaller Co²⁺ radius (0.745 Å, high spin) than Mn²⁺ one (0.83 Å, high spin) and increased average redox potential of mixed-polyanion structure (from the average voltage of ~ 3.8 V for Co-free sample to ~ 4 V for Co-doped sample) [77,108].

Firstly, Tang et al. [108] have prepared CNT-decorated $\text{Na}_4\text{Mn}_2\text{Co}(\text{PO}_4)_2(\text{P}_2\text{O}_7)/\text{C}$ microsphere structure ($\text{NM}_2\text{CPP}/\text{C}-\text{CNTs}$), through the typical spray-drying method, by mixing aqueous solutions of $\text{Mn}(\text{NO}_3)_2$, $\text{Co}(\text{NO}_3)_2 \cdot 6 \text{H}_2\text{O}$, citric acid (as both carbon source and chelating agent) and different concentration of CNTs (3.5 and 7 wt.%). The samples are heated at 350 °C for 3 h and 630 °C for 10 h in Ar. CNTs were found i) to control the morphology of mixed polyanionic compound, thus creating the microspherical network skeleton (composed of nanoparticles with an average size of 150 nm) instead of the large number of irregular micro pieces observed without CNT; ii) to increase the specific surface area (from 7.98 to 36.81 m² g⁻¹) thus providing larger number of active sites for Na⁺ ions, iii) to decrease the charge transfer resistance (i.e. to increase electron transport among NM_2CPP particles), iv) to increase sodium ion diffusion coefficient and v) consequently to increase specific capacity of composite. The optimal content of CNT in terms of the best electrochemical properties was found to be 5 wt.%. The initial discharge specific capacity of $\text{NM}_2\text{CPP}/\text{C}-5\text{wt.}\% \text{CNTs}$ in 1 M $\text{NaClO}_4/\text{EC}+\text{PC}+\text{FEC}$ amounts to 96.1 (71.65 % of the initial charge capacity), 93.5, 74.4 and 41 mAh g⁻¹ at

the current rates of 0.1, 0.5, 1 and 10 C (1 C = 128.7 mA g⁻¹), which is higher than that of $\text{NM}_2\text{CPP}/\text{C}$ amounting to 81, 79.6, 52.5 and 31.2 mAh g⁻¹, respectively (Fig. 17b). The capacity retention after 100 cycles at 0.5 C is 78.1 % ($\text{NM}_2\text{CPP}/\text{C}-5\text{wt.}\% \text{CNTs}$) and 35.1% ($\text{NM}_2\text{CPP}/\text{C}$), while $\text{NM}_2\text{CPP}/\text{C}-5\text{wt.}\% \text{CNTs}$ retains 76.4 % of the initial capacity after 150 cycles at 1 C. Redox peaks of $\text{NM}_2\text{CPP}/\text{C}-5\text{wt.}\% \text{CNTs}$, positioned at 3.89/3.58, 4.19/3.78 and 4.59/5.3 V vs. Na⁺/Na (Fig. 17b), are shifted towards higher potentials when compared to above indicated potentials of NMPP [77], due to Co-doping.

The energy density of $\text{Na}/\text{NaClO}_4/\text{EC}+\text{PC}+\text{FEC}/\text{NM}_2\text{CPP}/\text{C}-5\text{wt.}\% \text{CNTs}$ battery is estimated to be 371 Wh kg⁻¹ (at 0.1 C, based on the materials' level), which is still close to the value of Na cell containing Co and CNTs-free NMPP sample as cathode [77] amounting to 385 Wh kg⁻¹, (although at two-fold lower current). From practical point of view, $\text{NM}_2\text{CPP}/\text{C}-5\text{wt.}\% \text{CNT}$ has the large potential, since the sodium-ion battery such as hard carbon/ $\text{NaClO}_4/\text{EC}+\text{PC}+\text{FEC}/\text{NM}_2\text{CPP}/\text{C}-5\text{wt.}\% \text{CNTs}$ is capable of showing i) the high initial reversible capacity of 88.8, 74.8 and 57 mAh g⁻¹ at 0.1, 1 and 5 C, respectively, ii) the working voltage of 3.85 V and iii) energy density of 249.9 Wh kg⁻¹, with the capacity retention of 75.1 % (at 0.5 C) after 100 cycles.

Next, Ryu et al. [121] have synthesized Co-substituted $\text{Na}_4\text{Mn}_2\text{Co}(\text{PO}_4)_2(\text{P}_2\text{O}_7)/\text{C}$ ($\text{Na}_4\text{Mn}_{2.4}\text{Co}_{0.6}(\text{PO}_4)_2\text{P}_2\text{O}_7$) particles (100–200 nm) in the form of the composite with rGO sheet (denoted as NMCMP/rGO), Fig. 17c. NMCMP is first prepared through the solution combustion synthesis (using $\text{Na}_4\text{P}_2\text{O}_7$, $\text{Mn}(\text{NO}_3)_2 \cdot \text{H}_2\text{O}$, $\text{Co}(\text{NO}_3)_2 \cdot$

6 H₂O and NH₄H₂PO₄ as reactants) followed by heating at 600 °C (in Air for 6 h) and then it is dispersed with GO solution through the ball milling and heated at 600 °C for 2 h (in Ar) to get the reduced graphene oxide. Still, traces of impurity phases (less than 2 %) such as Mn₂O₃, and Na₂MnP₅O₁₅ are detected in NMCMP/rGO. The additional NaMnPO₄ phase is detected in NMMP/rGO with the total amount of impurities less than 5 %. Mn²⁺/Mn³⁺ oxidation/reduction process can be evidenced within 3.6–4 V vs. Na⁺/Na for both Co-free and Co-doped samples, while the additional redox process of Co²⁺/Co³⁺ is recognized at ~ 4.5 V (vs. Na⁺/Na) in CV of NMCMP/rGO (Fig. 17c), and is found to be faster than Mn redox process. Additionally, the partial Co substitution on Mn sites 1) reduces the degree of octahedral distortion; 2) facilitates the Mn²⁺/Mn³⁺ redox reaction; 3) facilitates the A → B phase transition during sodium deinsertion thus providing its completion and reversibility (this transition is incomplete in the Co absence since both A and B phases have been observed at 4.8 V vs. Na⁺/Na); 4) suppresses the lattice distortion thus reducing the total volume change (5.7 % for Co-doped structure vs. 7.0 % for Co-free structure); 5) decreases the reaction resistance and 6) increases the sodium diffusion coefficient. As a result, the higher specific capacity and better cyclic stability of NMCMP/rGO vs. NMMP/rGO are obtained, as illustrated in Fig. 17c. The initial specific capacity of NMMP/rGO, measured in 1 M NaPF₆ in EC/DEC, amounts to 74.7, 47, 31.9, 21.3 and 16.1 mAh g⁻¹ at 0.05, 0.1, 0.2, 0.5 and 1 C (1 C = 130 mA g⁻¹), while the corresponding values of NMCMP/rGO are found to be 89.4, 75.9, 64.2, 48.3 and 34.2 mAh g⁻¹, respectively. The capacity retention, after 40 cycles, is found to be 59.8 % (Co-free) and 76.8 % (with Co).

As in the case of NNPP, the future research concerning NMPP should be focused on developing different synthesis/strategies of this material, aimed at improving the specific capacity of this material and its cyclic performance.

4. The role of binder in the polyanionic electrode performance

Apart from the synthesis of active powder, which tailors the material properties, the electrode design can be critical for the electrochemical performance as well. Typically, the electrode is made of the active material, conductive additive and binder (attached to the Al current collector), in an appropriate ratio, that should ensure its uniform dispersion at particle level, proper electrochemical wiring and the mechanical stability upon long cycling (the prevention of the contact loss between active particles and current collector during cycling). Although less attention has been paid to the role of inactive components, the type and amount of binder could be pivotal in the final electrochemical properties, especially at higher loadings [122]. Design of the polymer binder has been attracting specific attention recently in the battery community. Some researchers are concentrated on finding alternative and sustainable solutions to replace the conventional poly(vinylidene difluoride) dissolved in N-methyl pyrrolidone, (PVdF^{NMP}), mostly focusing on the aqueous electrode processing route which uses cheaper and environmentally more friendly aqueous binders such as carboxymethyl cellulose (CMC), alginate, polyacrylic acid (PAA) and so on. These green alternative binders, enriched in COOH groups, offer advantages in terms of cost, toxicity and conductivity of the electrode (the use of toxic, flammable and expensive NMP would be avoided) [123], as well as simplicity and rapidness of its preparation. Moreover, they are able to provide better electrochemical properties of the electrode material, when compared to PVdF^{NMP}, especially for the materials possessing large volume changes during cycling such as silicon [124]. Moreover, the carboxyl methylcellulose/styrene-butadiene rubber CMC/SRN has already been commercialized for graphite-based anode [122]. Still, the choice of the binder is strongly influenced by the type of the material.

Regarding polyanionic compounds, PVdF^{NMP} is usually used as a binder while the focus is on development of synthesis strategies, aimed at improving electrochemical properties. Still, other binders such as CMC and PAA, dissolved in water (CMC_{aq} and PAA_{aq}),

turned out to be better solution than conventional PVdF [65,125,126]. Namely, improved rate capability and cycling stability of Nasicon Na₃V₂(PO₄)₂F₃ (75 mAh g⁻¹ for CMC vs. 18 mAh g⁻¹ for PVdF at 70 °C, with the retention of ~ 79 % vs. ~ 55 % over 3500 cycles at 30 °C in 1 M NaClO₄/EC+PEC+5wt.% FEC, 1C=128 mA g⁻¹) [126], Na₃V₂O_{2x}(PO₄)₂F_{3-2x}-rGO (108 mAh g⁻¹ for CMC vs. 103 mAh g⁻¹ at 0.1 C for PVdF), with the retention of 98 % over 250 cycles vs. 84 % over 60 cycles at 0.1 C in 1 M NaClO₄/PC+2wt.% FEC, 1C=130 mA g⁻¹) [125] and Na₂FePO₄F/C (66.8 mAh g⁻¹ vs. 25.1 mAh g⁻¹ at 4 °C, with the retention of ~ 92 % vs. ~ 81 % over 200 cycles at 1C in 1 M NaClO₄/PC+2 wt.% FEC, 1C=130 mA g⁻¹) [65] were achieved with the use of both CMC (10 wt.%) and PAA binders (10 wt.%) instead of PVdF. These aqueous binders were found to i) accelerate the charge transfer process during cycling; ii) facilitate Na⁺ ion diffusion, iii) improve the adhesion between active material and binder; iv) improve dispersivity of active particles in electrode slurries and their integrity during cycling, when compared to PVdF binder.

Besides, the development of binder-free flexible electrodes has attracted attention in recent years [127]. Design of binder-free electrodes by directly growing on different carbonaceous substrates (carbon cloth, carbon paper, graphene, carbon nanofibers) has been considered as an efficient strategy in providing outstanding rate performance and ultra-long cycling. This type of electrodes enables the integration of active material and current collector as a whole, thus avoiding the use of the binder. This way, the closer connection of active particles and current collector is achieved which reduces the contact resistance, thus facilitating the electron transfer. Thanks to the flexible nature of these electrodes, flexibility of battery device can be achieved [127,128]. Different binder-free polyanionic cathodes such as NaVPO₄F/C@carbon fibers [129], Na₃V₂(PO₄)₃@carbon nanofibers [130], Na₃V₂(PO₄)₃@carbon paper (NVP@CP) [131], Na₃V₂(PO₄)₃@carbon cloth [132], Na₂FeP₂O₇@porous carbon cloth [133] Na₃(VO)₂(PO₄)₂F@graphene foam [134] were made through the different template free and template-assisted methods such as electrospinning method [127,130] and impregnation-carbonization techniques assisted by freeze-drying [131], sol-gel [132] and solvothermal process [134]. These electrodes deliver high-rate performance over long cycling (up to 3000 cycles).

Most electrodes of examined mixed polyanionic cathode are prepared with PVdF^{NMP} (5 % or 10 wt.%), as listed in Table S1, while CMC_{aq} is only used as a binder for the preparation of Na₄Co₃(PO₄)₂(P₂O₇)-MWCNT [67] and Na₄Ni₃(PO₄)₂P₂O₇ [98]. Actually, Kumar et al [67,98] have used CMC since they have previously shown that CMC improved sodium storage properties of sodium vanadium oxy-fluorophosphate [125]. Regarding the amount of PVdF, 5 wt.% was mostly used for the preparation of NCPP [68,69,109,110], while one study uses 10 % of PVdF thus maintaining percent of conductive additive to 10 %. Electrodes of other polyanionic compounds including NFPP, NMPP and NNPP [47,50,63,64,71,77,96,99,102,107,108,112,115–117,121] mostly contain 10 wt.% of PVdF, while the amount of conductive additive is 20 or 10 wt.%. By surveying the Table S1, in terms of used binder, additive and active material ratio, it is difficult to conclude, with certainty, whether the amount of binder influences the cycling stability, since different synthesis procedures and different electrolytes were also used. It can be assumed that 10 % of PVdF, used in the electrode of hollow Al-doped Na₄Co₃(PO₄)₂(P₂O₇) microspheres [111], is favorable for such a long cycling, over 8000 charge/discharge cycles, due to the stronger bonding effect needed to maintain the active material-support contact. Also, we can notice that the NFPP-based electrode containing 10 wt.% of PVdF [112] shows higher capacity retention (97% over 100 cycles at C/20) than the electrode with 5 wt.% of PVdF (90 % over 50 cycles at 1 C) [114] in the common electrolyte (1 M NaClO₄/PC+EC), while the similar procedure for preparation of the active powder was used. Still, it should be borne in mind that different current rates were used, which can have an impact on anode polarization and consequently on the capacity retention. On the other hand, no capacity fade

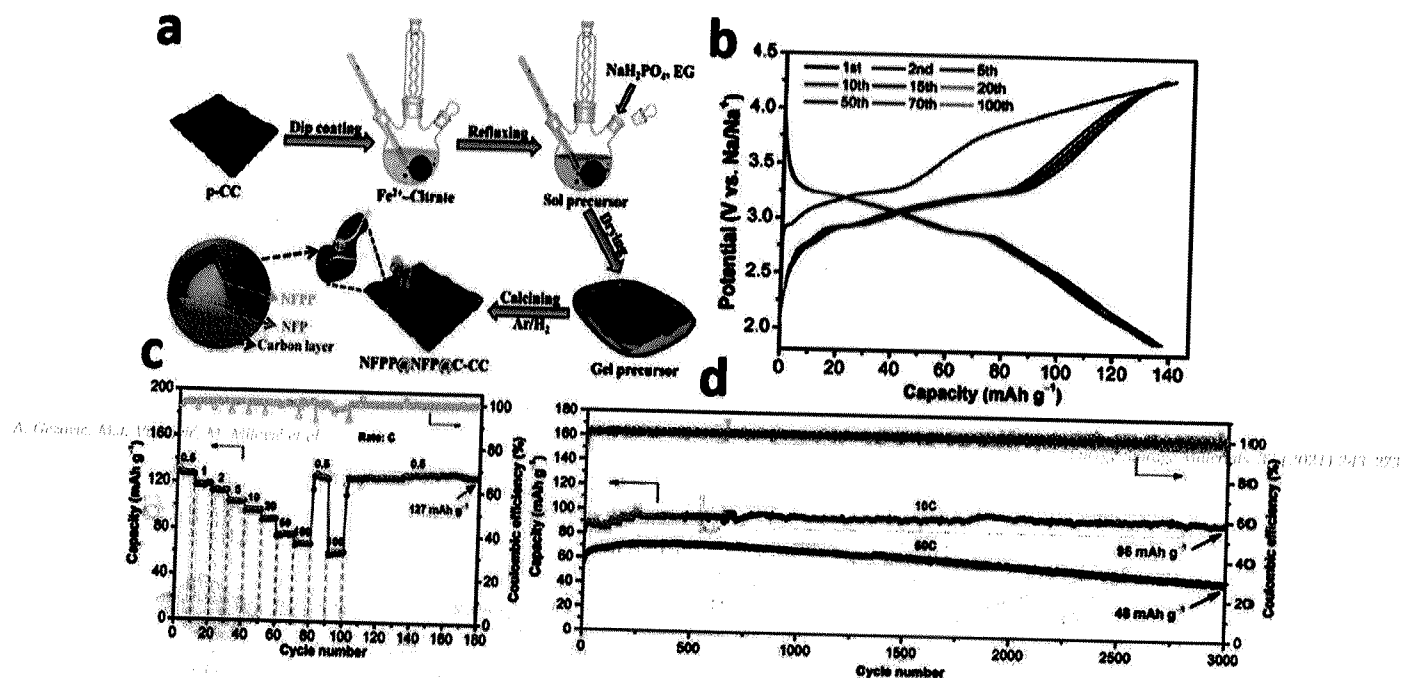


Fig. 18. a) Schematic illustration of the synthesis process of binder-free NFPP@NFP@C-CC electrode and its b) charge/discharge profiles at 0.1 C rate, c) Rate performance at different current rates and d) long-term cyclic stability at 10 C and 50 C for 3000 cycles obtained in a 1 M NaClO₄/PC+FEC, (1 C = 129 mA g⁻¹). (Reprinted with permission from ref. [119], Copyright 2019, Elsevier).

observed over 3000 cycles for the Na₄Fe₃(PO₄)₂(P₂O₇)@NaFePO₄@C (NFPP@NFP@C-CC) [119], grown on a flexible carbon cloth (CC) substrate (Fig. 18a-d), without the use of any binders and additives. Among all examined mixed-polyanionic cathodes (Table S1), this electrode actually shows the best sodium-storage capacity (Fig. 18a-d). It is the consequence of avoiding the insulator behavior of the binder, achieved through the sol-gel-based, dip-coating method. By growing the NFPP@NFP particles on the pretreated carbon cloth consisting of carbon fibers, the strong anchoring of active particles with the support can be achieved, thus enabling the easier electron transfer process between support and active material. This method, which implies in-situ preparation of flexible binder-free NFPP@NFP@C-CC cathode (with the capacity of 136 mAh g⁻¹@0.1 C, 97 mAh g⁻¹@10 C and 68 mAh g⁻¹@100C) [119], was shown to be more effective than the method for the preparation of binder-free Na₂FeP₂O₇ electrode on porous carbon cloth [133] in terms of simplicity, control of chemical composition and sodium storage capability (95 mAh g⁻¹@0.1 C, 68 mAh g⁻¹@10 C).

To summarize, the binder influence on the electrochemical properties of common Na₄M₃(PO₄)₂(P₂O₇) electrode is still not systematically studied. Numerous studies are still needed to evaluate the best optimal solutions as the most commercialization potential. The role of binder is especially critical issue for higher loadings, required for the commercial purpose. Of course, the selection of binder is in the strong correlation with both material properties and the type of the electrolyte.

5. The influence of the electrolyte formulation on polyanionic electrode performance

Besides materials' properties, the nature of the electrolyte is the crucial in tailoring the interface suitable for high-performance sodium-ion batteries. Passerini et al. [25] have published recently a comprehensive review related to the progress, status and perspective of electrolytes for Na-ion rechargeable batteries. The most commonly used electrolytes are carbonate-based liquid electrolytes composed of typical salts (NaClO₄, NaPF₆, NaTFSI, NaFSI, NaBF₄) dissolved in cyclic carbonates such as propylene carbonate (PC) and ethylene carbonate (EC) or in their combination with any linear carbonates such as ethyl methyl carbonate (EMC),

dimethyl carbonate (DMC) and diethyl carbonates (DEC). Besides, different ether-based, Ionic Liquids-based, aqueous, highly concentrated and solid-state electrolytes have been examined.

5.1. Nonaqueous organic electrolytes

An important aspect, regarding the role of the electrolyte in the final sodium storage performance of a certain electrode material, is not only related to the examined electrode interface, but also to the reactivity of Na metal electrode (acting as a reference and/or counter electrode) with the corresponding electrolyte. Sodium metal reacts with different organic carbonate electrolytes (NaClO₄/EC+DMC, NaPF₆/EC+DMC, NaClO₄/PC and NaClO₄/EC+DEC [112,135]) to a varying extent, depending on the type of solvent. This process is more pronounced if the sodium half-cell is underwent to potentiodynamic cycling. However, the fluoroethylene carbonate (FEC) additive was found to be an effective solution for Na-ion batteries, which improves their performance, thus suppressing undesired electrolyte decomposition reactions at the Na metal (or hard-carbon electrode) [136,137]. Still, positive effect of FEC is not always observed [138,139].

Electrolytes which are used for the examination of polyanionic NMPP cathode are listed in Table S1. As can be seen, most common electrolyte salts such as NaPF₆ and NaClO₄ are dissolved in the solvent mixtures of PC+EC [77,97,112,114,140,141], EC+DMC [67,98,116,117], EC+DEC [68,69,96,109,110,121], PC+FEC [50,107,119], EC+PC+FEC [99,108,141] or EC+DEC+FEC [63,64,102,111]. By examining the influence of two electrolytes (1 M NaClO₄/EC+PC and 1 M NaClO₄/EC+DEC) on the electrochemical performance of the common Na/NFPP half-cell, Jang et al. [112] showed that 1 M NaClO₄/EC+PC is a more suitable, thus providing the high reversible capacity of 122 mAh g⁻¹ over 100 cycles, with a high coulombic efficiency of ~ 99%. Namely, EC+DEC-based electrolyte reacts with Na metal (as evidenced by the color change of separator soaked by this electrolyte) thus forming decomposition products (sodium alkyl carbonates and reactive organic radical species), identified by ¹³C nuclear magnetic resonance (NMR) spectroscopy. The products diffuse towards NFPP cathode thus accelerating the electrolyte decomposition at higher potentials, which leads

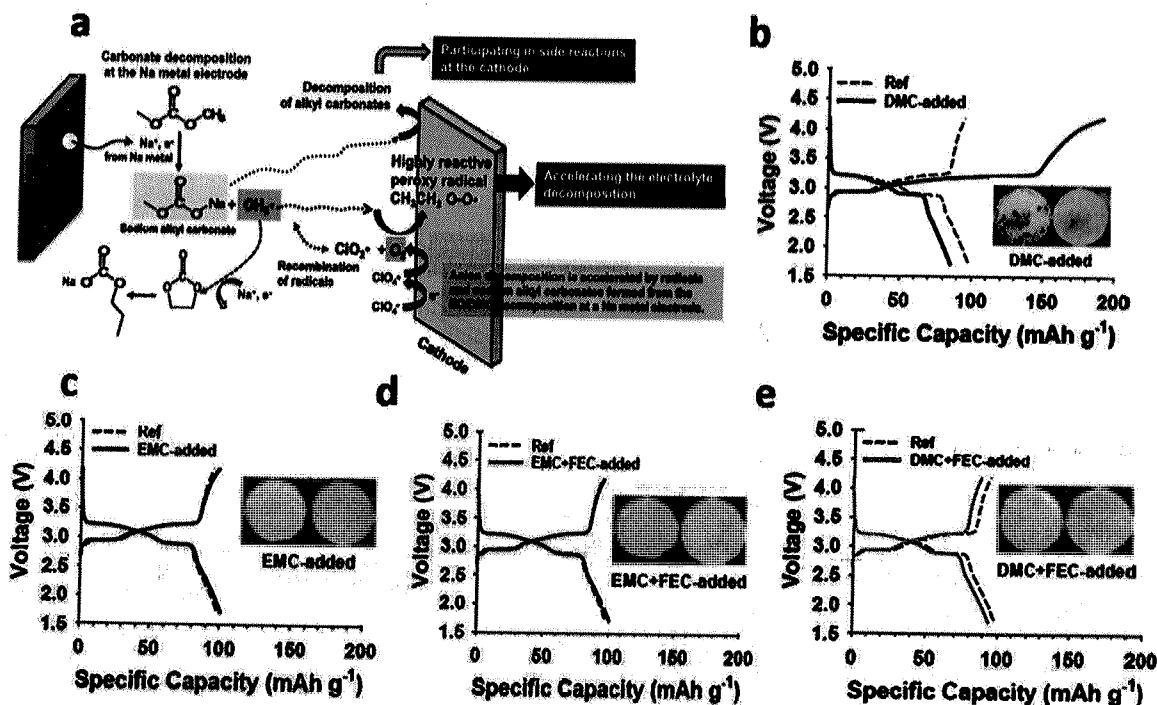


Fig. 19. a) Schematic illustration of the decomposition process of DMC-containing electrolyte at the Na metal anode (dissolved by-products diffuse to the NFPP cathode); the voltage profiles of NFPP, measured at C/20 C (1 C = 100 mA g⁻¹) and 30 °C, in b) 0.5 M NaClO₄/EC+PC+DMC, c) 0.5 M NaClO₄/EC+PC+EMC, d) 0.5 M NaClO₄/EC+PC+DMC+FEC and e) 0.5 M NaClO₄/EC+PC+DMC+FEC+EMC. Insets show the color change of the GFF separator before and after wetting with the corresponding electrolyte (Reprinted with permission from ref. [141], Copyright 2016, Elsevier).

to the appearance of two additional plateaus in the charging curve of Na/NFPP cell (Fig. 10a). This results in the cell overcharging, thus reducing its coulombic efficiency and reversible capacity.

When any of the linear carbonates (DMC, EMC or DEC) is added to the solvent mixture of EC+PC (at the expense of the PC fraction), the sodium storage performance becomes disrupted [141], despite the fact that the addition of low viscous linear carbonates improves NaClO₄/EC+PC ionic conductivity (following the order DEC, EMC, DMC) and wettability of hydrophobic polyethylene (PE) separator (following the order DMC, EMC, DEC). Namely, these carbonate-containing electrolytes undergo decomposition by reacting with the Na anode, which is more pronounced during cycling. It is also confirmed by ¹³C NMR spectroscopy of these electrolytes after their contact with the Na metal anode (without any applied potentials). Specifically, DMC undergoes irreversible decomposition at the Na metal anode thus forming dissolved by-products (sodium alkyl carbonate and CH₃• radical) which may diffuse to the NFPP cathode and further decompose at higher potentials during Na/NFPP charging (Fig. 19a). This contributes to an additional conveyed charge (Fig. 19b), which is not observed in the case of Li/NFPP cell. Mentioned by-products are also identified upon reaction of Na with EMC and DEC-based electrolytes, but the initial charge excess is not observed (Fig. 19c), due to the less pronounced reactivity when compared to DMC. It is evidenced by different color intensity of the separator, soaked by these linear carbonates-containing electrolytes. More importantly, the electrolyte decomposition byproducts were not identified when the FEC additive was added in any of DMC, EMC- and DEC-based electrolytes. FEC suppresses the reaction between Na and electrolyte effectively, thus forming stable electrode electrolyte interface (SEI) on the Na metal (Fig. 19d,e). As a result, the Na//NaClO₄/EC+PC+DMC+FEC//NFPP cell does not suffer overcharging (c), while its coulombic efficiency is improved (from 91–98 % up to 99.3%). However, if compared to FEC-free cell, it displayed reduced capacity, due to formation of thick NaF resistive layer on the cathode surface, which acts as an additional barrier for Na ion diffusion. Since

the amount of NaF, formed on the cathode upon cycling of the cell containing DEC+FEC-based electrolyte, is small, this film does not present diffusion barrier for Na ions in that cell. As a result, the capacity of the Na/EC+PC+DEC//NFPP cell is not reduced upon FEC addition into electrolyte. Its value is the highest among cells which use all three carbonates (DMC+FEC, EMC+FEC and DEC+FEC) as electrolytic components (90.5 mAh g⁻¹ without noticeable capacity loss over 300 cycles, while the coulombic efficiency is 99.5 %).

Let's discuss obtained electrochemical performance from the aspect of the electrolyte composition. If we compare the experimental results, obtained by Jang's and Lee's groups (Fig. 5c in [112] and Fig. 2b in ref [141]), the first overcharging of Na//1 M NaClO₄/EC+DEC+PC//NFPP is not observed, while it happens in the of Na//1 M NaClO₄/EC+DEC//NFPP cell. One can conclude that either PC slows down the reaction between DEC and Na metal, or such difference is simply governed by specific material properties. On the other hand, we can notice that the decomposition of DMC is not observed at Na metal [117], during cycling of half-cell using NFPP film and 1M NaClO₄/EC+DMC electrolyte, since the capacity is quite stable over 500 cycles. If we compare this behavior with Lee's results [141] on decomposing DMC component in the mixture of EC+PC and if we consider this difference from the aspect of the electrolyte, one can assume that PC accelerates DMC decomposition. However, the other reason for such difference could lie in different NFPP electrode engineering applied in references [141] and [117]. Therefore, the main question which arises here is related to the role of PC and/or material properties on the decomposition rate of linear carbonates at the sodium metal surface. This issue remains the subject matter for further researches.

The fact that the choice of the electrolyte determines the sodium storage performance of polyanionic cathode is clearly demonstrated by Kumar et al. [67], who showed different CV behavior for the common NCPP electrode (containing CMC binder) if measured in 1 M NaPF₆ in EC:DMC and if measured in 1 M NaClO₄/PC+FEC. Since FEC addition in PC can be favorable for sodium storage performance [119], the reason

for poorer performance of NCPP electrode [67], in 1 M NaClO₄/PC+FEC can be attributed to the "bad combination" of CMC and FEC binder [139]. Their synergy can cause an additional resistive layer on the Na metal thus increasing the cell polarization resistance. At the cathode side, the oxidation of Al in PC+FEC-based electrolyte could be more intensive within the used potential interval (from 4 to 4.8 V vs. Na), since this electrolyte may start to decompose at 3.8 V vs. Na on the Al foil [136] (the interval stability up to 4.8 V is shown for Pt current collector). Additional reason could be in the Al corrosion due to increased pH value of the CMC-based slurry. Unlike NaPF₆-based electrolyte, NaClO₄-based electrolyte does not contain fluorine which can passivate the current collector [142].

Beside the most common, carbonate-based organic electrolytes, ionic liquids (ILs) and concentrated electrolytes with organic solvents are also used for examining mixed polyanionic cathode [140]. By comparing the electrochemical behavior of NNPP in NaTFSI-Py₁₃FSI with that in NaPF₆/EC+DEC (1:1), Passerini et al [96] found an improved sodium storage in ILs-based electrolyte (63 mAh g⁻¹ vs. 40 mAh g⁻¹). Also, a wider potential window was provided with ILs- (3–5.1 V vs. Na⁺/Na) than with standard, carbonated-based electrolyte (3–4.9 V vs. Na⁺/Na), which is crucial for high-voltage material such as NNPP. Furthermore, the use of ultraconcentrated electrolyte (5 M) composed of sodium bis (fluorosulfonyl)imide in 1,2 dimethoxyethane (NaFSI-DME) shows good compatibility with NFPP, without corrosion of Al collector [140]. This highly concentrated electrolyte (conductivity of 0.584 S cm⁻¹) provides a high oxidation stability of Al collector (up to ~ 5 V vs. Na⁺/Na), reversible Na plating/stripping and low decomposition rate at Na metal. As a result, the high and stable redox behavior of Na//NaFSI-DME/NFPP cell was observed during 300 charging/discharging cycles. By comparing the sodium storage performance of NFPP in 5 M NaFSI-DME with that in typical 1M NaPF₆/EC+PC electrolyte, the improved behavior in first case was observed. Actually, the slightly higher initial capacity (116.2 vs. 111.4 mAh g⁻¹) and more noticeable improvement of the capacity efficiency (~ 99 vs. ~ 96 %) and capacity retention (~ 94 vs. ~ 85 %) upon 300 cycles, was observed in the case of concentrated NaFSI-DME electrolyte.

Although the conventional liquid-based electrolytes provide high-rate performance of metal-ion batteries, their use bears potential environmental risk mostly caused by flammable and volatile nature of the organic solvent. In this context, two types of safer and reliable alternative batteries, which use aqueous or solid-state electrolytes, have drawn attention.

5.2. Aqueous electrolytes

Apart from safety issues, aqueous electrolytes offer the higher ionic conductivity, lower price and simple manufacture process in comparison to the organic electrolyte. By comparing NFPP behavior in an organic solution (1 M NaClO₄ in EC:PC) and in 1 M Na₂SO₄ in H₂O [114], both higher capacity and better cyclic stability were observed in organic electrolyte. As we have already mentioned, the side reactions with water result in the capacity fade during cycling. So, the development of various strategies including particles coating procedures are needed to prevent the capacity fade and improve the capacity itself.

Generally, the main drawback and at the same time the main challenge with aqueous electrolyte is the lower voltage window limited by the electrolytic decomposition of water. By using highly concentrated salts in appropriate solvents, the potential window of aqueous solution could be extended up to 4 V [143], which opened a new door for future research directions in the field of aqueous rechargeable batteries. Lee et al [115] showed that the use of highly concentrated NaClO₄ (17 M), instead of 1 M NaClO₄ aqueous solution, resulted in shifting of the OER onset potential towards more positive potentials (from 4 to 4.4 V vs. Na⁺/Na) and HER onset potential toward more negative value (from 2.3 to 1.7 V vs. Na⁺/Na). As a result, a wider potential region of 2.7 V was obtained in 17 M NaClO₄. By comparing the sodium

performance of NFPP in different aqueous electrolytes, such as 17 M NaClO₄, 1 M NaClO₄ and 9.26 M NaCF₃SO₃ (in the form of full cell with NaTi₂(PO₄)₃), the capacity retention after 200 cycles was found to be improved significantly in concentrated aqueous solution (75, 18 and 63 % for 17 M NaClO₄, 1 M NaClO₄ and 9.26 M NaCF₃SO₃, respectively). Besides, the coulombic efficiency of NFPP-based cell after 200 cycles is significantly higher in 17 M NaClO₄ (~ 99%) than in 1 M NaClO₄ (~ 68 %), while the similar values are obtained between 17 M NaClO₄/H₂O and NaCF₃SO₃/H₂O.

Taking into account the possibility of broadening a potential window of aqueous electrolyte as well as the fact that the strategies for the high and stable capacitive performance are successfully developed for aqueous rechargeable batteries, further developments of this specific family of polyanionic compounds for aqueous rechargeable Na-ion batteries are worthy of investigations and remain a challenge.

5.3. Solid-state electrolytes

Solid-state electrolytes present potential solution to mitigate safety issues of conventional liquid electrolytes (mostly related to flammability and leakage of the electrolyte), thus allowing a high thermal stability, wider electrochemical stability window (> 5 V), longer life cycle and excellent mechanical/flexible properties. Besides, they simplify the cell-assembly process in terms of avoiding the separator wetting procedure by the electrolyte. On the other hand, there are big challenges regarding lower ionic conductivity, at a room temperature, when compared to liquid electrolytes, as well as the issues of controlling electrode/electrolyte interface and engineering processes [25]. Generally, solid-state electrolytes can be classified into conductive inorganic ceramic/glass-ceramic electrolytes, solid polymer electrolytes (SPEs) and their composite/hybrid versions. There are two types of inorganic solid electrolytes (ISEs): sulphide- (Na₃PS₄, Na₃SbS₄, Na₂S–SiS₂, Na₂S–GeS₂) and oxide-based organic electrolytes (β -Alumina electrolyte, Nasicon), while solid polymer electrolytes (SPEs) can be roughly divided into gel polymer and solvent-free solid polymer electrolytes [25,144].

β -Alumina electrolyte was the first fast ion conductor used in Na-S and Na-metal chloride batteries [144], while the main focus is currently on alternative sodium super ionic conductors such as NASICON with a general formula Na_{1+2x+y+z}M_xM_yM_{z-x-y}Si₂R_{3-z}O₁₂, where M is replaced by divalent, trivalent or tetravalent cations, while R can be Si or As [144].

Let's consider some developments of polyanionic structures for solid-state batteries. The first works on the use of Nasicon (Na₃Zr₂Si₂PO₁₂) as the solid electrolyte for both room and mid-high temperature sodium batteries were performed using polyanionic Na₃V₂(PO₄)₃ cathode [145,146]. The ionic conductivity of Nasicon Na₃Zr₂Si₂PO₁₂ was found to be ~ 9.4 × 10⁻⁴ S cm⁻¹ at a room temperature [145], while its value at 200 ° C amounted to ~ 1.5 × 10⁻³ S cm⁻¹ [146]. The initial capacity of Na₃V₂(PO₄)₃ (NVP), in the form of symmetrical NVP/Nasicon/NVP battery cycled at a room temperature within 0.01–1.9 V, was 80 % of the discharge capacity (68 mAh g⁻¹ @ 1.2 μ A cm⁻²) obtained for the symmetrical liquid NVP/NaClO₄-PC/NVP cell [145]. It was ~ 58 % of NVP theoretical capacity (117 mAh g⁻¹). However, deep capacity decay was obtained within the first five cycles. The improved rate capability of this symmetrical solid-state sodium cell, was obtained under higher temperature of 200 ° C [146]. Actually, when the NVP/Na₃Zr₂Si₂PO₁₂/cell operates at C/10 (97 μ A cm⁻²) under 200 ° C, its initial capacity could reach ~ 85 % of the NVP theoretical value. The capacity of ~ 50 mAh g⁻¹ was evidenced at C/2, showing a gradual decline over 20 cycles. Afterwards, different polyanionic Na₃V₂(PO₄)₃, NaTi₂(PO₄)₃, Na₃(VOPO₄)₂F, NaFePO₄ cathodes were examined in the combination with both organic and polymer solid electrolytes [147–149]. Different solid polymer-based electrolytes are summarized in the paper of Qiao et al [149]. By combining NVP as the cathode with Na/C as metal anode and NaFSI-based solid polymer (PEO) as the electrolyte, Zhao et al. [150] constructed full solid-state cell which at 80 ° C dis-

plays the high capacity ($\sim 111 \text{ mAh g}^{-1}$ at 0.1 C and 92 mAh g^{-1} at 2 C where 1 C is 117 mA g^{-1}) and ultrahigh capacity retention (92 % after 200 cycles and over 80 % after 5000 cycles) for a relatively large mass loading of $6\text{--}8 \text{ mg cm}^{-2}$ [150].

Generally, ISEs offer advantages over SPEs in terms of higher ionic conductivity ($10^{-4} \text{ S cm}^{-1}$ vs. $10^{-5} \text{ S cm}^{-1}$), higher cation transference number (~ 1 vs. $\sim 0.2\text{--}0.4$), higher resistance to the shocks and vibrations, and wider electrochemical potential window, while they are too hard and brittle unlike highly flexible and lightweight SPEs. Their hybridization in terms of making an ion-conducting ceramic/polymer composite is an effective way to afford advantages of both individual components. Kim et al. [151] proposed the use of such NASICON-based composite hybrid solid electrolyte (HSE), composed of NASICON ceramic powder (70wt%), a poly(vinylidene fluoride-hexafluoropropylene) (PVdF HFP) and ether-based electrolyte such as 1 M sodium triflate (NaCF_3SO_3)/TEGDME liquid electrolyte, for sodium battery (C/NaFePO_4). The initial specific capacity of NaFePO_4 in this half-cell amounted to 131 mAh g^{-1} at a 0.2 C rate, while the full cell arrangement with carbon anode, displayed 120, 103 and 75.4 mAh g^{-1} at rates 0.2, 0.5 and 1 C, respectively. The average voltage of this full HC/HSE/ NaFePO_4 cell was 2.6 V, while the capacity retention was found to be 96 % after 200 cycles.

Although various aforementioned polyanionic structures have been examined for solid-state batteries, according to the best of our knowledge, there is no attempt of examining interface between $\text{Na}_4\text{M}_3(\text{PO}_4)_2(\text{P}_2\text{O}_7)$ electrode and solid electrolyte interface. So, there is much space for studies of $\text{Na}_4\text{M}_3(\text{PO}_4)_2(\text{P}_2\text{O}_7)$ electrochemical properties, using various solid-state electrolytes, especially polymer-based ones which are successfully used for other polyanion compounds. Surely, it will define one of the future directions and, at the same time, present a great challenge in the field of the future energy storage.

6. Conclusions, challenges and opportunities for moving forward

6.1. The crucial issues

The sodiation/desodiation performance of $\text{Na}_4\text{M}_3(\text{PO}_4)_2(\text{P}_2\text{O}_7)$, experienced large advancement since 2013, especially $\text{Na}_4\text{Fe}_3(\text{PO}_4)_2(\text{P}_2\text{O}_7)$ one. Nevertheless, there are still lots of vague and unclarified issues, crucial for the "commercial design" of this material. Herein, we would like to summarize contradictions appearing in the literature and some unexplored segments, as the challenges for further research directed to the improvement sodium interfacial processes.

First, the issue of the full capacity upon deinsertion/insertion of Na^+ ions has not been entirely addressed. Different values of theoretical capacity have been reported, based on the transfer of three or four Na ions. Some authors regarded that the extraction of the fourth Na ion from $\text{Na}_4\text{Co}_3(\text{PO}_4)_2(\text{P}_2\text{O}_7)$ can only occur above 4.8 V vs. Na^+/Na , but the question remains whether it is followed by $\text{Co}^{3+}\text{--}\text{Co}^{4+}$ transition or the lattice oxygen oxidation. Otherwise, the partial extraction of all four Na ions may occur during redox process within the 4.1–4.7 V voltage interval. Furthermore, Kim et al. [47] highlighted that the theoretical capacity of $\text{Na}_4\text{Fe}_3(\text{PO}_4)_2(\text{P}_2\text{O}_7)$ should be 129 mAh g^{-1} (3 Na^+) instead of 170 mAh g^{-1} (4 Na^+), due to the pillar role of the remaining Na ion. This is in line with the three Fe ions in +2 oxidation state. Guided by Kim's studies, most authors have adopted theoretical capacity including three Na ion transfers, not only for Fe but also for Mn and Ni-based mixed phosphates. Regarding the structural characterization, we have also noticed some inconsistencies in the interpretation of Infrared and Raman spectra i.e. in the assignment of vibrational modes (as displayed in the section 2.1). Although the interpretation of Infrared spectra is difficult due to overlap of certain vibrational modes, we believe that an appropriate commitment can clarify some issues.

The next crucial issue is related to the determination of the Na^+ reaction path through the solid channel structure during charging/discharging procedure. The reported sequences of Na extraction are

not unambiguous, which is probably the consequence of distinctive experimental and theoretical approaches. Further observations, relying on combined experimental and theoretical studies, still require more attention, in order to match the final outputs, or, at least, to explain causes of discrepancies. Nevertheless, there are general conclusions about the low activation barrier for diffusion of all Na ions through the polyanionic framework, especially for ions with a fewer coordination number, which are assumed to leave the solid skeleton first.

Let us also shed more light on the importance of the synthesis procedure and the lack of explanation concerning the synthesis conditions and their influence to the final composition of polyanionic powder. Aqueous solutions of different salts such as oxalates, nitrates, acetates etc were generally used as the source of transition metals, while $\text{Na}_4\text{P}_2\text{O}_7$ or NaH_2PO_4 were mainly used as Na and P source. One can notice some differences between reactants acting as a phosphorous source. In some syntheses, both $\text{Na}_4\text{P}_2\text{O}_7$ and NaH_2PO_4 (or NaH_2PO_4) reactants, in the amount corresponding to the targeted stoichiometric composition, were used as the source of phosphorus (usually in the solid-state procedures), while some other procedures (for instance solution-based synthesis such as sol-gel one) used phosphate salts exclusively. The second case implies the thermal phosphate to pyrophosphate conversion. However, there is no general explanation as to why the phosphate decomposition is actually prevented under certain synthesis conditions and how $\text{PO}_4 \rightarrow \text{P}_2\text{O}_7$ thermal conversion can be adjusted/controlled to avoid the excess of phosphate or pyrophosphate phase. Formation of an additional phase (NaFePO_4 , $\text{Na}_2\text{FeP}_2\text{O}_7$...), in numerous synthesis of $\text{Na}_4\text{M}_3(\text{PO}_4)_2(\text{P}_2\text{O}_7)$, is practically inevitable (Table S1). The amount of mixed polyanionic phase, in the synthesized sample, as well as the type and amount of the secondary phase strongly depend on the synthesis conditions. For instance, the NFPP can be prepared by the solid-state reaction method, but only with the assistance of ball-milling. Also, the quenching of the sample can increase the content of the desired phase in the sample, but it deteriorates its structural and electrochemical properties. Notably, the temperature strongly controls the chemical composition. Furthermore, the amount of sodium should be controlled since it may determine the phase composition. On the other hand, the template method offers the possibility of obtaining the pure NFPP phase with an impressive ultra-fast rate capability. To summarize, optimization/tailoring of synthesis conditions, aimed at getting pure phase, still requires more attention.

Lastly, the achievement of high sodium storage properties of polyanionic compounds, which is closely related to the previous discussion, is of the crucial importance. The NFPP was shown to be the mostly investigated polyanionic cathode material, with the best performance. Its sodium storage performance has been gradually improving (Table S1), as the synthesis methods evolved over time, from the simple toward more complex procedures. The high and stable capacity of this compound, obtained by the solid-state reaction method, can be achieved at a lower current rate (128 mAh g^{-1} , 1 C = 120 mAh g^{-1}), while its rate capability was limited to 1 C (and barely to 10 C when too low capacity was measured). The sol-gel synthesis procedure enables the rate capability to extend from 10 C to 50 C, whereas NFPP gradually improves columbic capacity with the progress of sol-gel procedure, thus delivering the value of 78 mAh g^{-1} at 10 C [50], 85 mAh g^{-1} at 10 C, 78 mAh g^{-1} at 20 C [107] and $\sim 80 \text{ mAh g}^{-1}$ at 20 C [99] up to 97 mAh g^{-1} at 10 C [119]. Finally, the ultra-fast sodium storage properties (up to 200 C) have been achieved by the means of novel template [63] and ultra-spray methods [102], which provide the capacity of 79 mAh g^{-1} at 100 C or 35 mAh g^{-1} at 200 C, along with the long-term cyclability over 4000–6000 cycles.

On the other hand, such outstanding rate properties still remain a great challenge for Co, Ni and Mn-based compounds. Namely, the capacity of these compounds is generally lower than that of NFPP, especially at high current rates and upon long-term cycling. One of the reasons is the occurrence of different sodiation/desodiation redox potentials, depending on the type of transition metal. Namely, the average

sodium redox potentials of $\text{Na}_4\text{M}_3(\text{PO}_4)_2(\text{P}_2\text{O}_7)$ are found to be ~ 3.2 V (Fe), ~ 3.8 V (Mn), ~ 4.5 V (Co), ~ 4.8 V (Ni). The lowest redox potential implies less change of free Gibbs energy upon charging/discharging, which can lead to better structural stability. In addition to that, the sodiation/desodiation redox process of NFPP was found to be imperfect single-phase reaction, while the several biphasic transitions characterized the redox switching of Co, Ni, Mn-based compounds. Otherwise, the higher thermal stability of NCPP, NNPP and NMPP than NFPP, could provide the high crystallinity, favorable for the prolonged cycling stability. Anyhow, the novel synthesis/strategies of high-voltage polyanionic compounds (Co, Ni and Mn), aimed at improving capacity/stability, need to be developed. A lack of developed synthesis methods of Co, Ni and Mn-based compounds can be identified as a critical issue in overcoming inferior properties. Unlike NFPP which is synthesized by versatile synthesis procedures, only few methods, for Co, Ni and Mn-based compounds, have been reported so far. Namely, the sol-gel and ultra-spray-pyrolysis are used for the synthesis of NCPP, while the NNPP have been developed by the sol-gel and solid-state methods. The discharge capacity of NCPP at lower currents is below the theoretical one, amounting to ~ 100 mAh g^{-1} at 0.2 C, where 1 C = 170 mAh g^{-1} (Table S1). Its maximum rate capability is found at 20 C, with the corresponding coulombic capacity of 80 mA h g^{-1} . If someone replaces the certain fraction of Co with Al, the modified material will deliver higher rate capability (73.4 mAh g^{-1} at 50 C). Further, the NNPP in the form of composite with carbon, delivers even lower capacity, amounting to ~ 74 mAh g^{-1} at 0.1 C (1 C = 127 mA g^{-1}), with a very poor cyclic stability. Its capacity at higher currents has not been reported, while the oxygen release upon redox reaction is the major obstacle that needs to be overcome in the future. The solid-state, spray drying and gel-combustion methods were used for the synthesis of NMPP, whereas the dual strategy, including carbon coating and Co doping, is shown as an effective way to improve kinetics of the electrochemical reaction. The theoretical capacity of this Mn-based compound is withdrawn at low currents rates of 1 C (1 C = 130 mAh g^{-1}), while the maximum reported current rate is 10 C with the corresponding capacity of 41 mAh g^{-1} . Regarding NMPP, a great progress is made in terms of improving its electrochemical properties with respect to other Mn-based compounds, without the negative impact of the Jahn-Teller Distortion. Although NMPP shows significantly lower capacity than NFPP, observation that the diffusion barrier for Na ion decreases upon P_2O_7 distortion, at the final stage of charging (for Na1-Na4 pathway from 560 meV to 306 meV), appears encouraging. The same distortion in NFPP crystal lattice causes the narrowing of its Na diffusion channels thus leading to the significant increase of the activation energy for Na motion (it became even higher than 500 eV) and pronounced polarization (at the highest potentials) in the charge/discharge curves.

One should bear in mind that Fe and Mn are the most attractive components, from the sustainable and economic point of view. Accordingly, the research on Mn-based compounds, aimed at reaching/overcoming Fe-based compounds, seems to be the most challenging and promising in the future. Besides, $\text{Na}_4\text{M}_3(\text{PO}_4)_2(\text{P}_2\text{O}_7)$ type of polyanionic compound is found to be functional as cathode material, in various full battery cell configurations with the hard carbon as anode material (section 6.3). The best capacity can reach the value of 100 mAh g^{-1} (based on the cathode mass). One can conclude that two-electrode cell arrangement still requires a lot of attention in terms of improving electrochemical performance, in order for this class of materials to penetrate the battery market.

In addition to the structure and synthesis, the choice of the electrolyte is of the vital importance for the capacity and especially its retention. As elaborated above, its nature influences the interface properties and various interfacial processes related to decomposition of solvent components, additive and degradation of the active material as well, which further determine the sodium storage performance. By screening the table S1, one can notice that the performance of NFPP electrodes, which can withstand a large number of cycles in carbonate-based elec-

trolytes (more than 3000 cycles) refers to the electrolyte containing FEC additive. Actually, when the material's properties are adjusted via synthesis to enable high-rate performance, it seems that the presence of FEC is favorable for long-term cyclic stability. However, it also depends on the type of binder and solvent mixture. For example, the positive effects of FEC to the performance are not evidenced with CMC binder (as explained above) [139] and with highly concentrated NaFSI-DME [140]. Regarding other types of this new class of polyanionic structures (NCPP, NNPP and NMPP), rational synthesis methods, strategies and electrolyte formulations should be further developed to adjust the interface for the advanced battery performance of these structures.

6.2. Effective strategies to improve the kinetics of polyanionic cathode

In the $\text{Na}_4\text{M}_3(\text{PO}_4)_2(\text{P}_2\text{O}_7)$ structure, the MO_6 octahedra are linked with $(\text{PO}_4)^{3-}$ groups to form layers in the bc plane, which are bridged along the a-axis by $(\text{P}_2\text{O}_7)^{4-}$ groups (Fig. 3), thus forming 3D diffusion channels. Such opened 3D framework allows diffusion of Na ions along all three directions, offering an advantage over other polyanions which enable the Na ion diffusion through 1D channel (NaFePO_4) or 2D channels ($\text{Na}_2\text{FePO}_4\text{F}$). To achieve the fast-redox reaction, the rapid transport of electrons, that encounter Na ions within the framework, should be provided as well. The anchoring of the $\text{NaM}_3(\text{PO}_4)_2(\text{P}_2\text{O}_7)$ nanoparticles with conductive matrix of large specific surface area (1D, 2D, and 3D) can result in creation of 3D interconnected porous conductive framework and enhancement of the contact electrode/electrolyte area. So, this is an effective strategy to facilitate both electron and ionic wiring of $\text{NaM}_3(\text{PO}_4)_2(\text{P}_2\text{O}_7)$ particles, and boost kinetics of the mixed polyanionic cathode. There are several strategic approaches:

- i) Embedding of mixed polyanionic nanoparticles into 3D interconnected carbon network, which provides thin and uniform carbon layer (with a few nm) around active particles [50,63,77,96,97,99]. The carbon coating prevents the growth of $\text{Na}_4\text{M}_3(\text{PO}_4)_2(\text{P}_2\text{O}_7)$ particles during the synthesis procedure, thus providing reduced dimensions which shorten the path of electrons and ions. One can see, from the Table S1, that sub-micron/micron NCPP and NNPP particles (> 200 nm) are usually obtained. So, reduction of Co- and Ni-based polyanions materials to nano-dimensions (below 200 nm), through different approaches including carbon coating, should be one of the future directions towards improved properties. On the other hand, the reduced dimension of Fe- and Mn-based particles (especially NFPP), from 30 to 200 nm, have been synthesized. These nanodimensions of NFPP particles, coated by thin and homogeneous 2 - 3 nm carbon layer, provide an excellent performance [63]. Despite producing NMPP particles with the size of ~ 100 nm, achievement of the high rate performance and long capacity retention remains a challenge.
- ii) Carbon nanotubes wrapping of micro/nano spheres and growth of active particles on multi-walled carbon nanotubes (MWCNTs) [64,67,108,111]. Tang et al. [108,111] have prepared carbon nanotube (CNT)-modified $\text{Na}_4\text{Mn}_2\text{Co}(\text{PO}_4)_2(\text{P}_2\text{O}_7)$ (NM₂CPP/CNTs) and Al-doped $\text{Na}_4\text{Co}_3(\text{PO}_4)_2(\text{P}_2\text{O}_7)$ (Al-NCPP/CNT) microspheres with hollow structure, by using spray drying methods. These hollow microspheres (composed of nanoparticles), with shell thickness of ~ 465 nm, can allow large reaction area and fast mass transfer, thus shortening Na^+ diffusion distance. Moreover, they are able to accommodate the large volume changes during charge/discharge which is crucial for long-term cycling. Benefits of highly conductive surface CNTs are indicated in the subsection 3.4.2. As a result, Al-NCPP/CNT hollow structure is capable of delivering not only the high capacity and rate capability, but also exceptional cycling stability over 8000 cycles (for the small electrode loadings of 1.3 mg cm^{-2}). When compared to other carbon-coated polyanionic hollow spheres

($\text{Na}_2\text{FePO}_4\text{F}/\text{C}$, $\text{Na}_2\text{MnPO}_4\text{F}/\text{C}$, $\text{Na}_3\text{V}_2(\text{PO}_4)_3/\text{C}$) [152–154], the Al-NCPP/CNT hollow structure possesses higher rate capability and longer cycling life. By growing NFPP particles on MWCNTs [64], the high rate capability and an excellent capacity retention of NFPP/MWCNTs composite was also achieved.

- iii) 3D decorating of mixed-polyanions particles with conductive graphene network, which is able to prevent the aggregation of nanoparticles [102,121]. Namely, the encapsulation of mixed polyanion particles into 3D network of graphene sheets was found to enhance the electronic wiring and supply the electrode with many nanovoids for Na^+ diffusion. Such unique structure is able to accommodate large volume changes during cycling and deliver theoretical capacity, the outstanding rate capability and ultralong cycling life (up to 200 C and over 6000 cycles) [102].
- iv) carbon coating of nanoparticles + embedding of polyanionic nanoparticles into cross-linked porous graphene network [98,107]. 3D porous conductive network, composed of in-situ formed amorphous carbon layer and cross-linked graphene sheets, restricts the aggregation of polyanionic nanoparticles, increases electrode/electrolyte contact area and improves electron transport and dispersity of electrode particles. Such unique NPFC@AC-rGO structure [107] exhibits an excellent sodium storage performance, especially at the high rate of 20 C and the low temperature of -15°C .

Synergy of amorphous carbon with CNTs [108] and graphene sheets [107] in the mixed polyanionic composite, is considered to improve the electrochemical properties. Still, the sodium storage performance of published 3D hierarchical micro/nano phosphate structures (the capacity, rate capability and capacity retention) are inferior when compared to the performance of carbon-coated $\text{Na}_3\text{V}_2(\text{PO}_4)_3$ (NVP/C) [155]. Carbon framework of NVP/C consists of graphene-like coating layers and interconnected nanofibers. Therefore, there is still considerable room for further improvements of existing 3D conductive mixed polyanion structures. One approach should be directed to the carbon surface chemistry and its tailoring through the heteroatoms (N, S...) doping, which facilitates the charge transfer process.

6.3. Comparison with other polyanionic structures

Representative properties of different polyanionic-type materials are presented in the Table S2 (Supp.Data) in order to compare their electrochemical behavior with mixed-polyanionic compound. Although the comparison between different polyanionic structures is inappropriate, since the electrochemical performance varies depending on the used synthesis method or the type of the electrolyte, some advantages/disadvantages can be derived, as listed in the paper of Jin et al. [87]. Besides operating voltage (Fig. 2), the main advantage of 3D mixed-polyanionic framework over other polyanionic structures, (with a common transition metal M) such as phosphates (olivine and maricite NaMPO_4), fluorophosphates ($\text{Na}_2\text{MPO}_4\text{F}$) and pyrophosphates ($\text{Na}_2\text{MP}_2\text{O}_7$), is in term of the rate capability. Although the capacity of mixed phosphate-pyrophosphate structure, at lower current rates, can be slightly lower or comparable with the capacity of individual phosphates and pyrophosphates, its values are usually higher at higher currents (Table S2). Let's compare some binder-free polyanionic cathodes. We can see that the capacity of the binder-free NFPP@NFP@C-CC electrode in 1 M $\text{NaClO}_4/\text{PC}+5\%\text{FEC}$ (136 mAh g^{-1} at 0.1 C, 1 C = 129 mA g^{-1}) [119] is lower than the capacity of binder-free maricite NaFePO_4/C (NFP@C) in 1 M $\text{NaClO}_4/\text{PC}+5\%\text{FEC}$ [156], at slow current rates (145 mAh g^{-1} at 0.2 C, 1 C = 154 mA g^{-1}), while their values are comparable at high current rates (97 mAh g^{-1} at 10 C, 1 C = 129 mA g^{-1} and 84 at 10 C, 1 C = 154 mA g^{-1} , respectively). However, NFPP@NFP@C-CC can withstand current rates up to 100 C [119], while the maximal reported current rate of NFP@C is 50 C [156]. Furthermore, the NFPP@NFP@C-CC capacity, at all current rates, is higher than

the capacity values measured for free-standing pyrophosphates, which amount to 95 mAh g^{-1} at 0.1 C and 68 mAh g^{-1} at 10 C (1 C = 97 mA g^{-1}). On the other hand, the improved capacity of NFPP@NFP@C-CC, at ultrahigh current rates ranging from 10–200 C (68 mAh g^{-1} at 100 C, 1 C = 129 mA g^{-1}), remains the challenge when compared to the free-standing $\text{Na}_3\text{V}_2(\text{PO}_4)_3/\text{C}$ -CC (NVP@C-CC) electrode [132] (96.8 mAh g^{-1} at 100 C or 69.9 mAh g^{-1} at 200 C, 1 C = 117 mA g^{-1}). Still, their capacities are comparable at lower current rates. The operating voltage of NFPP is slightly lower than that of NVP (3.2 V vs. 3.4 V), while the operating potential of NVP is lower than the potential of Mn, Co and Ni-based mixed polyanions.

If we compare $\text{Na}_4\text{M}_3(\text{PO}_4)_2(\text{P}_2\text{O}_7)$ (M = Fe) with vanadium based-fluorophosphate $\text{Na}_3(\text{VO}_{1-x}\text{PO}_4)_2\text{F}_{1+2x}$ (mostly $\text{Na}_3\text{V}_2(\text{PO}_4)_2\text{O}_2\text{F}_3$, $\text{Na}_3\text{V}_2(\text{PO}_4)_2\text{F}_3$) [157,158], the lower operating potential will be observed for Fe and Mn-based polyanions, while Co and Ni-based mixed compounds would have a higher voltage. Besides, the $\text{Na}_4\text{M}_3(\text{PO}_4)_2(\text{P}_2\text{O}_7)$ matches fluorophosphates (based on material level in half-cell) in terms of the capacity and rate capability [157], but achievement of energy performance, as those of $\text{Na}_3\text{V}_2(\text{PO}_4)_2\text{F}_3/\text{C}$ -based prototype cell is still a challenge [157–159]. Still, Fe-based mixed polyanionic material offers an advantage in terms of the price and toxicity, while the high cost and toxicity of both V- and Co-based phosphates present the obstacle. Besides, there are high requirements for the synthesis equipment of the vanadium-based fluorophosphates [87]. On the other hand, the difficult control of the NFPP synthesis conditions, which is strongly related to an insufficient understanding of the reaction processes, is recognized as one of the critical issues.

Furthermore, Na-based silicate polyanion materials are also considered as the potential cathodes for SIBs [87] due to the high theoretical capacity when extracting two Na ions per unit formula (276 mAh g^{-1} for $\text{Na}_2\text{FeSiO}_4$), thermal stability, low cost and high abundance of elements (the $\text{Na}_2\text{FeSiO}_4$ is the cheapest compound due to abundant Na-Fe-Si resources). However, these compounds have low electronic conductivity, which causes difficult extraction of the second Na ion (occurring above 4 V vs. Na^+/Na) [160]. When compared with silicates, mixed $\text{Na}_4\text{M}_3(\text{PO}_4)_2(\text{P}_2\text{O}_7)$ compounds possess lower theoretical capacity, but higher voltage, while the eco-aspect of $\text{Na}_4\text{M}_3(\text{PO}_4)_2(\text{P}_2\text{O}_7)$ depends on the metal (Fe and Mn provide cheap and eco-friendly material unlike Co and Ni). Although Na-silicates possess high theoretical capacity (based on two Na ions followed by two electron process of $\text{Fe}^{2+}/\text{Fe}^{4+}$ redox pair), its utilization is usually limited due to difficult deinsertion of the second Na. Besides, it is a matter of the structural stability when two Na ions are extracted. In that case, advantage of the higher capacity over mixed polyanions would be annulled. On the other hand, mixed $\text{Na}_4\text{M}_3(\text{PO}_4)_2(\text{P}_2\text{O}_7)$ could offer not only higher operating potential but also higher cycling and rate capability (Table S1 and Table S2). Difficulties in obtaining a phase pure material is typical for both silicate and mixed polyanion materials.

6.4. Full cell configurations

Survey of constructed two-electrode full cells containing mixed polyanionic cathode and suitable anode is given in the Table S3. As we can see, different structures such as hard carbon (HC), $\text{Li}_4\text{Ti}_5\text{O}_{12}$, $\text{NaTi}_2(\text{PO}_4)_3$, (PPy)-coated Fe_3O_4 and CHC were employed as anodes thus providing cells with different operating voltages and capacities. Regarding mixed-polyanionic cathode materials, the most reported cells include NFPP and NCPP structures, while only one cell is reported for NMPP. This clearly indicates that practical development of this class of polyanionic materials as cathode are in the infancy thus leaving a lot of space for further progress and improvement. The comparison between listed full Na-ion cells is difficult since the electrochemical parameters are calculated differently (based on cathode mass, based on anode mass or based on both anode and cathode masses). However, several common issues can be noticed. First, the specific capacity of mixed-polyanionic cathode and its retention upon cycling, in full-cell arrangement, is lower

than in the half-cell configuration, using Na anode (comparison with Table S1), thus indicating incomplete possible utilization of this compound. The reason lies in the insufficient sodium storage performance of anode materials to match cathode performance, compatibility issues between electrodes and/or two-electrode cell construction. Second, the first irreversible capacity loss is typical for all assembled Na-ion full cells (Table S3), which can be attributed mostly to the formation of SEI layer on the anode surface. This irreversible capacity loss is between 20 - 40 % ($Q_{\text{discharge}}/Q_{\text{charge}}$) depending on the cell and applied current, while it is significantly reduced (5 - 10 %) when the anode is previously cycled in Na-full cell, which results in good coulombic efficiency (expressed as the discharge to charge capacity ratio) during further cycling.

The irreversible capacity loss is also evidenced for some other full Na-ion cells containing polyanionic cathodes [65,125]. Deng et al. [65] showed that the initial coulombic efficiency of the $\text{Na}_2\text{FePO}_4\text{F}$ -based cathode, calculated as the ratio of charge (deinsertion) and discharge (insertion) capacity, can be tailored by controlling the charging cut-off voltage ($Q_{\text{charge}}/Q_{\text{disch}}$ increases with the increase of the cut-off anodic potential). However, they have demonstrated that the charging of the Na/ $\text{Na}_2\text{FePO}_4\text{F}$ -based cathode up to higher voltage (2 - 4.5 V), followed by discharge-charge towards lower voltage (2 - 4 V), during subsequent cycling, can increase the initial coulombic efficiency ($Q_{\text{charge}}/Q_{\text{disch}}$) of the cathode (when compared to the constant cycling within lower or higher voltage interval) and improve cycling stability of the cell. However, this strategy is not effective for full HC/ $\text{Na}_2\text{FePO}_4\text{F}$ cell, where the constant cycling in the extended voltage interval (0 - 4.5 V) causes the best cycling performance. The mentioned cycle modes should also be checked for the mixed polyanionic cathode in order to see whether the initial coulombic efficiency of the material (that actually means the increase of the irreversible capacity loss) and consequently the cyclic performance can be improved by the cycling at higher voltages (overcharging). It is difficult for this strategy to be successfully applied for the high-voltage NCPP and NNPP cathodes due to issues related to electrolyte decomposition, but it could be a good way for improving performance of NFPP and NMPP-based cells. By comparing charge discharge/curves of all reported HC/NFPP-based cells [64, 99, 107, 119], we can notice that the cell cycled up to 4 V [64,99] shows the best discharge/charge ratio (after initial irreversible change) when compared to the other cells, cycled up to 3.2 V.

Generally, relatively poor capacity retention of the full Na-ion cell with mixed-polyanionic cathode is observed. It is more pronounced when compared to the performance in the half-cell configurations with the same cathode (Table S1) or some other hybrid systems (composed of polyanionic anode and carbon cathode) [161]. Actually, the cyclic performance is limited to several hundreds of cycles, which is in the range with full cells containing other polyanionic structures as cathode such as $\text{Na}_3\text{V}_2(\text{PO}_4)_3$, VOPO_4 [162–165]. On the other hand, same mixed-polyanionic cathodes can withstand several thousands of cycles in half-cell configurations. Apart from the improvement, related to anode materials and configurations, better understanding of the electrode/electrolyte interface is needed as well. Comprehensive approach of morphological and structural changes (the local atomic environment, diffusion coefficients, Na diffusion pathways and barriers) during charging /discharging, along with the developments of synthesis strategies and electrolyte formulations, is necessary to break a long-term cycling barrier.

In spite of the mentioned weaknesses, one can notice advantages of the mixed-polyanionic-based cells when compared to other polyanionic cathodes. HC/NCPP-based full cell [111] could provide higher operating voltage (~ 4.3 V) than other high-performance cells (~ 3.2 V) such as HC/ $\text{Na}_3\text{V}_2(\text{PO}_4)_3$ [164,165] and HC/ $\text{Na}_{3.5}\text{V}_2(\text{PO}_4)_2\text{F}_3$ [166]. However, further challenges should relate to the increase of capacity and its stability upon long-term cycling. The reduction of NCPP particles to nano-dimension, the anchoring of NCPP particles with some heteroatom-doped carbon and replacement of Co fraction with a certain ion could be effective future strategies, which would improve energy of

NCPP-based cell, reduce its toxicity and price, thus maintaining the high operating voltage. On the other hand, ion doping of NFPP and NMPP with a suitable cation or anion, capable of increasing voltage and electronic conductivity, would be a good direction for further improvement of energy performance of full Na-ion cell with NFPP and NMPP cathode.

Sodium phosphate polyanion materials were also used as electrodes of hybrid devices, preferably electrochemical capacitors. Hybrid capacitors, especially sodium-ion hybrid capacitors [100, 161], are extensively studied as potential devices which satisfy requirements of both high energy density and high-power density, at a low cost. Although $\text{Na}_4\text{M}_3(\text{PO}_4)_2(\text{P}_2\text{O}_7)$ type materials, have not been studied till now as the electrodes of hybrid capacitors, they should be treated as perspective ones, on the basis of following two examples with simpler phosphate polyanionic materials. First, Thangavel et al. [167] reported bio-inspired sodium ion hybrid capacitor, one electrode of which was polyanionic material $\text{Na}_3\text{V}_2(\text{PO}_4)_3$ and the second one was a cinnamon-derived highly porous carbon. In an organic electrolyte, this hybrid capacitor delivered energy density of 118 Wh kg^{-1} and a power density of 850 W kg^{-1} . It displayed also high cycling stability, the highest ever reported for sodium ion-based intercalation compounds. Second, Thangavel et al. [168] constructed a new type hybrid capacitor consisting of sodium super ionic conductor $\text{NaTi}_2(\text{PO}_4)_3$ /graphene nanosheets composite as an intercalation electrode, and 2D graphene nanosheets as an adsorption electrode. This capacitor displayed energy density of 80 Wh kg^{-1} and a respectable specific power of 8 kW kg^{-1} . The capacity fade was only 0.13 % per 1000 cycles, and 90 % after 75 000 cycles.

To confirm good perspective of these materials, we may outline excellent electrochemical half-cell behavior of $\text{Na}_4\text{M}_3(\text{PO}_4)_2(\text{P}_2\text{O}_7)/\text{C}$ composite described by Chen et al. [99], Yuan et al. [102] and Ma et al. [119].

6.5. Future considerations

Based on the total overview, the universal concept to obtain the high-performance mixed-polyanionic electrode (on the research level) is still difficult to derive due to interplay between key electrode and electrolyte components (material, binder and electrolyte) that control interface. Additional studies are needed in order to determine contribution of these individual components and their combining effect to the electrochemical activity of the $\text{Na}_4\text{M}_3(\text{PO}_4)_2(\text{P}_2\text{O}_7)$. In the strict relation to this, high-rate performance, high specific energy and excellent cycling stability with high safety, still remain the challenge, especially in the case of the structures with higher operating voltage, while many bottlenecks need to be solved. Specifically, future issues, which should be addressed, include following aspects/topics:

- Key fundamental questions, regarding the influence of the synthesis conditions/parameters to the final composition of $\text{Na}_4\text{M}_3(\text{PO}_4)_2(\text{P}_2\text{O}_7)$ phase, must be understood for each type of $\text{Na}_4\text{M}_3(\text{PO}_4)_2(\text{P}_2\text{O}_7)$. Namely, one has to deal with the following questions: i) How to adjust synthesis conditions to obtain completely pure polyanionic phase (identified as the bottleneck); ii) what parameters are determining formation of this phase and whether it depends on the specific synthesis; ii) does the pure phase show the best performance or whether its synergy with secondary polyanionic phases is more appropriate solution. Although some NFPP electrodes [99,102,119] hold the promise in the sodium batteries, further development of rational synthesis methods and strategies to design various nanoarchitectures (including impregnation with different conductive matrices), with improved energy/power performance, are highly needed, especially for i) higher currents/loadings; ii) NCPP, NMPP and NNPP electrodes and iii) full-cell configurations.
- the influence of the binder to the electrochemical properties of the common $\text{Na}_4\text{M}_3(\text{PO}_4)_2(\text{P}_2\text{O}_7)$ electrode is not yet systematically reported. The comparison of electrochemical properties of the common $\text{Na}_4\text{M}_3(\text{PO}_4)_2(\text{P}_2\text{O}_7)$ electrode, containing different binders, is nec-

essary. Since PVDF is the most common binder for the electrodes, examined so far (Table S1), the future directions should be focused more on the aqueous alternative binders, especially if we keep in mind the fact that CMC can cause better performance of polyanionic NVP cathode than PVDF [125]. Since the best performance among all examined $\text{Na}_4\text{M}_3(\text{PO}_4)_2(\text{P}_2\text{O}_7)$ samples is achieved for binder-free electrode, this processing way should also be pushed for all types of this specific polyanionic family and compared with other binder-containing powder electrodes, not only in terms of the electrochemical performance, but also concerning cost, simplicity and environmental compatibility.

- the influence of the electrolyte to the mixed-polyanionic cathode is examined in few studies, but the research in this field needs to be intensified more. Since individual solvent components are decisive for the final performance of polyanionic electrode (especially in terms of the capacity retention) their role in different interface processes (the decomposition rates of carbonate-based components at the metal surface, FEC-induced processes, the synergistic process of binder and FEC...) should be specified and elaborated.
- Since few papers are related to the examination in an aqueous electrolyte, while the use of this polyanionic cathode with the solid-state electrolyte has not been reported yet, these fields remain completely open. Moreover, the examination of comparative electrochemical behavior of the $\text{Na}_4\text{M}_3(\text{PO}_4)_2(\text{P}_2\text{O}_7)$ cathode in nonaqueous and aqueous electrolytes would be an effective strategy to understand sodium insertion mechanism better.
- All future issues, outlined above, should be elaborated through the various physicochemical and electrochemical methods and understood from the theoretical aspect in order to explain structural/morphological/electrochemical relations more profoundly and anticipate some future steps. The special focus should be on the study of Na-ion sequence during charging/discharging, in order to overcome ambiguity and find out the reason for discrepancy between theory and experiment. This would result in more accurate conclusions on the sodium redox mechanism of polyanionic materials, as an important link for their high energy performance.

Declaration of Competing Interest

The authors declare that they have no known competing financial interests or personal relationships that could have appeared to influence the work reported in this paper.

Acknowledgments

A. G. would like to thank to the Ministry of Science of Montenegro for selecting her to receive the "Scholarship for Doctoral Research in Montenegro". A. G and V. G. gratefully acknowledge the financial support from Ministry of Science of Montenegro under the same project entitled "Ecological cathode materials for lithium/sodium ion batteries". This research is supported by the Science Fund of the Republic of Serbia, PROMIS, #6062667, HISUPERBAT (M.V. and M.M. gratefully acknowledge this financial support). A.G., M.V., V.G. and R.D. are indebted for financial support by NATO through the Science for Peace and Security (SPS) Programme, the project SPC G5836 - SUPERCAR. M. V., M. M. and S.M. would also like to acknowledge for support Ministry of Education, Science and Technological Development of the Republic of Serbia, Contract number: 451-03-68/2020-14/200146". The continuous support for research in the field of energy storage through the bilateral project Montenegro-Serbia with title "Development of ecological Li-ionic batteries" is also acknowledged by V.G. and M.V. R. D. acknowledges support from Slovenian research agency through ARRS-MS-BI-ZP bilateral project and P2-0393 core research program. S.M. is indebted to the Serbian Academy of Sciences and Arts for supporting the study through the project "Electrocatalysis in the contemporary process of energy conversion".

Supplementary materials

Supplementary material associated with this article can be found, in the online version, at doi:10.1016/j.ensm.2021.02.011.

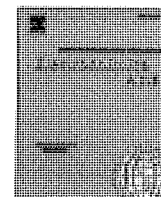
References

- [1] J.B. Goodenough, K.S. Park, The Li-ion rechargeable battery: A perspective, *J. Am. Chem. Soc.* 135 (2013) 1167–1176, doi:10.1021/ja3091438.
- [2] M.S. Whittingham, Lithium batteries and cathode materials, *Chem. Rev.* 104 (2004) 4271–4301, doi:10.1021/cr020731c.
- [3] J.B. Goodenough, Y. Kim, Challenges for rechargeable Li batteries, *Chem. Mater.* 22 (2010) 587–603, doi:10.1021/cm901452z.
- [4] D. Bresser, K. Hosoi, D. Howell, H. Li, H. Zetsel, K. Amine, S. Passerini, Perspectives of automotive battery R&D in China, Germany, Japan, and the USA, *J. Power Sources.* 382 (2018) 176–178, doi:10.1016/j.jpowsour.2018.02.039.
- [5] B. Dunn, H. Kamath, J.M. Tarascon, Electrical energy storage for the grid: A battery of choices, *Science* 334 (2011) 928–935, doi:10.1126/science.1212741.
- [6] B. Scrosati, J. Garche, Lithium batteries: Status, prospects and future, *J. Power Sources* 195 (2010) 2419–2430, doi:10.1016/j.jpowsour.2009.11.048.
- [7] M. Hu, X. Pang, Z. Zhou, Review Recent progress in high-voltage lithium ion batteries, *J. Power Sources.* 237 (2013) 229–242, doi:10.1016/j.jpowsour.2013.03.024.
- [8] C.P. Grey, J.M. Tarascon, Sustainability and in situ monitoring in battery development, *Nat. Mater.* 16 (2017) 45–56, doi:10.1038/nmat4777.
- [9] D. Larcher, J.M. Tarascon, Towards greener and more sustainable batteries for electrical energy storage, *Nat Chem* 7 (2015) 19–29, doi:10.1038/NCHEM.2085.
- [10] D. Buchholz, A. Moretti, R. Kloepsch, S. Nowak, V. Siozios, M. Winter, S. Passerini, Toward Na-ion batteries - Synthesis and characterization of a novel high capacity Na ion intercalation material, *Chem. Mater.* 25 (2013) 142–148, doi:10.1021/cm3029615.
- [11] A. Ponrouch, J. Bitenc, R. Dominko, N. Lindahl, P. Johansson, M.R. Palacin, Multivalent rechargeable batteries, *Energy Storage Mater.* 20 (2019) 253–262, doi:10.1016/j.ensm.2019.04.012.
- [12] J. Bitenc, N. Lindahl, A. Vizintin, M.E. Abdelhamid, R. Dominko, P. Johansson, Concept and electrochemical mechanism of an Al metal anode – organic cathode battery, *Energy Storage Mater* 24 (2020) 379–383, doi:10.1016/j.ensm.2019.07.033.
- [13] D. Aurbach, Z. Lu, A. Schechter, Y. Gofer, H. Gizar, R. Turgeman, Y. Cohen, M. Moshkovich, E. Levi, Prototype systems for rechargeable magnesium batteries, *Nature* 407 (2000) 724–727, doi:10.1038/35037553.
- [14] V. Verma, S. Kumar, W. Manalastas, R. Satish, M. Srinivasan, Progress in Rechargeable Aqueous Zinc- and Aluminum-Ion Battery Electrodes: Challenges and Outlook, *Adv. Sustain. Syst.* 3 (2019) 1800111, doi:10.1002/adsu.201800111.
- [15] J. Ming, J. Guo, C. Xia, W. Wang, H.N. Alshareef, Zinc-ion batteries: Materials, mechanisms, and applications, *Mater. Sci. Eng. R Rep.* 135 (2019) 58–84, doi:10.1016/j.mser.2018.10.002.
- [16] M. Vujković, B.S. Paunković, M. Mitrić, I. Stojković-Simatović, C.A.C. Sequeira, S. Mentus, Versatile insertion capability of $\text{Na}_{1.2}\text{V}_3\text{O}_8$ nanobelts in aqueous electrolyte solutions, *Electrochim. Acta.* 147 (2014) 167–175, doi:10.1016/j.electacta.2014.08.137.
- [17] M. Vujković, M. Mitrić, S. Mentus, High-rate intercalation capability of $\text{NaTi}_2(\text{PO}_4)_3/\text{C}$ composite in aqueous lithium and sodium nitrate solutions, *J. Power Sources.* (2015) 288, doi:10.1016/j.jpowsour.2015.04.132.
- [18] V. Pamoleras, P. Serras, I. Villaluenga, K.B. Hueso, J. González, T. Rojo, Na-ion batteries, recent advances and present challenges to become low cost energy storage systems, *Energy Environ. Sci.* 5 (2012) 5884–5901, doi:10.1039/c2ee02781j.
- [19] M. Balogun, Y. Luo, W. Qiu, P. Liu, Y. Tong, Review article A review of carbon materials and their composites with alloy metals for sodium ion battery anodes, *Carbon* 98 (2016) 162–178, doi:10.1016/j.carbon.2015.09.091.
- [20] C. Masquelier, L. Croguennec, Polyanionic (phosphates, silicates, sulfates) frameworks as Electrode Materials for rechargeable Li (or Na) Batteries, *Chem. Rev.* 113 (2013) 6552–6591, doi:10.1021/cr3001862.
- [21] C. Vaalma, D. Buchholz, M. Weil, S. Passerini, A cost and resource analysis of sodium-ion batteries, *Nat. Rev. Mater.* 3 (2018) 18013 doi:10.1038/natrevmats.2018.13.
- [22] L. Li, Y. Zheng, S. Zhang, J. Yang, Z. Shao, Z. Guo, Recent progress on sodium ion batteries: potential high-performance anodes, *Energy Environ. Sci.* 11 (2018) 2310–2340, doi:10.1039/c8ee01023d.
- [23] S. Kim, D. Seo, X. Ma, G. Ceder, K. Kang, Electrode Materials for Rechargeable Sodium-Ion Batteries: Potential Alternatives to Current Lithium-Ion Batteries, *Adv. Energy Mater.* 2 (2012) 710–721, doi:10.1002/aenm.201200026.
- [24] H. Pan, Y.S. Hu, L. Chen, R Room-temperature stationary sodium-ion batteries for large-scale electric energy storage, *Energy Environ. Sci.* 6 (2013) 2338–2360, doi:10.1039/c3ee40847g.
- [25] G.G. Eshetu, G.A. Elia, M. Armand, M. Forsyth, S. Kornaba, T. Rojo, S. Passerini, Electrolytes and interphases in sodium-based rechargeable batteries: Recent advances and perspectives, *Adv. Energy Mater.* 10 (2020) 2000093, doi:10.1002/aenm.202000093.
- [26] T. Perveen, M. Siddiq, N. Shahzad, R. Ihsan, A. Ahmad, M.I. Shahzad, Prospects in anode materials for sodium ion batteries - A review, *Renew. Sustain. Energy Rev.* 119 (2020) 109549, doi:10.1016/j.rser.2019.109549.
- [27] M. Chen, Q. Liu, S. Wang, E. Wang, X. Guo, High-Abundance and Low-Cost Metal-Based Cathode Materials for Sodium-Ion Batteries: Problems, Progress, and Key Technologies 9 (2019) 1803609, doi:10.1002/aenm.201803609.

- [28] Y. You, A. Manthiram, Progress in High-Voltage Cathode Materials for Rechargeable Sodium-Ion Batteries, *Adv. Energy Mater.* 8 (2017) 1701785, doi:10.1002/aenm.201701785.
- [29] Y.Y. Fang, J. Zhang, L. Xiao, X. Ai, Y. Cao, H. Yang, Phosphate framework electrode materials for sodium ion batteries, *Adv. Sci.* 4 (2017) 1600392, doi:10.1002/advs.201600392.
- [30] P. Barpanda, L. Lander, S. Nishimura, A. Yamada, Polyanionic insertion materials for sodium-ion batteries, *Adv. Energy Mater.* 8 (2018) 1703055, doi:10.1002/aenm.201703055.
- [31] M. Vujković, S. Mentus, Potentiodynamic and galvanostatic testing of $\text{NaFe}_{0.95}\text{V}_{0.05}\text{PO}_4/\text{C}$ composite in aqueous NaNO_3 solution, and the properties of aqueous $\text{Na}_{1.2}\text{V}_3\text{O}_8/\text{NaNO}_3/\text{NaFe}_{0.95}\text{V}_{0.05}\text{PO}_4/\text{C}$ battery, *J. Power Sources*. 325 (2016) 185–193, doi:10.1016/j.jpowsour.2016.06.031.
- [32] M. Vujković, S. Mentus, Fast sodiation/desodiation reactions of electrochemically delithiated olivine LiFePO_4 in aerated aqueous NaNO_3 solution, *J. Power Sources*. 247 (2014) 184–188, doi:10.1016/j.jpowsour.2013.08.062.
- [33] A.K. Padhi, K.S. Nanjundaswamy, J.B. Goodenough, Phospho-olivines as Positive-Electrode Materials for Rechargeable Lithium Batteries, *J. Electrochem. Soc.* 144 (1997) 1188–1194, doi:10.1149/1.1837571.
- [34] C. Masquelier, A.K. Padhi, K.S. Nanjundaswamy, J.B. Goodenough, New Cathode Materials for Rechargeable Lithium Batteries: The 3-D framework structures $\text{Li}_3\text{Fe}_2(\text{XO}_4)_3$ ($\text{X}=\text{P}, \text{As}$), *J. Solid State Chem.* 135 (1998) 228–234, doi:10.1006/jssc.1997.7629.
- [35] A.K. Padhi, K.S. Nanjundaswamy, C. Masquelier, S. Okada, J.B. Goodenough, Effect of structure on the $\text{Fe}^{3+}/\text{Fe}^{2+}$ redox couple in iron phosphates, *J. Electrochem. Soc.* 144 (1997) 1609–1613, doi:10.1149/1.1837649.
- [36] Y. Niu, Y. Zhang, M. Xu, A review on pyrophosphate framework cathode materials for sodium-ion batteries, *J. Mater. Chem. A* 7 (2019) 15006–15025, doi:10.1039/C9TA04274A.
- [37] D.V. Anishchenko, M.V. Zakharkin, V.A. Nikitina, K.J. Stevenson, E.V. Antipov, Phase boundary propagation kinetics predominately limit the rate capability of NASICON-type $\text{Na}_{3-x}\text{Mn}_x\text{V}_{2-x}(\text{PO}_4)_3$ ($0 \leq x \leq 1$) materials, *Electrochim. Acta*. 354 (2020) 136761, doi:10.1016/j.electacta.2020.136761.
- [38] M.V. Zakharkin, O.A. Drozhzhin, S.V. Ryzantsev, D. Chernyshov, M.A. Kirsanova, I.V. Mikheev, E.M. Pazhetnov, E.V. Antipov, K.J. Stevenson, Electrochemical properties and evolution of the phase transformation behavior in the NASICON-type $\text{Na}_{3-x}\text{Mn}_x\text{V}_{2-x}(\text{PO}_4)_3$ ($0 \leq x \leq 1$) cathodes for Na-ion batteries, *J. Power Sources*. 470 (2020) 228231, doi:10.1016/j.jpowsour.2020.228231.
- [39] A.J. Fernández-Ropero, D. Saurel, B. Acebedo, T. Rojo, M. Casas-Cabanas, Electrochemical characterization of NaFePO_4 as positive electrode in aqueous sodium-ion batteries, *J. Power Sources*. 291 (2015) 40–45, doi:10.1016/j.jpowsour.2015.05.006.
- [40] N.V. Kosova, V.R. Podugolnikov, E.T. Devyatkina, A.B. Slobodyuk, Structure and electrochemistry of NaFePO_4 and $\text{Na}_2\text{FePO}_4\text{F}$ cathode materials prepared via mechanochemical route, *Mater. Res. Bull.* 60 (2014) 849–857, doi:10.1016/j.matresbull.2014.09.081.
- [41] I.V. Tereshchenko, D.A. Aksonov, O.A. Drozhzhin, I.A. Presniakov, A.V. Sobolev, A. Zhugayevych, D. Striukov, K.J. Stevenson, E. Antipov, A.M. Abakumov, The Role of Semilabile Oxygen Atoms for Intercalation Chemistry of the Metal-Ion Battery Polyanion Cathodes, *J. Am. Chem. Soc.* 140 (2018) 3994–4003, doi:10.1021/jacs.7b12644.
- [42] M. Milović, D. Jugović, N. Cvjetičanin, D. Uskoković, A.S. Milošević, Z.S. Popović, F.R. Vukajlović, Crystal structure analysis and first principle investigation of F doping in LiFePO_4 , *J. Power Sources*. 241 (2013) 70–79, doi:10.1016/j.jpowsour.2013.04.109.
- [43] D. Jugović, M. Mitrić, M. Milović, N. Cvjetičanin, B. Jokić, A. Umićević, D. Uskoković, The influence of fluorine doping on the structural and electrical properties of the LiFePO_4 powder, *Ceram. Int.* 43 (2017) 3224–3230, doi:10.1016/j.ceramint.2016.11.149.
- [44] G. Longoni, J.E. Wang, Y.H. Jung, D.K. Kim, C.M. Mari, R. Ruffo, The Na_2FePO_4 -carbon nanotubes composite as high rate cathode material for sodium ion batteries, *J. Power Sources*. 302 (2016) 61–69, doi:10.1016/j.jpowsour.2015.10.033.
- [45] D. Jugović, M. Mitrić, M. Milović, V.N. Ivanovski, S. Škapin, B. Dojčinović, D. Uskoković, Structural and electrochemical properties of the $\text{Li}_2\text{FeP}_2\text{O}_7/\text{C}$ composite prepared using soluble methylcellulose, *J. Alloys Compd.* 786 (2019) 912–919, doi:10.1016/j.jallcom.2019.01.392.
- [46] F. Sanz, C. Parada, J.M. Rojo, C. Ruíz-Valero, Synthesis, structural characterization, magnetic properties, and ionic conductivity of $\text{Na}_4\text{M}^{\text{II}}_3(\text{PO}_4)_2(\text{P}_2\text{O}_7)$ ($\text{M}^{\text{II}} = \text{Mn}, \text{Co}, \text{Ni}$), *Chem. Mater.* 13 (2001) 1334–1340, doi:10.1021/cm001210d.
- [47] H. Kim, I. Park, D.H. Seo, S. Lee, S.W. Kim, W.J. Kwon, Y.U. Park, C.S. Kim, S. Jeon, K. Kang, New Iron-Based Mixed-Polyanion Cathodes for Lithium and Sodium Rechargeable Batteries: Combined First Principles Calculations and Experimental Study, *J. Am. Chem. Soc.* 134 (2012) 10369–10372, doi:10.1021/ja3038646.
- [48] F. Sanz, C. Parada, U. Amador, M.A. Monge, C. Ruíz-Valero, $\text{Na}_4\text{Co}_3(\text{PO}_4)_2\text{P}_2\text{O}_7$, a new sodium cobalt phosphate containing a three-dimensional system of large intersecting tunnels, *J. Solid State Chem.* 123 (1996) 129–139, doi:10.1006/jssc.1996.0161.
- [49] B. Senthilkumar, C. Murugesan, L. Sharma, S. Lochab, An overview of mixed polyanionic cathode materials for sodium-ion batteries, *Small Methods* 3 (2019) 1800253, doi:10.1002/smt.201800253.
- [50] X. Wu, G. Zhong, Y. Yang, Sol-gel synthesis of $\text{Na}_4\text{Fe}_3(\text{PO}_4)_2(\text{P}_2\text{O}_7)/\text{C}$ nanocomposite for sodium ion batteries and new insights into microstructural evolution during sodium extraction, *J. Power Sources*. 327 (2016) 666–674, doi:10.1016/j.jpowsour.2016.07.061.
- [51] A. Gutierrez, N.A. Benedek, A. Manthiram, Crystal-chemical guide for understanding redox energy variations of $\text{M}^{2+}/\text{M}^{3+}$ couples in polyanion cathodes for lithium-ion batteries, *Chem. Mater.* 25 (2013) 4010–4016, doi:10.1021/cm401949n.
- [52] P. Barpanda, G. Liu, C.D. Ling, M. Tamaru, M. Avdeev, S.C. Chung, Y. Yamada, A. Yamada, $\text{Na}_2\text{FeP}_2\text{O}_7$: A safe cathode for rechargeable sodium-ion batteries, *Chem. Mater.* 25 (2013) 3480–3487, doi:10.1021/cm401657c.
- [53] P. Barpanda, T. Ye, S. Nishimura, S. Chung, Y. Yamada, M. Okubo, H. Zhou, A. Yamada, Electrochemistry Communications, Sodium iron pyrophosphate: A novel 3.0 V iron-based cathode for sodium-ion batteries, *Electrochem. Commun.* 24 (2012) 116–119, doi:10.1016/j.elecom.2012.08.028.
- [54] M. Casas-Cabanas, V.V. Roddatis, D. Saurel, P. Kubiak, J. Carretero-González, V. Palomares, P. Serras, T. Rojo, Crystal chemistry of Na insertion/deinsertion in $\text{FePO}_4\text{-NaFePO}_4$, *J. Mater. Chem.* 22 (2012) 17421–17423, doi:10.1039/c2jm33639a.
- [55] N.V. Kosova, D.O. Rezepova, O.A. Podgornova, A.B. Slobodyuk, S.A. Petrov, M. Avdeev, A comparative study of structure, air sensitivity and electrochemistry of sodium iron pyrophosphates $\text{Na}_{2-x}\text{Fe}_{1+x}\text{P}_2\text{O}_7$ ($x = 0; 0.44$), *Electrochim. Acta* 235 (2017) 42–55, doi:10.1016/j.electacta.2017.03.058.
- [56] H. Kim, R.A. Shaloor, C. Park, S.Y. Lim, J.S. Kim, Y.N. Jo, W. Cho, K. Miyasaka, R. Kahraman, Y. Jung, J.W. Choi, $\text{Na}_2\text{FeP}_2\text{O}_7$ as a promising iron-based pyrophosphate cathode for sodium rechargeable batteries: A combined experimental and theoretical study, *Adv. Funct. Mater.* 23 (2013) 1147–1155, doi:10.1002/adfm.201201589.
- [57] J. Clark, P. Barpanda, A. Yamada, M.S. Islam, Sodium-ion battery cathodes $\text{Na}_2\text{FeP}_2\text{O}_7$ and $\text{Na}_2\text{MnP}_2\text{O}_7$, *J. Mater. Chem. A* 2 (2014) 11807–11812, doi:10.1039/c4ta02383h.
- [58] S.M. Wood, C. Bames, E. Kendrick, M.S. Islam, Sodium Ion Diffusion and Voltage Trends in Phosphates $\text{Na}_4\text{M}_3(\text{PO}_4)_2\text{P}_2\text{O}_7$ ($\text{M} = \text{Fe}, \text{Mn}, \text{Co}, \text{Ni}$) for Possible High-Rate Cathodes, *J. Phys. Chem. C* 119 (2015) 15935–15941, doi:10.1021/acs.jpcc.5b04648.
- [59] S.P. Ong, V.L. Chevrier, G. Hautier, A. Jain, C. Moore, S. Kim, X. Ma, G. Ceder, Voltage, stability and diffusion barrier differences between sodium-ion and lithium-ion intercalation materials, *Energy Environ. Sci.* 4 (2011) 3680–3688, doi:10.1039/c1ee01782a.
- [60] B.B.V. Chowdary, S. Chandana, B. Chaitanya, First-Principles Study of Olivine-Type NaMnPO_4 As Positive Electrode Materials for Rechargeable Sodium Ion Batteries, *Int. J. Adv. Res.* 5 (2017) 1298–1303, doi:10.21474/ijar01/3637.
- [61] R. Tripathi, S.M. Wood, M.S. Islam, L.F. Nazar, Na-Ion Mobility in Layered $\text{Na}_2\text{FePO}_4\text{F}$ and Olivine $\text{Na}[\text{Fe,Mn}]\text{PO}_4$, *Energy Environ. Sci.* 6 (2013) 2257–2264, doi:10.1039/C3EE40914G.
- [62] K.M. Bui, V.A. Dinh, S. Okada, T. Ohno, Hybrid functional study of the NASICON-type $\text{Na}_3\text{V}_2(\text{PO}_4)_3$: crystal and electronic structures, and polaron-Na vacancy complex diffusion, *Phys. Chem. Chem. Phys.* 17 (2015) 30433–30439, doi:10.1039/c5cp05323d.
- [63] X. Pu, H. Wang, T. Yuan, S. Cao, S. Liu, L. Xu, H. Yang, X. Ai, Z. Chen, Y. Cao, $\text{Na}_4\text{Fe}_3(\text{PO}_4)_2(\text{P}_2\text{O}_7)/\text{C}$ nanospheres as low-cost, high-performance cathode material for sodium-ion batteries, *Energy Storage Mater.* 22 (2019) 330–336, doi:10.1016/j.ensm.2019.02.017.
- [64] Y. Cao, X. Xia, Y. Liu, N. Wang, J. Zhang, D. Zhao, Y. Xia, Scalable synthesizing nanospherical $\text{Na}_4\text{Fe}_3(\text{PO}_4)_2(\text{P}_2\text{O}_7)$ growing on MCNTs as a high-performance cathode material for sodium-ion batteries, *J. Power Sources*. 461 (2020) 228130, doi:10.1016/j.jpowsour.2020.228130.
- [65] X. Deng, W. Shi, J. Sunarso, M. Liu, Z. Shao, A Green Route to a $\text{Na}_2\text{FePO}_4\text{F}$ -Based Cathode for Sodium Ion Batteries of High Rate and Long Cycling Life, *ACS Appl. Mater. Interfaces*. 9 (2017) 16280–16287, doi:10.1021/acsami.7b03933.
- [66] N. Böckenfeld, A. Balducci, Determination of sodium ion diffusion coefficients in sodium vanadium phosphate, *J. Solid State Electrochem.* 18 (2014) 959–964, doi:10.1007/s10008-013-2342-6.
- [67] P.R. Kumar, R. Essehli, H.B. Yahia, R. Amin, I. Belharouak, Electrochemical studies of a high voltage $\text{Na}_4\text{Co}_3(\text{PO}_4)_2\text{P}_2\text{O}_7$ -MWCNT composite through a selected stable electrolyte, *RSC Adv* 10 (2020) 15983–15989, doi:10.1039/d0ra02349c.
- [68] M. Nose, H. Nakayama, K. Nobuhara, H. Yamaguchi, S. Nakanishi, $\text{Na}_4\text{Co}_3(\text{PO}_4)_2\text{P}_2\text{O}_7$: A novel storage material for sodium-ion batteries, *J. Power Sources* 234 (2013) 175–179, doi:10.1016/j.jpowsour.2013.01.162.
- [69] M. Nose, S. Shiotani, H. Nakayama, K. Nobuhara, S. Nakanishi, H. Iba, $\text{Na}_4\text{Co}_2\text{Mn}_{0.3}\text{Ni}_{0.3}(\text{PO}_4)_2\text{P}_2\text{O}_7$: High potential and high capacity electrode material for sodium-ion batteries, *Electrochem. Commun.* 34 (2013) 266–269, doi:10.1016/j.elecom.2013.07.004.
- [70] H. Moriwake, A. Kuwabara, C.A.J. Fisher, M. Nose, H. Nakayama, S. Nakanishi, H. Iba, Y. Ikuhara, Crystal and electronic structure changes during the charge-discharge process of $\text{Na}_4\text{Co}_3(\text{PO}_4)_2\text{P}_2\text{O}_7$, *J. Power Sources*. 326 (2016) 220–225, doi:10.1016/j.jpowsour.2016.07.006.
- [71] H. Kim, I. Park, S. Lee, H. Kim, K.Y. Park, Y.U. Park, H. Kim, J. Kim, H.D. Lim, W.S. Yoon, K. Kang, Understanding the electrochemical mechanism of the new iron-based mixed-phosphate $\text{Na}_4\text{Fe}_3(\text{PO}_4)_2(\text{P}_2\text{O}_7)$ in a Na rechargeable battery, *Chem. Mater.* 25 (2013) 3614–3622, doi:10.1021/cm4013816.
- [72] S.M. Oh, S.T. Myung, J. Hassoun, B. Scrosati, Y.K. Sun, Reversible NaFePO_4 electrode for sodium secondary batteries, *Electrochem. Commun.* 22 (2012) 149–152, doi:10.1016/j.elecom.2012.06.014.
- [73] J. Kim, D.H. Seo, H. Kim, I. Park, J.K. Yoo, S.K. Jung, Y.U. Park, W.A. Goddard III, K. Kang, Unexpected discovery of low-cost maricite NaFePO_4 as a high-performance electrode for Na-ion batteries, *Energy Environ. Sci.* 8 (2015) 540–545, doi:10.1039/c4ee03215b.
- [74] S. Li, J. Guo, Z. Ye, X. Zhao, S. Wu, J.X. Mi, C.Z. Wang, Z. Gong, M.J. McDonald, Z. Zhu, K.M. Ho, Y. Yang, A Zero-Strain $\text{Na}_2\text{FeSiO}_4$ as Novel Cathode Mate-

- rial for Sodium-Ion Batteries, *ACS Appl. Mater. Interfaces*. 8 (2016) 17233–17238, doi:10.1021/acsmi.6b03969.
- [75] K. Saravanan, C.W. Mason, A. Rudola, K.H. Wong, P. Balaya, The first report on excellent cycling stability and superior rate capability of $\text{Na}_3\text{V}_2(\text{PO}_4)_3$ for sodium ion batteries, *Adv. Energy Mater.* 3 (2013) 444–450, doi:10.1002/aenm.201200803.
- [76] Y. Kawabe, N. Yabuuchi, M. Kajiyama, N. Fukuhara, T. Inamasu, R. Okuyama, I. Nakai, S. Komaba, Synthesis and electrode performance of carbon coated $\text{Na}_2\text{FePO}_4\text{F}$ for rechargeable Na batteries, *Electrochem. Commun.* 13 (2011) 1225–1228, doi:10.1016/j.elecom.2011.08.038.
- [77] H. Kim, G. Yoon, I. Park, K.Y. Park, B. Lee, J. Kim, Y.U. Park, S.K. Jung, H.D. Lim, D. Ahn, S. Lee, K. Kang, Anomalous Jahn-Teller behavior in a manganese-based mixed-phosphate cathode for sodium ion batteries, *Energy Environ. Sci.* 8 (2015) 3325–3335, doi:10.1039/c5ee01876e.
- [78] V. Priyanka, G. Savithiri, R. Subadevi, M. Sivakumar, An emerging electrochemically active maricite NaMnPO_4 as cathode material at elevated temperature for sodium-ion batteries, *Appl. Nanosci.* 10 (2020) 3945–3951, doi:10.1007/s13204-020-01506-8.
- [79] C.S. Park, H. Kim, R.A. Shaker, E. Yang, S.Y. Lim, R. Kahraman, Y. Jung, J.W. Choi, Anomalous manganese activation of a pyrophosphate cathode in sodium ion batteries: A combined experimental and theoretical study, *J. Am. Chem. Soc.* 135 (2013) 2787–2792, doi:10.1021/ja312044k.
- [80] X. Lin, X. Hou, X. Wu, S. Wang, M. Gao, Y. Yang, Exploiting $\text{Na}_2\text{MnPO}_4\text{F}$ as a high-capacity and well-reversible cathode material for Na-ion batteries, *RSC Adv* 4 (2014) 40985–40993, doi:10.1039/c4ra05336b.
- [81] M. Law, V. Ramar, P. Balaya, $\text{Na}_2\text{MnSiO}_4$ as an attractive high capacity cathode material for sodium-ion battery, *J. Power Sources*. 359 (2017) 277–284, doi:10.1016/j.jpowsour.2017.05.069.
- [82] A. Gutierrez, S. Kim, T.T. Fister, C.S. Johnson, Microwave-Assisted Synthesis of NaCoPO_4 Red-Phase and Initial Characterization as High Voltage Cathode for Sodium-Ion Batteries, *ACS Appl. Mater. Interfaces*. 9 (2017) 4391–4396, doi:10.1021/acsmi.6b14341.
- [83] P. Barpanda, J. Lu, T. Ye, M. Kajiyama, S.C. Chung, N. Yabuuchi, S. Komaba, A. Yamada, A layer-structured $\text{Na}_2\text{CoP}_2\text{O}_7$ pyrophosphate cathode for sodium-ion batteries, *RSC Adv* 3 (2013) 3857–3860, doi:10.1039/c3ra23026k.
- [84] J.C. Treacher, S.M. Wood, M.S. Islam, E. Kendrick, $\text{Na}_2\text{CoSiO}_4$ as a cathode material for sodium-ion batteries: Structure, electrochemistry and diffusion pathways, *Phys. Chem. Chem. Phys.* 18 (2016) 32744–32752, doi:10.1039/c6cp06777h.
- [85] K. Kubota, K. Yokoh, N. Yabuuchi, S. Komaba, $\text{Na}_2\text{CoPO}_4\text{F}$ as a High-voltage Batteries, Na-ion batteries, *Electrochemistry* 82 (2014) 909–911, doi:10.5796/electrochemistry.82.909.
- [86] S. Chakraborty, A. Banerjee, T. Watcharatharapong, R.B. Araujo, R. Ahuja, Current computational trends in polyanionic cathode materials for Li and Na batteries, *J. Phys. Condens. Matter Top.* 30 (2018) 283003, doi:10.1088/1361-648X/aac62d.
- [87] T. Jin, H. Li, K. Zhu, P.F. Wang, P. Liu, L. Jiao, Polyanion-type cathode materials for sodium-ion batteries, *Chem. Soc. Rev.* 49 (2020) 2342–2377, doi:10.1039/C9CS00846B.
- [88] J.Y. Sun, S.T. Myung, Y.K. Sun, Sodium-ion batteries: present and future, *Chem. Soc. Rev.* 46 (2017) 3529–3614, doi:10.1039/c6cs00776g.
- [89] Y. Fang, L. Xiao, Z. Chen, X. Ai, Y. Cao, H. Yang, Recent Advances in Sodium - Ion Battery Materials, *Electrochem. Energy Rev.* 1 (2018) 294–323, doi:10.1007/s41918-018-0008-x.
- [90] X. Pu, H. Wang, D. Zhao, H. Yang, X. Ai, S. Cao, Z. Chen, Y. Cao, Recent Progress in Rechargeable Sodium-Ion Batteries: toward High-Power Applications, *Small* 15 (2019) 1805427, doi:10.1002/sml.201805427.
- [91] D. Bin, F. Wang, A.G. Tamirat, L. Suo, Y. Wang, C. Wang, Y. Xia, Progress in Aqueous Rechargeable Sodium-Ion Batteries, *Advanced Energy Mater.* 8 (2018) 1703008, doi:10.1002/aenm.201703008.
- [92] S. Guo, J. Li, Q. Xu, Z. Ma, H. Xue, Recent achievements on polyanion-type compounds for sodium-ion batteries: Syntheses, crystal chemistry and electrochemical performance, *J. Power Sources*. 361 (2017) 285–299, doi:10.1016/j.jpowsour.2017.07.002.
- [93] Q. Ni, Y. Bai, F. Wu, C. Wu, Polyanion-Type Electrode Materials for Sodium-Ion Batteries, *Adv. Sci.* 4 (2017) 1600275, doi:10.1002/adv.201600275.
- [94] R. Liu, Z. Liang, Z. Gong, Y. Yang, Research Progress in Multielectron Reactions in Polyanionic Materials for Sodium-Ion Batteries, *Small* 3 (2018) 1800221, doi:10.1002/smt.201800221.
- [95] M. Zarrabaitia, M. Jáuregui, N. Sharma, J.C. Pramudita, M. Casas-Cabanas, $\text{Na}_4\text{Co}_3(\text{PO}_4)_2\text{P}_2\text{O}_7$ through Correlative Operando X-ray Diffraction and Electrochemical Impedance Spectroscopy, *Chem. Mater.* 31 (2019) 5152–5159, doi:10.1021/acscchemmater.9b01054.
- [96] H. Zhang, I. Hase, D. Buchholz, B. Qin, D. Geiger, S. Jeong, U. Kaiser, S. Passerini, Exploring the Ni redox activity in polyanionic compounds as conceivable high potential cathodes for Na rechargeable batteries, *NPG Asia Mater* 9 (2017) e370–e378, doi:10.1038/am.2017.41.
- [97] N.V. Kosova, V.A. Belotserkovsky, Sodium and mixed sodium/lithium iron orthopyrophosphates: Synthesis, structure and electrochemical properties, *Electrochim. Acta.* 278 (2018) 182–195, doi:10.1016/j.electacta.2018.05.034.
- [98] P.R. Kumar, H.B. Yahia, I. Belharouak, M.T. Sougrati, S. Passerini, R. Amin, R. Essehli, Electrochemical investigations of high-voltage $\text{Na}_4\text{Ni}_3(\text{PO}_4)_2\text{P}_2\text{O}_7$ cathode for sodium-ion batteries, *J. Solid State Electrochem.* 24 (2020) 17–24, doi:10.1007/s10008-019-04448-6.
- [99] M. Chen, W. Hua, J. Xiao, D. Cortie, W. Chen, E. Wang, Z. Hu, Q. Gu, X. Wang, S. Indris, S.L. Chou, S.X. Dou, NASICON-type air-stable and all-climate cathode for sodium-ion batteries with low cost and high-power density, *Nat. Commun.* 10 (2019) 1–11, doi:10.1038/s41467-019-09170-5.
- [100] L.N. Zhao, T. Zhang, H.L. Zhao, Y.L. Hou, Polyanion-type electrode materials for advanced sodium-ion batteries, *Mater. Today Nano.* 10 (2020) 100072, doi:10.1016/j.mtnano.2020.100072.
- [101] R. Essehli, B.El Bali, S. Benmokhtar, H. Fuess, I. Svoboda, S. Oubbadi, Synthesis, crystal structure and infrared spectroscopy of a new non-centrosymmetric mixed-anion phosphate $\text{Na}_4\text{Mg}_3(\text{PO}_4)_2(\text{P}_2\text{O}_7)_2$, *J. Alloys Compd.* 493 (2010) 654–660, doi:10.1016/j.jallcom.2009.12.181.
- [102] T. Yuan, Y. Wang, J. Zhang, X. Pu, X. Ai, Z. Chen, H. Yang, Y. Cao, 3D graphene decorated $\text{Na}_4\text{Fe}_3(\text{PO}_4)_2(\text{P}_2\text{O}_7)$ microspheres as low-cost and high-performance cathode materials for sodium-ion batteries, *Nano Energy* 56 (2019) 160–168, doi:10.1016/j.nanoen.2018.11.011.
- [103] N.V. Kosova, O.A. Podgornova, E.T. Devyatkina, V.R. Podugolnikov, S.A. Petrov, Effect of Fe^{2+} substitution on the structure and electrochemistry of LiCoPO_4 prepared by mechanochemically assisted carbothermal reduction, *J. Mater. Chem. A.* 2 (2014) 20697–20705, doi:10.1039/c4ta04221b.
- [104] H. Zhou, S. Upreti, N.A. Chernova, G. Hautier, G. Ceder, M.S. Whittingham, Iron and manganese pyrophosphates as cathodes for lithium-ion batteries, *Chem. Mater.* 23 (2011) 293–300, doi:10.1021/cm102922q.
- [105] N.V. Kosova, A.M. Tsapina, A.B. Slobodyuk, S.A. Petrov, Structure and electrochemical properties of mixed transition-metal pyrophosphates $\text{Li}_2\text{Fe}_{1-y}\text{Mn}_y\text{P}_2\text{O}_7$ ($0 \leq y \leq 1$), *Electrochim. Acta.* 174 (2015) 1278–1289, doi:10.1016/j.electacta.2015.06.070.
- [106] B. Senthilkumar, G. Ananya, P. Ashok, S. Ramaprabhu, Synthesis of Carbon coated $\text{Nano-Na}_4\text{Ni}_3(\text{PO}_4)_2\text{P}_2\text{O}_7$ as a Novel Cathode Material for Hybrid Supercapacitors, *Electrochim. Acta.* 169 (2015) 447–455, doi:10.1016/j.electacta.2015.04.088.
- [107] X. Ma, X. Wu, P. Shen, Rational Design of $\text{Na}_4\text{Fe}_3(\text{PO}_4)_2(\text{P}_2\text{O}_7)$ Nanoparticles Embedded in Graphene: Toward Fast Sodium Storage Through the Pseudocapacitive Effect, *ACS Appl. Energy Mater.* 1 (2018) 6268–6278, doi:10.1021/acsaem.8b01275.
- [108] L. Tang, X. Liu, Z. Li, X. Pu, J. Zhang, Q. Xu, H. Liu, Y.G. Wang, Y. Xia, CNT-Decorated $\text{Na}_4\text{Mn}_2\text{Co}(\text{PO}_4)_2\text{P}_2\text{O}_7$ Microspheres as a Novel High-Voltage Cathode Material for Sodium-Ion Batteries, *ACS Appl. Mater. Interfaces* 11 (2019) 27813–27822, doi:10.1021/acsmi.9b07595.
- [109] M. Nose, K. Nobuhara, S. Shiotani, H. Nakayama, S. Nakanishi, H. Iba, Electrochemical Li^+ insertion capabilities of $\text{Na}_{4-x}\text{Co}_3(\text{PO}_4)_2\text{P}_2\text{O}_7$ and its application to novel hybrid-ion batteries, *RSC Adv* 4 (2014) 9044–9047, doi:10.1039/c3ra45836a.
- [110] S. Nakanishi, M. Nose, H. Nakayama, H. Iba, Study of New Active Materials for Rechargeable Sodium-Ion Batteries, *Adv. Sci. Technol.* 93 (2014) 137–145, doi:10.4028/www.scientific.net/ast.93.137.
- [111] X. Liu, L. Tang, Z. Li, J. Zhang, Q. Xu, H. Liu, Y. Wang, Y. Xia, Y. Cao, X. Ai, An Al-doped high voltage cathode of $\text{Na}_4\text{Co}_3(\text{PO}_4)_2\text{P}_2\text{O}_7$ enabling highly stable 4 V full sodium-ion batteries, *J. Mater. Chem. A.* 7 (2019) 18940–18949, doi:10.1039/c9ta04450g.
- [112] J.Y. Jang, H. Kim, Y. Lee, K.T. Lee, K. Kang, N.S. Choi, Cyclic carbonate based-electrolytes enhancing the electrochemical performance of $\text{Na}_4\text{Fe}_3(\text{PO}_4)_2(\text{P}_2\text{O}_7)$ cathodes for sodium-ion batteries, *Electrochem. Commun.* 44 (2014) 74–77, doi:10.1016/j.elecom.2014.05.003.
- [113] N.V. Kosova, A.A. Shindrov, Effect of Mixed Li^+/Na^+ -ion Electrolyte on electrochemical performance of $\text{Na}_4\text{Fe}_3(\text{PO}_4)_2(\text{P}_2\text{O}_7)$ in hybrid batteries, *Batteries* 5 (2019) 39, doi:10.3390/batteries5020039.
- [114] A.J. Fernández-Ropero, M. Zarrabaitia, M. Reynaud, T. Rojo, M. Casas-Cabanas, Toward Safe and Sustainable Batteries: $\text{Na}_4\text{Fe}_3(\text{PO}_4)_2(\text{P}_2\text{O}_7)$ as a Low-Cost Cathode for Rechargeable Aqueous Na-Ion Batteries, *J. Phys. Chem. C* 122 (2018) 133–142, doi:10.1021/acs.jpcc.7b09803.
- [115] M.H. Lee, S.J. Kim, D. Chang, J. Kim, S. Moon, K. Oh, K.Y. Park, W.M. Seong, H. Park, G. Kwon, B. Lee, K. Kang, Toward a low-cost high-voltage sodium aqueous rechargeable battery, *Mater. Today*. 29 (2019) 26–36, doi:10.1016/j.mattod.2019.02.004.
- [116] S. Baskar, R. Angalakuthi, C. Murugesan, S.B. Krupanidhi, P. Barpanda, Exploration of Iron-Based Mixed Polyanion Cathode Material for Thin-Film Sodium-Ion Batteries, *ECS Trans* 85 (2018) 227–234, doi:10.1149/08513.0227ecst.
- [117] B. Senthilkumar, A. Rambabu, C. Murugesan, S.B. Krupanidhi, P. Barpanda, Iron-Based Mixed Phosphate $\text{Na}_4\text{Fe}_3(\text{PO}_4)_2(\text{P}_2\text{O}_7)$ Thin Films for Sodium-Ion Microbatteries, *ACS Omega* 5 (2020) 7219–7224, doi:10.1021/acsomega.9b03835.
- [118] K. Sada, C. Murugesan, S. Baskar, P. Barpanda, Potassium Intercalation into Sodium Metal Oxide and Polyanionic Hosts: Few Case Studies, *ECS Trans* 85 (2018) 207–214, doi:10.1149/08513.0207ecst.
- [119] X. Ma, Z. Pan, X. Wu, P.K. Shen, $\text{Na}_4\text{Fe}_3(\text{PO}_4)_2(\text{P}_2\text{O}_7)$ @ NaFePO_4 @C core-double-shell architectures on carbon cloth: A high-rate, ultrastable, and flexible cathode for sodium ion batteries, *Chem. Eng. J.* 365 (2019) 132–141, doi:10.1016/j.cej.2019.01.173.
- [120] F. Sanz, C. Parada, J.M. Rojo, C. Ruiz-Valero, Crystal structure, magnetic properties, and ionic conductivity of a new mixed-anion phosphate $\text{Na}_4\text{Ni}_3(\text{PO}_4)_2(\text{P}_2\text{O}_7)_2$, *Chem. Mater.* 11 (1999) 2673–2679, doi:10.1021/cm981105a.
- [121] S. Ryu, J.E. Wang, J.H. Kim, R. Ruffo, Y.H. Jung, D.K. Kim, A study on cobalt substitution in sodium manganese mixed-anion phosphates as positive electrode materials for Na-ion batteries, *J. Power Sources*. 444 (2019) 227274, doi:10.1016/j.jpowsour.2019.227274.
- [122] F. Zou, A. Manthiram, A Review of the Design of Advanced Binders for High-Performance Batteries, *Adv. Energy Mater.* 10 (2020) 1–28, doi:10.1002/aenm.202002508.
- [123] D. Bresser, D. Buchholz, A. Moretti, A. Varzi, S. Passerini, Alternative binders for sustainable electrochemical energy storage—the transition to aqueous electrode processing and bio-derived polymers, *Energy Environ. Sci.* 11 (2018) 3096–3127, doi:10.1039/c8ee00640g.

- [124] I. Kovalenko, B. Zdyrko, A. Magasinski, B. Hertzberg, Z. Milicev, R. Burtovyy, I. Luzinov, G. Yushin, A major constituent of brown algae for use in high-capacity Li-ion batteries, *Science* 334 (2011) 75–79, doi:10.1126/science.1209150.
- [125] P.R. Kumar, Y.H. Jung, S.A. Ahad, D.K. Kim, A high rate and stable electrode consisting of a $\text{Na}_3\text{V}_2\text{O}_{2x}(\text{PO}_4)_2\text{F}_{3-2x}$ -rGO composite with a cellulose binder for sodium-ion batteries, *RSC Adv* 7 (2017) 21820–21826, doi:10.1039/c7ra01047h.
- [126] J. Zhao, X. Yang, Y. Yao, Y. Gao, Y. Sui, B. Zou, H. Ehrenberg, G. Chen, F. Du, Moving to Aqueous Binder: A Valid Approach to Achieving High-Rate Capability and Long-Term Durability for Sodium-Ion Battery, *Adv. Sci.* 5 (2018) 1700768, doi:10.1002/advs.201700768.
- [127] T. Jin, Q. Han, L. Jiao, Binder-Free Electrodes for Advanced Sodium-Ion Batteries, *Adv. Mater.* 32 (2020) 1806304, doi:10.1002/adma.201806304.
- [128] H. Li, M. Xu, Z. Zhang, Y. Lai, J. Ma, Engineering of Polyanion Type Cathode Materials for Sodium-Ion Batteries: Toward Higher Energy/Power Density, *Adv. Funct. Mater.* 30 (2020) 2000473, doi:10.1002/adfm.202000473.
- [129] T. Jin, Y. Liu, Y. Li, K. Cao, X. Wang, L. Jiao, Electrospun $\text{NaVPO}_4\text{F}/\text{C}$ Nanofibers as Self-Standing Cathode Material for Ultralong Cycle Life Na-Ion Batteries, *Adv. Energy Mater.* 7 (2017) 1700087, doi:10.1002/aenm.201700087.
- [130] Q. Ni, Y. Bai, Y. Li, L. Ling, L. Li, G. Chen, Z. Wang, H. Ren, F. Wu, C. Wu, 3D Electronic Channels Wrapped Large-Sized $\text{Na}_3\text{V}_2(\text{PO}_4)_3$ as Flexible Electrode for Sodium-Ion Batteries, *Small* 14 (2018) 1702864, doi:10.1002/smll.201702864.
- [131] K. Kretschmer, B. Sun, J. Zhang, X. Xie, H. Liu, G. Wang, 3D Interconnected Carbon Fiber Network-Enabled Ultralong Life $\text{Na}_3\text{V}_2(\text{PO}_4)_3$ @Carbon Paper Cathode for Sodium-Ion Batteries, *Small* 13 (2017) 1603318, doi:10.1002/smll.201603318.
- [132] D. Guo, J. Qin, Z. Yin, J. Bai, Y.K. Sun, M. Cao, Achieving high mass loading of $\text{Na}_3\text{V}_2(\text{PO}_4)_3$ @carbon on carbon cloth by constructing three-dimensional network between carbon fibers for ultralong cycle-life and ultrahigh rate sodium-ion batteries, *Nano Energy* 45 (2018) 136–147, doi:10.1016/j.nanoen.2017.12.038.
- [133] H.J. Song, D.S. Kim, J.C. Kim, S.H. Hong, D.W. Kim, An approach to flexible Na-ion batteries with exceptional rate capability and long lifespan using $\text{Na}_3\text{Fe}_2\text{O}_7$ nanoparticles on porous carbon cloth, *J. Mater. Chem. A* 5 (2017) 5502–5510, doi:10.1039/c7ta00727b.
- [134] D. Chao, C.H.M. Lai, P. Liang, Q. Wei, Y.S. Wang, C.R. Zhu, G. Deng, V.V.T. Doan-Nguyen, J. Lin, L. Mai, H.J. Fan, B. Dunn, Z.X. Shen, Sodium Vanadium Fluorophosphates (NVOPF) Array Cathode Designed for High-Rate Full Sodium Ion Storage Device, *Adv. Energy Mater.* 8 (2018) 1–8, doi:10.1002/aenm.201800058.
- [135] K. Pfeifer, S. Arnold, J. Becherer, C. Das, J. Maibach, H. Ehrenberg, S. Dsoke, Can Metallic Sodium Electrodes Affect the Electrochemistry of Sodium-Ion Batteries? Reactivity Issues and Perspectives, *ChemSusChem* 12 (2019) 3312–3319, doi:10.1002/cssc.201901056.
- [136] S. Komaba, T. Ishikawa, N. Yabuuchi, W. Murata, A. Ito, Y. Ohsawa, Fluorinated ethylene carbonate as electrolyte additive for rechargeable Na batteries, *ACS Appl. Mater. Interfaces* 3 (2011) 4165–4168, doi:10.1021/am200973k.
- [137] S. Komaba, W. Murata, T. Ishikawa, N. Yabuuchi, T. Ozeki, T. Nakayama, A. Ogata, K. Gotoh, K. Fujiwara, Electrochemical Na insertion and solid electrolyte interphase for hard-carbon electrodes and application to Na-ion batteries, *Adv. Funct. Mater.* 21 (2011) 3859–3867, doi:10.1002/adfm.201100854.
- [138] L. Wu, D. Buchholz, D. Bressler, L. Gomes Chagas, S. Passerini, Anatase TiO_2 nanoparticles for high power sodium-ion anodes, *J. Power Sources* 251 (2014) 379–385, doi:10.1016/j.jpowsour.2013.11.083.
- [139] M. Dahbi, T. Nakano, N. Yabuuchi, T. Ishikawa, K. Kubota, M. Fukunishi, S. Shibahara, J.Y. Son, Y.T. Cui, H. Oji, S. Komaba, Sodium carboxymethyl cellulose as a potential binder for hard-carbon negative electrodes in sodium-ion batteries, *Electrochim. Commun.* 44 (2014) 66–69, doi:10.1016/j.elecom.2014.04.014.
- [140] J. Lee, Y. Lee, J. Lee, S.M. Lee, J.H. Choi, H. Kim, M.S. Kwon, K. Kang, K.T. Lee, N.S. Choi, Ultraconcentrated sodium Bis(fluorosulfonyl)imide-based electrolytes for High-Performance Sodium metal batteries, *ACS Appl. Mater. Interfaces* 9 (2017) 3723–3732, doi:10.1021/acsami.6b14878.
- [141] Y. Lee, J. Lee, H. Kim, K. Kang, N.S. Choi, Highly stable linear carbonate-containing electrolytes with fluoroethylene carbonate for high-performance cathodes in sodium-ion batteries, *J. Power Sources* 320 (2016) 49–58, doi:10.1016/j.jpowsour.2016.04.070.
- [142] V. Dall'Asta, D. Buchholz, L.G. Chagas, X. Dou, C. Ferrara, E. Quartarone, C. Tealdi, S. Passerini, Aqueous Processing of $\text{Na}_0.44\text{MnO}_2$ Cathode Material for the Development of Greener Na-Ion Batteries, *ACS Appl. Mater. Interfaces* 9 (2017) 34891–34899, doi:10.1021/acsami.7b09464.
- [143] C. Yang, J. Chen, T. Qing, X. Fan, W. Sun, A. von Cresce, M.S. Ding, O. Borodin, J. Vatamanu, M.A. Schroeder, N. Eidson, C. Wang, K. Xu, 4.0 V Aqueous Li-Ion Batteries, *Joule* 1 (2017) 122–132, doi:10.1016/j.joule.2017.08.009.
- [144] Y. Wang, S. Song, C. Xu, N. Hu, J. Molenda, L. Lu, Development of solid-state electrolytes for sodium-ion battery—A short review, *Nano Mater. Sci.* 1 (2019) 91–100, doi:10.1016/j.nanoms.2019.02.007.
- [145] Y. Noguchi, E. Kobayashi, L.S. Plashnitsa, S. Okada, J.I. Yamaki, Fabrication and performances of all solid-state symmetric sodium battery based on NASICON-related compounds, *Electrochim. Acta* 101 (2013) 59–65, doi:10.1016/j.electacta.2012.11.038.
- [146] F. Lalère, J.B. Leriche, M. Courty, S. Boulineau, V. Viallet, C. Masquelier, V. Seznec, An all-solid state NASICON sodium battery operating at 200°C, *J. Power Sources* 247 (2014) 975–980, doi:10.1016/j.jpowsour.2013.09.051.
- [147] W. Zhou, Y. Li, S. Xin, J.B. Goodenough, Rechargeable Sodium All-Solid-State Battery, *ACS Cent. Sci.* 3 (2017) 52–57, doi:10.1021/acscentsci.6b00321.
- [148] R. Asakura, D. Reber, L. Duchêne, S. Payandeh, A. Remhof, H. Hagemann, C. Battaglia, 4 V Room-Temperature All-Solid-State Sodium Battery Enabled By a Passivating Cathode/Hydroborate Solid Electrolyte Interface, *Energy Environ. Sci.* 13 (2020) 5048–5058, doi:10.1039/d0ee01569e.
- [149] L. Qiao, X. Judez, T. Rojo, M. Armand, H. Zhang, Review—Polymer Electrolytes for Sodium Batteries, *J. Electrochem. Soc.* 167 (2020) 070534, doi:10.1149/1945-7111/ab7aa0.
- [150] C. Zhao, L. Liu, Y. Lu, M. Wagemaker, L. Chen, Y.S. Hu, Revealing an Interconnected Interfacial Layer in Solid-State Polymer Sodium Batteries, *Angew. Chemie - Int. Ed.* 58 (2019) 17026–17032, doi:10.1002/anie.201909877.
- [151] J.K. Kim, Y.J. Lim, H. Kim, G.B. Cho, Y. Kim, A hybrid solid electrolyte for flexible solid-state sodium batteries, *Energy Environ. Sci.* 8 (2015) 3589–3596, doi:10.1039/c5ee01941a.
- [152] A. Langrock, Y. Xu, Y. Liu, S. Ehrman, A. Manivannan, C. Wang, Carbon coated hollow $\text{Na}_2\text{FePO}_4\text{F}$ spheres for Na-ion battery cathodes, *J. Power Sources* 223 (2013) 62–67, doi:10.1016/j.jpowsour.2012.09.059.
- [153] L. Wu, Y. Hu, X. Zhang, J. Liu, X. Zhu, S. Zhong, Synthesis of carbon-coated $\text{Na}_2\text{MnPO}_4\text{F}$ hollow spheres as a potential cathode material for Na-ion batteries, *J. Power Sources* 374 (2018) 40–47, doi:10.1016/j.jpowsour.2017.11.029.
- [154] J. Mao, C. Luo, T. Gao, X. Fan, C. Wang, Scalable synthesis of $\text{Na}_3\text{V}_2(\text{PO}_4)_3/\text{C}$ porous hollow spheres as a cathode for Na-ion batteries, *J. Mater. Chem. A* 3 (2015) 10378–10385, doi:10.1039/c5ta01007a.
- [155] Y. Fang, L. Xiao, X. Ai, Y. Cao, H. Yang, Hierarchical Carbon Framework Wrapped $\text{Na}_3\text{V}_2(\text{PO}_4)_3$ as a Superior High-Rate and Extended Lifespan Cathode for Sodium-Ion Batteries, *Adv. Mater.* 27 (2015) 5895–5900, doi:10.1002/adma.201502018.
- [156] Y. Liu, N. Zhang, F. Wang, X. Liu, L. Jiao, L.Z. Fan, Approaching the Downsizing Limit of Maricite NaFePO_4 toward High-Performance Cathode for Sodium-Ion Batteries, *Adv. Funct. Mater.* 28 (2018) 1–9, doi:10.1002/adfm.201801917.
- [157] J.Z. Guo, P.F. Wang, X.L. Wu, X.H. Zhang, Q. Yan, H. Chen, J.P. Zhang, Y.G. Guo, High-Energy/Power and Low-Temperature Cathode for Sodium-Ion Batteries: In Situ XRD Study and Superior Full-Cell Performance, *Adv. Mater.* 29 (2017) 1–8, doi:10.1002/adma.201701968.
- [158] T. Broux, F. Fauth, N. Hall, Y. Chatillon, M. Bianchini, T. Barnine, J.B. Leriche, E. Suard, D. Carlier, Y. Reynier, L. Simonin, C. Masquelier, L. Croguennec, High Rate Performance for Carbon-Coated $\text{Na}_3\text{V}_2(\text{PO}_4)_2\text{F}_3$ in Na-Ion Batteries, *Small Methods* 3 (2019) 1–12, doi:10.1002/smt.201800215.
- [159] G. Yan, S. Mariyappan, G. Rouse, Q. Jacquet, M. Deschamps, R. David, B. Mirvaux, J.W. Freeland, J.M. Tarascon, Higher energy and safer sodium ion batteries via an electrochemically made disordered $\text{Na}_3\text{V}_2(\text{PO}_4)_2\text{F}_3$ material, *Nat. Commun.* 10 (2019), doi:10.1038/s41467-019-08359-y.
- [160] B. Ali, A. ur-Rehman, F. Ghafoor, M.I. Shahzad, S.K. Shah, S.M. Abbas, Interconnected mesoporous $\text{Na}_2\text{FeSiO}_4$ nanospheres supported on carbon nanotubes as a highly stable and efficient cathode material for sodium-ion battery, *J. Power Sources* 396 (2018) 467–475, doi:10.1016/j.jpowsour.2018.06.049.
- [161] F. Li, Z. Zhou, Micro/Nanostructured Materials for Sodium Ion Batteries and Capacitors, *Small* 14 (2018) 1–25, doi:10.1002/smll.201702961.
- [162] H. Li, L. Peng, Y. Zhu, D. Chen, X. Zhang, G. Yu, An advanced high-energy sodium ion full battery based on nanostructured $\text{Na}_2\text{Ti}_3\text{O}_7/\text{VOPO}_4$ layered materials, *Energy Environ. Sci.* 9 (2016) 3399–3405, doi:10.1039/c6ee00794e.
- [163] N. Wang, Z. Bai, Y. Qian, J. Yang, Double-Walled Sb@ TiO_2 -xNanotubes as a Superior High-Rate and Ultralong-Lifespan Anode Material for Na-Ion and Li-Ion Batteries, *Adv. Mater.* 28 (2016) 4126–4133, doi:10.1002/adma.201505918.
- [164] W. Ren, X. Yao, C. Niu, Z. Zheng, K. Zhao, Q. An, Q. Wei, M. Yan, L. Zhang, L. Mai, Cathodic polarization suppressed sodium-ion full cell with a 3.3 V high-voltage, *Nano Energy* 28 (2016) 216–223, doi:10.1016/j.nanoen.2016.08.010.
- [165] X. Liang, X. Ou, F. Zheng, Q. Pan, X. Xiong, R. Hu, C. Yang, M. Liu, Surface Modification of $\text{Na}_3\text{V}_2(\text{PO}_4)_3$ by Nitrogen and Sulfur Dual-Doped Carbon Layer with Advanced Sodium Storage Property, *ACS Appl. Mater. Interfaces* 9 (2017) 13151–13162, doi:10.1021/acsami.7b00818.
- [166] B. Zhang, R. Dugas, G. Rouse, P. Rozier, A.M. Abakumov, J.M. Tarascon, Insertion compounds and composites made by ball milling for advanced sodium-ion batteries, *Nat. Commun.* 7 (2016) 1–9, doi:10.1038/ncomms10308.
- [167] R. Thangavel, K. Kaliyappan, K. Kang, X. Sun, Y.S. Lee, Going beyond Lithium Hybrid Capacitors: Proposing a New High-Performing Sodium Hybrid Capacitor System for Next-Generation Hybrid Vehicles Made with Bio-Inspired Activated Carbon, *Adv. Energy Mater.* 6 (2016) 1–9, doi:10.1002/aenm.201502199.
- [168] R. Thangavel, B. Moorthy, D.K. Kim, Y.S. Lee, Pushing the Energy Output and Cyclability of Sodium Hybrid Capacitors at High Power to New Limits, *Adv. Energy Mater.* 7 (2017) 1–10, doi:10.1002/aenm.201602654.



An effective approach to reaching the theoretical capacity of a low-cost and environmentally friendly $\text{Na}_4\text{Fe}_3(\text{PO}_4)_2(\text{P}_2\text{O}_7)$ cathode for Na-ion batteries

Aleksandra Gezović^a, Miloš Milović^b, Danica Bajuk-Bogdanović^c, Veselinka Grudić^a, Robert Dominko^{d,e}, Slavko Mentus^{c,f}, Milica J. Vujković^{c,g,*}

^a Faculty of Metallurgy and Technology, University of Montenegro, Cetinjski put bb, 81000 Podgorica, Montenegro

^b Institute of Technical Sciences of SASA, Knez Mihajlova 35/IV, 11000, Belgrade, Serbia

^c University of Belgrade - Faculty of Physical Chemistry, Studentski trg 12-14, Belgrade, Serbia

^d National Institute of Chemistry, Hajdrihova 19, SI-1000 Ljubljana, Slovenia

^e FKKT, University of Ljubljana, Večna pot 117, 1000 Ljubljana, Slovenia

^f Serbian Academy of Sciences and Arts, Knez Mihajlova 35, 11158 Belgrade, Serbia

^g Center for Interdisciplinary and Multidisciplinary Studies, University of Montenegro, Podgorica, Montenegro

ARTICLE INFO

Keywords:

$\text{Na}_4\text{Fe}_3(\text{PO}_4)_2(\text{P}_2\text{O}_7)$

$\text{Na}_2\text{FeP}_2\text{O}_7$ secondary phase

Sol-gel synthesis

The critical role of pH

Na-ion batteries

ABSTRACT

$\text{M}_4\text{Fe}_3(\text{PO}_4)_2(\text{P}_2\text{O}_7)$ specific family has appeared as a new class of polyanionic compounds for sodium-ion batteries, capable of offering a higher operating voltage than individual phosphates and pyrophosphates. The study addresses the issue of $\text{Na}_4\text{Fe}_3(\text{PO}_4)_2\text{P}_2\text{O}_7$ (NFPP) sol-gel synthesis when both phosphates and pyrophosphates act as reactants, leading to successful production of NFPP under controlled synthesis conditions, capable of reaching the theoretical capacity. Spontaneous citric-assisted sol-gel reaction, between PO_4^{3-} and $\text{P}_2\text{O}_7^{2-}$ units occurring at pH of 3 (which follows NFPP stoichiometry), leads to the formation of pyrophosphate ($\text{Na}_2\text{FeP}_2\text{O}_7$, NFP) with a certain amount of the mixed phase. Fe-oxalate coordination is dominant at low pH while the citric acid protonation suppresses direct Fe-citric complexation. pH adjustment to a neutral value changes the complexation and reaction pathway, allowing direct Fe(II)-citric coordination and subsequent oxidation. The exchange of Fe-oxalate with the soluble ferric ammonium citrate complex happens under neutral pH and therefore leads to the formation of NFPP as the dominant phase, liberated from NFP. Furthermore, a series of samples, developed by varying citric-to-Fe molar ratio and controlling pH, served as a platform to identify and solve problems regarding the unambiguous FTIR assignment of the polyanionic NFP/NFPP mixture. FTIR and CV methods are proposed as assisting tools for XRD to identify NFP admixture. Finally, and most importantly, NFPP phase formed under neutral pH has a higher sodiation/desodiation capacity than NFPP/NFP heterostructure, reaching a theoretical value at a rather high current of 1 A g^{-1} , which has not been attained in the literature.

1. Introduction

Huge demand for green and renewable energy resources has launched the expansion of electrochemical energy storage technology, where high-energy Li-ion batteries take over the leading role [1]. Nevertheless, limited lithium resources related to its high cost and difficulties in extraction and recycling procedures, are shifting research interests towards safer and more sustainable developments [2,3]. Post-lithium ion batteries, based on Earth-abundant elements, play a rising role in the energy storage field, where huge interests are focused on Na-ion rechargeable batteries, due to the low cost and abundance of sodium [4–7].

Three classes of materials, namely sodium transition metal oxides, Prussian blue analogues and polyanionic materials have been extensively investigated to solve the cathode issue of Na-ion batteries and make them competitive with Li-ion technology. Polyanionic-type structures may enable rapid diffusion for Na^+ ions with sufficient structural stability due to a three-dimensional framework, built on tetrahedral anions $(\text{XO}_4)^n^-$ or their derivatives $(\text{X}_m\text{O}_{3m+1})^n^-$ ($\text{X} = \text{P}, \text{Si}, \text{S}, \text{Se}, \text{Mo}, \text{W}, \dots$) corner- or edge-shared with MO_6 polyhedrons ($\text{M} =$ transition metal) [8–12]. A combination of different polyanion units, so-called "anions engineering" [13] was found as an operative way to tune the redox properties of polyanionic cathode and develop new structures that match Li insertion materials. A specific family of

* Corresponding author at: Milica Vujković, University of Belgrade - Faculty of Physical Chemistry, Studentski trg 12–14, 11158 Belgrade, Serbia
E-mail address: milica.vujkovic@ffh.bg.ac.rs (M.J. Vujković).

isostructural polyanions with mixed phosphate and pyrophosphate structural units $\text{Na}_4\text{M}_3(\text{PO}_4)_2(\text{P}_2\text{O}_7)$, determined by Sanc et al [14,15], have attracted attention as novel Na-ion cathodes due to lower barrier for Na-ion diffusion, low volume changes during cycling and higher redox potential over individual phosphate and pyrophosphate compounds [16,17]. For instance, the $\text{Fe}^{2+}/\text{Fe}^{3+}$ redox potential increases in the order FePO_4 , NaFePO_4 , $\text{Na}_2\text{FeP}_2\text{O}_7$, or $\text{Na}_2\text{FePO}_4\text{F}$, amounting to 2.4, 2.7, 3.0 and 3.2 V vs. Na^+/Na , while the volume changes of approximately 4%, 2% and 17% follow $\text{Na}_4\text{Fe}_3(\text{PO}_4)_2\text{P}_2\text{O}_7$, $\text{Na}_2\text{FeP}_2\text{O}_7$ and NaFePO_4 , respectively [6].

Kim and coworkers [16,17] have proposed $\text{Na}_4\text{Fe}_3(\text{PO}_4)_2(\text{P}_2\text{O}_7)$ (NFPP) with the orthorhombic crystal structure (Pn21 a space group) as a promising mixed polyanionic cathode for SIBs, using solid-state synthesis with the ball-milling assistance. Its theoretical capacity was calculated per 3 Na^+ ions and amounts to 129 mAh g^{-1} . Several authors [18–22] have used Kim's procedure to improve the sodium storage performance of the mixed polyanionic phase with different modification strategies [18,19,22] and electrolyte formulations [20,21]. Various synthesis procedures including sol-gel [23–25], solution-combustion [26], template [27] and spray-drying methods [28–31] have also been developed. Their survey can be found in our recent review paper [6], where we elaborated on certain difficulties related to the NFPP synthesis and parameters affecting the phase composition. Namely, the individual phosphates ($\text{Na}_2\text{FeP}_2\text{O}_7$) and pyrophosphates (NaFePO_4) are usually obtained as accompanied phases for this type of compound. Through the introduction of Fe defects into the NFPP framework to the composition of $\text{Na}_4\text{Fe}_{2.91}(\text{PO}_4)_2\text{P}_2\text{O}_7$ Zhao et al [32] found an effective way to avoid impurities and obtain a pure phase with improved properties. Unlike the solid-state method, which usually used $\text{Na}_4\text{P}_2\text{O}_7$ and $\text{NH}_4\text{H}_2\text{PO}_4$ as the phosphorous source, sol-gel and combustion procedures of NFPP used phosphates salts exclusively (without pyrophosphates) [23–26] where $\text{PO}_4 \rightarrow \text{P}_2\text{O}_7$ thermal conversion allows the formation of NFPP framework. We found no reports aimed at the use of the sol-gel route with phosphates and pyrophosphates as reactants, which will be the topic of this work. That is why we undertook this study, and a brief summary of

the results is as follows: If the mentioned components are mixed, to follow $\text{Na}_4\text{Fe}_3(\text{PO}_4)_2(\text{P}_2\text{O}_7)$ stoichiometry, together with a certain amount of a citric acid which provides a pH of 3, the pyrophosphate $\text{Na}_2\text{FeP}_2\text{O}_7$ (NFP) appears as the dominant phase. pH increase of the reaction suspension, adjusted either through a certain amount of citric acid or ammonium hydroxide, was found to change the reaction pathway, thereby increasing the relative amount of the mixed NFPP phase in the NFPP/NFP heterostructure. When pH is 7, the NFPP phase is liberated from NFP and can reach theoretical capacity (at a relatively high current rate of 8 C) as well as high-rate capability in the Na-containing aqueous electrolyte. The production of the final polyanionic composition, depending on the synthesis conditions, is explained from the aspect of Fe-complexation by carefully following the colors during each stage of synthesis procedures.

2. Experimental

2.1. Samples preparation

$\text{Na}_4\text{Fe}_3(\text{PO}_4)_2\text{P}_2\text{O}_7/\text{C}$ was synthesized by the sol-gel route using $\text{FeC}_2\text{O}_4 \cdot 2\text{H}_2\text{O}$, $\text{Na}_4\text{P}_2\text{O}_7$ and $\text{NH}_4\text{H}_2\text{PO}_4$ as Fe and P sources, according to the procedure illustrated in Fig. 1. First, a certain amount of $\text{FeC}_2\text{O}_4 \cdot 2\text{H}_2\text{O}$ (0.01 mol) was mixed with citric acid $\text{C}_6\text{H}_8\text{O}_7 \cdot \text{H}_2\text{O}$ (0.015) in 30 mL of distilled water, under magnetic stirring at a room temperature. Furthermore, the stoichiometric amount of $\text{Na}_4\text{P}_2\text{O}_7$ and $\text{NH}_4\text{H}_2\text{PO}_4$, together with a certain amount of sucrose (25wt%), were added to the citric-oxalate yellow suspension. The yellow suspension displayed a pH of 3 and 25vol% NH_4OH was added, drop by drop, until the pH was 7. A rapid yellow-to-green colour change was observed after the pH adjustment. The suspension was heated at 60°C until evaporation and a gradual colour alteration from light to dark green was observed. After around two hours, this green colour turned brown and became completely transparent (Fig. 1a). Upon evaporation, the gel's colour remained brown (Fig. 1, above) marked by the gelatinous colour of sucrose. The change from dark brown to light green gel was detected

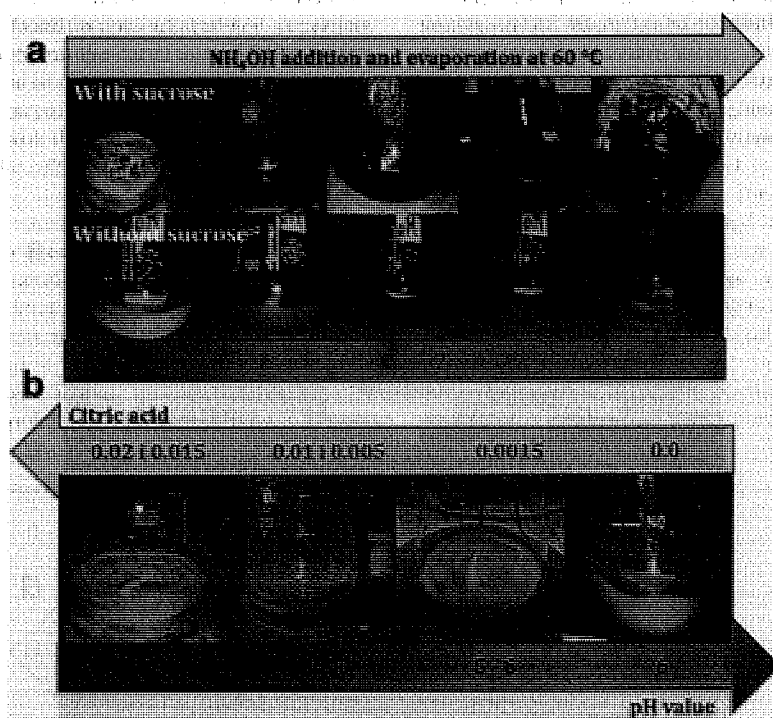


Fig. 1. a) Reaction path of $\text{Na}_4\text{Fe}_3(\text{PO}_4)_2\text{P}_2\text{O}_7/\text{C}$ formation using a citric-assisted sol-gel route with and without sucrose, when both phosphate and pyrophosphate are used as reactants; pH of the suspension is adjusted to 7; b) the color of suspension during the citric-assisted sol-gel route when the different molar concentration of citric acid is used and determines the pH. When there are two concentrations, the color of the suspension is practically the same.

(Fig. 1.b, below) in the absence of sucrose. In the next step, the obtained gel was dried at 160 °C over 1.5 h in the Air atmosphere to form a black powder precursor (lighter in the sucrose absence), which was then calcinated at 500 °C under Ar/H₂ (95:5) to the final black powder, designated as NFPP/SC_pH7 (with sucrose) and NFPP/C_pH7 (without sucrose).

Described colour changes are not observed when it comes to spontaneous reaction at a pH of 3. In this case, the turbid yellow-brown colour of the suspension was noticed (Fig.S1). Namely, the yellow suspension first evaporated at 60 °C to a light brown gel. Then the gel was heated at 150 °C to a brown precursor and further at 500 °C (under 95% Ar/5%H₂) to the final black powder. The sample is labeled as NFPP/SC_pH3. An amber gel color and less intensive brown precursor were registered in the absence of sucrose (Fig.S2), while the final black powder was labeled as NFPP/C_pH3.

In addition, different samples were prepared by spontaneous sol-gel process using the same amount of oxalate, phosphate, pyrophosphate and different molar fractions of citric acid in amounts of 0.02, 0.01, 0.005, 0.0015 and 0 (Fig. 1c). This way, the suspension pH varied from 3 to 6 and changes from intense to pale yellow with green shades were observed. The precursor samples are shown in Fig.S3.

2.2. Samples characterizations

X-ray powder diffraction (XRD) patterns were conducted on a Philips 1050 diffractometer using CuK α radiation in the interval of 2 θ from 8° to 70°. The step size of 0.02° and a counting time of 5 s per step were used. Qualitative and semi-quantitative phase analysis has been performed in Eva software. The unit cell parameters have been extracted from the whole powder pattern refinement via Le Bail method [33] in Topas software.

The thermogravimetric analysis coupled with simultaneous differential thermal analysis (TG/DTA) of samples was done using the Thermobalance TA.SDT Model 2090. Powder samples were heated from 25–750 °C under Air atmosphere, at a heating rate of 10 °C min⁻¹.

The Fourier-transform Infrared spectra (FTIR) of obtained samples were collected in the wavenumber range of 4000–400 cm⁻¹ at 64 scans per spectrum and 2 cm⁻¹ resolution, using Avatar System 370 spectrometer (Thermo Nicolet, USA). The technique of KBr pellet was used.

The Raman spectra were recorded using a DXR Raman Microscope (Thermo Scientific). The samples were excited by the 532 nm emission line of a diode laser with 2 mW of power focused on a 2.1-mm spot on the surface of the sample through a 10x microscope objective. The spectrum was obtained as an average of three measurements on different places on the sample surface (10 exposures, 10 s each, per place).

2.3. Electrode preparation and electrochemical characterizations

For electrochemical measurements, the slurry was made by mixing 85 wt% of active composite material, 10 wt.% of the carbon black (Cabot Vulcan XC-72R, and 5% of the poly(vinylidene fluoride) (PVdF) as a binder, in a certain amount of N-methyl-2-pyrrolidone as a solvent. After homogenisation in an ultrasonic bath, a thin layer of the slurry was deposited onto conductive glassy carbon support. The formed electrodes, carrying different samples, were dried at 140 °C for 4 h under the vacuum. To test working electrodes in a three-electrode cell connected with a Gamry 1010E device, a wide platinum foil and saturated calomel electrode (SCE) were used as a counter and reference electrode, respectively. The electrochemical investigations including Cyclic Voltammetry (CV) and Chronopotentiometry (CP) were performed in the air-equilibrated 6 M NaNO₃. Cyclic voltammograms and chronopotentiograms were measured within the electrochemical stability window of the aqueous electrolyte, by varying scan rates from 1 to 400 mV s⁻¹ (for CV) and current densities from 0.25 to 10 A g⁻¹ (for CP).

3. Results and discussion

3.1. Composition vs. synthesis conditions

XRD pattern of NFPP/SC_pH3 sample, synthesized by the spontaneous sol-gel process, revealed the heterostructure Na₂FeP₂O₇/NaFe₄(PO₄)₃P₂O₇ (NFP/NFPP), as shown in Fig. 2. The Na₂FeP₂O₇ is formed as the dominant phase in the amount of \approx 74 wt.%, while the remaining \approx 26 wt.% corresponds to the amount of targeted mixed NaFe₄(PO₄)₃P₂O₇ phase. The refined pattern of NFPP/SC_pH3 is presented in Fig.S5a. The obtained unit cell parameters of Na₄Fe₃(PO₄)₂P₂O₇ (a=18.05 Å, b=6.57 Å, c=10.69 Å) and Na₂FeP₂O₇ (a=6.41 Å, b=9.58 Å, c=11.07 Å, α =64.49°, β =85.74°, γ =73.13°) correspond to those reported in references [17,32,34] The formed heterostructure is the consequence of the thermally-induced phosphate \rightarrow pyrophosphate conversion. That is a reason why the reported sol-gel procedure of Na₄Fe₃(PO₄)₂P₂O₇ [23–25] did not involve pyrophosphates as reactants, but only phosphates which were able to undergo partial decomposition to pyrophosphate under appropriate synthesis conditions, as suggested by Wu [23]. Moreover, the sucrose addition into the reaction mixture was found to catalyze the phosphate thermolysis (Fig.S4), since the lower amount of Na₂FeP₂O₇ (\approx 63 wt.%) versus Na₄Fe₃(PO₄)₂P₂O₇ (\approx 37 wt.%) was found in the sample without sucrose (NFPP/C_pH3).

To find synthesis conditions that favour NaFe₄(PO₄)₃P₂O₇ formation, the initial amount of citric acid was changed. As its molar concentration varied from 0.02 to 0, the amount of the mixed polyanion phase was found to increase, from 14 to 38 wt% (Fig. 3), while at the same time NFP fraction decreases. Still, NFP phase dominates all NFPP/NFP samples. Searching for an explanation, pH of the initial suspension appeared as a key link. pH increase, induced by the citric acid decrease, favors the formation of NFP phase. When the pH of the synthesis was directly adjusted to neutral value (NFPP/SC_pH7), thus maintaining the same amount of citric acid (0.015 mol) as for NFPP/SC_pH3, the mixed phase was formed as the major one, while the sodium pyrophosphate phase is not formed at all (Fig. 2 and Fig. 3). Still, the small amount of maricite-type NaFePO₄, typical accompanying phase, is also formed. The refined pattern of NFPP/SC_pH7 is shown in Fig.S5b. The obtained lattice parameters of Na₄Fe₃(PO₄)₂P₂O₇ (a=18.04 Å, b=6.54 Å, c=10.67 Å) and NaFePO₄ (a=6.71 Å, b=9.01 Å, c=5.07 Å) match those reported in references [17,30,32,35] Unlike the reaction under acidic conditions,

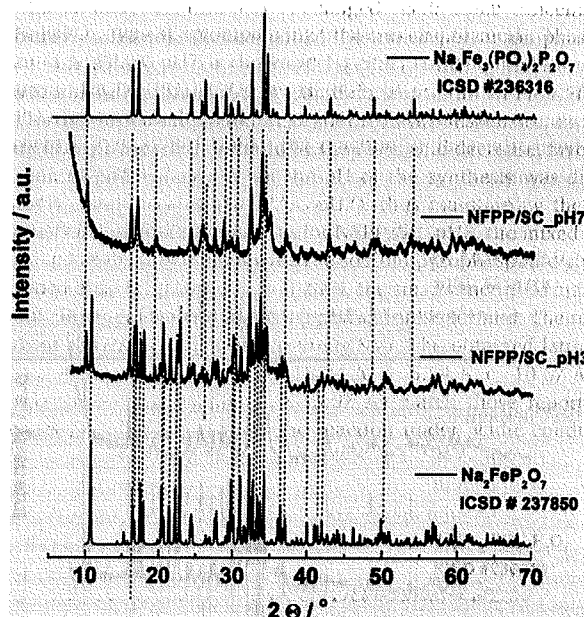


Fig. 2. XRD patterns (CuK α radiation) of NFPP/SC_pH3 and NFPP/SC_pH7 compared to Na₄Fe₃(PO₄)₃P₂O₇ and Na₂FeP₂O₇ databases using.

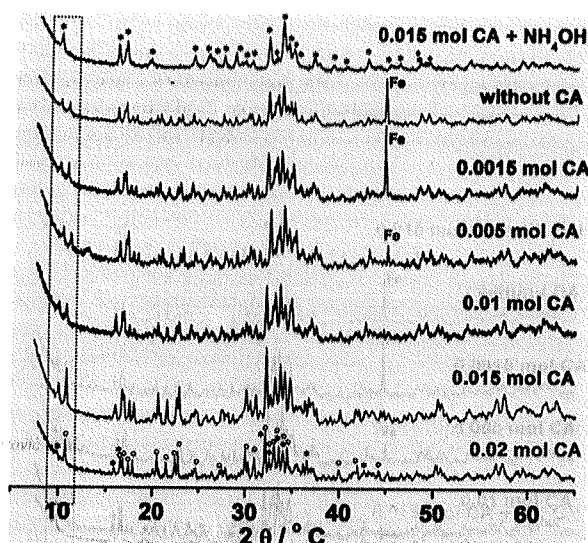


Fig. 3. XRD patterns (CuK α radiation) of samples prepared by spontaneous sol-gel reaction using different fractions of citric acids from 0.02 mol to 0, without pH adjustment. XRD pattern at the top shows the sample with adjusted pH to 7 and 0.015 mol citric concentration. Symbols * and ♦ denote Na₄Fe₃(PO₄)₂P₂O₇ and NaFePO₄, respectively.

the sucrose presence did not significantly change the phase composition when the pH was 7. Thus, if the sol-gel reaction is allowed to proceed at neutral pH, both pyrophosphates and phosphates react with each other, thus forming Na₄Fe₃(PO₄)₂P₂O₇.

3.2. Thermal behavior

Further, we measured the TG/DTA curves of examined samples in oxidizing, synthetic air atmosphere, Fig. 4. Generally, two parallel processes can be observed during thermal heating of polyanionic samples above 200 °C. The first one is Fe²⁺ to Fe³⁺ oxidation of polyanionic phases, which results in final NaFeP₂O₇, Na₄P₂O₇, Fe₂O₃ and Na₃Fe₂(PO₄)₃ products, according to Eqs. (1)-(3) in Supp. Data. These processes are accompanied by the corresponding mass increase. However, it cannot be evidenced from TG/DTA curves in Fig. 4a,b due to parallel carbon combustion to CO₂ which is responsible for the observed mass decrease. The weight loss and carbon fraction become higher with the citric acid increase, since it acts as a carbon source (Fig. 4b). By considering the theoretical weight gain of the sample, induced by these oxidation processes, the carbon amount in the Na₄Fe₃(PO₄)₃P₂O₇/

Na₂FeP₂O₇ heterostructure is estimated to be ≈ 15 (NFPP/C₃) and ≈ 20 wt.% (NFPP/SC₃), while its value in NFPP/SC₇ and NFPP/SC₇ is found to be higher amounting to ≈ 34 and ≈ 36 wt.%, respectively. The small amount of carbon originates from sucrose (ranging from 2-5 wt. %), as can be seen in Fig.S6, while the major part comes from the citric acid combustion. One can see that the carbon content is strongly influenced by the pH of the reaction mixture. The observed difference between NFPP (pH=7) and NFPP/NFP -based (pH=3) samples can be attributed to different combustion rates of citric acid due to diverse nature of Fe complexes formed under varied pH (please see explanation in section 3.3). Namely, the combustion process was alleviated in the presence of NFP (evidenced by the smaller slope of the TG curve within 400 -600 °C range) which resulted in lower amount of carbon.

From TG/DTA curves of NFPP/SC_{pH3} and NFPP/SC_{pH7} (Fig. 4a), we can conclude that the Na pyrophosphate presence in the sample attenuates the carbon combustion kinetics thus making it happen in two steps (at 362 and 444 °C). We can also notice that the appearance of the second DTA peak (Fig. 4b) follows the trend of increasing citric acid and consequently Na pyrophosphate amount. This can be attributed to a different carbonization degree of carbon that surrounds pyrophosphate particles. This type of carbon is probably more graphitized since a higher temperature is needed for its removal upon heating. Such observed behavior was also confirmed in TG/DTA curves of the sample prepared under a pH of 3, with and without sucrose. From the TG curve of the NFPP/C_{pH3} sample (without sucrose) one can see an additional exothermic peak at 530 °C (Fig.S5), which can be attributed to the combustion's completion to pyrophosphates under air atmosphere rather than to the remained Fe²⁺ to Fe³⁺ oxidation process. This conclusion is based on the phase composition of both NFP/C₃ and NFP/SC₃ samples and the fact that the second DTA peak is more pronounced in the presence of sucrose (due to higher Na₂FeP₂O₇ fraction). In other words, sucrose catalyzes the phosphate to pyrophosphate combustion (in line with XRD), since the released heat provides more energy for the pyrophosphate formation.

3.3. FTIR study

To identify vibrational modes, belonging to individual polyanionic phases, the Infrared spectra of examined samples have been measured. When it comes to the mixture of phosphate phases, the assignment of individual modes is aggravated due to their overlapping, while their mutual interaction can cause modes' shifting. Regarding Na₄Fe₃(PO₄)₂P₂O₇, we have noticed that the specification of individual modes is not fully consistent in the literature, which can be influenced by the presence of secondary phases which are usually inevitable in the synthesis. A series of our samples can serve as an excellent guide for the

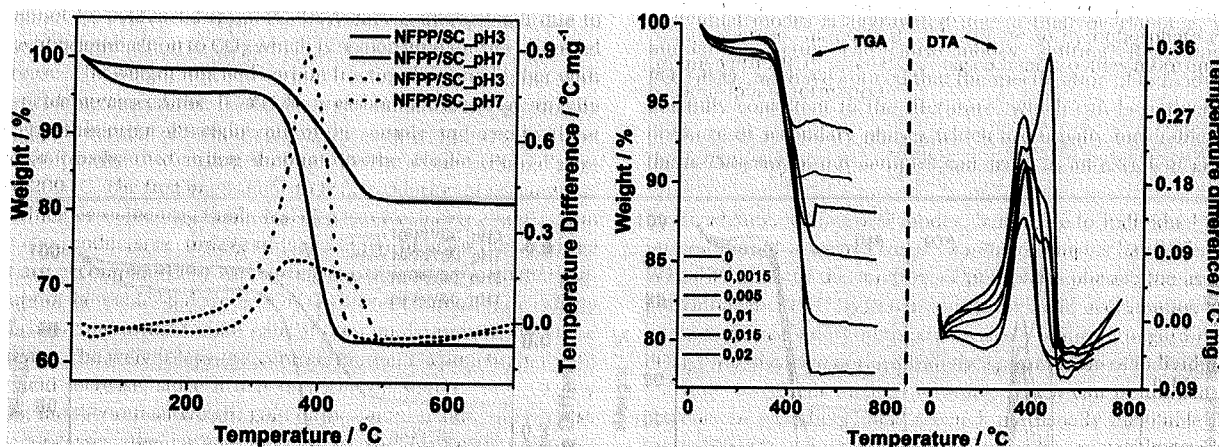


Fig. 4. TG/DTA curve of NFPP/NFP samples prepared under different pH using 0.015 mol citric concentration of citric acid (a) and different molar citric acid concentrations from 0.02 to 0 (b).

assignment of individual modes belonging to the pyrophosphate and mixed $\text{PO}_4\text{-P}_2\text{O}_7$ phase when they both appear in the sample. First, let's identify the vibrational modes of samples with (NFPF/SC_pH3) and without $\text{Na}_2\text{FeP}_2\text{O}_7$ (NFPF/SC_pH7), shown in Fig. 5. inevitable in the synthesis. Differentiation of modes belonging to individual phosphate phases is aggravated due to their overlapping and shifting, positions of characteristic vibrational modes are not fully consistent, which is probably influenced by the presence of secondary phases, usually

To facilitate the assignment process, three spectral regions (A, B and C) are typically recognized:

- A. Vibrational modes, within the high-frequency region, correspond to asymmetric ($1200\text{-}990\text{ cm}^{-1}$) and symmetric ($990\text{-}890\text{ cm}^{-1}$) P-O stretching vibrations in PO_3 and PO_4 units. Those belonging to the mixed NFPF phase (1120, 1178, 1165, 1129, 1103, 1080, 1034, 993, 980, 953 cm^{-1}) can be easily identified in the sample with an adjusted pH, while in the sample with pH of 3, characteristic P-O bands of the pure sodium Fe pyrophosphate [36] (here positioned at 1160, 1102, 1042, 993, 953 cm^{-1}) are superimposed to those of the mixed phase.
- B. Vibrational modes, within the middle-frequency range, are attributed to typical asymmetric and symmetric bridging P-O-P vibrations of the pyrophosphate group. Interestingly, in the spectrum of NFPF/SC_pH7, there are three bands (shoulder at 905, 879, and 718 cm^{-1}) belonging to the mixed phase instead of two. However, the band at 905 cm^{-1} is positioned at the P-O/P-O-P boundary and it is difficult to specify the region to which it belongs. On the other hand, two typical pyrophosphate bands of NaFeP_2O_7 (at 905 and 737 cm^{-1}) and the contribution of those from the mixed phase (shoulder at 905, 879, and 718 cm^{-1}) can be clearly identified in the spectrum of NFPF/SC_pH 3.
- C. Low-frequency bands are attributed to O-P-O bending modes in PO_4 units. Two bands of pyrophosphate phase, which are active in this region [36], match those positioned left (557 cm^{-1}) and right (529 cm^{-1}) from the main band at 542 cm^{-1} which belongs to the mixed phase. So, their intensity increases with the appearance of the pyrophosphate phase in the mixture. Two additional modes at the lowest frequencies can be identified for both NFPF and NFP phases. Those belonging to NFPF are positioned at 480 & 456 cm^{-1} , while NFP modes are slightly shifted towards lower wavenumbers (more precisely at 488 & 461 cm^{-1}).

A comparison of samples with and without sucrose (Fig.S7) confirms the previous assignment. One can see that assigned $\text{Na}_2\text{FeP}_2\text{O}_7$ modes (1160, 1102, 1041, 993, 953, 905, 741, 557, 529, 488, 456 cm^{-1}) become more pronounced in the spectrum of heterostructure with the

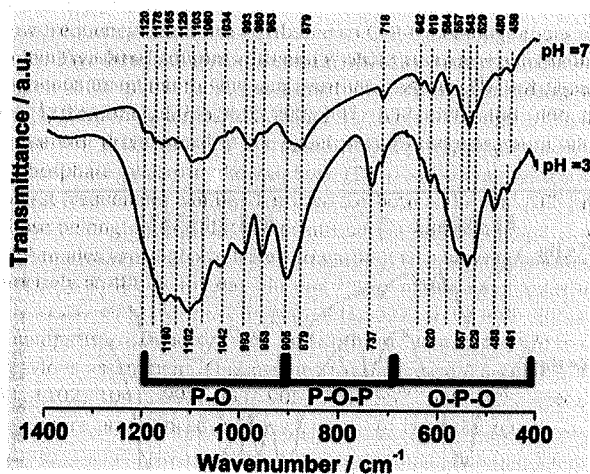


Fig. 5. FTIR spectra of NFPF/SC_pH3 and NFPF/SC_pH7.

higher fractions of $\text{Na}_2\text{FeP}_2\text{O}_7$. Their positions are slightly shifted when compared to the pure sodium pyrophosphate phase ($1158, 1092, 1036, 1012, 1002, 957, 905, 739, 667, 601, 567, 530, 489\text{ cm}^{-1}$) [36]. This can be attributed to the interaction of pyrophosphate with the surrounding mixed phase which makes its bonds weaker. Assignment of $\text{Na}_2\text{FeP}_2\text{O}_7$ modes is also confirmed in spectra of samples with different molar citric acid concentrations (Fig. 6), where their gradual fade in relative intensity can be observed as the citric acid amount decreases, due to a decreased sodium pyrophosphate fraction. In the middle region, we can follow the change from one band (905 or 737 cm^{-1}), which mostly belongs to sodium pyrophosphate, to the other one (879 or 718 cm^{-1}) belonging to the mixed phase at a slightly lower frequency. The splitting of the low-frequency bridging mode (737 and 718 cm^{-1}) is observed when both of these phases are in the mixture and can be an indication of occurring $\text{Na}_2\text{FeP}_2\text{O}_7$ as an accompanied phase of NFPF.

All assigned FTIR bands in our samples, including detected shoulders, are summarized and compared with the literature data (Table 1). $\text{Na}_4\text{Fe}_3(\text{PO}_4)_3\text{P}_2\text{O}_7$ - belonging bands match the reported ones, with certain discrepancies. First, if we compare modes of as-prepared NFPF/SG_pH7 ($\text{Na}_4\text{Fe}_3(\text{PO}_4)_3\text{P}_2\text{O}_7/\text{NaFePO}_4 \approx 92\%/8\text{wt}\%$) and NFP450 ($\text{Na}_4\text{Fe}_3(\text{PO}_4)_3\text{P}_2\text{O}_7/\text{NaFePO}_4 \approx 89\%/11\text{wt}\%$) prepared by Kosova et al [19] (shown in Fig. 6a in ref.15), we can notice one substantial difference in the position of the mid-frequency band (718 vs. 737 cm^{-1}). However, this divergence is strange due to the following reasons: 1. the position of this band for pure $\text{Na}_4\text{Fe}_3(\text{PO}_4)_3\text{P}_2\text{O}_7$ was found to be around 720 cm^{-1} [27,28], which is in accordance with our results; 2. our composition is quite similar to the NFP450, which indicates that the observed difference cannot be attributed to the influence of the secondary maricite phase. The reason for the mentioned discrepancy can be either the different crystallinity of mixed phases or some inadvertent omission in Kosova's paper, with the following explanation. According to Kosova [19], the low-frequency P-O-P band is positioned at 737 cm^{-1} , based on Fig. 6a and Table 7 in ref.15. However, a closer inspection of Fig. 6b in ref. [15], which summarizes FTIR spectra of several NFP-based samples, including NFP450, reveals the characteristic position of this band at $\approx 720\text{ cm}^{-1}$, while the new band, with slightly higher frequency ($\approx 737\text{ cm}^{-1}$), rises when the sodium pyrophosphate appears. This matches our observation regarding the appearance of two bands in the middle frequency region (resembling a band's splitting) when it comes to the formation of a phosphate-pyrophosphate heterostructure. Moreover, our results unambiguously show that P-O-P vibration at around 718 cm^{-1} band can be attributed to the mixed phase, while the 737 cm^{-1} band originates from sodium pyrophosphate. Based on all of this, FTIR should serve to identify $\text{Na}_2\text{FeP}_2\text{O}_7$ as an accompanying phase, which is

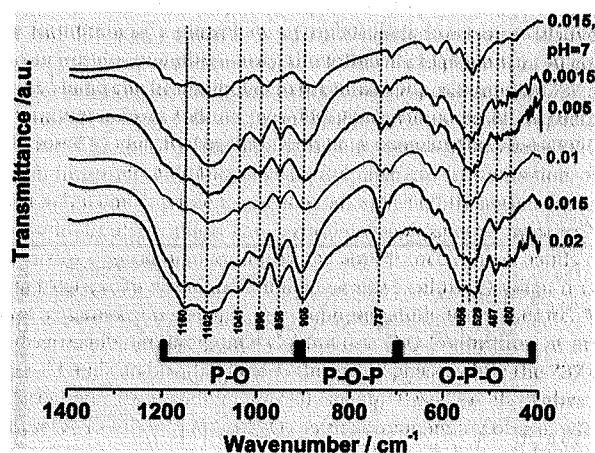


Fig. 6. FTIR spectra of NFPF/NFP samples prepared by sol-gel route using different citric acid concentrations which determine pH. Only FTIR at the top corresponds to the sample with 0.015 mol concentration of citric acid, when pH is adjusted to 7.

Table 1
Survey of assigned FTIR bands for different phosphate-based compounds.

≈ Wavenumbers / cm ⁻¹ and assignment				
Polyanionic composition	P-O _{asym/sym} (1200- 900 cm ⁻¹)	P-O _{sym} (P-O-P) _{as}	P-O-P _{sym} (P-O-P) _{as}	O-P-O 700-400
This work				
Na ₄ Fe ₃ (PO ₄) ₃ P ₂ O ₇	1220,1178,1157, 1129, 1103, 1080, 1034,1022, 993 / 980,953	905 879 (P-O-P)	718	642,619, 584, 557, 547,529
Na ₂ FeP ₂ O ₇ bands	1160, 1105, 1041, 993, 956		905 737	557, 529, 487, 460
Literature data for Na₄Fe₃(PO₄)₃P₂O₇				
Na ₄ Fe ₃ (PO ₄) ₃ P ₂ O ₇ [15]	1199, 1177, 1165, 1134, 1104, 1085, 1046, 1022, 995 / 988, 957	903 (P-O-P)	737	644, 623, 583, 557 544, 529
Na ₄ Fe ₃ (PO ₄) ₂ P ₂ O ₇ / C [23]	1195, 1160, 1101 / 989,957	905 (P-O-P)	719 879	638, 621, 583, 548, 480, 460
Na ₄ Fe ₃ (PO ₄) ₂ P ₂ O ₇ / rGO [24]	1200, 1165, 1105, 1043 / 989, 956,	904 (P-O-P)	721 879	621, 584, 545
Na ₄ Fe ₃ (PO ₄) ₂ P ₂ O ₇ / MCNTs (impurities of NaFePO ₄ and Na ₂ FeP ₂ O ₇) [27]	1200, 1158, 1131, 1102, 1036 / 990	956 902 (P-O-P)	879 746, 721	646, 619, 543, 485, 460
Na ₄ Mg ₃ (PO ₄) ₂ P ₂ O ₇ [28]	1205, 1180, 1173, 1126, 1113, 1095, 1068, 1053, 1009 / 999, 968, 953	914 (P-O-P)	730	631, 590, 575, 561, 542 / 494, 471, 457
Na ₄ Fe ₃ (PO ₄) ₂ P ₂ O ₇ (impurities of NaFePO ₄ and Na ₂ FeP ₂ O ₇) [29]	1204, 1176, 1164, 1105, 1080, 1024, 986, 954	904 884 (P-O-P)	720	644, 622, 582, 543, 530, 482,458
Na ₄ Fe ₃ (PO ₄) ₂ P ₂ O ₇ impurities of NaFePO ₄ and Na ₂ FeP ₂ O ₇ [30]	1200*, 1161, 1105, 991	956 906 (P-O-P)	720	621, 584, 545, 482*, 458*
Literature data for Na₂FeP₂O₇				
Na ₂ FeP ₂ O ₇ [31]	1155, 1038, 1011, 958	910 (P-O-P)	738	567, 532, 488, 406
Na ₂ FeP ₂ O ₇ [26]	1158, 1092, 1036, 1012, 1002, 957	905 (P-O-P)	739	667, 601, 567, 530, 489,
Na ₂ FeP ₂ O ₇ [32]	1152, 1123, 1092, 1012,958,	913 (P-O-P)	738	620,566,531

* not indicated in the published FTIR but the band/shoulder is evidenced

particularly important when its small fraction is formed, hardly detectable by XRD [20]. There is one more issue regarding the specification of 905 cm⁻¹ vibrational mode of NFPP/SC_7, since it is positioned at P-O/P-O-P boundary.

According to Kosova [19], this mode is specified as P-O, while others [27,28,37,38] ascribed this band to the P-O-P region. We believe that this mode belongs to asymmetric P-O-P rather than P-O region and the appearance of three P-O-P modes of Na₄Fe₃(PO₄)₂P₂O₇ can be related to

the imperfection of Fe in the crystal lattice. In the case of NFPP/SC_pH3, two typical asymmetric and symmetric stretching P-O-P vibrational modes of Na₂FeP₂O₇ [36] can easily be recognized.

3.4. Electrochemical behavior

3.4.1. CV characterization

Sodium storage behavior of NFPP/SC_pH3 and NFPP/SC_pH7 samples was examined by cyclic voltammetry (Fig. 7). Initial CVs of these materials (Fig. 7a,b), measured at a scan rate of 20 mV s⁻¹ in NaNO₃, reveal their different redox shape, governed by phase composition. Different anodic behavior in the first cycle of NFPP/SC_pH3 (related to Na⁺ ion deinsertion) is the consequence of Na defect sites in NFP pristine [39]. Since the capacitive current arises along with redox processes, the shape of CV peaks is better defined at lower scan rates such as 5 mV s⁻¹ and 1 mV s⁻¹ (Fig. 7c,d).

Characteristic redox profile of Na, Fe-based pyrophosphate [39–42], composed of broad redox pair at lower potentials (-0.39/ -0.47 V vs. SCE or 2.56/2.48 V vs. Na⁺/Na) and three sharper redox peaks at higher potentials (0.03/-0.022, 0.19/0.06, 0.31/0.25 V vs. SCE or 2.99/2.93, 3.14/3.01, 3.26/3.2 V vs. Na⁺/Na), can be recognized in CV of the heterostructure (brown line in Fig. 7d). These redox peaks reflect the deinsertion/insertion processes of sodium ions from/into four energetically different sites of the pyrophosphate lattice, induced by Fe²⁺ ↔ Fe³⁺ oxidation [39]. Deinsertion of Na1 site along 001 channel of Na₂Fe₂P₂O₇, with an activation barrier of ≈ 0.48 eV [39], occurs during anodic reaction at the lowest potential of ≈ 0.4 V vs. SCE or 2.5 vs. Na⁺/Na (labeled as 1 in Fig. 7d), which is followed by a single-phase transition. Anodic processes at more positive potentials (labeled as 2, 3,4 in Fig. 7d) involve two-phase transitions occurring through the formation of intermediate phases where Na3-Na8 ions undergo extraction along 1D and/or 2D channels of pyrophosphate structure with comparable barriers of ≈ 0.54 eV [39]. Reverse processes happen during the cathodic scan, where the presence of the mixed polyanionic phase and capacitive current blur CV contours. Redox peaks of the mixed phase are superimposed to both Na₂Fe₂P₂O₇-belonging peaks and capacitive current. They can be clearly evidenced in the phase liberated from pyrophosphate (Fig. 7d, green line at pH7). Several anodic peaks at -0.16, -0.08, 0.03, 0.19, 0.31 0.38 V vs. SCE (or 2.79, 2.87, 2.98, 3.14, 3.26, 3.33 V vs. Na⁺/Na) reflect the extraction of three Na⁺ ions from distinguishable Na sites of mixed polyanion lattice, through a single-phase reaction, with low diffusion energy barriers from 0.02-0.5 eV [17]. Corresponding cathodic peaks are not distinguished (green line in Fig. 7d) as in the case of organic electrolytes [19], due to the faster kinetics of processes in an aqueous electrolyte (closer peak potential positions) and certain contribution of the capacitive current. Four redox pairs (positioned at 2.79/2.5, 2.98/2.88, 3.14/3.11 and 3.26/3.19 V vs. Na⁺/Na), are typically observed for NFPP in literature [19]. Additional redox peaks, observed here at 2.87 and 3.33 V vs. Na⁺/Na (Fig. 7d), may be correlated to the higher structural disorder and Fe sites impurity.

3.4.1.1. Specific capacity vs. scan rate. Cycling at different scan rates show that CV's shape is quite preserved with a certain distortion at ultrahigh scan rates, due to ohmic resistance. The integration of measured CVs provides specific capacity as the function of scan rate (Fig. 8), which is higher for the mixed phase without Na₂FeP₂O₇. Its kinetic behavior strongly depends on the applied scan rate range due to different determining processes at lower and higher currents.

At smaller scan rates (5–50 mV s⁻¹), the capacity fade of the NFPP/SC_pH7 is a little slower than NFPP/SC_pH3 due to better diffusivity of Na⁺ ions through 3 D framework of the NFPP phase. Smaller scan rates reveal enough time for ions to penetrate into 3D channels of the mixed phase, which provides a higher amount of accumulated ions (138 mA h g⁻¹ vs. 72 at 5 mV s⁻¹). One can conclude that the higher fraction of the

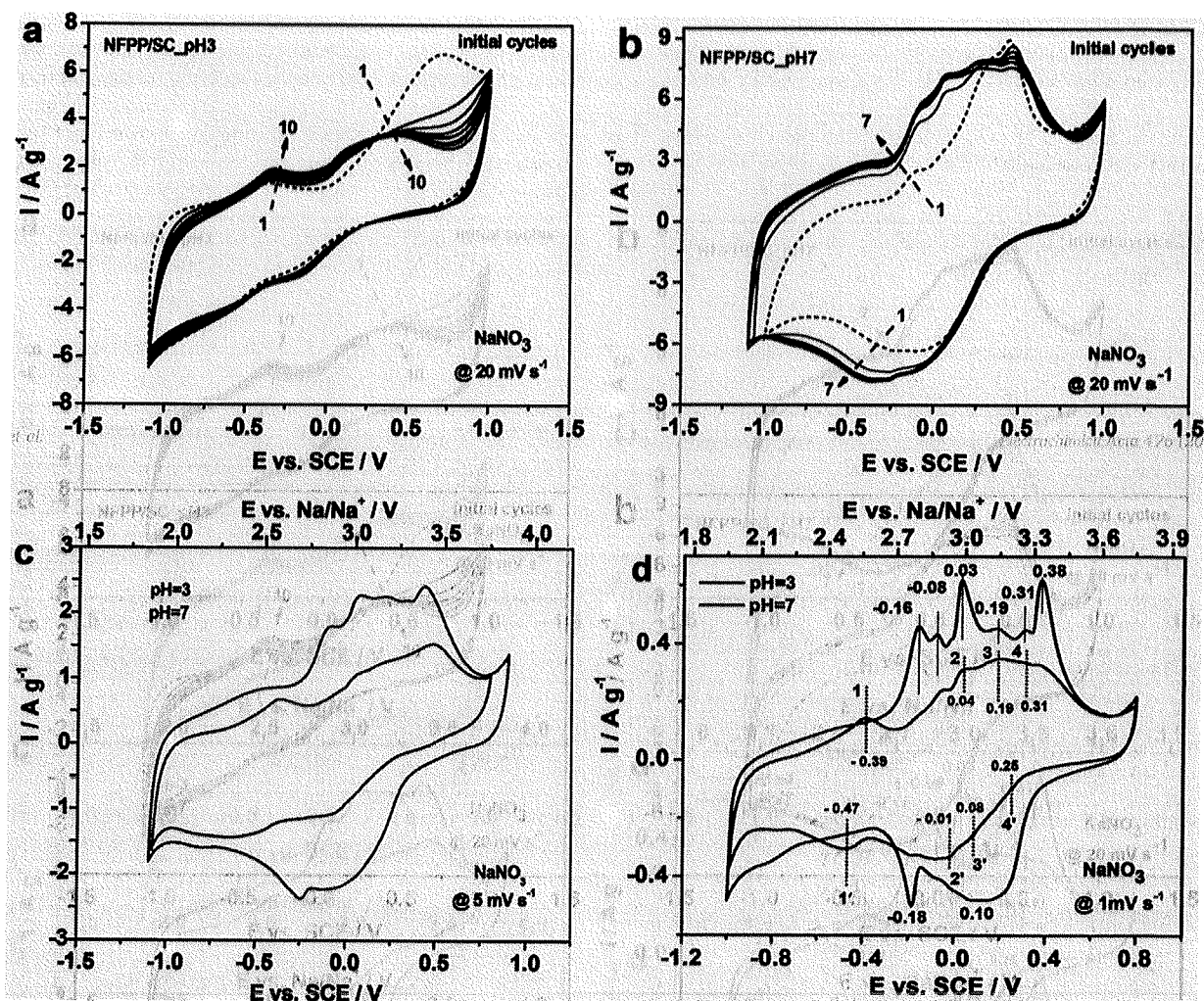


Fig. 7. Initial (a,b) and stabilized (c,d) cyclic voltammograms of NFPP/SC_pH3 and NFPP/SC_pH7 measured in NaNO_3 at 20, 5 and 1 mV s^{-1} . The scale of CV, measured at lower scan rates, is also converted versus Na/Na^+ .

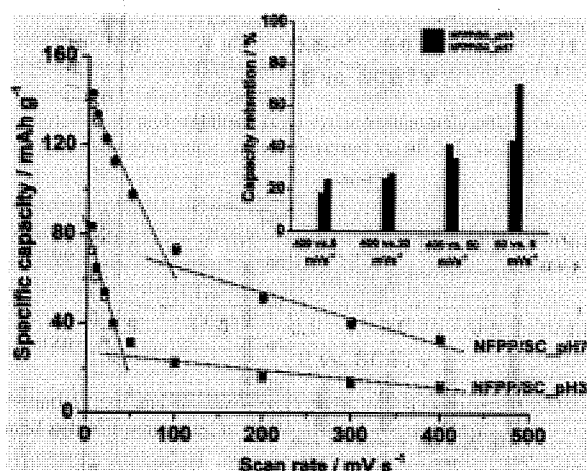


Fig. 8. The specific coulombic capacity versus scan rate. Emptied and filled symbols present dissociation and sodiation capacity, respectively. The dotted line illustrates the relative capacity fade rate and the kinetic behavior as the scan rate increases. The inset chart represents the capacity retention (%) calculated on the basis of the retained capacity at 400 mV s^{-1} (with respect to those at 5, 20 and 50 mV s^{-1}) and 50 mV s^{-1} (with respect to one at 5 mV s^{-1}).

electrode "inner part" (mostly related to the less accessible bulk phase) is utilized for NFPP_pH7 than for NFPP_pH3. The opposite behavior was observed at higher scan rates. The electronic transport becomes an issue and lower capacity fade is observed for the phase with $\text{Na}_2\text{FeP}_2\text{O}_7$, which can be associated with the more graphitized nature of the carbon that surrounds it, as shown by both TG/DTA (Fig. 4) and Raman spectra (Fig S8). Namely, more graphitized carbon requires a higher temperature to be released under air flow (two DTA peaks at ≈ 362 and ≈ 444 °C for NFPP/SC_pH3 and one DTA peak at ≈ 380 °C for NFPP/SC_pH7). Also, the higher I_G/I_D ratio of Raman bands in NFPP/SC_pH3 than in NFPP/SC_pH7 confirms the more graphitized nature of carbon in the presence of NFP phase. Still, the significantly better specific capacity of NFPP phase, when it is liberated from $\text{Na}_2\text{FeP}_2\text{O}_7$ can be observed at high polarization rate of 50 mV s^{-1} (Fig. 9).

Further decrease of the scan rate below 5 mV s^{-1} (to the value of 1 mV s^{-1}), leads to a bit higher capacity of NFPP/NFP heterostructure, while there is no further capacity enhancement for the mixed phase (Fig.S9). Although theoretically impossible, a lower value was measured at 1 mV s^{-1} than at 5 and 10 mV s^{-1} , due to more pronounced instability of the phase upon a slow scan rate of 1 mV s^{-1} and a little shorter potential interval. One can say that the limiting capacity of the mixed phase (close to the theoretical value based on three Na^+ ions) is reached at 1 and 5 mV s^{-1} .

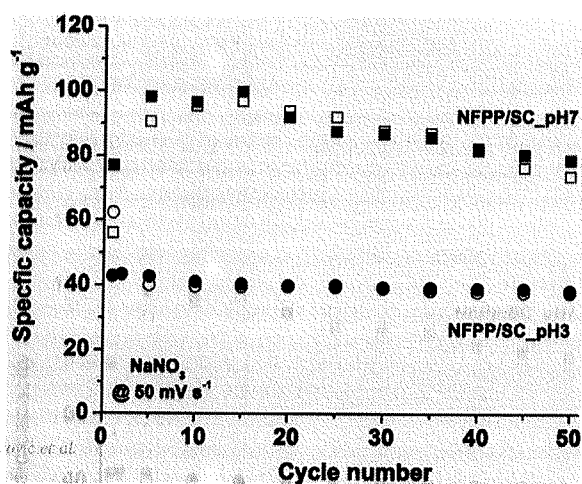


Fig. 9. Cyclic stability of NFP/SC_pH3 and NFP/SC_pH7, measured at 50 mV s^{-1} .

3.4.1.2. Contribution of $\text{Na}_4\text{Fe}_3(\text{PO}_4)_2\text{P}_2\text{O}_7$ and $\text{Na}_2\text{FeP}_2\text{O}_7$ phases to the redox behavior of mixture. If we look at CVs of samples with different molar citric concentrations (Fig. 10) and consequently the ratio of $\text{Na}_2\text{FeP}_2\text{O}_7$ and $\text{Na}_4\text{Fe}_3(\text{PO}_4)_2\text{P}_2\text{O}_7$ phases, we can notice their individual contribution to the total redox behavior. Several conclusions can be derived. First, $\text{Na}_2\text{FeP}_2\text{O}_7$ presence decreases the current response of the composite and the best behavior was observed when the sample was liberated from this phase. Second, the pyrophosphate shifts the right side of the cathodic part towards lower potentials and the shifting trend follows the increase in pyrophosphate fraction. So, ions need more energy to be inserted into the mixed phase in the presence of the pyrophosphate. Furthermore, the relative ratio of current peaks, at positive potentials, changes with the ratio of individual phases, depending on the amount of the mixed phase. For its larger fraction, the peak's intensity at 0 V vs. SCE (or 2.95 V vs. Na^+/Na) is more pronounced over the other two, while it is less pronounced when it comes to a smaller fraction. Last but not least, the contribution of pyrophosphate can be reflected through the appearance of the broad redox pair at low potentials (around -0.39/-0.43 V vs. SCE or 2.56/2.52 V vs. Na^+/Na), which belongs to this phase exclusively.

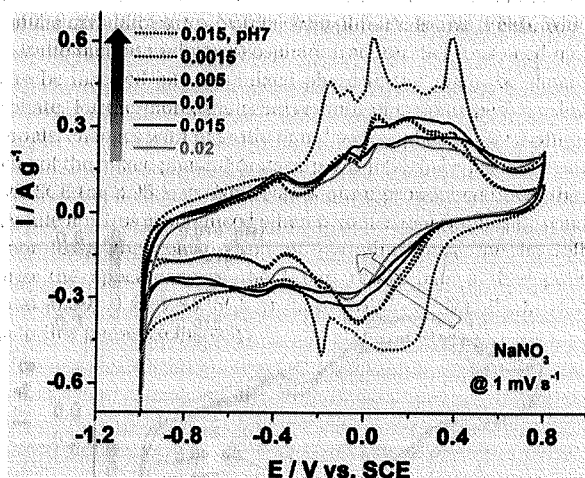


Fig. 10. CV of samples prepared with different amount of citric acid which determines the fraction of $\text{Na}_2\text{FeP}_2\text{O}_7$ and carbon in the mixture. The current is normalized per estimated active mass of the sample.

3.4.2. Chronopotentiometry

3.4.2.3. Higher vs. lower current rates. The galvanostatic profile of samples was first measured at 1 A g^{-1} (Fig. 11) and then at lower current rates ranging from 0.5 to 0.25 A g^{-1} . Although redox plateaus are not well defined, they can be expected over the curves, according to the potentials of CV maxima. Low current redox behavior is influenced by the composition of the sample. While the sodiation/desodiation capacity of NFP_pH3 increases upon the current decrease from 1 A g^{-1} to 0.25 A g^{-1} , its value for NFP_pH7 is practically insensitive to the same change in current, which is in accordance with CV measurements (Fig. S7). Therefore, NFP/SC_pH7 is capable of achieving theoretical capacity at a relatively high current rate of 1 A g^{-1} ($\approx 8\text{C}$), which is also close to the scan rate of 5 mV s^{-1} ($\approx 4.5 \text{ C}$).

The capacity values of NFP/SC_pH3 during anodic/cathodic scan, based on the estimated active mass, are found to be 106/112, 100.7/111, 86/96, 81/91 mA h g^{-1} at 0.12, 0.25, 0.5 and 1 A g^{-1} . The capacity exceeds the theoretical value of $\text{Na}_2\text{FeP}_2\text{O}_7$ (97 mA h g^{-1}) due to the redox contribution of the mixed phase. In literature, the capacity of $\text{Na}_2\text{FeP}_2\text{O}_7/\text{C}$ in an organic electrolyte was found to be close to the theoretical value using both three-electrode and coin-cell configurations [42–45]. Although NFP electrodes can offer higher capacity in aqueous than in organic electrolyte [46], the achievement of the theoretical value in an aqueous medium for this type of material is still challenging [46,47]. Generally, the reduction of NFP particle's size to nano dimensions (20–50 nm) [44] or its impregnation with multiple-walled carbon nanotube (MWCNT) [42] and reduced Graphene oxide (rGO) [45] were found to be effective strategies for pushing NFP to theoretical limit [42,44]. The integration of $\text{Na}_2\text{FeP}_2\text{O}_7$ with NFPP, achieved through the spontaneous citric-assisted sol-gel reaction, can be regarded as one more effective way to improve its electrochemical performance.

When the mixed phase is liberated from the pyrophosphate, higher capacity was obtained amounting to 135 mA h g^{-1} (anodic) and 141 mA h g^{-1} (cathodic) at 1 A g^{-1} . The anodic capacity is close to the theoretical value of NFPP based on the extraction of 3 Na^+ ions, while the cathodic capacity is slightly higher than the theoretical one (141 mA h g^{-1}), which can be attributed to the participation of evolved hydrogen due to side reaction of water reduction at limiting negative potentials. Further current decrease only leads to the increase of the cathodic capacity due to the water decomposition reaction.

When the current returns to the value of 1 A g^{-1} (after low current rates), different behavior between samples is observed, as shown in Fig. 11a,b. A significant capacity drop of NFP/SC_pH3 has been detected (about $\approx 27\%$) since smaller currents probably cause some structural rearrangements responsible for the capacity fade. As a result, poor rate capability was observed (Fig. 11c,d). Unlike NFP/SC_pH3 (Fig. 11a), a small fade was observed after low currents for NFP/SC_7 (Fig. 11b) followed by a high-rate capability (Fig. 11d). The material was found to withstand ultrahigh current rates amounting to 78 C , reaching the capacity of $\approx 80 \text{ mAh g}^{-1}$. This behavior follows the trend observed by CV within corresponding scan rates from 5 to 50 mV s^{-1} , where diffusion behavior still determines the kinetics of the redox process.

The measured specific capacity of the NFPP synthesized here exceeds the literature values obtained in literature, in aqueous electrolyte [21, 22]. Namely, the achievement of NFPP theoretical capacity at such high current rates was not observed in literature. Also, the specific capacity is significantly greater than the capacity NFPP-based samples (prepared by sol-gel), measured in the organic electrolyte under the common current regime [23–25]. Nevertheless, it is the consequence of the faster conductivity of aqueous electrolyte.

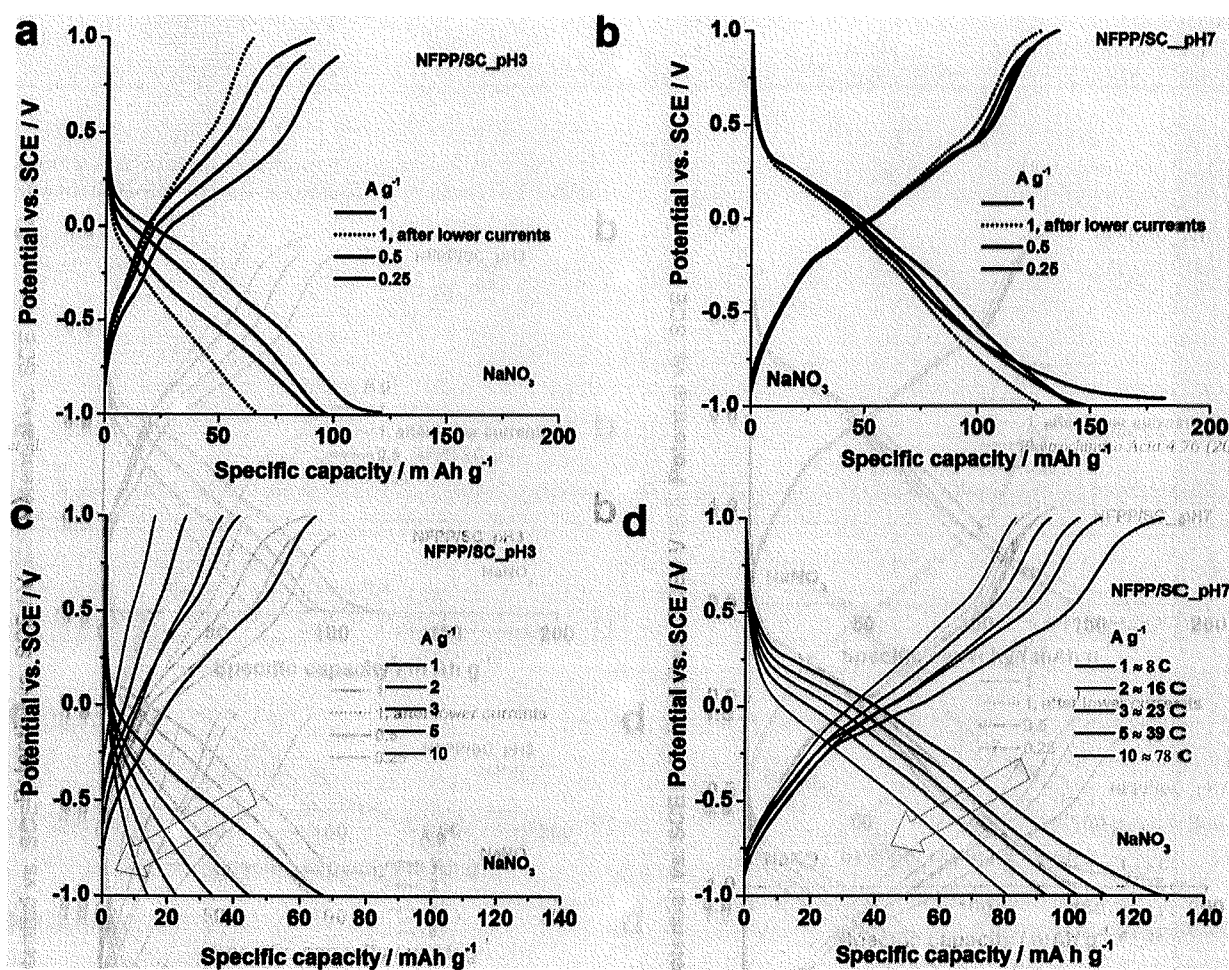


Fig. 11. CP curves of NFPP/SC_pH3 (a,c) and NFPP/SC_pH7 (b,d) at low (a,b) and high currents (c,d). After low currents of 1, 0.5 and 0.25 A g^{-1} , the current was returned to the initial value of 1 A g^{-1} and the response was shown by a dashed curve in a,b.

3.5. Suggestion for the $\text{Na}_2\text{FeP}_2\text{O}_7$ identification in $\text{Na}_4\text{Fe}_3(\text{PO}_4)_2\text{P}_2\text{O}_7/\text{Na}_2\text{FeP}_2\text{O}_7$

Sodium pyrophosphate, $\text{Na}_2\text{FeP}_2\text{O}_7$ is almost an inevitable phase upon $\text{Na}_4\text{Fe}_3(\text{PO}_4)_2\text{P}_2\text{O}_7$ formation, even if the stoichiometry of the mixed phase is adjusted. Although pyrophosphate identification does not seem an issue, due to its highly intensive and numerous X-ray reflections, we would like to shed light on some problems, in the literature, and indicate some helpful insights in that regard.

First, let's look at the results of Cao et al [37] who refined a highly pure mixed phase just by mentioning the presence of impurities such as $\text{Na}_2\text{FeP}_2\text{O}_7$ and NaFePO_4 maricite. We can conclude that their FTIR and CV also confirmed $\text{Na}_2\text{FeP}_2\text{O}_7$ presence, based on the splitting of the symmetrical bridging mode or appearing of the characteristic redox pair at lower potentials. However, there is one more interesting thing here. In many papers with pure or almost pure NFPP phase, XRD region at low angles, below 13° or 15° of 2θ is not presented, while $\text{Na}_2\text{FeP}_2\text{O}_7$ has an intensive reflection at 11 of 2θ . We suggest that this region must be shown because it includes not only the intensive reflection of $\text{Na}_2\text{FeP}_2\text{O}_7$ at 11° of 2θ (if it appears), but also the reflection of the mixed phase at 9° of 2θ . This is significant when a small concentration of pyrophosphate is present in the mixture, and can only be detected based on this low-angle reflection, as shown by Ma [24]. Also, we suggest that CV and FTIR can help identify this phase with certainty due to the highly sensitive response of these methods to the small sodium pyrophosphate fraction.

To recapitulate, our results show that the splitting of low-frequency

symmetric P-O-P mode indicates the pyrophosphate formation in the mixture. Namely, two closely positioned bands at ≈ 718 and $\approx 737 \text{ cm}^{-1}$ in the middle infrared frequency range (it looks like a band splitting) belong to NFPP and NFP phases, respectively. This is also in line with published FTIR diagrams [19,37] where $\text{Na}_2\text{FeP}_2\text{O}_7$ appeared as an accompanying phase of NFPP. Furthermore, CV can serve to identify $\text{Na}_2\text{FeP}_2\text{O}_7$ based on its typical low-potential redox pair, which cannot be attributed to the mixed phase. These peaks are related to a single-phase transition of pyrophosphate lattice and they are very pronounced in CV of $\text{Na}_4\text{Fe}_3(\text{PO}_4)_2\text{P}_2\text{O}_7/\text{Na}_2\text{FeP}_2\text{O}_7$, even with a small amount of $\text{Na}_2\text{FeP}_2\text{O}_7$ [24,37].

3.6. pH-triggered sol-gel reaction of $\text{Na}_4\text{Fe}_3(\text{PO}_4)_2\text{P}_2\text{O}_7$

Wu and coworkers [23] were the first who proposed a sol-gel route of NFPP by mixing Fe powder with citric acid, accompanied by adding phosphate and ethylene glycol into a jade-green ferrous citrate solution. The mixed polyanionic phase is formed at 400 and 500 $^\circ\text{C}$ by decomposing the phosphate to pyrophosphate fraction when Na to Fe ratio follows the stoichiometry. If not, the excess of phosphate or pyrophosphate is observed. This procedure was adopted by other authors [24,45] while one more route, using sodium phytate, ferrous oxalates and phosphate [48], has been recently proposed. This study shows that the thermal phosphate decomposition can be prevented upon sol-gel + thermal treatment and the mixed phase can be obtained using both phosphates and pyrophosphates as reactants. Let's consider the reaction path of the sol-gel process, illustrated in Fig. 12.

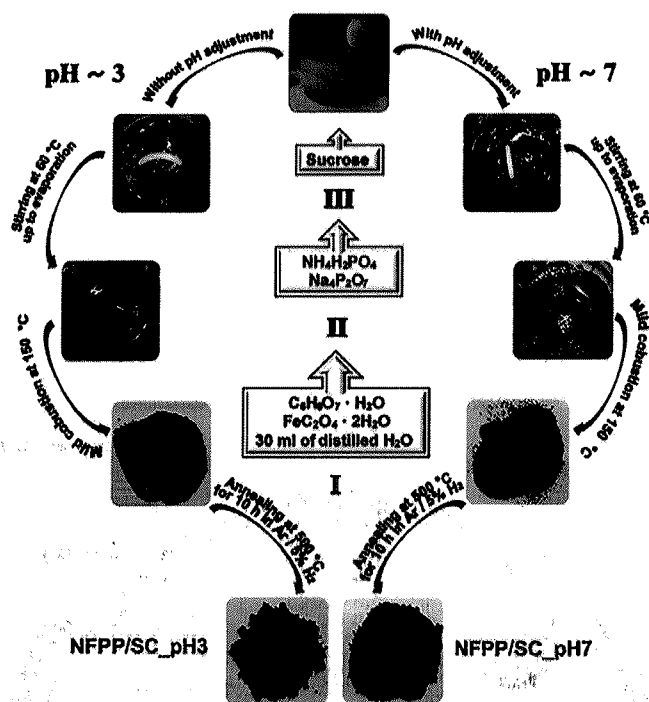


Fig. 12. Sol-gel scheme of NFPP/SC with and without pH adjustment.

First, let's explain our procedure. We used the 0.015 mol citric acid and 0.01 mol Fe, since such ratio corresponds to one used in the sol-gel route reported by Wu et al [23]. Under these conditions the authors obtained a pure NFPP phase by using phosphate salts exclusively and Fe metal as a precursor. When both phosphates and pyrophosphates were used, together with FeC_2O_4 oxalate (under the same mole level), the excess of pyrophosphate was observed due to thermal $\text{PO}_4 \rightarrow \text{P}_2\text{O}_7$ decomposition, which is in line with Wu's observation. To examine the phase composition with the change of citric acid concentration, following the order 0.015, 0.01, 0.005, and 0.0015 we found that citric acid decrease favors the formation of the mixed phase, due to pH increase. When the pH was adjusted with NH_4OH to 7, NFPP was obtained as a major phase. To confirm the trend of changing NFPP/NFP ratio with the citric acid concentration, we also prepared one sample with a citric acid content, higher than the initial 0.015, amounting to 0.02 mol citric acid concentration. As expected, such prepared sample showed a higher amount of $\text{Na}_2\text{FeP}_2\text{O}_7$ than the sample with 0.015 mol citric acid concentration.

In Wu's procedure [23], Fe metal was mixed with citric acid thus forming a jade-green coloured solution, which can be a recognizable step for the successful production of NFPP. As indicated by these authors, the green colour is observed only after 15 h mixing of Fe powder with citric acid. When we mixed $\text{Fe}_2\text{C}_2\text{O}_4$ and citric acid, the yellow suspension was observed even after prolonged mixing, without the appearance of the green colour. Fe (II)-oxalate complex remains since Fe^{2+} to Fe^{3+} oxidation is very slow at low pH (induced by citric acid), while protonation of citrate carboxylic groups, at lower pH, suppresses their direct coordination with Fe ions [49]. When the citric acid is not added, pH is found to be around 6 and pale yellow colour of suspension with greenish tinge is observed (Fig. 1). The reason is the faster Fe^{2+} to Fe^{3+} oxidation at elevated pH [49]. As a result of mentioned processes, the brown colour of gel was observed upon its evaporation, thus indicating that Fe species mostly remain in the oxalate form. In the absence of sucrose, the colour is umber (Fig.S2) due to a higher degree of Fe (II) to Fe (III) oxalate oxidation, since sucrose can be a reducing agent at low pH via its hydrolysis product. The sucrose absence makes the powder's color less intense (Fig. 13). One can conclude that predominance of Fe (II)/Fe (III) oxalates in the reaction mixture leads to $\text{Na}_2\text{FeP}_2\text{O}_7$

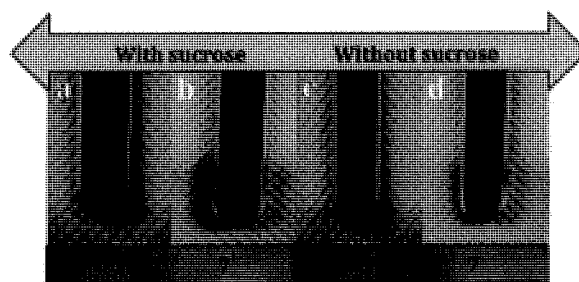


Fig. 13. NFPP_pH3 and NFPP_pH7 precursors obtained by citric-assisted sol-gel route with and without sucrose addition.

formation. Indirect-type Fe-citrate coordination is possible, to a minor extent, via hydrogen bonds of citrate with OH- groups of iron-hydroxo complex which is also formed together with iron-oxalate, under pH of 3 [50]. This behavior can be correlated with the formation of a certain NFPP fraction in NFPP/SC_3 sample.

On the other hand, when the pH of Fe oxalate+citric acid suspension was adjusted to a neutral value, the yellow-to-green colour change was observed (Fig. 12., right side). The green colour can be attributed to the formation of Fe(II) citrate complex since the citric acid becomes deprotonated at neutral pH (except for the proton on the hydroxyl group) and hence reacts rapidly with Fe(II) thus forming a green complex. The green colour becomes more intensive and darker over time and turns into dark brown (due to $\text{Fe}^{2+} \rightarrow \text{Fe}^{3+}$ oxidation facilitated at elevated pH), which afterwards becomes completely transparent (Fig. 1). It can be attributed to the formation of ferric ammonium citrate solution. The presence of OH^- ions facilitates oxidation, thus making the formed complex dissolved and capable of reacting with phosphates and pyrophosphates to the NFPP precursor. Otherwise, these changes are not observed when it comes to spontaneous reaction corresponding to pH of 3. The turbid yellow-brown solution was observed which indicates the phosphate precipitation and its thermal decomposition to NFP phase.

The various nature of complexes formed under pH of 3 and 7 can be responsible for the different carbon content in NFPP and NFPP/NFP composites. Therefore, the higher amount of carbon in NFPP/SC_pH7 (≈ 35 wt.%) than in NFPP/SC_pH7 (≈ 20 wt.%) can be attributed to the more pronounced catalytic properties of Fe ions towards citric acid combustion due to their greater proximity under neutral pH value (Fe-citrate complex dominance). At lower pH, the steric hindrance of oxalates alleviates the catalytic effect of Fe and slows down the citrate combustion.

The question regarding the formation of green Fe (III) oxalates upon the neutralizing of the suspension arises here. Upon pH adjustment to 7, the green color of suspension was attributed to Fe (II) citrate rather than Fe (III) oxalate complex. This was proven by observing colors of two separate suspensions: with and without citric acid. The observed green color during synthesis of NFPP/SC_pH7 (in the presence of citric acid) didn't match the one observed in the synthesis without citric acid, when Fe (III) oxalates were formed under neutralizing pH. Additionally, color changes, during the entire synthesis process of NFPP/SC_pH7, match the change of Fe (II)citrate to ammonium Fe (III) citrate rather than Fe (III) oxalates (Fig. 1 and Fig.S10). Let's explain. To check Fe (III) oxalate contribution, the same reaction was performed without citric acid (at pH=7 adjusted with NH_4OH). A soft green shade is observed which becomes somewhat intensive over time, while the solid green colour can only be observed upon raising pH to 8-9. However, the behavior of Fe (III) oxalates, during evaporation in the absence of citric acid, does not match the reaction path observed in Fig. 1, since the blur suspension was observed over the entire process (Fig.S10), without transparent brown colour. One can conclude that the brown colour of the solution (when the citric acid is added) is still related to the ammonium Fe (III)-citrate complex. As mentioned in the Experimental section, this brown colour gradually fades during evaporation thus producing light-green gel (Fig.

S11). This can be the consequence of the conformation changes of ammonium citrate complex due to water evaporation. Explicitly, there are two ferric ammonium citrate forms, brown and green, depending on pH. Liberation of water can change pH and type of complex. As mentioned, when it comes to Fe-citrate coordination, the combustion path results in the formation of the mixed polyanionic phase.

To summarize this section, pH appeared as a key link to determine the type of Fe-based complex in the sol-gel process through the control of Fe-citrate bonding and consequently final polyanionic composition. Of course, it does not mean that a similar effect would not occur using some other synthesis, under specific conditions. The results open up new aspects for the synthesis of the NFPP phase with promising sodium storage properties.

4. Conclusions

So far, a sol-gel route for $\text{Na}_4\text{Fe}_3(\text{PO}_4)_2\text{P}_2\text{O}_7$ production used phosphate salts exclusively as a phosphorous source, where their partial thermal conversion to pyrophosphates allows the formation of the mixed-phase polyanionic framework. In this contribution, we showed that $\text{Na}_4\text{Fe}_3(\text{PO}_4)_2\text{P}_2\text{O}_7$ could be successfully obtained by citric-assisted sol-gel process, using both phosphate and pyrophosphate as reactants, when the pH of the reaction suspension was adjusted to a neutral value. Namely, when it comes to this spontaneous reaction (without pH adjustment), $\text{Na}_2\text{FeP}_2\text{O}_7$ is formed as the dominant phase due to phosphate to pyrophosphate decomposition. Its fraction decreases on account of increasing NFPP fraction (23wt% \rightarrow 42wt%), as the pH of the suspension increases (2-3 \rightarrow 6-7), which is controlled by the amount of citric acid (0.02 \rightarrow 0). pH adjustment to a neutral value with ammonium-hydroxide, changes the reaction path and the nature of Fe-based complex, thus making it more dissolved and capable of reacting with both phosphate and pyrophosphates. It leads to the formation of the mixed polyanion as the major one, liberated from $\text{Na}_2\text{FeP}_2\text{O}_7$. Such obtained phase shows promising sodium storage performance, measured in an aqueous medium, higher than the one measured for NFPP/NFP heterostructure and capable of reaching theoretical capacity at a relatively high current of 1 A g^{-1} .

A series of samples with different $\text{Na}_4\text{Fe}_3(\text{PO}_4)_2\text{P}_2\text{O}_7/\text{Na}_2\text{FeP}_2\text{O}_7$ ratios were developed, by changing the citric acid to Fe ratio, with the purpose to understand the key factors responsible for the final NFPP composition and its interrelation with the secondary pyrophosphate phase, $\text{Na}_2\text{FeP}_2\text{O}_7$. Through a literature survey and careful observation of suspension color under different stages of synthesis procedures, some crucial issues regarding the reaction path of NFPP sol-gel have been addressed. Namely, the type of the complex, influenced by the initial amount of citric acid and pH of suspension, was found to determine the reaction/combustion path and final polyanionic composition. These parameters actually control Fe-complexation and oxidation, including the type of Fe-coordination, where the dominant complex species switches from oxalate to citrate, as the pH rises. Since the citric acid is highly protonated, under low pH and is not able to directly interact with Fe (II) species, Fe ions remain mostly coordinated with oxalates, which precipitate to pyrophosphates. pH enhancement deprotonates carboxylic groups of citric acid, thus "activating" them to coordinate directly with ferrous ions and further form soluble ammonium ferric citrate complex responsible for the formation of the mixed phase.

Furthermore, both FTIR and CV are proposed as assisting tools to XRD for the identification of sodium pyrophosphate fraction in the $\text{Na}_4\text{Fe}_3(\text{PO}_4)_2\text{P}_2\text{O}_7/\text{Na}_2\text{FeP}_2\text{O}_7$ mixture since these methods are recognized as highly sensitive to the small $\text{Na}_2\text{FeP}_2\text{O}_7$ amount. Therefore, we suggest the following steps for the successful identification of a small sodium pyrophosphate fraction in the heterostructure:

1. Low-angle X-ray region should be always presented (above 5° of 2 θ) since the best way to distinguish $\text{Na}_2\text{FeP}_2\text{O}_7$ from $\text{Na}_4\text{Fe}_3(\text{PO}_4)_2\text{P}_2\text{O}_7$

is by using different positions of the low-angle intensive reflections at 9° of 2 θ (for NFPP) and 11° of 2 θ (for NFP) in Cu K α radiation.

2. FTIR can identify the pyrophosphate fraction based on the splitting of the low-frequency symmetric P-O-P mode (718 and 737 cm^{-1}) in the middle-frequency interval.
3. An appearance of the broad low-potential redox pair (at -0.39/-0.43 V vs. SCE or 2.56/2.52 V vs. Na^+/Na) can identify NFP presence in the mixture, where its current response is quite pronounced when it comes to the small pyrophosphate fractions.

Additionally, several samples with different NFPP and NFP ratios, allowed us to unambiguously assign vibrational modes of these phases and to successfully correlate the CV profile with the phase composition. The characteristic CV behavior was observed, for the heterostructure, with a high and a low amount of the mixed phase. The influence of the pyrophosphate phase on the redox behavior of NFPP is reflected through decreased capacity, more difficult intercalation of Na ions and appearance of the low-potential redox pair.

The results give meaningful insight into NFPP synthesis, which can be helpful for the broad family of polyanionic compounds in light of tailoring their sodium storage properties.

CRedit authorship contribution statement

Aleksandra Gezović: Investigation, Methodology, Writing – original draft. **Miloš Milović:** Investigation, Writing – review & editing. **Danica Bajuk-Bogdanović:** Formal analysis. **Veseljka Grudić:** Writing – review & editing, Supervision. **Robert Dominko:** Writing – review & editing. **Slavko Mentus:** Writing – review & editing, Supervision. **Milica J. Vujković:** Conceptualization, Investigation, Methodology, Writing – original draft, Writing – review & editing, Supervision.

Declaration of Competing Interest

The authors declare that they have no known competing financial interests or personal relationships that could have appeared to influence the work reported in this paper.

Data availability

No data was used for the research described in the article.

Acknowledgments

This research was supported by the NATO Science for Peace and Security Programme under grant G5836-SUPERCAR. A.G. gratefully acknowledges to Ministry of Science and Technological Development Montenegro for the "Scholarship for Doctoral Research in Montenegro". M.M., D.B.B. and M.V. also acknowledge the Ministry of Science, Technological Development and Innovation of the Republic of Serbia (Contract No. 451-03-68/2022-14/200175 and Contract number: 451-03-47/2023-01/200146) for support. M.V. also acknowledges Bilateral project Serbia-Germany. R.D. also acknowledges support from the Slovenian research agency through the P2-0423 core research program. S.M. acknowledges the support of the Serbian Academy of Sciences and Arts through the project F-190.

Supplementary materials

Supplementary material associated with this article can be found, in the online version, at doi:10.1016/j.electacta.2023.143718.

- [47] Y.H. Jung, C.H. Lim, J.H. Kim, D.K. Kim, $\text{Na}_2\text{FeP}_2\text{O}_7$ as a positive electrode material for rechargeable aqueous sodium-ion batteries, *RSC Adv* 4 (2014) 9799–9802, <https://doi.org/10.1039/c3ra47560c>.
- [48] X. Li, Y. Meng, D. Xiao, Three-dimensional hole graphene modified $\text{Na}_4\text{Fe}_3(\text{PO}_4)_2(\text{P}_2\text{O}_7)/\text{C}$ as a high-performance cathode for rechargeable sodium-ion batteries, *Chem. - A Eur. J.* 29 (2023), <https://doi.org/10.1002/chem.202203381>.
- [49] N. Pham, T.D. Waite, A. Ninh Pham, T. David Waite, Oxygenation of Fe(II) in the presence of citrate in aqueous solutions at pH 6.0–8.0 and 25°C: interpretation from an Fe(II)/Citrate speciation perspective, *J. Phys. Chem. A* 112 (2008) 643–651.
- [50] G. Pliego, J.A. Zazo, J.A. Casas, J.J. Rodriguez, Fate of iron oxalates in aqueous solution: The role of temperature, iron species and dissolved oxygen, *J. Environ. Chem. Eng.* 2 (2014) 2236–2241, <https://doi.org/10.1016/j.jece.2014.09.013>.

2. Declaration of competing interest

[47] Y.H. Jung, C.H. Lim, J.H. Kim, D.K. Kim, $\text{Na}_2\text{FeP}_2\text{O}_7$ as a positive electrode material for rechargeable aqueous sodium-ion batteries, *RSC Adv* 4 (2014) 9799–9802, <https://doi.org/10.1039/c3ra47560c>.

[48] X. Li, Y. Meng, D. Xiao, Three-dimensional hole graphene modified $\text{Na}_4\text{Fe}_3(\text{PO}_4)_2(\text{P}_2\text{O}_7)/\text{C}$ as a high-performance cathode for rechargeable sodium-ion batteries, *Chem. - A Eur. J.* 29 (2023), <https://doi.org/10.1002/chem.202203381>.

2. Declaration of competing interest

[49] N. Pham, T.D. Waite, A. Ninh Pham, T. David Waite, Oxygenation of Fe(II) in the presence of citrate in aqueous solutions at pH 6.0–8.0 and 25°C: interpretation from an Fe(II)/Citrate speciation perspective, *J. Phys. Chem. A* 112 (2008) 643–651.

[50] G. Pliego, J.A. Zazo, J.A. Casas, J.J. Rodriguez, Fate of iron oxalates in aqueous solution: The role of temperature, iron species and dissolved oxygen, *J. Environ. Chem. Eng.* 2 (2014) 2236–2241, <https://doi.org/10.1016/j.jece.2014.09.013>.



**Europass
Curriculum Vitae**



Lične informacije

Ime / Prezime **Aleksandra Gezović**
Datum rođenja 01.01.1995. godine
Adresa Univerzitet Cme Gore, Metalurško-tehnološki fakultet, Cetinjski put bb, Podgorica, Cma Gora
E-mail gezovic.a@ucg.ac.me

Trenutna aktivnost Saradnik u nastavi; Student doktorskih studija na Metalurško-tehnološkom fakultetu, Univerzitet Cme Gore.

Oblasti istraživanja Elektrohemija, Hemija materijala, Korozija (Zeleni inhibitori), Materijali za skladištenje i konverziju energije (Li-, Najsionske baterije, superkondenzatori na bazi ugljenika).

Radno iskustvo

Datum Od novembra 2021. godine
Profesija **Saradnik u nastavi na katedni za Opštu i neorgansku hemiju**
Ime i adresa poslodavca Univerzitet Cme Gore, Metalurško-tehnološki fakultet, Cetinjski put bb, Podgorica, Cma Gora
Datum 15.01.2017.-15.10.2017.godine
Profesija **Laborant** u laboratoriji za Analitičku hemiju i laboratoriji za instrumentalne metode
Ime i adresa poslodavca Univerzitet Cme Gore, Metalurško-tehnološki fakultet, Cetinjski put bb, Podgorica, Cma Gora
Tip poslovanja ili sektor Pripravnički staž u okviru programa stručnog usavršavanja lica sa visokim obrazovanjem, koji realizuje Vlada Cme Gore

Obrazovanje

Datum 10.2017.-09.2018. godine
Kvalifikacija **Master fizikohemičar**
Naziv teze „Na_{0.44}MnO₂ kao katodni materijal za vodene natrijum-jonske baterije“
Oblast istraživanja Fizička hemija materijala, Elektrohemija – oblast litijum/natrijum-jonskih baterija
Naziv ustanove koja je izdala kvalifikaciju Univerzitet u Beogradu, Fakultet za fizičku hemiju
Datum 09.2016.-09.2017. godine
Kvalifikacija **Specijalista hemijske tehnologije**
Naziv teze „Korozija bakra u 0.51 M rastvoru NaCl i njegova zaštita ekstraktom propolisa“
Oblast istraživanja Fizička hemija, Elektrohemija, Elektrohemijski procesi i proizvodi
Naziv ustanove koja je izdala kvalifikaciju Univerzitet Cme Gore, Metalurško-tehnološki fakultet
Datum 09.2013.-09.2016. godine
Kvalifikacija **Bečelor hemijske tehnologije**
Naziv teze /
Oblast istraživanja
Naziv ustanove koja je izdala kvalifikaciju Univerzitet Cme Gore, Metalurško-tehnološki fakultet

Lične sposobnosti

Jezik **Engleski B2**
Tečničke sposobnosti i kompetencije UV/VIS spektroskopija, Infracrvena spektroskopija sa Furijeovom transformacijom (FTIR), Rendgenska difrakcija praha, Elektrohemijska mjerenja: Ciklična voltometrija, Hronopotenimetrija, Galvanostatsko punjenje/praznjenje
Računarske sposobnosti i kompetencije Microsoft Office, OriginLab, Sigma-Plot, Adobe Illustrator

Projekti

Datum / Ime / Uloga **2023 – 2025 / Ugljenici izvedeni iz biomase kao anode u natrijum-jonskim baterijama, Bilateralni projekat između Cme Gore i Slovenije / Učesnik, mladi istraživač**
Datum / Ime / Uloga **2023 – 2025 / Izrada visokovrijednosnih proizvoda recikliranjem otpada u industriji aluminijuma, Bilateralni projekat između Cme Gore i Slovenije / Učesnik, mladi istraživač**
Datum / Ime / Uloga **2021 – 2024 / SUPERCAR „Baterije i superkondenzatori na bazi ugljenika (Carbon-based Batteries and Supercapacitors)“ G5836, odobren u okviru NATO programa Nauka za mir i bezbjednost (Science for Peace and Security Programme). Projekat između Slovenije, Srbije i Cme Gore / Učesnik, mladi istraživač**

Datum / Ime / Uloga	2020 – 2022 / BIOUGALJ "Zelena hemija za održivu energiju: Zelena hemija za održivu energiju: Aktivni ugljenik dobijen od biomase kao elektroda za skladištenje električne energije", Nacionalni, naučno-istraživački projekat, podržan od Ministarstva nauke Crne Gore / Učesnik, mladi istraživač
Datum / Ime / Uloga	2019-2023 / Mreža zelenog hemijskog inženjerstva ka unapređenju održivih procesa, COST Akcija CA18224 / Učesnik, mladi istraživač
Datum / Ime / Uloga	10.2019.-11.2019. / Materijali za skladištenje energije, Program gostujućeg predavača, podržan od Ministarstva nauke Crne Gore / Učesnik, mladi istraživač
Ostale aktivnosti	<ul style="list-style-type: none"> ▪ Član organizacionog tima i predavač na ljetnoj školi za studente "Fizičko-hemijske metode karakterizacije materijala za skladištenje energije", 19.09.-25.09.2022. ▪ Član tehničkog odbora, „Savremene baterije i superkondenzatori – Internacionalni simpozijum Beograd 2022“, 01.06.-02.06.2022, Beograd, Srbija ▪ Predavač – „Kako baterije mijenjaju svijet?“ na inženjerskoj ljetnoj školi nauke u Pljevljima, podržanoj od strane NGO "Korak sa naukom", 2021 ▪ Učesnik "Crnogorskse ljetnje startup škole", 2019
Trening/mobilnost	<ul style="list-style-type: none"> ▪ Gostujući istraživač na Nacionalnom institutu za hemiju, Ljubljana, Slovenija – Laboratorija za moderne baterijske sisteme (Šef laboratorije Prof. Robert Dominko), realizovano u okviru NATO programa Nauka za mir i bezbjednost (SUPER CAR), G5836, June 30 - July 29, 2022 ▪ Gostujući istraživač doktorskih studija na Univerzitetu u Beogradu, Fakultetu za fizičku hemiju, pod supervizorstvom dr. Milice Vuković, realizovano kroz projekat EKAMAB, "Ekološki polianjonski katodni materijali za litijum-natrijum-jonske baterije", 15.02.-15.05.2019. godine, 15.02.-15.03.2020. godine, 15.06.-15.08.2020. godine
Ostala dostignuća	<ul style="list-style-type: none"> ▪ Nagrada za najbolju poster prezentaciju na „Twenty-third Annual YUCOMAT 2022 Conference, Herceg Novi, Crna Gora, 29.08.02.09.2022. godine ▪ Stipendija Ministarstva nauke Crne Gore za doktorska istraživanja u Crnoj Gori kroz projekat EKAMAB, "Ekološki polianjonski katodni materijali za litijum-natrijum-jonske baterije", za period od 01.2019.-10.2021. godine



**Europass
Curriculum Vitae**

Bibliografija

Lične informacije

Ime / Prezime **Aleksandra Gezović**
Datum rođenja 01.01.1995. godine
Adresa Univerzitet Crne Gore, Metalurško-tehnološki fakultet, Cetinjski put bb, Podgorica, Crna Gora
E-mail gezovic.a@ucg.ac.me

Istraživačke / naučne aktivnosti

Publikacije

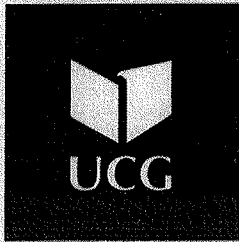
1. **Aleksandra Gezović**¹, Miloš Milović¹, Danica Bajuk-Bogdanović¹, Veselinka Grudić¹, Robert Dominko¹, Slavko Mentus¹, Milica J. Vujković¹, An effective approach to reaching the theoretical capacity of a low-cost and environmentally friendly $\text{Na}_4\text{Fe}_3(\text{PO}_4)_2(\text{P}_2\text{O}_7)$ cathode for Na-ion batteries, *Electrochimica Acta*, 476 (2024) 143718 <https://doi.org/10.1016/j.electacta.2023.143718>
2. **Aleksandra Gezović**¹, Jana Mišurović¹, Branislav Milovanović¹, Mihajlo Etinski¹, Jugoslav Krstić¹, Veselinka Grudić¹, Robert Dominko¹, Slavko Mentus¹, Milica J. Vujković¹, High Al-ion storage of vine shoots-derived activated carbon: New concept for affordable and sustainable supercapacitors, *Journal of Power Sources*, 538 (2022) 231561 <https://doi.org/10.1016/j.jpowsour.2022.231561>
3. **A. Gezović**[#], M.J. Vujković^{#,*}, M. Milović¹, V. Grudić¹, R. Dominko¹, S. Mentus¹, Recent developments of $\text{Na}_4\text{M}_3(\text{PO}_4)_2(\text{P}_2\text{O}_7)$ as the cathode material for alkaline-ion rechargeable batteries: challenges and outlook, *Energy Storage Materials*, 37 (2021) 243-273 <https://doi.org/10.1016/j.ensm.2021.02.011>
4. V. Grudić¹, I. Bošković¹, and **A. Gezović**¹, Inhibition of Copper Corrosion in NaCl Solution by Propolis Extract, *Chem. Biochem. Eng. Q.*, 32 (3) (2018) 299-305 <https://doi.org/10.15255/CABEQ.2018.1357>

Konferencije

1. Jana Mišurović, **Aleksandra Gezović**, Veselinka Grudić, Milica Vujković, Capacitive behaviour of biomass-derived activated carbon in Al-ion containing electrolytes, 2nd International Conference on Chemo and Bioinformatics, Kragujevac, Serbia, September 28-29, **2023**
2. **Aleksandra Gezović**, Veselinka Grudić, Slavko Mentus, Milica Vujković, Electrochemical behaviour of $\text{Na}_4\text{Fe}_3(\text{PO}_4)_2\text{P}_2\text{O}_7$ cathode in the lithium nitrate aqueous solution, Twenty-fourth Annual YUCOMAT 2023 Conference, Herceg Novi, Montenegro, September 4 - September 8, **2023**
3. Jana Mišurović, **Aleksandra Gezović**, Blaž Tratnik, Alen Vižintin, Veselinka Grudić, Robert Dominko, Milica Vujković, Sodium-ion storage mechanism investigation of vine shoots-derived hard carbon, Twenty-fourth Annual YUCOMAT 2023 Conference, Herceg Novi, Montenegro, September 4 - September 8, **2023**
4. Milica Vujković, **Aleksandra Gezović**, Danica Bajuk-Bogdanović, Slavko Mentus, Core issues of the sol-gel process for designing a high-quality polyanionic $\text{Na}_4\text{Fe}_3(\text{PO}_4)_2(\text{P}_2\text{O}_7)$ phase, Twenty-fourth Annual YUCOMAT 2023 Conference, Herceg Novi, Montenegro, September 4 - September 8, **2023**
5. Milica J. Vujković, **Aleksandra Gezović**, Jana Mišurović, Veselinka Grudić, Robert Dominko, Razvoj materijala za baterijske sisteme nove generacije, Savremena stremjenja u elektrohemiji u procesu prelaska na obnovljive izvore energije Naučni skup posvećen 100-godišnjici rođenja inostranog člana SANU ĐŽ. O'M. Bokrisa, Srpska akademija nauka i umjetnosti, Beograd, Srbija 5. jun **2023**
6. Zorica B. Leka, Danijela M. Čukić, **Aleksandra R. Gezović**, Examination of the mechanochemical reaction of Fe(II)- salt with iminodiacetate-dithiocarbamate-ligand (idadc3-), 59th MEETING OF THE SERBIAN CHEMICAL SOCIETY Novi Sad, Serbia, 1-2 June **2023**
7. **Aleksandra Gezović**, Jana Mišurović, Jugoslav Krstić, Alen Vižintin, Veselinka Grudić, Robert Dominko, Milica Vujković, How does activation affect Na storage properties of carbon obtained from vine shoots?, Materials for Sustainable Development Conference (MATSUS) (Materials-for-Sustainable-Development-Conference) Proceedings of MATSUS23 & Sustainable Technology Forum València (STECH23) (MATSUS23), #SusBat - Enabling Beyond Classical Li-ion Batteries through materials development and sustainability València, Spain, **2023** March 6th - 10th
8. Milica Vujković, **Aleksandra Gezović**, Danica Bajuk Bogdanović, Tamara Petrović, Veselinka Grudić, Slavko Mentus, What Drives the Synthesis of Mixed Polyanionic $\text{Na}_4\text{Fe}_3(\text{PO}_4)_2\text{P}_2\text{O}_7$ Cathode Material and Determines its Electrochemical Behavior?, Materials for Sustainable Development Conference (MATSUS) (Materials-for-Sustainable-Development-Conference) Proceedings of MATSUS23 & Sustainable Technology Forum València (STECH23) (MATSUS23), #SusBat - Enabling Beyond Classical Li-ion Batteries through materials development and sustainability València, Spain, **2023** March 6th - 10th
9. Jana Mišurović, **Aleksandra Gezović**, Blaž Tratnik, Alen Vižintin, Veselinka Grudić, Robert Dominko, Milica Vujković, Vine shoots-derived hard carbon as an anode for Na-ion batteries, Materials for Sustainable Development Conference (MATSUS) (Materials-for-Sustainable-Development-Conference) Proceedings of MATSUS23 & Sustainable Technology Forum València (STECH23) (MATSUS23), #SusBat - Enabling Beyond Classical Li-ion Batteries through materials development and sustainability València, Spain, **2023** March 6th - 10th
10. Tamara Petrović, Miloš Milović, **Aleksandra Gezović**, Jana Mišurović, Veselinka Grudić, Milica Vujković, Hybrid aqueous Ca-ion battery: Design and Performance, Twentieth Young Researchers Conference – Materials Science and Engineering, November 30 – December 2, **2022**, Belgrade, Serbia
11. **Aleksandra Gezović**, Miloš Milović, Danica Bajuk-Bogdanović, Veselinka Grudić, Slavko Mentus, Milica Vujković, pH-triggered sol-gel synthesis of $\text{Na}_4\text{Fe}_3(\text{PO}_4)_2\text{P}_2\text{O}_7$ cathode material, Twenty-third Annual YUCOMAT 2022 Conference, Herceg Novi, Montenegro, August 29 - September 2, **2022**
12. Jana Mišurović, **Aleksandra Gezović**, Jugoslav Krstić, Branislav Milovanović, Veselinka Grudić, Slavko Mentus, Milica Vujković, Comparative study of biomass-derived carbon interfacial processes in Aluminum-based and conventional acidic electrolyte, Twenty-third Annual YUCOMAT 2022 Conference, Herceg Novi, Montenegro, August 29 - September 2, **2022**
13. **Aleksandra Gezović**, Jana Mišurović, Jugoslav Krstić, Nikola Simović, Veselinka Grudić, Robert Dominko, Slavko Mentus, Milica J. Vujković, Al-ion Charge Storage Ability of Vine Shoots-derived Carbon, Contemporary Batteries and Supercapacitors – International Symposium Belgrade 2022, June 1-2, **2022**, Belgrade, Serbia
14. Milica J. Vujković, **Aleksandra Gezović**, Danica Bajuk-Bogdanović, Veselinka Grudić, Slavko Mentus, Towards alternative Li-free Electrode Materials: Synthesis and Phase Composition Interrelation, Contemporary Batteries and Supercapacitors – International Symposium Belgrade 2022, June 1-2, **2022**, Belgrade, Serbia
15. Veselinka Grudić, **Aleksandra Gezović**, Jana Mišurović, Jugoslav Krstić, Milica Vujković, Activated Carbon Derived from Vine Shoots as Electrode Material for High-Performance Supercapacitors, 22nd Annual Conference on Material Science YUCOMAT 2021 Herceg Novi, September 3-7, **2021**, Herceg Novi, Montenegro
16. **Aleksandra Gezović**, Milica Vujković, Veselinka Grudić, Miloš Milović, Danica Bajuk-Bogdanović and Slavko Mentus, Three-dimensional $\text{Na}_4\text{Fe}_3(\text{PO}_4)_2\text{P}_2\text{O}_7/\text{Na}_2\text{FeP}_2\text{O}_7$ polyanionic heterostructure: the synthesis and electrochemical behavior in the aqueous lithium and sodium nitrate solutions; 71st Annual Meeting of the International Society of Electrochemistry, 30th August to 4th September, **2020**
17. **Aleksandra Gezović**, Veselinka Grudić, Miloš Milović, Danica Bajuk-Bogdanović, Milica Vujković, Polyanionic cathode material $\text{Na}_4\text{Fe}_3(\text{PO}_4)_2\text{P}_2\text{O}_7/\text{C}$ for aqueous sodium-ion batteries, Twenty-first YUCOMAT 2019 & Eleventh WRTCS 2019, September 2-6, **2019**, Herceg Novi, Montenegro
18. **Gezović Aleksandra**, Vujković Milica, Jugović Dragana, Janković Častvan Ivona, Stojković Simatović Ivana, Mentus Slavko, Synthesis, characterization and electrochemical properties of $\text{Na}_{0.44}\text{MnO}_2$ in NaNO_3 and LiNO_3

aqueous solution, 14th International Conference on Fundamental and Applied Aspects of Physical Chemistry, September 24-28, 2018, 407-410, Belgrade, Serbia

19. **Aleksandra Gezović**, Milica Vujković, Dragana Jugović, Ivona Janković-Častvan and Ivana Stojković Simatović, "Na_{0.44}MnO₂ as a cathode material for aqueous sodium-ion batteries" 3rd International Symposium on Materials for Energy Storage and Conversion-mESC-IS, September 10th-12th, 2018, Belgrade, Serbia
 20. Stojan Božović, Sanja Martinez, Veselinka Grudić and **Aleksandra Gezović**, "Synergistic effect of propolis, tannin and benzoate on the corrosion behaviour of metals in 0.51 M NaCl solution", 23rd International conference of materials protection and industrial finish, KORMAT 2018, Zagreb, Hrvatska
-



Univerzitet Crne Gore
adresa / address_Cetinjska br. 2
81000 Podgorica, Crna Gora
telefon / phone_00382 20 414 255
fax_00382 20 414 230
mail_rektorat@ucg.ac.me
web_www.ucg.ac.me
University of Montenegro

Broj / Ref 03 - 2402
Datum / Date 04.06.2020

Crna Gora
UNIVERZITET CRNE GORE
METALURŠKO-TEHNOLOŠKI FAKULTET

Broj 799
Podgorica, 05.06 2020 god.

Na osnovu člana 72 stav 2 Zakona o visokom obrazovanju („Službeni list Crne Gore“ br 44/14, 47/15, 40/16, 42/17, 71/17, 55/18, 3/19, 17/19, 47/19) i člana 32 stav 1 tačka 9 Statuta Univerziteta Crne Gore, Senat Univerziteta Crne Gore na sjednici održanoj 04.06.2020. godine, donio je

ODLUKU O IZBORU U ZVANJE

Na osnovu člana 72 stav 2 Zakona o visokom obrazovanju
Dr Veselinka Grudić bira se u akademsko zvanje redovni profesor Univerziteta Crne Gore za oblasti **Fizička hemija i Hemijsko inženjerstvo**, na Metalurško-tehnološkom fakultetu Univerziteta Crne Gore, na neodređeno vrijeme.



**SENAT UNIVERZITETA CRNE GORE
PREDSJEDNIK**

Prof. dr Danilo Nikolić, rektor

Prof. dr Veselinka Grudić- biografija

Rođena sam 03.01.1972. godine u Pljevljima. Osnovnu školu sam završila u Pljevljima, a srednju školu u Podgorici sa odličnim uspjehom. Metalurško-tehnološki fakultet-odsjek Neorganska tehnologija (opšti smjer), Univerziteta u Podgorici upisala sam 1990/91. godine. Diplomirala sam 1995. godine i stekla zvanje diplomirani inženjer neorganske tehnologije. Poslijediplomske studije na Fakultetu za fizičku hemiju, Univerziteta u Beogradu upisala sam 1995. godine. Magistarski rad pod naslovom: "Kinetika elektrodnih reakcija metala u aprotičnim elektrolitičkim rastvorima" odbranila sam u februaru 1999. godine, Doktorsku disertaciju pod naslovom: "Oksidacija halogenidnih jona u aprotičnim elektrolitičkim rastvorima" odbranila sam marta 2004. godine na Fakultetu za fizičku hemiju, Univerziteta u Beogradu.

Zaposlena sam na Metalurško-tehnološkom fakultetu u Podgorici od 1995. godine kao asistent – stažista sa punim radnim vremenom na Katedri za fizičku hemiju i elektrohemiju. U zvanje asistenta sam izabrana 2000. godine na istoj katedri. Tokom rada kao asistent- stažista bila sam angažovana na izvođenju vježbi iz predmeta: Elektrohemija i Zaštitne prevlake. Od oktobra 2002. godine izvodila sam vježbe iz predmeta Hemijska termodinamika, a od oktobra 2003. godine sam angažovana u nastavi iz istog predmeta. U zvanje Višeg stručnog saradnika, za izvođenje vježbi iz predmeta: Fizička hemija i elektrohemija, Elektrohemija, Neorganska hemija i Hemija na Poljoprivrednom fakultetu izabrana sam 2005. godine. U zvanje docenta izabrana sa 2009. godine za predmete: Hemijska termodinamika, Tehnološke operacije II, Hemijski izvori struje i Zaštitne prevlake. U zvanje vanrednog profesora izabrana sam 2015. godine za predmete: Hemijska termodinamika, Tehnološke operacije II, Elektrohemija, Hemijski izvori struje i Zaštitne prevlake. 2020. godine izabrana sam u zvanje redovni profesor za oblasti Fizička hemija i Hemijsko inženjerstvo.

Moja profesionalna orijentacija je u području sinteze i karakterizacije materijala za skladištenje energije, elektrohemijskog ispitivanja različitih površinskih procesa na granici elektroda / elektrolit, ispitivanje mehanizma i kinetike sorpcionih procesa, kao i zaštita metalnih materijala od korozije primjenom inhibitora. Bila sam mentor jedne doktorske disertacije, više od 40 specijalističkih radova, dva magistarska rada, a trenutno sam mentor jedne doktorske disertacije i pet master radova. Publikovala sam više od 70 naučnih i konferencijskih radova, od kojih je 21 radova SCI indeksiranih publikacija. Aktivno sam učestvovala, kao rukovodilac ili član radnog tima, u realizaciji 18 naučno - istraživačkih i bilateralnih projekata. U prethodnom periodu bila sam član organizacionog/naučnog odbora nekoliko međunarodnih/regionalnih konferencija.

Univerzitet Crne Gore mi je dodijelio priznanja za postignute rezultate i doprinos razvoju naučno-istraživačkog, umjetničkog i stručnog rada na Metalurško-tehnološkom fakultetu u 2018. i 2019. godini.

Prof. dr Veselinka Grudić-bibliografija (odabrani radovi)

1. Aleksandra Gezović, Miloš Milović, Danica Bajuk-Bogdanović, **Veselinka Grudić**, Robert Dominko, Slavko Mentus, Milica J Vujković, An effective approach to reaching the theoretical capacity of a low-cost and environmentally friendly $\text{Na}_4\text{Fe}_3(\text{PO}_4)_2(\text{P}_2\text{O}_7)$ cathode for Na-ion batteries, *Electrochimica Acta*, 476 2024, 143718,
2. A. Gezović, J. Mišurović, B. Milovanović, M. Etinski, J. Krstić, **V. Grudić**, R. Dominko, S. Mentus, M. J. Vujković*, High Al-ion storage of vine shoots-derived activated carbon: New concept for affordable and sustainable supercapacitors, *Journal of Power Sources* 538, 2022, 231561.
3. A. Gezović#, M. J. Vujković#,*, M. Milović, **V. Grudić**, R. Dominko, S. Mentus, Recent developments of $\text{Na}_4\text{M}_3(\text{PO}_4)_2(\text{P}_2\text{O}_7)$ as the cathode material for alkaline-ion rechargeable batteries: challenges and outlook, *Energy Storage Materials*, 37, 2021, 243-273.
4. Stojan Božović, Tena Gvozdanović, Ana Kraš, **Veselinka Grudić**, Stanislav Kurajica, Sanja Martinez, Rust layer growth and modification by a tannin-based mixture for lowering steel corrosion rates in neutral saline solution, *Corros. Eng. Sci. Technol.*, 2020, 55, 1-9.
5. **Veselinka Grudić**, Sanja Martinez, Bojana Knežević and Ivana Bošković, Corrosion inhibition of steel in a sodium chloride solution by natural honey, *Materials Testing* 61(9), 2019, 881-884.
6. **Grudić Veselinka**, Ivana Bošković, Dragan Radonjić, Željko Jaćimović, Bojana Knežević, The Electrochemical Behavior of Al Alloys in NaCl Solution in the Presence of Pyrazole Derivative, *Iranian Journal of Chemistry & Chemical Engineering*, 38 (2), 93, 2019, 127-138
7. V. Grudić, I. Bošković, A. Gezović "Inhibition of Copper Corrosion in NaCl Solution by Propolis Extract ", *Chemical and Biochemical Engineering Quarterly*, 32 (3), 2018, 299-305.
8. Stojan Božović, Sanja Martinez and **Veselinka Grudić**, "A Novel Environmentally Friendly Synergistic Mixture for Steel Corrosion Inhibition in 0.51 M NaCl", *Acta Chimica Slovenica*, 66, 2019, 112-122.
9. **Veselinka Grudić**, Ivana Bošković, Sanja Martinez, Bojana Knežević, "Study of corrosion inhibition for mild steel in NaCl solution by propolis extract", *Macedonian Journal of Chemistry and Chemical Engineering*, 37 (2), 2018, 203-213,
10. **Grudić Veselinka V.**, Blagojević Nada Z., Vukašinović-Pešić Vesna L., Brašanac Snežana R., "Kinetics of degradation of ascorbic acid by cyclic voltammetry method", *CI&CEQ*, 21(2), 2015, 351-357.

Република Србија
**МИНИСТАРСТВО НАУКЕ,
 ТЕХНОЛОШКОГ РАЗВОЈА И ИНОВАЦИЈА**
 Комисија за стицање научних звања

Број: 660-01-00001/2421
 28.02.2023. године
 Београд

На основу члана 24. став 2. и члана 76. став 7. Закона о науци и истраживањима ("Службени гласник Републике Србије", број 49/19), члана 3. ст. 2. и 4. и члана 40. Правилника о стицању истраживачких и научних звања ("Службени гласник Републике Србије", број 159/20) и захтева који је поднео

Факултет за физичку хемију у Београду

Комисија за стицање научних звања на седници одржаној 28.02.2023. године, донела је

**ОДЛУКУ
 О СТИЦАЊУ НАУЧНОГ ЗВАЊА**

Др Милоша Вуковић

стиче научно звање
Научни саветник

у области природно-математичких наука – хемија

О Б Р А З Л О Ж Е Њ Е

Факултет за физичку хемију у Београду

утврдио је предлог број 2015 од 08.12.2022. године на седници Наставно-научног већа Факултета и поднео захтев Комисији за стицање научних звања 2022 од 08.12.2022. године за доношење одлуке о испуњености услова за стицање научног звања *Научни саветник*.

Комисија за стицање научних звања је по претходно прибављеном позитивном мишљењу Митинског научног одбора за хемију на седници одржаној 28.02.2023. године разматрала захтев и утврдила да именована испуњава услове из члана 76. став 7. Закона о науци и истраживањима ("Службени гласник Републике Србије", број 49/19), члана 3. ст. 1. и 3. и члана 40. Правилника о стицању истраживачких и научних звања ("Службени гласник Републике Србије", број 159/20) за стицање научног звања *Научни саветник*, па је одлучила као у изрени ове одлуке.

Довољенством ове одлуке именована стиче сва права која јој на основу ње по закону припадају.

Одлуку доставити подносиоцу захтева, именованој и архиви Министарства науке, технолошког развоја и иновација у Београду.

ПРЕДСЕДНИК КОМИСИЈЕ

Проф. др Снежана Станковић
 проф. др Снежана Станковић

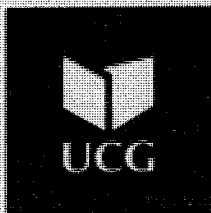


Dr MILICA VUJKOVIĆ - Кратка биографија

Милица Вујковић је рођена у Никшићу, Црна Гора. Научни саветник је на Факултету за физичку хемију, Универзитета у Београду, где је докторирала из области литијум-јонских батерија (2013. године). Од 2011 године, њен научно-истраживачки рад усмерен је на развој материјала за складиштење и конверзију енергије укључујући батерије, суперкондензаторе, електролизере итд. Позивни је предавач престижног MESC+ мастер програма (2019-2023), а од новембра 2023. године је и гостујући предавач на Универзитету Црне Горе. Била је један од организатора симпозијума о батеријама на реномираном 71. ISE скупу у Београду 2020. године и COIN2022 симпозијума (www.coin202.org) одржаном у Српској академији наука и уметности. За своје научно истраживачке резултате награђивана је неколико пута: награда за најбољу докторску тезу од Друштва за истраживање материјала Србије, награда Привредне коморе Београда за најбољу докторску тезу 2013. године и за најбољи патент 2012/2013, Награда Фондације Ђоке Влајковића за најбољи научни рад младих научника Универзитета у Београду 2018. и 2021. године, награда за најбољи постер на Елмини 2022. конференцији. Одржала је неколико позивних предавања на реномираним научним институцијама/конференцијама. Кординира/ла је са 6 пројеката међу којима је и међународни SuperCar-NATOSPS пројекат 2021-2023, билатерални пројекат Србија-Њемачка 2024-2026 и национални HiSuperBat пројекат из програма Промис 2020-2022, финансиран од стране Фонда за Науку Републике Србије. Поред тога, учествовала/учествује у 11 међународних/националних пројекта. Коаутор је 50 научних радова цитираних 1260 пута (h=20), 80 конференцијских саопштења, 1-ог поглавља у монографији и 3 национална патента.

Релевантне публикације:

1. A. Gezović, J. Mišurović, B. Milovanović, M. Etinski, J. Krstić, V. Grudić, R. Dominko, S. Mentus, **M. J. Vujković***, High Al-ion storage of vine shoots-derived activated carbon: New concept for affordable and sustainable supercapacitors, *Journal of Power Sources* 538 (2022) 231561. IF2022=9.719.
2. A. Gezović[#], **M. J. Vujković^{#,*}**, M. Milović, V. Grudić, R. Dominko, S. Mentus, Recent developments of $\text{Na}_4\text{M}_3(\text{PO}_4)_2(\text{P}_2\text{O}_7)$ as the cathode material for alkaline-ion rechargeable batteries: challenges and outlook, *Energy Storage Materials*, 37, 2021, 243-273. IF2020=17.789.
2. **M. J. Vujković**, M. Etinski, B. Vasić, B. Kuzmanović, D. Bajuk-Bogdanović, R. Dominko, S. Mentus, Polyaniline as a charge storage material in an aqueous aluminum-based electrolyte: Can aluminum ions play the role of protons?, *Journal of Power Sources*, 482 (2021) 228937. IF2020=9.127.
3. **Milica Vujković***, Dušan Mladenović, Miloš Milović, Tamara Petrović, Danica Bajuk – Bogdanović, Biljana Šljukić – Paunković, Slavko Mentus, Sodium-pillared vanadium oxides as next-gen materials: Does co-inserted water control the cyclic stability of vanadates in an aqueous electrolyte? *Electrochimica Acta*, 425, 2022, 140603. IF2021=7.336. <https://doi.org/10.1016/j.electacta.2022.140603>
4. **M. Vujković**, D. Bajuk-Bogdanović, Lj. Matović, M. Stojmenović, S. Mentus, Mild electrochemical oxidation of zeolite templated carbon in acidic solutions, as a way to boost its charge storage properties in alkaline solutions, *Carbon*, 138 (2018) 369; IF2018=7.466.
5. J. Senčanski, D. Bajuk-Bogdanović, D. Majstorović, E. Tchernychova, J. Papan, **M. Vujković***, The synthesis of $\text{Li}(\text{Co-Mn-Ni})\text{O}_2$ cathode material from spent-Li ion batteries and the proof of its functionality in aqueous lithium and sodium electrolytic solutions, *J. Power Sources* 342 (2017) 690; IF2017=6.945.
6. Z. Jovanović* D. Bajuk-Bogdanović, S. Jovanović, Ž. Mravik, J. Kovač, I. Holclajtner-Antunović, **M. Vujković**, The role of surface chemistry in the charge storage properties of graphene oxide, *Electrochimica Acta* 258 (2017) 1228; IF2017=5.116.
7. Z. Jovanović*, I. Holclajtner-Antunović, D. Bajuk-Bogdanović, S. Jovanović, Ž. Mravik, **M. Vujković**, *Effect of thermal treatment on the charge storage properties of graphene oxide/12-tungstophosphoric acid nanocomposite*, *Electrochemistry Communications* 83 (2017) 36; IF2017=4.660.
8. **M. Vujković**, S. Mentus, Potentiodynamic and galvanostatic testing of $\text{NaFe}_{0.95}\text{V}_{0.05}\text{PO}_4/\text{C}$ composite in aqueous NaNO_3 solution, and the properties of aqueous $\text{Na}_{1.2}\text{V}_3\text{O}_8/\text{NaNO}_3/\text{NaFe}_{0.95}\text{V}_{0.05}\text{PO}_4/\text{C}$ battery, *J. Power Sources*, 325 (2016) 185; IF2016=6.395.
9. **M. Vujković**, S. Mentus, High-rate intercalation capability of $\text{NaTi}_2(\text{PO}_4)_3/\text{C}$ composite in aqueous lithium and sodium nitrate solutions, *J. Power Sources*, 288 (2015) 176-186. doi:10.1016/j.jpowsour.2015.04.132. (IF2016=6.395).
10. **M. Vujković**, S. Mentus, Fast sodiation/desodiation reactions of electrochemically delithiated olivine LiFePO_4 in aerated aqueous NaNO_3 solution, *J. Power Sources*, 247 (2014) 184-188. doi:10.1016/j.jpowsour.2013.08.062. (IF2014=6.217).

**Univerzitet Crne Gore**

adresa / address: Cetinjska br. 2
81000 Podgorica, Crna Gora
telefon / phone: 00382 20 414 255
fax: 00382 20 414 230
mail: rektorat@ucg.ac.me
web: www.ucg.ac.me

University of MontenegroBrod / Ref 03-1402Datum / Date 24.09.2021

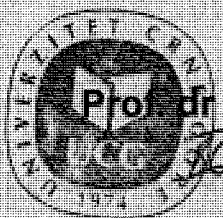
Crna Gora
UNIVERZITET CRNE GORE
METALURŠKO-TEHNOLOŠKI FAKULTET

Brod 14024 / 21
Podgorica, 09.10 - 20 god.

Na osnovu člana 72 stav 2 Zakona o visokom obrazovanju („Službeni list Crne Gore“ br 44/14, 47/15, 40/16, 42/17, 71/17, 55/18, 3/19, 17/19, 47/19, 72/19 i 74/20) i člana 32 stav 1 tačka 9 Statuta Univerziteta Crne Gore, Senat Univerziteta Crne Gore na sjednici održanoj 24.09.2021. godine, donio je

**ODLUKU
O IZBORU U ZVANJE**

Dr IVANA BOŠKOVIĆ bira se u akademsko zvanje redovni profesor Univerziteta Crne Gore iz oblasti **Fizička hemija** na **Metalurško-tehnološkom fakultetu Univerziteta Crne Gore**, na neodređeno vrijeme.

**SENAT UNIVERZITETA CRNE GORE
PREDSJEDNIK****Prof. dr Vladimir Božović, rektor**

PROF. DR IVANA BOŠKOVIĆ- BIOGRAFIJA

Rodjena je 26. 08. 1971. u Titogradu. Osnovnu školu i gimnaziju Slobodan Škerović u Titogradu završila je 1990. godine. Studije neorganske tehnologije je završila na Metalurško-tehnološkom fakultetu u Podgorici 1995. godine. Zaposlila se na istom fakultetu 1995. godine kao asistent-pripravnik na Katedri za fizičku hemiju i elektrohemiju. Poslijediplomske studije na Fakultetu za Fizičku hemiju u Beogradu je završila 1999. godine, a doktorske studije na istom fakultetu 2005. godine i stekla zvanje doktora fizičko-hemijskih nauka. U periodu od 2014. do 2016. godine obavljala je poslove prodekana za istraživanje i razvoj na Metalurško-tehnološkom fakultetu. Redovni je profesor i od 2021. godine prodekan za nastavu Metalurško-tehnološkog fakulteta. Naučno-istraživački rad je dominantno u oblasti fizičke hemije, fizičke hemije materijala i zaštite životne sredine.

PROF. DR IVANA BOŠKOVIĆ- BIOGRAFIJA

Prof. dr. Ivana Bošković-Škerović rođena je 26. 08. 1971. u Titogradu. Osnovnu školu i gimnaziju Slobodan Škerović u Titogradu završila je 1990. godine. Studije neorganske tehnologije je završila na Metalurško-tehnološkom fakultetu u Podgorici 1995. godine. Zaposlila se na istom fakultetu 1995. godine kao asistent-pripravnik na Katedri za fizičku hemiju i elektrohemiju. Poslijediplomske studije na Fakultetu za Fizičku hemiju u Beogradu je završila 1999. godine, a doktorske studije na istom fakultetu 2005. godine i stekla zvanje doktora fizičko-hemijskih nauka. U periodu od 2014. do 2016. godine obavljala je poslove prodekana za istraživanje i razvoj na Metalurško-tehnološkom fakultetu. Redovni je profesor i od 2021. godine prodekan za nastavu Metalurško-tehnološkog fakulteta. Naučno-istraživački rad je dominantno u oblasti fizičke hemije, fizičke hemije materijala i zaštite životne sredine.

BIBLIOGRAFIJA (10 izabranih referenci)

1. **I. Bošković**, S. Mentus, J.M.Pješčić, (2005): Ta₂O₅ templated growth of droplet-like platinum particles by potentiodynamic polarization of tantalum in aqueous solution of hexachloroplatinic acid, *Electrochemistry Communications*, Vol.7, No. 8, pp. 797-802, ISSN: 1388-2481, DOI:10.1016/j.elecom.2005.05.001
2. **I. Bošković**, S. Mentus and M.Pješčić, (2006): Electrochemical behavior of an Ag/TiO₂ composite surfaces, *Electrochimica Acta*, Vol.51, No.14, pp. 2793-2799, ISSN: 0013-4686
3. **I. Bošković**, S. Nenadović, Lj. Kljajević, I.Vukanac, N. Stanković, J. Luković and M. Vukčević (2018): Radiological and physicochemical properties of red/mud based geopolymers, *Nuclear Protection & Radiation*, Vol.33, No.2, pp. 188-194, ISSN: 1451-3994, DOI:10.2298/NTRP.1802188B
4. V. Grudić, **I. Bošković** and A. Gezović (2018): Inhibition of copper corrosion in NaCl solution by propolis extract, *Chemical Biochemical Engineering Quarterly*, Vol. 32, No.3, pp. 299-305, ISSN: 0352-9568, DOI:10.15255/CABEQ.2018.1357
5. **I. Bošković**, V. Grudić, M. Ivanović, I. Milašević, (2018): Investigation of Reduction and Precipitation Rate of Colloidal Gold Particles Obtained in the Process of Electrical and Electronic Waste Recycling, *Iranian Journal of Chemistry & Chemical Engineering*, Vol. 37, No. 2, pp. 133-138, ISSN: 1021-9986
6. **I. Bošković**, M. Vukčević, S. Nenadović, M. Mirković, M. Stojmenović, V.Pavlović and Lj. Kljajević, (2019): Characterization of Red mud/metakaolin-based geopolymers as modified by Ca(OH)₂, *Materiali in Tehnologije*, 53 (3) 341 ISSN:1580-2949, DOI: 10.17222/mit.2018.130
7. A. Occhicone, M. Vukčević, **I. Bošković** and C. Ferone (2021): Red Mud-Blast Furnace Slag-Based Alkali-Activated Materials, *Sustainability*, Vol.13, No. 20, pp.11298-11313, ISSN: 2071-1050, DOI: 10.3390
8. M.Vukčević, **I. Bošković**, B. Potparić, S. Nenadović, L.Kljajević, N. Jović-Orsini (2021): Characterisation of metakaolin-based geopolymers as modified by organic phase, *Journal of Environmental Protection and Ecology*, Vol.22, No.1, pp. 127-138, ISSN: 1311-5065
9. A. Occhicone, M. Vukčević, **I. Bošković**, S. Mingione and C. Ferone (2022): Alkali-Activated Red Mud and Construction and Demolition Waste-Based Components: Characterization and Environmental Assessment, *Materials*, Vol. 15, pp. 1617-1631, ISSN: 1996-1944, DOI:10.3390/ma15020694
10. S. Nenadović, J. Gulicovski, M. Mirković, Lj. Kljajević, **I. Bošković**, M. Vukčević and M. Nenadović (2022): Structural, Mechanical and Chemical Properties of Low Content Carbon Geopolymer, *Sustainability*, Vol. 14, pp. 4885-4898, , ISSN: 2071-1050, DOI:10.3390/su14094885



Република Србија
**МИНИСТАРСТВО ПРОСВЕТЕ,
НАУКЕ И ТЕХНОЛОШКОГ РАЗВОЈА**
Комисија за стицање научних звања

Број: 660-01-00001/2064

22.02.2022. године

Београд

На основу члана 24. став 2. и члана 76. став 6. Закона о науци и истраживањима ("Службени гласник Републике Србије", број 49/19), члана 3. ст. 2. и 4. и члана 40. Правилника о стицању истраживачких и научних звања ("Службени гласник Републике Србије", број 159/20) и захтева који је поднео

Института техничких наука САНУ у Београду

Комисија за стицање научних звања на седници одржаној 22.02.2022. године, донела је

**ОДЛУКУ
О СТИЦАЊУ НАУЧНОГ ЗВАЊА**

Др Милош Миловић

стиче научно звање

Виши научни сарадник

у области природно-математичких наука - физичка хемија

О Б Р А З Л О Ж Е Њ Е

Института техничких наука САНУ у Београду.

утврдио је предлог број 366/1 од 22.10.2021. године на седници Научног већа Института и поднео захтев Комисији за стицање научних звања број 370/1 од 25.10.2021. године за доношење одлуке о испуњености услова за стицање научног звања **Виши научни сарадник**.

Комисија за стицање научних звања је по претходно прибављеном позитивном мишљењу Матичног научног одбора за хемију на седници одржаној 22.02.2022. године разматрала захтев и утврдила да именовани испуњава услове из члана 76. став 6. Закона о науци и истраживањима ("Службени гласник Републике Србије", број 49/19), члана 3. ст. 1. и 3. и члана 40. Правилника о стицању истраживачких и научних звања ("Службени гласник Републике Србије", број 159/20) за стицање научног звања **Виши научни сарадник**, па је одлучила као у изреци ове одлуке.

Доношењем ове одлуке именовани стиче сва права која му на основу ње по закону припадају.

Одлуку доставити подносиоцу захтева, именованом и архиви Министарства просвете, науке и технолошког развоја у Београду.

ПРЕДСЕДНИК КОМИСИЈЕ

Ђорђевић

Др Ђурђица Јововић,
научни саветник

ПРВИ ПОМОЋНИК ПРЕДСЕДНИКА ВЛАДЕ



Институт техничких наука САНУ

Бр. 165/1

12.04. 20 22. год.

Кнез Михајлова 35/IV, Београд, ПФ 377
Тел: 2636-994, 2185-437, Факс: 2185-263

Милош Миловић - СТРУЧНА БИОГРАФИЈА

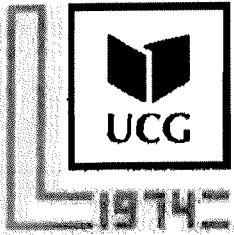
Милош Драгош Миловић рођен је 1987. године у Приштини. Основну школу започео у Приштини, а завршио у Рашки, као и средњошколско гимназијско образовање. Године 2006. уписује Факултет за физичку хемију Универзитета у Београду. Мастер рад „Креирање неуронске мреже у циљу процене садржаја гвожђа у мозгу оболелих од амиотрофичне латералне склерозе“ одбранио је 2011. године. Докторске студије уписује 2011. на истом факултету, а докторски рад под називом “Синтеза, структурна и електрохемијска својства LiFePO_4 и $\text{Li}_2\text{FeSiO}_4$ као катодних материјала за литијум-јонске батерије“ одбранио је 2016. У Институту техничких наука САНУ запослен је од децембра 2011. Од 2022. је у звању вишег научног сарадника. У област научног интересовања спадају: хемијски извори струје, литијум-јонске батерије, електродни материјали, хемија чврстог стања, кристалографија. До сада је објавио 21 рад у међународним часописима. Хиршов индекс М. Миловића је 7, а цитираност је 176 (према бази Scopus од 17.03.2024). Рецензент је у неколико часописа. Члан је Српског керамичког друштва и Српског кристалографског друштва. Члан је научног одбора конференције Младих истраживача (Young Researchers' Conference). Био је члан неколико комисија за избор у научна звања пред научним већима Института техничких наука САНУ и Института за нуклеарне науке „Винча“. Награђен је Повешом Универзитета у Београду као најбољи студент генерације Факултета за физичку хемију који је дипломирао у школској 2010/11. Награда је из 2012. Добитник је дипломе „Павле Савић“, коју додељује Друштво физикохемичара Србије за успех постигнут на студијама физичке хемије. Награда је из 2014. Добитник је стипендије Међународне уније за кристалографију (IUCr) за учешће на XXV конференцији Српског кристалографског друштва: 25th Conference of the Serbian Crystallographic Society, 2018. Добитник је награде за најбољу постер презентацију на конференцији: 3rd International Symposium on Materials for Energy Storage and Conversion mESC-IS 2018.

Листа најзначајнијих радова

1. **Miloš Milović**, Dragana Jugović, Nikola Cvjetičanin, Dragan Uskoković, Aleksandar S. Milošević, Zoran S. Popović, Filip R. Vukajlović, Crystal structure analysis and first principle investigation of F doping in LiFePO_4 , *Journal of Power Sources* 241 (2013) 70-79, DOI: [10.1016/j.jpowsour.2013.04.109](https://doi.org/10.1016/j.jpowsour.2013.04.109)
2. Dragana Jugović, **Miloš Milović**, Valentin N. Ivanovski, Max Avdeev, Robert Dominko, Bojan Jokić, Dragan Uskoković, Structural study of monoclinic $\text{Li}_2\text{FeSiO}_4$ by X-ray diffraction and Mössbauer spectroscopy, *Journal of Power Sources* 265 (2014) 75-80, DOI: [10.1016/j.jpowsour.2014.04.121](https://doi.org/10.1016/j.jpowsour.2014.04.121) (ИФ=6.217, област: 2/28 Electrochemistry; бр хетероцитата: 10)
3. **Miloš Milović**, Dragana Jugović, Miodrag Mitrić, Robert Dominko, Ivana Stojković-Simatović, Bojan Jokić, Dragan Uskoković, The use of methylcellulose for the synthesis of $\text{Li}_2\text{FeSiO}_4/\text{C}$ composites, *Cellulose* 23 (2016) 239-246, DOI: [10.1007/s10570-015-0806-9](https://doi.org/10.1007/s10570-015-0806-9)
4. Jugović, D., Mitrić, M., **Milović, M.**, Cvjetičanin, N., Jokić, B., Umićević, A., Uskoković, D. The influence of fluorine doping on the structural and electrical properties of the LiFePO_4 powder, (2017) *Ceramics International*, 43 (3), pp. 3224-3230. DOI: [10.1016/j.ceramint.2016.11.149](https://doi.org/10.1016/j.ceramint.2016.11.149)
5. Jugović, D., **Milović, M.**, Popović, M., Kusigerski, V., Škapin, S., Rakočević, Z., Mitrić, M. Effects of fluorination on the structure, magnetic and electrochemical properties of the P2-type Na_xCoO_2 powder, (2019) *Journal of Alloys and Compounds*, 774, pp. 30-37. DOI: [10.1016/j.jallcom.2018.09.372](https://doi.org/10.1016/j.jallcom.2018.09.372)
6. Jugović, D., **Milović, M.**, Popović, M., Kusigerski, V., Škapin, S., Rakočević, Z., Mitrić, M. Effects of fluorination on the structure, magnetic and electrochemical properties of the P2-type Na_xCoO_2 powder, (2019) *Journal of Alloys and Compounds*, 774, pp. 30-37. DOI: [10.1016/j.jallcom.2018.09.372](https://doi.org/10.1016/j.jallcom.2018.09.372)
7. **Milović, M.D.**, Vasić Aničijević, D.D., Jugović, D., Aničijević, V.J., Veselinović, L., Mitrić, M., Uskoković, D. On the presence of antisite defect in monoclinic $\text{Li}_2\text{FeSiO}_4$ – A combined X-Ray diffraction and DFT study, (2019) *Solid State Sciences*, 87, pp. 81-86. DOI: [10.1016/j.solidstatesciences.2018.11.008](https://doi.org/10.1016/j.solidstatesciences.2018.11.008)
8. **Milović, M.**, Jugović, D., Vujković, M., Kuzmanović, M., Mraković, A., Mitrić, M. Towards a green and cost-effective synthesis of polyanionic cathodes: comparative electrochemical behaviour of LiFePO_4/C , $\text{Li}_2\text{FeP}_2\text{O}_7/\text{C}$ and $\text{Li}_2\text{FeSiO}_4/\text{C}$ synthesized using methylcellulose matrix, (2021) *Bulletin of Materials Science*, 44 (2), art. no. 144. DOI: [10.1007/s12034-021-02397-3](https://doi.org/10.1007/s12034-021-02397-3)
9. Gezović, A., Vujković, M.J., **Milović, M.**, Grudić, V., Dominko, R., Mentus, S. Recent developments of $\text{Na}_4\text{M}_3(\text{PO}_4)_2(\text{P}_2\text{O}_7)$ as the cathode material for alkaline-ion rechargeable batteries: challenges and outlook, (2021) *Energy Storage Materials*, 37, pp. 243-273. DOI: [10.1016/j.ensm.2021.02.011](https://doi.org/10.1016/j.ensm.2021.02.011)

10. **Milović, M., Vujković, M., Jugović, D., Mitrić, M.** Electrochemical and structural study on cycling performance of γ - LiV_2O_5 cathode, (2021) *Ceramics International*, 47 (12), pp. 17077-17083. [DOI: 10.1016/j.ceramint.2021.03.016](https://doi.org/10.1016/j.ceramint.2021.03.016)

10. Milović, M., Vujković, M., Jugović, D., Mitrić, M. Electrochemical and structural study on cycling performance of γ - LiV_2O_5 cathode, (2021) *Ceramics International*, 47 (12), pp. 17077-17083. [DOI: 10.1016/j.ceramint.2021.03.016](https://doi.org/10.1016/j.ceramint.2021.03.016)



Univerzitet Crne Gore

- ☑ Cetinjska 2
- ☑ 81000 Podgorica, Crna Gora
- ☑ t: +382 20 411 233
- ☑ r: info@ucg.ac.me
- ☑ www.ucg.ac.me

University of Montenegro

Rezi / Rez: 03-1389

Datum / Date: 23. 02 2024

Na osnovu člana 72 stav 2 Zakona o visokom obrazovanju („Službeni list Crne Gore“, br. 44/14, 47/15, 40/16, 42/17, 71/17, 55/18, 3/19, 17/19, 47/19, 72/19 i 74/20 i 104/21, 86/22 i 125/23) i člana 32 stav 1 tačka 9 Statuta Univerziteta Crne Gore, Senat Univerziteta Crne Gore, na sjednici održanoj 23.2.2024. godine, donio je

University of Montenegro

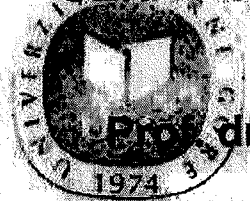
ODLUKU O IZBORU U ZVANJE

Na osnovu člana 72 stav 2 Zakona o visokom obrazovanju („Službeni list Crne Gore“, br. 44/14, 47/15, 40/16, 42/17, 71/17, 55/18, 3/19, 17/19, 47/19, 72/19 i 74/20 i 104/21, 86/22 i 125/23) i člana 32 stav 1 tačka 9 Statuta Univerziteta Crne Gore, Senat Univerziteta Crne Gore, na sjednici održanoj 23.2.2024. godine, donio je

Dr MARTIN ČALASAN bira se u akademsko zvanje **vanredni profesor Univerziteta Crne Gore** za oblast **Električne mašine i pogoni** na **Elektrotehičkom fakultetu Univerziteta Crne Gore**, na period od pet godina.

SENAT UNIVERZITETA CRNE GORE

PREDSJEDNIK



Prof. dr Vladimir Božović, rektor

Na osnovu člana 72 stav 2 Zakona o visokom obrazovanju („Službeni list Crne Gore“, br. 44/14, 47/15, 40/16, 42/17, 71/17, 55/18, 3/19, 17/19, 47/19, 72/19 i 74/20 i 104/21, 86/22 i 125/23) i člana 32 stav 1 tačka 9 Statuta Univerziteta Crne Gore, Senat Univerziteta Crne Gore, na sjednici održanoj 23.2.2024. godine, donio je

SENAT UNIVERZITETA CRNE GORE

PREDSJEDNIK



Prof. dr Vladimir Božović, rektor

Na osnovu člana 72 stav 2 Zakona o visokom obrazovanju („Službeni list Crne Gore“, br. 44/14, 47/15, 40/16, 42/17, 71/17, 55/18, 3/19, 17/19, 47/19, 72/19 i 74/20 i 104/21, 86/22 i 125/23) i člana 32 stav 1 tačka 9 Statuta Univerziteta Crne Gore, Senat Univerziteta Crne Gore, na sjednici održanoj 23.2.2024. godine, donio je

Ćalasan Martin - Biografija

Rođen sam 05. oktobra 1986. godine u Plužinama. Osnovnu školu sam pohađao u mjestu Brezna, Opština Plužine, a Gimnaziju, prirodno matematički smjer, u Plužinama. Za uspjeh u osnovnoj i srednjoj školi dobitnik sam diplome »Luča 1« i nosilac priznanja »Đak generacije«.

Školske 2005/2006. započeo sam studije na Elektrotehničkom fakultetu Univerziteta Crne Gore, odsjek Energetika i automatika. Osnovne studije završio sam u junu 2008. godine sa prosječnom ocjenom 9.86. Nakon druge i treće godine studija dobio sam novčane nagrade Elektrotehničkog fakulteta za najboljeg studenta odsjeka Energetika i automatika. Specijalističke studije, smjer Industrijska elektrotehnika, na istom fakultetu, završio sam u junu 2009. godine sa prosječnom ocjenom 10.00. Tokom osnovnih i specijalističkih studija bio sam korisnik stipendija Vlade Republike Crne Gore za talentovane studente i učenike, Opštine Plužine, Regulatorne agencije za energetiku i Elektroprivrede Crne Gore AD Nikšić (EPCG).

Magistarske studije na Elektrotehničkom fakultetu Univerziteta Crne Gore, smjer Industrijska elektrotehnika, završio sam odbranom magistarske teze naslova »*Simulacioni model i dinamika statičkog pobudnog sistema sinhronih generatora u HE "Perućica"*«, pod mentorstvom prof. dr Milutina Ostojića, u junu 2010. godine s opštim uspjehom 10, čime sam stekao akademski naziv magistra elektrotehničkih nauka.

Doktorsku disertaciju naslova »*Upravljanje prekidačkim reluktantnim generatorom i tolopogije energetske pretvarača za rad u kontinualanom režimu*«, pod mentorstvom prof. dr Vladana Vujičića, redovnog profesora Elektrotehničkog fakulteta Univerziteta Crne Gore, odbranio sam 15.06.2017. godine, čime sam stekao naučni stepen doktora elektrotehničkih nauka.

U zvanje DOCENTA za oblast Električne mašine i pogoni (Električne mašine – osnovne studije – studijski program Energetika i automatika; FACTS i HVDC komponente energetske elektronike – master studije – studijski program Elektroenergetski sistemi; Električni pogoni – master studije – studijski program Automatika i Industrijska elektrotehnika; Upravljanje i regulacija električnih pogona – master studije - studijski program Automatika i Industrijska elektrotehnika) na Elektrotehničkom fakultetu Univerziteta Crne Gore, izabran sam na sjednici Senata UCG na sjednici od 12.02.2019. godine. U dosadašnjem radu na Elektrotehničkom fakultetu u Podgorici, Pomorskom fakultetu u Kotoru i Mašinskom fakultetu u Podgorici izvodio sam nastavu iz većeg broja predmeta iz izborne oblasti - oblasti električnih mašina i pogona. Na doktorskim studijama na Elektrotehničkom fakultetu ustanovio sam i predmet Sistemi za skladištenje električne energije.

U dosadašnjem naučno-istraživačkom radu objavio sam oko 55 radova na SCI/SCIE listi, kao i oko 150 radova u ostalim časopisima, kao i na domaćim, regionalnim i međunarodnim konferencijama. Objavio sam knjigu »*Mašine jednosmjerne struje*« u izdanju Naučne knjige iz Beograda (Srbija), kao i nekoliko poglavlja u knjigama međunarodnih izdavača. Recenzirao sam preko 2000 radova u časopisima sa SCI/SCIE liste i bio sam učesnik nekoliko međunarodnih projekata. Bio sam jedan od urednika u šest specijalnih izdanja časopisa sa SCI/SCIE liste:

- [1] "Renewable Based Energy Distributed Generation" – časopis Energies (ISSN 1996-1073)
- [2] "Power System Dynamics, Operation, and Control including Renewable Energy Systems and Smart Grid: Technology and Applications" – časopis Electronics (ISSN 2079-9292)
- [3] „Energy Hubs in Modern Energy Systems with Renewables and Energy Storage“ – časopis Frontiers in Energy Research - Smart Grids (ISSN 2296-598X)
- [4] „Electrical Vehicles Technologies and the Power Quality Challenges“ - časopis International Transactions on Electrical Energy Systems (ISSN: 2050-7038)
- [5] „Mathematical Modeling in Energy Sector“ – časopis Energies (ISSN 1996-1073)
- [6] „Technical and Environmental Implications of Electrifying Waterborne Transportation Systems“ – časopis Water (ISSN 1996-1073).

U prethodnom periodu, bio sam i član organizacionog/naučnog odbora većeg broja međunarodnih, domaćih i regionalnih konferencija, dok sam održao i veći broj predavanja na naučnim skupovima, ljetnjim školama i stručnim savjetovanjima.

Za svoj nastavni i naučno-istraživački rad dobio sam sljedeće nagrade i priznanja:

- Priznanja UCG za postignute rezultate i doprinose razvoju naučno-istraživačkog, umjetničkog i stručnog rada na Elektrotehničkom fakultetu u 2019, 2020 i 2022. godini
- Nagradu CANU za 2020. godinu iz Fonda Crnogorske akademije nauka i umjetnosti za podsticanje podmlatka,
- DANUBIUS nagradu za mlade naučnike koju dodjeljuje Austrijsko ministarstvo za obrazovanje, nauku i istraživanje i Institut za Dunavsku regiju i Centralnu Evropu, u oktobru 2021. godine
- Nagrada Ministarstva nauke za najboljeg pronalazača u Crnoj Gori u 2017. godini,
- Nagrada Ministarstva nauke za najboljeg naučnika Crne Gore u 2022. godini, i
- Državnu nagradu OKTOIH za 2022. godinu.

Imam naučnu saradnju sa profesorima i istraživačima iz preko 10 zemalja i sa preko 25 međunarodnih institucija. U periodu od marta 2021. godine do septembra 2021. godine bio sam član Savjeta za nauku Vlade Crne Gore. Od juna 2022. godine član sam Odbora direktora Elektroprivrede Crne Gore. Član sam IEEE i CIGRE, dok sam od 2021. godine potpredsjednik Crnogorskog komiteta CIGRE – CG KO CIGRE.

Ćalasan Martin – bibliografija (odabrani SCI/SCIE radovi)

- [1] Z. M. Ali, M. Calasan, F.H. Gandoman, F. Jurado, Shady H.E. Abdel Aleem, „Review of batteries reliability in electric vehicle and E-mobility applications“, *Ain Shams Engineering Journal*, August 2023, 102442, <https://doi.org/10.1016/j.asej.2023.102442>
- [2] I. Knezevic, M. Calasan, T. Dlabac, „Novel Analytical Approaches for Induction Machine Direct Start-up Speed–Time Curve Modeling under Fan Load“, *Archiv für Elektrotechnik - Electrical Engineering*, Vol. AA, Issue BB, 2023, pp.AA-BB, <https://doi.org/10.1007/s00202-023-02039-3>
- [3] M. Micev, M. Ćalasan, M. Radulović, " Optimal tuning of the novel voltage regulation controller considering the real model of the automatic voltage regulation system," *Heliyon*, Vol. 9, No. 8, 2023, pp. e18707, <https://doi.org/10.1016/j.heliyon.2023.e18707>
- [4] M. Petronijevic, I. Radonjic, M. Dimitrijevic, L. Pantic, M. Calasan, „Performance evaluation of single-stage photovoltaic inverters under soiling conditions“, *Ain Shams Engineering Journal*, 2023, pp. 102353, <https://doi.org/10.1016/j.asej.2023.102353>
- [5] M. Ćalasan, A. Jovanović, V. Rubežić, D. Mujičić, A. Deriszadeh, “Notes on parameter estimation for single-phase transformer”, *IEEE Transactions on Industry Applications*, Vol. 56, Issue 4, pp. 3710 - 3718, jul 2020, <https://doi.org/10.1109/TIA.2020.2992667>, ISSN 0093-9994
- [6] M. Micev, M. P. Calasan, S. H. E. Abdel Aleem, H. M. Hasanien and D. Petrovic, "Two Novel Approaches for Identification of Synchronous Machine Parameters from Short-Circuit Current Waveform," *IEEE Transactions on Industrial Electronics*, Vol. 69, Issue 6, jun 2022, pp. 5536 – 5546, <https://doi.org/10.1109/TIE.2021.3086715>, ISSN: 2780046, ISSN: 0278-0046
- [7] A.Deriszadeh, M. P. Ćalasan, A. Alaei and J. F. Gieras, "A Novel Field Current Estimation Method for Brushless Wound-field Synchronous Machine," *IEEE Transactions on Transportation Electrification*, Volume: 8, Issue: 3, September 2022, pp. 3524 – 3533, <https://doi.org/10.1109/TTE.2022.3162173>, ISSN: 2332-7782
- [8] M. Micev, M. Ćalasan, M. Radulović, „Full Synchronous Machine Parameters Identification Based on Field and Armature Current During the Short-Circuit“, *IEEE Transactions on Industry Application*, Vol. 57, Iss. 6, pp. 5959 - 5968 <https://doi.org/10.1109/TIA.2021.3112141>, ISSN 0093-9994
- [9] M. Micev, M. Ćalasan, M. Radulović, S. H. E. Abdel Aleem, H. M. Hasanien and A. F. Zobaa, "Artificial Neural Network-Based Nonlinear Black-Box Modeling of Synchronous Generators," *IEEE Transactions on Industrial Informatics*, Vol. 19, Issue 3, March 2023, pp. 2826 – 2837, <https://doi.org/10.1109/TII.2022.3187740>, Print ISSN: 1551-3203
- [10] M. Micev, M. Ćalasan, D. Petrović, Z.M. Ali, N. V. Quynh, S. H. E. Abdel Aleem „Field Current Waveform-Based Method for Estimation of Synchronous Generator Parameters Using Adaptive Black Widow Optimization Algorithm“, *IEEE Access*, Vol. 8, pp. 207537-207550, <https://doi.org/10.1109/ACCESS.2020.3037510>, ISSN 2169-3536
- [11] A. Deriszadeh, O. Karabasoglu, M. P Calasan, F. Mehdipour „A Dynamic Functional Model of Diode Bridge Rectifier for Unbalanced Input Voltage Conditions“, *IET Power Electronics*, Vol. 14, Issue 3, beb. 2021., pp. 584-589, <https://doi.org/10.1049/pel2.12040>, ISSN 1755-4543
- [12] M. Micev, M. Ćalasan, D. Oliva, „Design and robustness analysis of an Automatic Voltage Regulator system controller by using Equilibrium Optimizer algorithm“, *Computers and Electrical Engineering*, Volume 89, January 2021, pp. 106930, <https://doi.org/10.1016/j.compeleceng.2020.106930>, ISSN 0045-7906
- [13] M. Rawa, Y. Al-Turkiab, H. Sindi, M. Ćalasan, Z.M.Ali, S.H.E. Abdel Aleem, „Current-voltage curves of planar heterojunction perovskite solar cells – Novel expressions based on Lambert W function and Special Trans Function Theory“, *Journal of Advanced Research*, Volume 44, Feb. 2023, pp. 91-108, <https://doi.org/10.1016/j.jare.2022.03.017>, Print ISSN: 2090-1232
- [14] M. Calasan, SHE Allem, H. Hasanien, Z Alaas, Z. Ali, „An innovative approach for mathematical modeling and parameter estimation of PEM fuel cells based on iterative Lambert W function“, *Energy*, Vol. 264, February 2023, pp. 126165, <https://doi.org/10.1016/j.energy.2022.126165>, Print ISSN: 0360-5442

- [15] M. Micev, M. Čalasan, D. Stipanović, M. Radulović, "Modeling the relation between the AVR setpoint and the terminal voltage of the generator using artificial neural networks," *Engineering Applications of Artificial Intelligence*, Vol. 120, April 2023, pp. 105852, <https://doi.org/10.1016/j.engappai.2023.105852>, Print ISSN: 0952-1976
- [16] M. Calasan, S.H.E. Abdel Aleem, A. F. Zobaa „A new approach for parameters estimation of double and triple diode models of photovoltaic cells based on iterative Lambert W function“, *Solar Energy*, Vol. 218 (2021) 392–412, <https://doi.org/10.1016/j.solener.2021.02.038>, ISSN 0038-092X
- [17] M. Calasan, S.H.E. Abdel Aleem, M. Bulatovic, Vesna Rubezic, Z.M. Ali, M. Micev „Design of controllers for automatic frequency control of different interconnection structures composing of hybrid generator units using the chaotic optimization approach“, *Electrical Power and Energy Systems*, Vol. 129 (2021), pp. 106879, <https://doi.org/10.1016/j.ijepes.2021.106879>, ISSN 0142-0615
- [18] M. Čalasan, S.H.E. Abdel Aleem, A.F. Zobaa, "On the root mean square error (RMSE) calculation for parameter estimation of photovoltaic models: A novel exact analytical solution based on Lambert W function", *Energy Conversion and Management*, Vol. 210, pp. 112716, April 2020, <https://doi.org/10.1016/j.enconman.2020.112716>, ISSN 0196-8904
- [19] O. Lukacevic, A. Akmalag, K. Alqunun, A. Farah, M. Calasan, Y. M. Ali, S. H. E. Abdel Aleem, "Optimal CONOPT solver-based coordination of bi-directional converters and energy storage systems for regulation of active and reactive power injection in modern power networks", *Ain Shams Engineering Journal*, Vol. 13, Issue 6, Nov. 2022, pp. 101803, <https://doi.org/10.1016/j.asej.2022.101803>, ISSN 2090-4479
- [20] E. M. Ahmed, S. Rakočević, M. Čalasan, Z. M. Ali, H. M. Hasanien, R. A. Turkey, S. H. E. Abdel Aleem, „BONMIN solver-based coordination of distributed FACTS compensators and distributed generation units in modern distribution networks“, *Ain Shams Engineering Journal*, vol. 13, no. 4, pp. 101664, 2022, doi: <https://doi.org/10.1016/j.asej.2021.101664>, ISSN 2090-4479
- [21] A. Taher, H. Hasanien, S.A. Aleem, M. T. Veliz, M. Calasan, R. Turkey, F. Jurado, „Optimal Model Predictive Control of Energy Storage Devices for Frequency Stability of Modern Power Systems“, *Journal of Energy Storage*, Volume 57, January 2023, pp. 106310, <https://doi.org/10.1016/j.est.2022.106310>, ISSN 2352-152X
- [22] M. Rawa, S. Alghamdi, A. H. Milyani, F. Hariri, B. Alghamdi, M. Ajour, M. Čalasan, Z. M. Ali, H. M. Hasanien, B. Popov, S.H.E. Abdel Aleem, „Thermal model of supercapacitors operating in constant power applications: New mathematical expressions for precise calculation of temperature change“, *Journal of Energy Storage*, Vol. 49, May 2022, pp. 104121, <https://doi.org/10.1016/j.est.2022.104121>, ISSN 2352-152X
- [23] M. Micev, M. Čalasan, Z. M. Ali, H.M. Hasanien, S. H. E. Abdel Aleem, "Optimal Design of Automatic Voltage Regulation Controller Using Hybrid Simulated Annealing- Manta Ray Foraging Optimization Algorithm," *Ain Shams Engineering Journal*, Vol. 12, Issue 1, March 2021, pp. 641-657, <https://doi.org/10.1016/j.asej.2020.07.010>, ISSN 2090-4479
- [24] M. Calasan, A.F. Zobaa, H.M. Hasanien, S. H. E. Abdel Aleem, Ziad M. Ali, "Towards accurate calculation of supercapacitor electrical variables in constant power applications using new analytical closed-form expressions", and Corrigendum, *Journal of Energy Storage*, Vol. 42 (48), pp. 102998 (104367), 2021, <https://doi.org/10.1016/j.est.2021.102998>, ISSN 2352-152X
- [25] M. Calasan, "Analytical solution for no-load induction machine speed calculation during direct start-up", *International Transactions on Electrical Energy Systems*, Vol. 29, Issue 4, 2019, pp. 1-12, <https://doi.org/10.1002/etep.2777>, ISSN 2050-7038
- [26] M. Calasan, A. Nedjc "Experimental Testing and Analytical Solution by Means of Lambert W-Function of Inductor Air Gap Length," *Electric Power Components and Systems (Formerly known as Electric Machines & Power Systems)* Vol. 46, Issue 7, 2018, <https://doi.org/10.1080/15325008.2018.1488012>, ISSN 1532-5008
- [27] T. Dlabac, M. Čalasan, M. Krčum, N. Marvučić, "PSO-based PID controller design for ship course keeping autopilot", *Shipbuilding/Brodogradnja*, Vol. 70, No. 4, pp. 1-15, 2019, <https://doi.org/10.21278/brod70401>, ISSN 0007-215X
- [28] A. Dedic, T. Konjic, M. Čalasan, F. Dedic, „Fuzzy C-Means Clustering Applied to Load Profiling of Industrial Customers“, *Electric Power Components and Systems (Formerly known as Electric Machines & Power Systems)*, Vol. 49, Issue 11-12, pp. 1068–1084, 2021, <https://doi.org/10.1080/15325008.2022.2049660>, ISSN 1532-5008
- [29] M. Čalasan, "An invertible dependence of the speed and time of the induction machine during no-load direct start-up", *Automatika - Journal for Control, Measurement, Electronics, Computing and*

Communications, Vol. 61, Issue 1, 2020, pp. 1411-149, <https://doi.org/10.1080/00051144.2019.1689725>,
ISSN: 0005-1144

- [30] M. Čalasan, L. Nikitović, S. Mujović, "CONOPT solver embedded in GAMS for optimal power flow", *Journal of Renewable and Sustainable Energy*, Vol. 11, pp. 1-16, 2019. <https://doi.org/10.1063/1.5113902>,
ISSN 1941-7012